Monte Carlo Studies of Ising Model Interfaces and Solid-On-Solid Models

Als Habilitationsschrift dem

Fachbereich Physik

der

Westfälischen Wilhelms-Universität, Münster

vorgelegt von

Klaus Pinn

– 1995 –

Monte Carlo Studies of Ising Model Interfaces and Solid-On-Solid Models

Als Habilitationsschrift dem

Fachbereich Physik

der

Westfälischen Wilhelms-Universität, Münster

vorgelegt von

Klaus Pinn

– 1995 –

This work is an account of some research on properties of Ising model interfaces and Solid-On-Solid models. It is based on a backbone of papers [BB1] – [BB9] that was produced together with several collaborators:

Michele Caselle,
Hans Gerd Evertz,
Roberto Fiore,
Fernando Gliozzi,
Martin Hasenbusch,
Gidi Lana,
Mihai Marcu,
Sorin Solomon,
Stefano Vinti.

I would like to thank them all for the enjoyable collaboration.

Articles by the Author and Collaborators
that form the Backbone of this Work[1]

[BB1] H.G. Evertz, M. Hasenbusch, M. Marcu, K. Pinn, and S. Solomon,
Phys. Lett. B 254 (1991) 185,
Stochastic Cluster Algorithms for Discrete Gaussian (SOS) Models.

[BB2] H.G. Evertz, M. Hasenbusch, M. Marcu, K. Pinn, and S. Solomon,
J. Phys. I France (1991) 1669,
High Precision Measurement of the SOS Surface Thickness in the Rough Phase.

[BB3] M. Hasenbusch, G. Lana, M. Marcu, and K. Pinn,
Phys. Rev. B 46 (1992) 10472,
Cluster Algorithm for a Solid-On-Solid Model with Constraints.

[BB4] M. Hasenbusch and K. Pinn,
Physica A 192 (1993) 342,
Surface Tension, Surface Stiffness, and Surface Width of the 3-dimensional Ising Model on a Cubic Lattice.

[BB5] H.G. Evertz, M. Hasenbusch, M. Marcu, and K. Pinn,
Physica A 199 (1993) 31,
The Solid-on-Solid Surface Width Around the Roughening Transition.

[BB6] M. Hasenbusch and K. Pinn,
Physica A 203 (1994) 189,
Comparison of Monte Carlo Results for the 3D Ising Interface Tension and Interface Energy with (Extrapolated) Series Expansions.

[BB7] M. Hasenbusch, M. Marcu, and K. Pinn,
Physica A 208 (1994) 124,
High Precision Renormalization Group Study of the Roughening Transition.

[BB8] M. Caselle, R. Fiore, F. Gliozzi, M. Hasenbusch, K. Pinn, and S. Vinti,
Nucl. Phys. B 432 (1994) 590,
Rough Interfaces Beyond the Gaussian Approximation.

[BB9] M. Hasenbusch, M. Marcu, and K. Pinn,
Physica A 211 (1994) 255,
The Sine Gordon Model: Perturbation Theory and Cluster Monte Carlo.

[1] For abstracts of these articles see the Bibliography

Contents

Introduction

In this work I will present and discuss results which relate to structure and phase transitions in interfaces that separate the two phases of 3-dimensional binary systems. The concrete models under study are the 3-dimensional Ising model and several 2-dimensional Solid-On-Solid (SOS) models. SOS models can be considered as approximations of interfaces that naturally arise when overhangs of the interface and bubbles of the bulk phases are neglected. They can also be regarded as statistical models in their own right.

Our research was motivated and inspired by the development of efficient Cluster Monte Carlo algorithms for the simulation of 2-dimensional SOS models [BB1, BB3, BB9] and for the interface of the 3-dimensional Ising model [132]. These algorithms are called Valleys-To-Mountains-Reflection (VMR) algorithms. Their efficiency comes from their ability to make large scale changes on the shape and structure of interface configurations. In many cases the so-called critical slowing down that hampers Monte Carlo simulations with local update algorithms could be strongly reduced or even completely eliminated.[2]

With efficient Monte Carlo algorithms at hand it was possible to perform very precise studies of interface properties. An account on some of these shall be given in this report.

We will begin with an introduction of interfaces in the 3-dimensional Ising model and to 2-dimensional Solid-On-Solid models in chapter 1. Interfaces of the type discussed in this work come in two phases: a rough phase at high temperatures and a smooth (rigid) phase at low temperatures. Various observables allow to distinguish the two phases. E.g., in the rough phase the interface width diverges when its area becomes infinite, while it stays finite in this limit in the smooth phase.

The phase transition separating the two phases of the interface is called roughening transition. It is generally believed to be of the Kosterlitz-Thouless (KT) type [1, 2]. The transition is of infinite order and governed by an essential singularity of the free energy and other quantities at the transition point.

The basic features of the KT transition can be derived from the KT flow equations. In chapter 2 I shall present a derivation of these equations (and certain generalizations thereof). The derivation is done in the framework of the continuum Sine Gordon model and based on approximations of an exact renormalization group differential equation. In a second section we move to the lattice Sine Gordon model. Using both the VMR cluster Monte Carlo algorithm

[2] For a report on simulations of the Discrete Gaussian model on random triangulated surfaces with our VMR algorithm, see [151]

and perturbation theory, "lines of constant roughness" are defined and determined. These lines are analogous to the KT flow lines in the rough phase.

Chapter 3 is devoted to a careful study of the behavior of the interface width in an SOS model, the Discrete Gaussian model. In the first section, we demonstrate that (in accordance with Kosterlitz-Thouless theory) the squared interface width grows logarithmically with the linear lattice extension in the rough phase. The second section is devoted to a study of the interfacial width of the same model in the vicinity of the roughening temperature T_R. This study is based on precise Monte Carlo data obtained with our VMR algorithm, combined with a renormalization group improved formula that describes the behavior on small lattices on both sides of T_R.

In chapter 4 we confirm the Kosterlitz-Thouless scenario for three SOS models, the Discrete Gaussian model, the Absolute-Value-SOS (ASOS) model, and the dual of the XY model. The method is based on a matching of the renormalization group flow of the candidate models with the flow of a bona fide Kosterlitz-Thouless model, the exactly solvable BCSOS model. Very precise estimates for the roughening couplings and other non-universal quantities are obtained.

Chapter 5 reports on three studies of interfaces in the 3-dimensional Ising model. In the first section, we determine the interface tension and interface energy throughout the whole range from zero temperature up to the bulk transition point. It is demonstrated that in the rough phase the large distance behavior is well described by a massless Gaussian dynamics. The interface stiffness coefficient is determined. Results for the interfacial width on large lattices are presented.

The second study is on a comparison of precise Monte Carlo data for the interface tension and (extrapolated) low temperature expansions. Our study reveals that (as a consequence of the roughening transition) these series have to be used with great care.

In the last section, we compare predictions of the Capillary Wave Model beyond its Gaussian approximation with Monte Carlo results for the energy gap and the surface energy of the 3-dimensional Ising model in the scaling region. It is found that the finite size effects of these quantities are well described by the Capillary Wave Model, expanded to two-loop order, i.e., one order beyond the Gaussian approximation.

Chapter 1

Ising Model Interfaces and Solid-On-Solid Models

We get in touch with interfaces in the 3-dimensional Ising model. Solid-On-Solid models are defined, and a sketch of a few of their basic properties is given.

1.1 Ising Model Interfaces

The Ising model has become a working horse for studies both in the Statistical Mechanics and the Euclidean Quantum Field Theory framework. The 2-dimensional model was exactly solved by Onsager in 1944 [139, 140]. This was the first nontrivial example where a phase transition could be exactly derived from the microscopic Hamiltonian.

Since then, properties of the Ising model have been subject to an incredible number of analytical and numerical studies.

We shall be concerned about the 3-dimensional model on the cubic lattice. We start from the Ising Hamiltonian,

$$H = -\sum_{<x,y>} s_x s_y \,, \qquad s_x = \pm 1 \,. \tag{1.1}$$

The sites of the simple cubic lattice are labeled by integer coordinates $x = (x_1, x_2, x_3)$. The sum in eq. (1.1) is over all (unordered) nearest neighbor pairs of sites in the lattice. We assume that suitable boundary conditions are specified on finite lattices. The partition function is

$$Z = \sum_{\{s\}} \exp\left(-\beta H\right) \,. \tag{1.2}$$

Here, the summation is over all possible configurations of the Ising spins. The pair interaction is normalized such that $\beta = 1/(k_B T)$, where k_B denotes Boltzmann's constant, and T is the temperature.

At a critical coupling $\beta = \beta_c$ the infinite volume limit of the model undergoes a second order phase transition. The (presently) most precise estimate for β_c was obtained in a Monte Carlo

Renormalization Group study of Baillie et al. [94]:

$$\beta_c = 0.221652(3)(1)\,. \tag{1.3}$$

The first error is due to statistical fluctuations while the second one is the estimate for the systematic effects from using a finite (small) number of blocking steps in the MCRG procedure. For the relevant critical exponents, the authors obtain

$$\begin{aligned} \nu &= 0.624(2)\,, \\ \eta &= 0.026(3)\,. \end{aligned} \tag{1.4}$$

The estimate for the correlation length exponent ν lies $2-3\sigma$ below that from other methods, like the ϵ-expansion and high temperature series analysis. For a detailed comparison and references see [94].

While in infinite volume, for $\beta > \beta_c$, the system shows a spontaneous symmetry breaking, in finite volume this cannot occur, and interfaces appear, separating extended domains of different magnetization.

Let us consider simple cubic lattices with extension L in the x_1- and x_2-directions and with extension $t = 2D+1$ in the x_3-direction.[1] We adopt the convention that the x_3-coordinate runs from $-D$ to $+D$. Let us generalize eq. (1.1) to

$$H = -\sum_{<x,y>} k_{xy}\, s_x s_y\,. \tag{1.5}$$

The lattice becomes a torus by regarding the uppermost plane as the lower neighbor plane of the lowermost plane. An analog identification is done for the other two lattice directions. For the Ising spin field s we will use two different boundary conditions: Periodic boundary conditions are defined by letting $k_{xy} = 1$ for all links $<x,y>$ in the lattice. To define antiperiodic boundary conditions in x_3-direction, we also set $k_{xy} = 1$ with the exception of the links connecting the uppermost plane ($x_3 = +D$) with the lowermost plane ($x_3 = -D$). These links carry an antiferromagnetic factor $k_{xy} = -1$.

For sufficiently large β and large enough L, the imposure of antiperiodic boundary conditions forces the system to develop exactly one interface, a region where the magnetization rapidly changes from a large negative value to a large positive value.

The Ising interface undergoes a *roughening transition* at an inverse temperature $\beta_R = 1/(k_{\rm B}T_R)$ that is nearly twice as large as the bulk transition coupling β_c given above.[2] The most precise estimate for the roughening coupling is $\beta_R = 0.4074(3)$ [37]. This value is consistent with a previous estimate $T_R/T_c = 0.542(5)$ in [35] and also with earlier results cited in [35].

What happens at the roughening transition? Roughly speaking, the large scale interface behavior changes from being rigid (smooth) at low temperature to being rough at high temperature. An important example is the behavior of the interfacial width in the limit of $L \to \infty$.

[1] In chapter 5, we shall also consider lattices of size L_1, L_2 in $x_1 - x_2$-direction, with $L_1 \neq L_2$

[2] A fundamental work on this issue is ref. [3]

We adopt the following definition of the interfacial width: A magnetization profile for lattice planes perpendicular to the x_3-direction is defined by

$$M(x_3) = L^{-2} \sum_{x_1, x_2} s_x \,. \tag{1.6}$$

The antiperiodic boundary condition allows one to shift the configuration in x_3-direction such that the interface comes close to $x_3 = 0$.

We introduce an auxiliary coordinate z that assumes half-integer values (labeling positions between adjacent lattice layers perpendicular to the x_3-direction). z takes values $-D+1/2, -D+3/2, \ldots, D-3/2, D-1/2$. Following [35], a normalized magnetization gradient is defined as

$$\rho(z) = \frac{1}{M(D) - M(-D)} \left[M(z + \tfrac{1}{2}) - M(z - \tfrac{1}{2}) \right] \,. \tag{1.7}$$

For a given configuration of the spin field, the position of the interface is defined as the sum over $z\rho(z)$. The square of the interface width is then defined [47, 35] as the expectation value

$$W^2 = \left\langle \sum_z \rho(z)\, z^2 - \left(\sum_z \rho(z)\, z \right)^2 \right\rangle \,. \tag{1.8}$$

(For a discussion of the subleties of this definition, see chapter 5). In the rough phase, i.e., for $\beta > \beta_R$, the interface width is predicted to diverge when $L \to \infty$. More precisely,

$$W^2 \simeq \text{const} + \frac{\beta_{\text{eff}}}{2\pi} \ln L \,. \tag{1.9}$$

This prediction is based on the assumption that in the rough phase the long distance properties of the Ising interface are described by a massless Gaussian dynamics.[3] In the smooth phase, the interfacial width has a finite limit when the interface extension goes to infinity.

Of course, the roughening transition also shows up in other observables, see, e.g., [155, 158, 159].[4] We shall discuss some of its aspects in this work.

Roughening can be observed in real life systems, like crystal surfaces. The roughening transition of a crystal surface can be macroscopically characterized by the disappearance of a facet of a given orientation from the equilibrium crystal shape. On the microscopic scale, the roughening transition is characterized by the vanishing of the free energy of a step on the facet. Strong fluctuations in the location of the facet appear. For a few quite recent papers on experiments and comparison with theory see, e.g., [18]-[21].

The roughening transition is also of importance in lattice gauge theories, see, e.g., [22]-[28].

[3] In the language of condensed matter physics this means that the degrees of freedom are uncoupled capillary waves with an energy proportional to the squared wave vector

[4] I would like to mention here two other useful reviews on surfaces and interfaces by Diehl [156] and by Jasnow [157]

1.2 Solid-On-Solid Models

A fairly good approximation of the Ising interface is given by Solid-On-Solid models to be introduced in this section. The SOS approximation amounts to ignoring overhangs of the Ising interface and bubbles in the two phases separated by the interface. For an early work on the SOS approximation of the Ising interface, see [5]. For a review of exact results on SOS type of models, see [155]. By duality [153] and other exact transformations (see, e.g., [6, 9, 10, 11, 12, 13]) SOS models are shown to be equivalent to a variety of other statistical models. We shall see a number of examples for these equivalences in this work.

All SOS models that we shall consider have in common that they are 2-dimensional lattice spin models. The spins h_x take values in an unbounded discrete set S (isomorphic to the integer numbers). The interaction energy (Hamiltonian) is invariant under global shifts $h_x \to h_x + M$ for $M \in S$. A typical partition function for such a model looks like [5]

$$Z = \sum_{\{h\}} \exp\left(- \sum_{<x,y>} V(h_x - h_y) \right) . \tag{1.10}$$

In this example, the Hamiltonian is a sum of contributions depending on pairs of nearest neighbor spins only. The summation in eq. (1.10) is over equivalence classes of spin configurations $\{h\}$. The classes are defined by identifying two configurations that differ only by a global shift $M \in S$.

Our first example of an SOS model is the Absolute-Value-Solid-On-Solid (ASOS) model. It can be considered as the SOS approximation of an (001) lattice plane interface of an Ising model on a simple cubic lattice. The model is defined by

$$V_{ASOS} = K^{ASOS} |h_x - h_y| . \tag{1.11}$$

The spin variables h_x take integer values. We interpret the h_x as heights with respect to a certain base. For finite positive K^{ASOS} the Hamiltonian will favor that neighboring spins take similar values. When K^{ASOS} is large enough, the surface will not fluctuate too wildly. As a consequence one expects that the surface thickness squared,[6]

$$W^2 = \lim_{|x-y|\to\infty} \langle (h_x - h_y)^2 \rangle , \tag{1.12}$$

is finite: the system is in the "smooth" phase. On the other hand, if K^{ASOS} is below a certain critical value, the surface becomes "rough", and the surface thickness diverges.

The transition between the two phases is called roughening transition. The theory of Kosterlitz and Thouless makes detailed predictions about the nature of this transition, see chapter 2.

In [BB7] (see also chapter 4) the roughening transition of the ASOS model was estimated to occur at $K_R^{ASOS} = 0.8061(3)$.

[5] A factor $1/(k_B T)$, where k_B denotes Boltzmann's constant and T the temperature, is absorbed in the definition of the interaction

[6] A definition of the interface thickness on *finite lattices* will be given later, see chapter 2

In [99] it was proved for a class of SOS models that for sufficiently small coupling K the 2-point correlation function $\langle (h_0 - h_x)^2 \rangle$ goes like $\ln(|x|)$ at large distance x. Furthermore, it follows from convergent cluster expansions that $\langle (h_0 - h_x)^2 \rangle$ stays bounded for all x if K is sufficiently large.

Let us now turn to the Discrete Gaussian (DG) model: It is of the type defined in eq. (1.10) with

$$V_{DG} = K^{DG} (h_x - h_y)^2 . \tag{1.13}$$

The spin variables h_x take integer values. Note that the Hamiltonian looks exactly like that of a continuous Gaussian model. However, the restriction of the h_x to integer values introduces a nontrivial interaction. The DG model will play a prominent role in this work. For an early paper on the physics of this model, see [7].

Precise estimates of the roughening coupling were determined in [BB7] and [BB5] (cf. chapters 3 and 4). The most accurate estimate is $K_R^{DG} = 0.6645(6)$.

The Discrete Gaussian model is dual to the XY model with Villain action [153]. This model is defined by the partition function

$$Z_V = \int_{-\pi}^{\pi} \prod_x d\Theta_x \prod_{<x,y>} B(\Theta_x - \Theta_y) , \tag{1.14}$$

with

$$B(\Theta) = \sum_{p=-\infty}^{\infty} \exp\left(-\tfrac{1}{2}\beta_V (\Theta - 2\pi p)^2\right) \tag{1.15}$$

and

$$\frac{1}{2\beta_V} = K^{DG} . \tag{1.16}$$

The index "V" here refers to "Villain". Let us note that in three dimensions, the DG model is dual to U(1) gauge theory with Villain action. This model was investigated rigorously by Göpfert and Mack [101], see also the work of Ito [102].

The XY model with "standard (cosine) action" has the partition function

$$Z_{XY} = \int_{-\pi}^{\pi} \prod_x d\Theta_x \exp\left(\beta^{XY} \sum_{<x,y>} \cos(\Theta_x - \Theta_y)\right) . \tag{1.17}$$

The standard action is the mostly discussed action for an XY model. The dual of this model is given by the partition function

$$Z_{XY}^{SOS} = \sum_{\{h\}} \prod_{<x,y>} I_{|h_x - h_y|}(\beta^{XY}) , \tag{1.18}$$

where the I_n are modified Bessel functions. Again h_x is integer. For an early study of the XY model with the help of exact transformations to other statistical models, see [6].

We finally introduce the Body Centered Solid-On-Solid (BCSOS) model. It will play a prominent role in chapter 4. The BCSOS model was introduced by van Beijeren [98] as a

SOS approximation of an interface in an Ising model on a body centered cubic lattice on a (001) lattice plane. For detailed analysis of this model with respect to roughening and surface structure, see [158, 16, 159]. The effective 2-dimensional lattice splits in two sublattices like a checker board. In the original formulation, on one of the sublattices the spins take integer values, whereas the spins on the other sublattice take half-integer values. We adopt a different convention: spins on "odd" lattice sites take values of the form $2n+\frac{1}{2}$, and spins on "even" sites are of the form $2n-\frac{1}{2}$, n integer. The partition function of the BCSOS model can be expressed as

$$Z_{BCSOS} = \sum_{\{h\}} \exp\left(-K^{BCSOS} \sum_{[x,y]} |h_x - h_y| \right) . \tag{1.19}$$

The sum is over next-to-nearest neighbor pairs $[x,y]$, and nearest neighbor spins h_x and h_y obey the constraint $|h_x - h_y| = 1$. Van Beijeren [98] showed that the BCSOS model is isomorphic to the F-model, which is a special six vertex model. The configurations of the BCSOS model are in one-to-one correspondence to the configurations of the F-model. The F-model can be solved exactly with transfer matrix methods [96, 97, 100]. The roughening transition occurs at

$$K_R^{BCSOS} = \tfrac{1}{2} \ln 2 . \tag{1.20}$$

The exact formula for the correlation length is [100]:

$$\begin{aligned} \frac{1}{\xi^{BCSOS}} &= -\ln\left\{ 2x^{1/2} \prod_{m=1}^{\infty} \left(\frac{1+x^{4m}}{1+x^{4m-2}} \right)^2 \right\} , \\ x &\equiv \exp\left(-\operatorname{arcosh}\left(\tfrac{1}{2}\exp(4K) - 1 \right) \right) . \end{aligned} \tag{1.21}$$

For $K \searrow K_R$, the correlation length behaves like

$$\xi^{BCSOS} \simeq \frac{1}{4} \exp\left(\frac{\pi^2}{8\sqrt{\frac{1}{2}\ln 2}} \kappa^{-\frac{1}{2}} \right) , \quad \kappa = \tfrac{K-K_R}{K_R} . \tag{1.22}$$

The essential singularity of the correlation length at the critical coupling K_R is typical for a KT model. It is instructive to compare the results of the exact and the asymptotic expression in the neighborhood of the critical point. Table 1.1 shows that at correlation length 189 there is still a relative deviation of 7 per cent between the exact result and the result from the asymptotic formula. This nicely explains why the determination of amplitudes (occuring as parameters in the asymptotic correlation length formula) from correlation length measurements in KT models is so difficult. (Cp. our discussion of this problem in ref. [BB7] and chapter 4.)

The free energy per volume is also exactly known. For $K > K_R$,

$$\begin{aligned} f^{BCSOS} &\equiv -\ln Z^{BCSOS}/\text{volume} \\ &= 2K - \left\{ \tfrac{1}{2}\lambda + \sum_{m=1}^{\infty} \frac{\exp(-m\lambda)\sinh(m\lambda)}{m\cosh(m\lambda)} \right\} , \\ \lambda &\equiv \operatorname{arcosh}\left(\tfrac{1}{2}\exp(4K) - 1 \right) . \end{aligned} \tag{1.23}$$

κ	ξ_{asympt}	ξ_{exact}	κ	ξ_{asympt}	ξ_{exact}
1.00	1.577	2.033	0.20	$0.2436 \cdot 10^2$	$0.2710 \cdot 10^2$
0.80	2.087	2.603	0.10	$0.1750 \cdot 10^3$	$0.1889 \cdot 10^3$
0.60	3.103	3.740	0.05	$0.2784 \cdot 10^4$	$0.2938 \cdot 10^4$
0.40	5.910	6.870	0.01	$0.3080 \cdot 10^9$	$0.3156 \cdot 10^9$

Table 1.1: Comparison of ξ^{BCSOS} from the asymptotic and the exact formula

For $K < K_R$, the free energy f^{BCSOS} has the following integral representation:

$$f^{BCSOS} = 2K - \frac{1}{4\mu}\int_0^\infty \frac{dx}{\cosh(\pi x/2\mu)} \ln\left(\frac{\cosh x - \cos 2\mu}{\cosh x - 1}\right) , \tag{1.24}$$

$$\mu \equiv \arccos\left(\tfrac{1}{2}\exp(4K) - 1\right) . \tag{1.25}$$

Figure 1.1 shows f^{BCSOS} in the neighborhood of the roughening coupling $K_R = \frac{1}{2}\ln 2$. The free energy and all its derivatives stay finite at the transition point (when suitably defined as limits from the right and from the left, respectively). However, there is an essential singularity. This can already be seen if one directly inserts $K = K_R$ in eq. (1.23) and in eq. (1.24). In both cases one obtains $\ln 2$, different from the right-left limits to be read off in figure 1.1. One can show [100] that for $K \searrow K_R$, the singular part of the free energy (note that eqs. (1.23) and (1.24) give the full free energy) vanishes according to

$$f_{\mathrm{sing}}^{BCSOS} \sim \exp\left(-\frac{\pi^2}{4\sqrt{\frac{1}{2}\ln 2}}\,\kappa^{-\frac{1}{2}}\right) , \quad \kappa = \tfrac{K-K_R}{K_R} . \tag{1.26}$$

There exist more SOS models of interest. One of them, the Sine Gordon model, will be discussed at length in the next chapter.

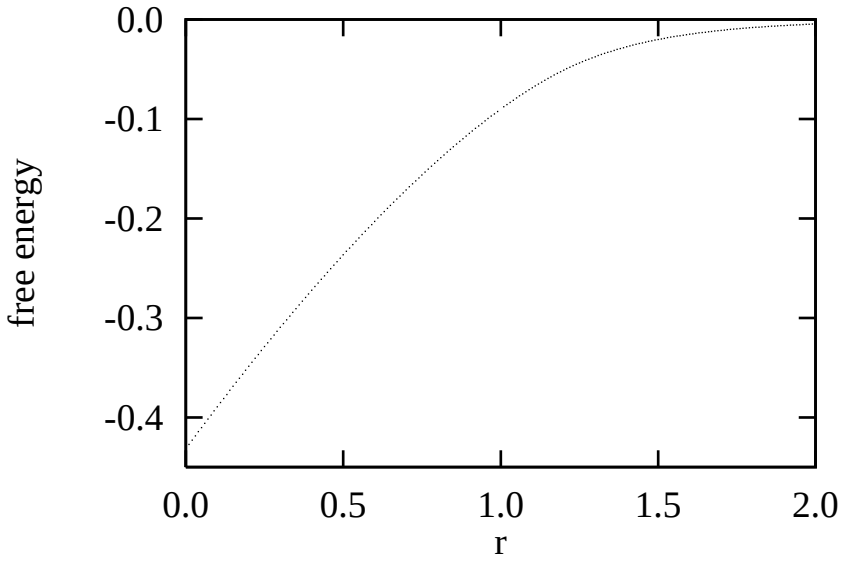

Figure 1.1: The free energy per volume of the BCSOS model as a function of $r = K^{BCSOS}/K_R^{BCSOS}$

Chapter 2

The Sine Gordon Model and the Kosterlitz-Thouless Scenario

In this chapter, we shall get in touch with Kosterlitz-Thouless physics visiting the Sine Gordon model. In the first section, I shall derive renormalization group flow equations that generalize the famous Kosterlitz-Thouless equations. The derivation is done in the continuum formulation. In the second section, "lines of constant roughness" shall be derived for the lattice Sine Gordon model. The analysis is based on a second order perturbative expansion in the fugacity z. The content of section 2.1 has not been published before, section 2.2 is based on ref. [BB9].

2.1 The Continuum Sine Gordon Model: Kosterlitz-Thouless Equations

The 2-dimensional continuum massless Sine Gordon (SG) model is defined by the partition function

$$\mathcal{Z} = \int d\mu_{\beta v}(\varphi)\, \exp[V(\varphi)]\,. \tag{2.1}$$

Here, $d\mu_{\beta v}$ denotes the Gaussian measure[1] with covariance βv, defined through

$$\int d\mu_{\beta v}(\varphi)\, \exp[i(k,\varphi)] = \begin{cases} \exp\left[-\frac{1}{2}\beta(k, Ck)\right] & , \text{ if } \int_x k_x = 0 \\ 0 & , \text{ else }. \end{cases} \tag{2.2}$$

We have introduced the notation

$$\int_x (.) = \int d^2x\, (.)\,, \qquad (\psi, \phi) = \int_x \psi_x \phi_x\,. \tag{2.3}$$

[1] For an introduction to Gaussian measures, see textbooks on quantum field theory. For mathematical aspects, see [103]

$\beta \geq 0$ can be interpreted as temperature. The kernel C is given by

$$C_{x,y} = \int_p \frac{\exp[ik(x-y)] - 1}{p^2} \exp(-p^2/\Lambda^2)\,,$$

where

$$\int_p (.) = \int \frac{d^2p}{(2\pi)^2}\,(.)\ . \tag{2.4}$$

We have provided the propagator with a cutoff Λ, formally $v = \exp(\Delta/\Lambda^2)(-\Delta)^{-1}$.

The (generalized) SG potential $V(\varphi)$ is given by

$$V(\varphi) = \sum_n \frac{z_n}{2} \int_x \cos(2\pi n \varphi_x) \equiv \int_x \mathcal{V}(\varphi_x)\,. \tag{2.5}$$

The sum runs over all integers n, and the fugacities[2] obey $z_{-n} = z_n$. A more formal way to write down the partition function of the Sine Gordon model is as follows:

$$Z = \int \prod_x d\varphi_x \, \exp\left[-\frac{1}{2\beta}(\varphi, -\Delta\varphi) + V(\varphi)\right]\,. \tag{2.6}$$

Here, Δ denotes the Laplacian, $\Delta = \partial^2/\partial x_1^2 + \partial^2/\partial x_2^2$.

The Sine Gordon model has been subject to many interesting theoretical and numerical studies. A fundamental work is ref. [4]. For the relation of the model with the 2-dimensional Coulomb gas, see refs. [9, 10, 11]. Renormalization group equations are derived and discussed in [8, 11], cp. also the present work. Rigorous results on the long-distance properties of the model in the massless phase and a rigorous construction of the model in the massive phase are reported in refs. [104, 105].

2.1.1 Infinitesimal Renormalization Group Step

Consider an infinitesimal renormalization group transformation [86, 87] such that the cutoff Λ is lowered to $\Lambda' = \Lambda(1-\epsilon)$, with $\epsilon > 0$ infinitesimal. This corresponds to a split of the propagator, $v = u + \Gamma$. The block spin propagator u has cutoff Λ'. Γ is called fluctuation propagator. For our choice of the cutoff, with $a \equiv \Lambda^{-1}$, and $a' = \Lambda'^{-1}$,

$$\begin{aligned}\Gamma_x &= \int_p \frac{\exp(ipx)}{p^2}\,[\exp(-a^2p^2) - \exp(-a'^2p^2)] \\ &= \int_{a^2}^{a'^2} d\lambda \int_p \exp(ipx - \lambda p^2)\,.\end{aligned} \tag{2.7}$$

The p-integration can be done:

$$\Gamma_x = \frac{1}{4\pi}\int_{a^2}^{a'^2} \frac{d\lambda}{\lambda} \exp\left(-\frac{1}{4}x^2/\lambda\right) = F(a'^2) - F(a^2)\,, \tag{2.8}$$

[2]The name fugacity for the coupling constant z will become clear later when we consider the Coulomb gas representation of the SG model, see also ref. [10]

with

$$\frac{d}{d\lambda}F(\lambda) = F'(\lambda) = \frac{\exp\left(-\frac{1}{4}x^2/\lambda\right)}{4\pi\,\lambda}\,. \tag{2.9}$$

For an infinitesimal renormalization group transformation we can write $\Gamma_x = \epsilon\gamma_x$. To see this, let $a' = (1+\epsilon)a$, i.e. $a'^2 = a^2 + 2a^2\epsilon$. Then

$$\Gamma_x = 2\,a^2 F'(a^2)\,\epsilon + O(\epsilon^2)\,, \tag{2.10}$$

and

$$\gamma_x = \frac{\exp\left(-\frac{1}{4}\Lambda^2 x^2\right)}{2\pi}\,. \tag{2.11}$$

We shall employ the convolution formula for Gaussian measures,

$$\int d\mu_{v_1+v_2}(\varphi)\,\mathcal{O}(\varphi) = \int d\mu_{v_1}(\varphi_1)\int d\mu_{v_2}(\varphi_2)\,\mathcal{O}(\varphi_1+\varphi_2)\,, \tag{2.12}$$

to rewrite the partition function eq. (2.1) as

$$\mathcal{Z} = \int d\mu_{\beta u}(\phi)\,\exp[V'(\phi)]\,. \tag{2.13}$$

The effective potential $V'(\phi)$ is given by

$$\exp[V'(\phi)] = \int d\mu_{\beta\Gamma}(\zeta)\,\exp[V(\phi+\zeta)]\,. \tag{2.14}$$

A very useful identity for Gaussian integrations is the following:

$$\int d\mu_v(\zeta)\,\mathcal{O}(\phi+\zeta)] = \exp\left[\frac{1}{2}\left(\frac{\delta}{\delta\phi}, v\frac{\delta}{\delta\phi}\right)\right]\,\mathcal{O}(\phi)\,. \tag{2.15}$$

Let us consider ϵ infinitesimal from now on. With the help of eq. (2.15) we find

$$V'(\phi) = V(\phi) + \epsilon\,\frac{\beta}{2}\int_x\int_y \gamma_{xy}\left\{\frac{\delta^2 V(\phi)}{\delta\phi_x\delta\phi_y} + \frac{\delta V(\phi)}{\delta\phi_x}\frac{\delta V(\phi)}{\delta\phi_y}\right\}\,. \tag{2.16}$$

This equation is more or less equivalent to Polchinski's exact RG differential equation [87]. We will now use eq. (2.16) to compute $V'(\phi)$ for the model defined by the potential eq. (2.5). One finds

$$\begin{aligned} V'(\phi) \quad &= V(\phi) \quad + \epsilon\,(2\pi)^2\frac{\beta}{2}\Big\{-\gamma_{oo}\sum_n n^2\frac{z_n}{2}\int_x \cos(2\pi n\phi_x) + \\ &\quad + \sum_{m,n} mn\frac{z_m}{2}\frac{z_n}{2}\int_x\int_y \gamma_{xy}\sin(2\pi m\phi_x)\sin(2\pi n\phi_y)\Big\}\,. \end{aligned} \tag{2.17}$$

2.1.2 Local Potential Approximation of the Effective Theory

Eq. (2.17) shows that the effective theory contains more interactions terms than the SG model we started from. We aim at an approximation of $V'(\phi)$ in the form

$$V'(\phi) = K'(\phi) + \int_x \mathcal{V}'(\phi_x)\,, \tag{2.18}$$

where $K'(\phi)$ is a kinetic term which is quadratic in ϕ and vanishes for constant ϕ, and $\mathcal{V}'$ denotes the zero momentum potential (per volume). We shall later also approximate the kinetic term by a constant times the Laplace operator.

The zero momentum potential is defined as follows:

$$\mathcal{V}'(\psi) = \text{volume}^{-1} V'(\phi)\Big|_{\phi_x=\psi}\,. \tag{2.19}$$

We find

$$\begin{aligned}\mathcal{V}'(\psi) \quad &= \mathcal{V}(\psi) \quad + \epsilon\,(2\pi)^2 \frac{\beta}{2}\Big\{-\gamma_{oo}\sum_n n^2 \frac{z_n}{2}\cos(2\pi n\psi) + \\ &\quad + \gamma_{(1)}\sum_{m,n} mn\frac{z_m}{2}\frac{z_n}{2}\sin(2\pi m\psi)\sin(2\pi n\psi)\Big\}\,.\end{aligned} \tag{2.20}$$

We have introduced the abbreviation

$$\gamma_{(1)} = 2\pi\int_0^\infty dr\, r\,\gamma_r\,. \tag{2.21}$$

Using that $\sin a \sin b = \frac{1}{2}[\cos(a-b) - \cos(a+b)]$ one arrives at

$$\mathcal{V}'(\psi) = \mathcal{V}(\psi) + \epsilon\sum_n \frac{y_n}{2}\cos(2\pi n\psi)\,. \tag{2.22}$$

The y_n are given by

$$y_n = (2\pi)^2\frac{\beta}{2}\left(-\gamma_{oo}\,n^2\,z_n + \tfrac{1}{2}\gamma_{(1)}\sum_m m(m+n)z_m z_{m+n}\right)\,. \tag{2.23}$$

Note that we determined the zero momentum potential exactly. For the kinetic term things are more difficult. Here we have to make an approximation. The contribution of the effective Hamiltonian eq. (2.17) to the kinetic term is given by

$$K'(\phi) = \epsilon\,\mathbf{SQ}(2\pi)^2\frac{\beta}{8}\sum_{m,n} mnz_m z_n\int_x\int_y \gamma_{xy}\sin(2\pi m\phi_x)\sin(2\pi n\phi_y)\,. \tag{2.24}$$

The operator $\mathbf{SQ}$ means that we have to take the quadratic part ($\mathbf{Q}$) in ϕ and subtract ($\mathbf{S}$) the zero momentum contributions. Taking the quadradic part is simple:

$$K'(\phi) = \epsilon\,\mathbf{S}(2\pi)^4\frac{\beta}{8}\sum_{m,n}(mn)^2 z_m z_n\int_x\int_y \gamma_{xy}\phi_x\phi_y\,. \tag{2.25}$$

For a general translational invariant kernel A_{xy},

$$\begin{aligned}(\phi, A\phi) &= \int_x \int_y \phi_x A_{xy} \phi_y \\ &= \sum_{n=0}^{\infty} \frac{i^n}{n!} \int_p |\tilde{\phi}_p|^2 \int_x A_{ox} (px)^n \,. \end{aligned} \tag{2.26}$$

Now let us assume that the kernel A is invariant under rotations, i.e. A depends only on $r = |x|$. Then (in two dimensions)

$$\int_x A_{ox} (px)^n = |p|^n \int_0^{\infty} r^{n+1} A_r \int_0^{2\pi} d\varphi \cos^n \varphi \,. \tag{2.27}$$

The integral over φ vanishes for odd n, and for even n we have

$$\int_0^{2\pi} d\varphi \cos^n \varphi = \frac{2\pi}{2^n} \frac{n!}{(n/2)!^2} \,. \tag{2.28}$$

Inserting this we find

$$(\phi, A\phi) = \sum_{n=0}^{\infty} \frac{(-\frac{1}{4})^n}{n!^2} A_{(n)} \, (\phi, (-\Delta)^n \phi) \,, \tag{2.29}$$

where the coefficients A_n are given by

$$A_{(n)} = 2\pi \int_0^{\infty} dr \, r^{2n+1} \, A_r \,. \tag{2.30}$$

We conclude that

$$\mathbf{S} \int_x \int_y \gamma_{xy} \phi_x \phi_y = -\frac{1}{4} \gamma_{(3)} (\phi, -\Delta\phi) + ... \tag{2.31}$$

The correction terms contain higher derivatives and are thus irrelevant operators with respect to the Gaussian fixed point. This may justify that we ignore these terms in the following. $\gamma_{(3)}$ is given by

$$\gamma_{(3)} = 2\pi \int_0^{\infty} dr \, r^3 \, \gamma_r \,. \tag{2.32}$$

Our approximation for the kinetic term will be

$$K'(\phi) = -\epsilon \, \kappa \, \frac{1}{2\beta} (\phi, -\Delta\phi) \,, \tag{2.33}$$

with

$$\kappa = (2\pi)^4 \, \gamma_{(3)} \, \frac{\beta^2}{16} \left(\sum_n n^2 z_n \right)^2 \,. \tag{2.34}$$

2.1.3 Rescaling of Units and Renormalization of β

We now turn to the renormalization of β and the rescaling of units. The starting point is our approximation for the effective potential

$$V'(\phi) = V(\phi) - \epsilon\,\kappa \frac{1}{2\beta}(\phi, -\Delta\phi) + \epsilon \sum_n \frac{y_n}{2} \int_x \cos(2\pi n \phi_x)\,. \tag{2.35}$$

The kinetic term will now be absorbed in the (block spin) propagator, thus leading to a renormalization of β:

$$\frac{1}{\beta'} = \frac{1}{\beta}(1+\epsilon\kappa) \qquad \rightarrow \qquad \beta' = \beta - \epsilon\beta\kappa\,. \tag{2.36}$$

Furthermore, we perform a variable transformation in the partition function eq. (2.13),

$$\phi_x = \varphi_{\lambda x}\,, \tag{2.37}$$

where $\lambda = \Lambda'/\Lambda = 1-\epsilon$. This transformation leads to a factor $(1+\epsilon)^2 = 1+2\epsilon$ in front of the fugacities. The propagator does not acquire a factor, but the cutoff is rescaled back from Λ' to Λ. The effective theory is therefore described by the coupling constants

$$\begin{aligned} z_n' &= z_n + \epsilon\,(2z_n + y_n)\,, \\ \beta' &= \beta - \epsilon\beta\kappa\,. \end{aligned} \tag{2.38}$$

A finite RG transformation can be obtained as the solution of the differential equation

$$\begin{aligned} \dot{z}_n &= 2z_n + y_n\,, \\ \dot{\beta} &= -\beta\kappa\,. \end{aligned} \tag{2.39}$$

The dot denotes derivative with respect to the scale parameter t. (Note that the change of length scale is $\exp t$.) Inserting the definitions of y_n and κ we get

$$\begin{aligned} \dot{z}_n &= (2 - \pi\beta n^2) z_n + A\beta \sum_m m(m+n)\, z_m z_{m+n}\,, \\ \dot{\beta} &= -B\beta^3 \left(\sum_m m^2 z_m \right)^2\,. \end{aligned} \tag{2.40}$$

We have used that $\gamma_{oo} = 2\pi$. The (scheme dependent) constants A and B are given by

$$\begin{aligned} A &= \pi^2\,\gamma_{(1)}\,, \\ B &= \pi^4\,\gamma_{(3)}\,. \end{aligned} \tag{2.41}$$

2.1.4 Recovering the Kosterlitz-Thouless Equations

We make the approximation that $z_n = 0$ for all $n \neq \pm 1$. Then the flow equations simplify to

$$\begin{aligned} \dot{z}_1 &= (2 - \pi\beta)\, z_1 \,, \\ \dot{\beta} &= -4B\beta^3 z_1^2 \,. \end{aligned} \tag{2.42}$$

Define $\pi\beta - 2 = x$. Note that $\beta = \frac{2}{\pi}$ is the critical point for $z_1 \to 0$. In order to study the flow in the vicinity of the fixed point one therefore expands $\beta^3 = (2/\pi)^3 + O(x)$. If we redefine the fugacity,

$$y = \frac{\sqrt{32B}}{\pi}\, z_1 \,, \tag{2.43}$$

the flow equations take the standard form

$$\begin{aligned} \dot{y} &= -xy \,, \\ \dot{x} &= -y^2 \,. \end{aligned} \tag{2.44}$$

2.1.5 Solution of the Kosterlitz-Thouless Equations

We consider the KT equations (2.44). It is easy to see that $dy^2/dt = dx^2/dt$. Therefore $E = y^2 - x^2$ is a constant of motion. We consider separately the three cases $E = 0$, $E < 0$, and $E > 0$.

$E = 0$: From $y^2 - x^2 = 0$ it follows that either $x = y$ or $x = -y$. In the first case one is on the critical trajectory that runs into the fixed point at $(x, y) = (0, 0)$. The second case corresponds to the expanding manifold that leaves the fixed point. On the critical trajectory y obeys the differential equation $\dot{y} = -y^2$, which has the solution

$$y(t) = \frac{1}{\frac{1}{y_0} + t} \,, \tag{2.45}$$

where $y_0 = y(t = 0)$. On the expanding manifold y obeys $\dot{y} = y^2$, and the solution is

$$y(t) = \frac{1}{\frac{1}{y_0} - t} \,. \tag{2.46}$$

Note that on this trajectory y diverges for finite t.

$E < 0$: We look at the solutions in the $x > 0$ region (the solutions for $x < 0$ can be obtained analogously). Let a denote the point where the trajectory hits the x-axis at infinite t. Define $x = a + f$. We then have the system of differential equations

$$\begin{aligned} \tfrac{dy^2}{dt} &= -2\,(a + f)y^2 \,, \\ \tfrac{df}{dt} &= -\,y^2 \,. \end{aligned} \tag{2.47}$$

It follows that

$$\frac{dy^2}{df} = 2\,(a+f)\,, \tag{2.48}$$

and therefore

$$y^2 = f^2 + 2af\,. \tag{2.49}$$

The integration constant vanishes because $y = 0$ for $f = 0$. We find the following differential equation for f:

$$\frac{df}{dt} = -f(f+2a)\,. \tag{2.50}$$

This equation can be solved by separation of variables

$$dt = -\frac{df}{2a}\left(\frac{1}{f} - \frac{1}{f+2a}\right)\,. \tag{2.51}$$

By integration we find

$$f(t) = 2a\left\{\left(1+\frac{2a}{f(t_0)}\right)\,\exp[2a(t-t_0)] - 1\right\}^{-1}\,. \tag{2.52}$$

$E > 0$: Define $\epsilon = \sqrt{E}$. From $y^2 = \epsilon^2 + x^2$ one obtains

$$\frac{dx}{dt} = -(\epsilon^2 + x^2)\,. \tag{2.53}$$

This differential equation can again be solved by separation of variables. The solution is

$$x(t) = \epsilon\,\tan\left(\arctan\frac{x(t_0)}{\epsilon} - \epsilon(t-t_0)\right)\,. \tag{2.54}$$

The flow diagram encodes the full information about the critical behavior, see figure 2.1. Region I ($E < 0$) corresponds to the massless phase. Here, the trajectories run exponentially fast (in the variable $t = \ln B$) to $y = 0$: the long distance behavior is that of a massless Gaussian model. The point where a trajectory hits the x-axis corresponds to a β-value that is called β_{eff}. It is the β-coupling of the free field theory describing the long distance behavior of all models that "come down" the trajectory. Note that this is a whole class of models which differ only in the "time" they need to reach the x-axis.

Regions II ($E > 0$) and III ($E < 0$) correspond to the massive phase. Here, with increasing length scale, the fugacity increases, and the global symmetry under shifts $\varphi_x \to \varphi_x + \text{integer}$ is spontaneously broken. The separatrix between regions I and II is the critical line. Models on this line are driven into the fixed point $(x, y) = (0, 0)$ which corresponds to $\beta = 2/\pi$ and $z = 0$. Note that the approach to the fixed point goes like $\sim t^{-1}$ on the critical trajectory.

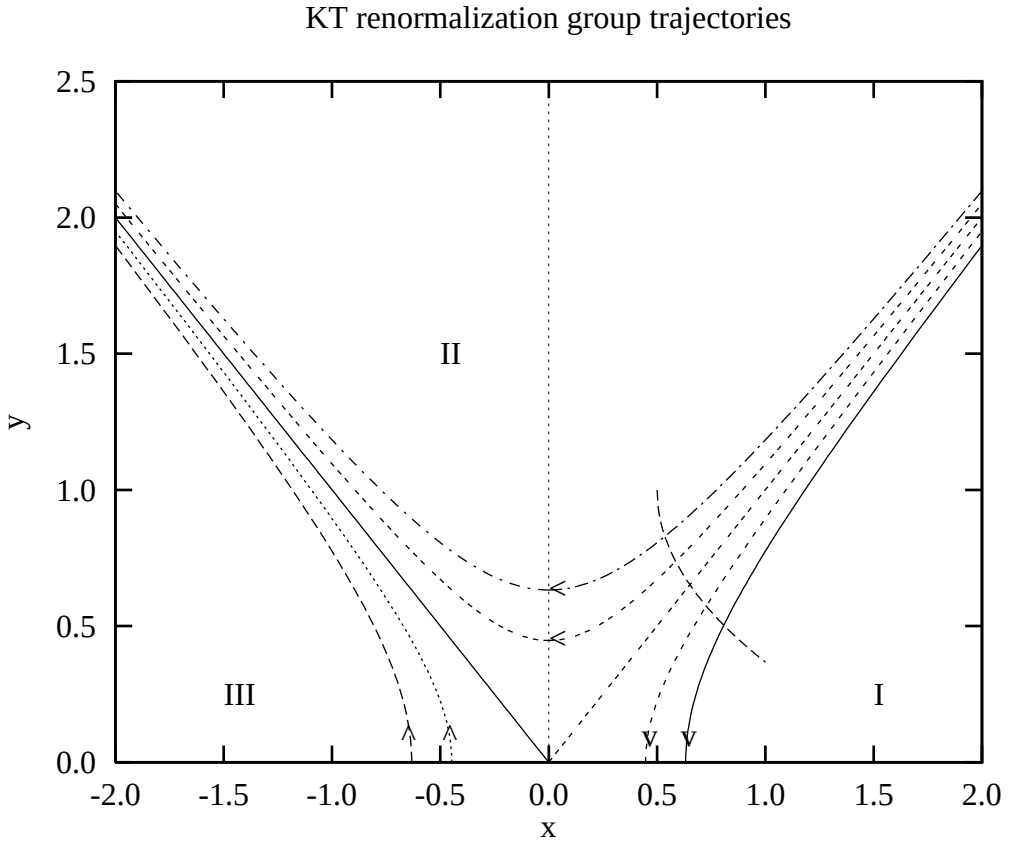

Figure 2.1: Renormalization group trajectories in a Kosterlitz-Thouless model. Region I ($E < 0$) corresponds to the massless phase. Here, the trajectories run exponentially fast (in the variable t) to $y = 0$: the long distance behavior is that of a Gaussian model. Regions II ($E > 0$) and III ($E < 0$) correspond to the massive phase. Here, with increasing length scale, the fugacity increases, and the global symmetry under shifts $\varphi_x \to \varphi_x + \text{integer}$ is spontaneously broken. The separatrix between regions I and II ($E = 0$) is the critical line. Models on this line are driven into the fixed point $(x, y) = (0, 0)$ which corresponds to $\beta = 2/\pi$ and $z = 0$. The meaning of the dotted line intersecting the trajectories in regions I and II is explained in the text

From the solutions of the flow equations one can derive (see, e.g., [146]) that the correlation length of a KT model diverges like

$$\xi^{KT} \simeq A \exp\left(C \left| \frac{\beta_c - \beta}{\beta_c} \right|^{-\frac{1}{2}} \right) , \tag{2.55}$$

for $\beta \to \beta_c$. Here, A, C, and β_c are non-universal constants, i.e. they have different values for different KT models. One should compare eq. (2.55) with with eq. (1.22).

The KT equations for the SG model were derived using several approximations. The most important assumption is that the fugacity is small. However, if one assumes that $(x, y) = (0, 0)$ is the fixed point that governs the critical behavior then the trajectories of a critical or nearly critical KT model will eventually enter the region where the fugacity is small and where the KT equations become valid. Depending on the details of the microscopic Hamiltonian, the "time" before the effective Hamiltonian comes close to the fixed point can be very long, i.e., the flow close to the critical line is very slow. This is one of the reasons why the unambigious confirmation of the KT scenario for realistic models is so difficult.

2.2 The Lattice Sine Gordon Model: Lines of Constant Roughness

The lattice Sine Gordon (SG) model Hamiltonian is

$$H(\varphi) = \frac{1}{2\beta} \sum_{<x,y>} (\varphi_x - \varphi_y)^2 - V(\varphi) . \tag{2.56}$$

The sum runs over all nearest neighbor pairs $< x, y >$ in the 2-dimensional square lattice, and

$$V(\varphi) = z \sum_x \cos(2\pi\varphi_x) . \tag{2.57}$$

We have chosen units such that the Boltzmann factor is $\exp(-H)$.

Compared to other SOS models the SG model is very suitable for analytical calculations, e.g., expansions in the fugacity z.

The variables φ_x have a natural interpretation as height variables. For sufficiently small temperature β a typical φ-configuration describes a more or less smooth surface (interface). In the thermodynamic limit the interface gets localized and has a finite width. The model is in the *smooth* phase.

For large β, however, the interface can freely wander. Furthermore, the interface width squared diverges logarithmically when the area becomes large. The model is in the *rough* phase.

The two phases are separated by a phase transition of infinite order, the roughening transition. The transition occurs on a critical line $\beta_c(z)$.

To make things more precise, we define the interface width W. On a finite periodic square lattice Λ with $N = L \times L$ sites, let

$$W^2 = \frac{1}{N^2} \sum_{x,y} \langle (\varphi_x - \varphi_y)^2 \rangle = 2 \langle (\varphi_x - \Phi)^2 \rangle \,. \tag{2.58}$$

Φ is the average of φ over the entire lattice,

$$\Phi = \frac{1}{N} \sum_x \varphi_x \,. \tag{2.59}$$

One can show (see, e.g., [BB9]) that for $z = 0$ and $L \to \infty$,

$$W^2 \to \frac{\beta}{\pi} \ln L + c \,, \tag{2.60}$$

where c is some constant.

The interface width can be used to distinguish between the two phases of the SG model: In the limit $L \to \infty$, for nonzero z,

$$W^2 \to \begin{cases} \frac{\beta_{\text{eff}}(z)}{\pi} \ln L + c', & \text{if } \beta \geq \beta_c(z) \,, \\ \text{finite}, & \text{else} \,. \end{cases} \tag{2.61}$$

This equation says that in the rough (large β) phase, the long distance behavior of the theory is that of a Gaussian model ($z = 0$) with infinite correlation length, but with a changed temperature β_{eff} that depends on the fugacity z.

It is known that for $z \to 0$, the critical temperature goes to $2/\pi$, see, e.g., [10]. Accordingly, the *critical line* is given as the set of points (z, β) with $\beta_{\text{eff}}(z) = 2/\pi$. For every z, the critical point $\beta_c(z)$ is the smallest value of β such that the interface width diverges for $L \to \infty$. At $\beta = \beta_c(z)$, the asymptotic ratio $W^2 / \ln L$ jumps from $2/\pi^2$ to zero.
More generally, we shall define *lines of constant roughness* in the rough phase of the model as those lines in the (z, β)-plane that belong to the same value of β_{eff}. Models that lie on the same line have identical long distance behavior (which is Gaussian in this particular model).

In this section, we shall derive an approximation of the lines of constant roughness from the perturbative expansion of the interface width W to second order in z.

It is always interesting to compare analytical results with numerical ones, especially when approximations are made in the analytical calculations. To make this comparison we employed a cluster algorithm for the simulation of the SG model [BB9].

2.2.1 Perturbation Theory for the Interface Width

Expectation values (correlation functions) of observables in the SG model are defined through

$$\langle \mathcal{O}(\varphi) \rangle = \frac{\int \prod_x d\varphi_x \exp\left[-H(\varphi)\right] \, \mathcal{O}(\varphi)}{\int \prod_x d\varphi_x \exp\left[-H(\varphi)\right]} \,. \tag{2.62}$$

The Hamiltonian $H(\varphi)$ is invariant under shifts $\varphi_x \to \varphi_x + n$ for all x, where n is an integer constant. As a consequence, expectation values are defined only for observables $\mathcal{O}(\varphi)$ that have the same global symmetry: In this case the infinite contribution from the zero mode associated with the symmetry is exactly cancelled in eq. (2.62).[3]

For the perturbation theory to be done in this section, it is convenient to rewrite eq. (2.62) with the help of a Gaussian measure. An integration measure $d\mu_{\beta C}(\varphi)$ is defined through its generating functional[4]

$$\int d\mu_{\beta C}(\varphi)\ \exp[i(k,\varphi)] = \begin{cases} \exp\left[-\frac{1}{2}\beta(k,Ck)\right] & \text{, if } \sum_x k_x = 0 \\ 0 & \text{, else .} \end{cases} \tag{2.63}$$

The covariance C is a matrix with elements

$$\begin{aligned} C_{xy} &= \frac{1}{N}\sum_{p\neq 0} \frac{\mathrm{e}^{ip(x-y)}-1}{\hat{p}^2}\,, \\ \hat{p}^2 &= 4 - 2\cos p_1 - 2\cos p_2\,, \end{aligned} \tag{2.64}$$

where the p_i, $i = 1, 2$, are summed over the values $\{0, ..., L-1\}\cdot(2\pi/L)$. The scalar product is defined by

$$(\phi,\psi) = \sum_x \phi_x \psi_x\,. \tag{2.65}$$

It is not difficult to show that the expectation value eq. (2.62) can be rewritten as

$$\langle \mathcal{O}(\varphi)\rangle = \frac{\int d\mu_{\beta C}(\varphi)\ \exp\left[V(\varphi)\right]\ \mathcal{O}(\varphi)}{\int d\mu_{\beta C}(\varphi)\ \exp\left[V(\varphi)\right]}\,. \tag{2.66}$$

The calculation of the interface width is started with the observation that for arbitrary observables $\mathcal{O}(\varphi)$,

$$\begin{aligned} \langle \mathcal{O}(\varphi)\rangle &= \frac{\int d\mu_{\beta C}(\varphi)\ \exp[V(\varphi)]\,\mathcal{O}(\varphi)}{\int d\mu_{\beta C}(\varphi)\ \exp[V(\varphi)]} \\ &= \frac{\int d\Phi \int d\mu_{\beta C}(\varphi)\ \delta(\Phi - \frac{1}{N}\sum_x \varphi_x)\ \exp[V(\varphi)]\,\mathcal{O}(\varphi)}{\int d\Phi \int d\mu_{\beta C}(\varphi)\ \delta(\Phi - \frac{1}{N}\sum_x \varphi_x)\ \exp[V(\varphi)]} \\ &= \frac{\int d\Phi \int d\mu_{\beta\Gamma}(\varphi)\ \exp[V(\Phi+\varphi)]\,\mathcal{O}(\Phi+\varphi)}{\int d\Phi \int d\mu_{\beta\Gamma}(\varphi)\ \exp[V(\Phi+\varphi)]}\,. \end{aligned} \tag{2.67}$$

Here, the Gaussian measure with covariance Γ is defined through

$$\int d\mu_\Gamma(\varphi)\,\mathcal{O}(\varphi) = \lim_{M\to 0} \frac{\int d\mu_{v_M}(\varphi)\,\delta(\sum_x \varphi_x)\mathcal{O}(\varphi)}{\int d\mu_{v_M}(\varphi)\,\delta(\sum_x \varphi_x)}\,, \tag{2.68}$$

[3] The **Z**-symmetry of the model is broken in the smooth phase, $\beta < \beta_c(z)$. Here, in the thermodynamic limit, expectation values of observables that are not **Z**-invariant, are defined

[4] Compare the corresponding defintions in the continuum case discussed in the previous section

where[5] $v_M = (-\Delta + M^2)^{-1}$. It is not difficult to demonstrate that

$$\Gamma_{xy} = \int d\mu_\Gamma(\varphi)\, \varphi_x \varphi_y = \frac{1}{N} \sum_{p \neq 0} \frac{\mathrm{e}^{ip(x-y)}}{\hat{p}^2}\,. \tag{2.69}$$

Correlation functions as occuring in eq. (2.67) can be computed with the help of the generating functional

$$\int d\mu_{\beta\Gamma}(\varphi)\, \exp\left[i(k,\varphi)\right] = \exp\left[-\tfrac{1}{2}\beta(k,\Gamma k)\right]\,. \tag{2.70}$$

The "effective observable" for the interface width is independent of Φ:

$$\mathcal{O}(\Phi + \varphi) = 2\,\varphi_x^2\,. \tag{2.71}$$

We therefore have

$$W^2 = 2\,\frac{\int d\mu_{\beta\Gamma}(\varphi)\ \varphi_x^2 \int d\Phi\ \exp[V(\Phi+\varphi)]}{\int d\mu_{\beta\Gamma}(\varphi)\ \int d\Phi\ \exp[V(\Phi+\varphi)]}\,. \tag{2.72}$$

We expand the Boltzmann factor:

$$\begin{aligned} \exp[V(\Phi+\varphi)] &= \sum_{n\geq 0} \frac{z^n}{n!} \sum_{x_1} \dots \sum_{x_n} \cos 2\pi(\varphi_{x_1} + \Phi) \dots \cos 2\pi(\varphi_{x_n} + \Phi) && (2.73) \\ &= \sum_{n\geq 0} \left(\frac{z}{2}\right)^n \frac{1}{n!} \sum_{x_1,s_1} \dots \sum_{x_n,s_n} \exp\left[i2\pi \left(\sum_{i=1}^n s_i \cdot (\varphi_{x_i} + \Phi)\right)\right]\,. && (2.74) \end{aligned}$$

The "charges" s_i are summed over the values ± 1. The Φ-integral leads to a δ-function that forces the sum of the s_i to be zero (neutrality condition). We shall indicate this constraint with a prime at the sums in the equations to follow. The Gaussian integrations in eq. (2.72) can now be done, leading to the representation

$$W^2 = 2\beta\Gamma_{oo} - K\,\frac{\sum_{n\geq 0} \left(\frac{z}{2}\right)^n Z'_n}{\sum_{n\geq 0} \left(\frac{z}{2}\right)^n Z_n}\,. \tag{2.75}$$

Here, we have defined

$$Z'_n = \frac{1}{n!} \sum_{x_1,s_1}{}' \dots \sum_{x_n,s_n}{}' \exp\left(-\tilde{\beta} \sum_{i<j}^n s_i C_{x_i x_j} s_j\right) \left(\sum_{i=1}^n C_{ox_i} s_i\right)^2\,, \tag{2.76}$$

and

$$Z_n = \frac{1}{n!} \sum_{x_1,s_1}{}' \dots \sum_{x_n,s_n}{}' \exp\left(-\tilde{\beta} \sum_{i<j}^n s_i C_{x_i x_j} s_j\right)\,. \tag{2.77}$$

[5] Δ denotes the usual lattice Laplacian

Furthermore, we have introduced the abbreviations

$$\begin{aligned} \tilde{\beta} &= (2\pi)^2 \beta \\ K &= \frac{2\tilde{\beta}^2}{(2\pi)^2} \,. \end{aligned} \tag{2.78}$$

In the derivation of eqs. (2.76) and (2.77) we exploited the fact that for neutral charge configurations s,

$$\sum_{i,j}^{n} s_i \Gamma_{x_i x_j} s_j = 2 \sum_{i<j}^{n} s_i C_{x_i x_j} s_j \,, \tag{2.79}$$

and

$$\sum_{i}^{n} \Gamma_{o x_i} s_i = \sum_{i}^{n} C_{o x_i} s_i \,. \tag{2.80}$$

Eq. (2.75) is the Coulomb gas representation of the interface width. The gas is a neutral gas with integer charges ± 1. A lattice site can be occupied by more than one charge. The representation is in the grand canonical ensemble, and z obviously plays the role of the fugacity for the charges s_i. A small z means that the dominant contributions to the sum come from systems with only a few charges present (dilute Coulomb gas). Note that it follows from this representation that a finite fugacity always makes the interface width smaller, because only positive terms are subtracted from the $z = 0$ result.[6] Furthermore, together with eq. (2.61) it follows that β_{eff} is smaller than β.

We now determine the coefficients in the expansion

$$W^2 = \sum_{n \geq 0} \left(\frac{z}{2} \right)^n W_n^2 \,. \tag{2.81}$$

One finds

$$\begin{aligned} W_n^2 &= 0 \quad \text{for } n \text{ odd} \\ W_0^2 &= 2\beta \Gamma_{oo} \\ W_2^2 &= -K Z_2' \\ W_4^2 &= -K (Z_4' - Z_2' Z_2) \\ W_6^2 &= -K (Z_6' - Z_2' Z_4 - Z_2' Z_4 + Z_2' Z_2^2) \\ W_8^2 &= \ldots \end{aligned} \tag{2.82}$$

Let us explicitly write down Z_2', Z_2, and Z_4':

$$Z_2' = \sum_{x,y} \exp\left(\tilde{\beta} C_{xy} \right) (C_{ox} - C_{oy})^2$$

[6] We here assume that the infinite sum over n converges. This is probably the case in the rough phase

$$
\begin{aligned}
&= \sum_{x\neq 0} \exp\left(\tilde{\beta} C_{ox}\right) \sum_y (C_{o,x+y} - C_{o,y})^2 \\
Z_2 &= L^2 \sum_x \exp\left(\tilde{\beta} C_{ox}\right) . \qquad (2.83)
\end{aligned}
$$

Finally,

$$
\begin{aligned}
Z_4' &= \frac{1}{4} \sum_{x_1,x_2,x_3,x_4} \exp\left[-\tilde{\beta}\left(C_{x_1x_2} - C_{x_1x_3} - C_{x_1x_4} - C_{x_2x_3} - C_{x_2x_4} + C_{x_3x_4}\right)\right] \cdot \\
&\quad \cdot \left(C_{ox_1} + C_{ox_2} - C_{ox_3} - C_{ox_4}\right)^2 \qquad (2.84)
\end{aligned}
$$

Of course, using translational invariance of C, the expression for Z_4' can be transformed in a similar way as for $n = 2$.

2.2.2 Lines of Constant Roughness

In the rough phase the behavior of the 2-dimensional SG model at large distance is that of a Gaussian model ($z = 0$), but with an effective $\beta_{\text{eff}} < \beta$. For the interface width this means that in the limit $L \to \infty$,

$$
W^2 \to \frac{\beta_{\text{eff}}(z)}{\pi} \ln L + c' . \qquad (2.85)
$$

We define lines of constant roughness as the sets of points (z, β) that belong to the same β_{eff}. Constant roughness here means that the models lying on the same line have identical long distance behavior. In this section we will use the expansion of the interface width to second order in z to determine the lines of constant roughness. With eq. (2.83) and the observation that

$$
\sum_y (C_{o,x+y} - C_{o,y})^2 = -2 \frac{1}{N} \sum_{p\neq 0} \frac{\mathrm{e}^{ipx} - 1}{(\hat{p}^2)^2} \qquad (2.86)
$$

one arrives at

$$
W^2 = W_o^2 + z^2 \frac{\tilde{\beta}^2}{(2\pi)^2} \sum_{x\neq 0} \exp\left(\tilde{\beta} C_{ox}\right) \frac{1}{N} \sum_{p\neq 0} \frac{\mathrm{e}^{ipx} - 1}{(\hat{p}^2)^2} + O(z^4) . \qquad (2.87)
$$

The first observation is that the $O(z^2)$ term of the $z = 0$ interface width also behaves like $\ln L$ for large L. To show this, we interchange the order of summation,

$$
\sum_{x\neq 0} \exp\left(\tilde{\beta} C_{ox}\right) \frac{1}{N} \sum_{p\neq 0} \frac{\mathrm{e}^{ipx} - 1}{(\hat{p}^2)^2} = \frac{1}{N} \sum_{p\neq 0} \frac{1}{\hat{p}^2} \underbrace{\sum_{x\neq 0} \exp\left(\tilde{\beta} C_{ox}\right) \frac{\mathrm{e}^{ipx} - 1}{\hat{p}^2}}_{D_p} . \qquad (2.88)
$$

Note that $D_p = A + O(p^2)$, and A has an infinite volume limit:

$$\begin{aligned} A_\infty = \lim_{L\to\infty}\lim_{p\to 0} D_p &= -\tfrac{1}{2}\lim_{p\to 0}\sum_{x\neq 0}\exp\left(\tilde{\beta}C_{ox}\right)\frac{(px)^2}{\hat{p}^2} \\ &= -\tfrac{1}{4}\sum_{x\neq 0}\exp\left(\tilde{\beta}C_{ox}\right)\,x^2\,. \end{aligned} \tag{2.89}$$

The x-sum now runs over the infinite lattice. The $O(p^2)$-terms in D_p will lead to corrections of W_o^2 that remain finite in the infinite volume limit. The limit $p \to 0$ in eq. (2.89) is a bit subtle. Note that the limit of $(px)^2/\hat{p}^2$ alone strongly depends on the direction in that the limit is taken in the 2-dimensional p-space. However, the limit is to be performed under the sum over x. Now divide this sum into a sum over equivalence classes X of points x on which C_{ox} takes the same value (these points are actually connected by lattice symmetries). Sum $(px)^2/\hat{p}^2$ over $x \in X$ and then let $p \to 0$. Then the limit becomes independent of the direction in that the limit is taken, and one arrives at the result given in eq. (2.89).

The large L approximation is thus

$$W^2 \to W_o^2 + z^2\frac{\tilde{\beta}^2}{(2\pi)^2}\underbrace{\frac{1}{N}\sum_{p\neq 0}\frac{1}{\hat{p}^2}}_{\Gamma_{oo}}\,A_\infty + \text{ const } + O(z^4)\,. \tag{2.90}$$

We apply the approximation formula [146]

$$C_{ox} \simeq -\frac{1}{2\pi}\left(\ln|x| + \tfrac{3}{2}\ln 2 + \gamma\right)\,, \tag{2.91}$$

where $\gamma = 0.5772...$ denotes Euler's constant. The approximation for A_∞ then is

$$A_\infty \approx -\tfrac{1}{4}\exp\left[-2\pi\beta(\tfrac{3}{2}\ln 2 + \gamma)\right]\underbrace{\sum_{x\neq 0}|x|^{2-2\pi\beta}}_{E_2(\pi\beta-1)}\,. \tag{2.92}$$

E_2 denotes the Epstein-ζ-function [138],

$$E_2(s) = \sum_{x\neq 0}\frac{1}{(x_1^2+x_2^2)^s}\,. \tag{2.93}$$

Note that replacing the "true" Coulomb propagator by its approximation eq. (2.91) will change A_∞ by a small finite amount (the approximation of the propagator has errors that decay like $1/|x|$). However, A_∞ diverges for $\beta \to 2/\pi$. Since the divergence comes from the large x contributions, the finite errors from the small distances can be neglected in this limit which will be of importance later.

Recall that $W_o^2 = 2\beta\Gamma_{oo}$. Therefore

$$W^2 \to 2\Gamma_{oo}\left(\beta - z^2\,\tfrac{1}{8}(2\pi)^2\beta^2\exp\left[-2\pi\beta(\tfrac{3}{2}\ln 2+\gamma)\right]\,E_2(\pi\beta-1)\right) + \text{ const } + O(z^4)\,. \tag{2.94}$$

If we define a $\Delta\beta$ function through

$$\beta_{\text{eff}} = \beta - z^2 \Delta\beta(\beta) + O(z^4)\,, \tag{2.95}$$

we find

$$\Delta\beta(\beta) = \frac{1}{8}(2\pi)^2\beta^2 \exp\left[-2\pi\beta(\tfrac{3}{2}\ln 2 + \gamma)\right]\; E_2(\pi\beta - 1)\,. \tag{2.96}$$

Let us now introduce a new variable

$$x = \beta - \frac{2}{\pi}\,. \tag{2.97}$$

x measures the distance from the critical point at vanishing fugacity z. For $\Delta x(x)$ one obtains

$$\Delta x(x) = \frac{1}{8}(2\pi)^2 \left(\frac{2}{\pi} + x\right)^2 \exp\left(-2\pi\left(\frac{2}{\pi} + x\right)\left(\tfrac{3}{2}\ln 2 + \gamma\right)\right)\; E_2(1 + \pi x)\,. \tag{2.98}$$

We are now able to obtain the lines of constant roughness. They will be parameterized in the form $z(x, x_{\text{eff}})$, where $x_{\text{eff}} = \beta_{\text{eff}} - \frac{2}{\pi}$:

$$z(x, x_{\text{eff}}) = \left(\frac{x - x_{\text{eff}}}{\Delta x(x)}\right)^{1/2}\,. \tag{2.99}$$

In figure 2.2, we show the lines of constant roughness for $x_{\text{eff}} = 0.0 \ldots 0.09$. The case $x_{\text{eff}} = 0.0$ corresponds to the critical line.

For the numerical evaluation of $\Delta x(x)$ we used that [138] the Epstein ζ-function E_2 can be written as the product

$$E_2(s) = 4\zeta_R(s)\,\beta(s)\,, \tag{2.100}$$

where $\zeta_R(s)$ denotes the Riemann ζ-function,

$$\zeta_R(s) = \sum_{n=1}^{\infty} n^{-s}\,, \tag{2.101}$$

and [141]

$$\beta(s) = \sum_{n=0}^{\infty} (-1)^n\,(2n+1)^{-s} = \frac{1}{2\Gamma(s)} \int_0^\infty dt\, \frac{t^{s-1}}{\cosh(t)}\,. \tag{2.102}$$

Figure 2.2 looks like a part I of the flow diagram of Kosterlitz and Thouless, cp. figure 2.1. The strong similarity becomes more evident if we expand $z(x, x_{\text{eff}})$ around $x = 0$. Using the expansions

$$\zeta_R(s) = \frac{1}{s-1} + \gamma + O(s-1)\,, \tag{2.103}$$

and

$$\beta(s) = \frac{\pi}{4}\left(1 + \left(\gamma + \ln 2\pi + 2\ln\frac{\Gamma(3/4)}{\Gamma(1/4)}\right)\,(s-1)\right) + O\Big((s-1)^2\Big)\,, \tag{2.104}$$

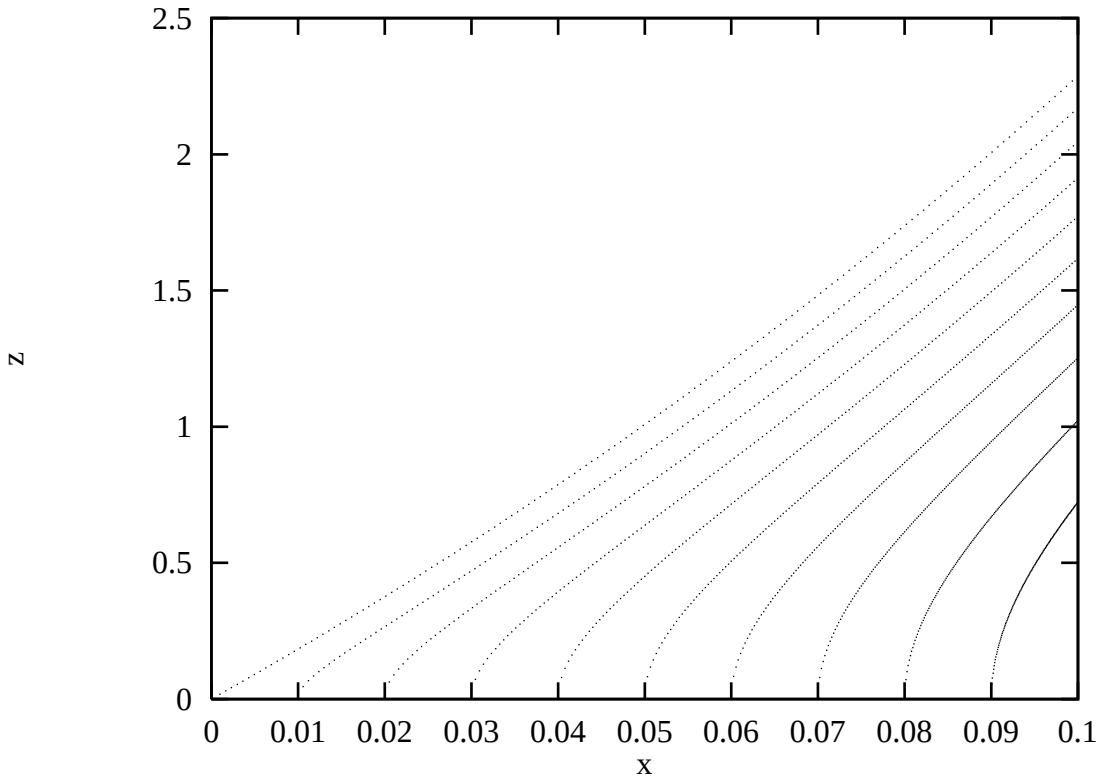

Figure 2.2: Lines of constant roughness in the rough phase of the 2-dimensional lattice Sine Gordon model for $x_{\text{eff}} = 0.0 \ldots 0.09$

we find

$$E_2(1+\pi x) = \frac{1}{x} + \kappa + O(x)\,, \tag{2.105}$$

with

$$\kappa = \pi\left(2\gamma + \ln 2\pi + 2\ln\frac{\Gamma(3/4)}{\Gamma(1/4)}\right) = 2.5849817\ldots\,. \tag{2.106}$$

If we plug in all our material, we find

$$z(x, x_{\rm eff}) = S\sqrt{x(x-x_{\rm eff})}\,\left(1+O(x)\right), \tag{2.107}$$

where $S = \exp((5/2)\ln 2 + 2\gamma) \approx 17.945$. The critical line in the vicinity of the fixed point $(z=0, x=0)$ is thus

$$z(x,0) = S\,x\left(1+O(x)\right). \tag{2.108}$$

For a comparison: The solutions of the KT equations in the rough phase are of the form

$$Y = \sqrt{E+X^2}\,, \tag{2.109}$$

with $E<0$. Y and X are proportional to the fugacity and to $\beta - 2/\pi$, respectively.[7] The case $E=0$ corresponds to the critical line.

2.2.3 Comparison of Perturbation Theory and Monte Carlo Results

Accuracy of the Perturbation Theory

We checked the accuracy of eq. (2.87) by a direct comparison with Monte Carlo results for the interface width obtained with the VMR cluster algorithm described in ref. [BB9].

In table 2.1 we compare the results at $\beta = 0.75$. For $z \le 1$ the deviations are fairly small. For $z = 1.5$ the relative error of the perturbative result is of order 1.5 per cent.

A similar statement is true for a set of β values that we chose to be close to the roughening point $\beta_c(z)$. Table 2.2 shows our results for the points $(z,\beta) = (0.5, 0.665)$, $(1.0, 0.700)$, and $(1.5, 0.720)$.

Table 2.3 shows the same comparison for two β values in the smooth phase. As is to be expected from the fact that W_0^2 and W_2^2 diverge logarithmically with L, the approximation fails completely for large L: the breaking of the symmetry under global integer shifts and the finiteness of W^2 for $L\to\infty$ are not reproduced by the perturbation theory.

[7] Note, however, that the corresponding constants are non-universal, i.e. dependent on the cutoff scheme. They can not be determined by a trivial computation

z	L	W^2_{MC}	W^2_{PT}
0.0	8	0.56751(75)	0.568942
0.0	16	0.73483(81)	0.734887
0.0	32	0.89919(92)	0.900489
0.0	64	1.06513(98)	1.065998
0.0	128	1.2324(11)	1.231483
0.0	256	1.3972(12)	1.396961
0.5	8	0.56602(78)	0.566367
0.5	16	0.73104(80)	0.731812
0.5	32	0.89795(92)	0.896745
0.5	64	1.05992(95)	1.061484
0.5	128	1.2264(10)	1.226138
0.5	256	1.3925(12)	1.390748
1.0	8	0.56079(85)	0.558644
1.0	16	0.72417(87)	0.722587
1.0	32	0.88976(92)	0.896745
1.0	64	1.05077(96)	1.061484
1.0	128	1.2148(11)	1.226138
1.0	256	1.3776(12)	1.372110
1.5	8	0.55412(86)	0.545772
1.5	16	0.71853(86)	0.707212
1.5	32	0.87879(92)	0.866793
1.5	64	1.04003(97)	1.025370
1.5	128	1.2015(11)	1.183376
1.5	256	1.3594(11)	1.341046

Table 2.1: Monte Carlo estimates for W^2 for different lattice sizes L and fugacities z. β is 0.75 always. The Monte Carlo (MC) results for the interface width squared can be compared with leading order perturbation theory (PT) given in the last column

z	β	L	$W^2_{\rm MC}$	$W^2_{\rm PT}$
0.5	0.665	8	0.49914(41)	0.498831
0.5	0.665	16	0.64426(39)	0.644232
0.5	0.665	32	0.78950(40)	0.788863
0.5	0.665	64	0.93364(39)	0.933018
1.0	0.700	8	0.51899(45)	0.514735
1.0	0.700	16	0.66990(42)	0.665522
1.0	0.700	32	0.81866(42)	0.814886
1.0	0.700	64	0.96894(42)	0.963367
1.5	0.720	8	0.52654(48)	0.515716
1.5	0.720	16	0.68148(44)	0.668146
1.5	0.720	32	0.83422(43)	0.818267
1.5	0.720	64	0.98679(43)	0.966976

Table 2.2: Monte Carlo estimates for the interface width close to $\beta_c(z)$, and comparison with perturbation theory

The Critical Line

We tried to determine $\beta_c(z)$ for $z = 0.5$, 1.0 and 1.5 using the *matching* method that we introduced in [BB7], cf. chapter 4. This method is based on a comparison of the blocked observables of the model in question with that of the BCSOS model. The BCSOS model is exactly solved and known to undergo a KT phase transition. The basic idea of our matching procedure is to simulate the BCSOS model at its known roughening temperature. One measures various block observables, e.g., the $A_{i,l}$ to be introduced below. One then searches for the critical coupling β_c and a scale transformation of the SOS model under consideration such that the blocked SOS observables match with that of the critical BCSOS model.

We measured a set of "block spin observables". To this end, the lattice was divided into four blocks x' of size $L/2 \times L/2$. Block spins $\phi_{x'}$ were then defined as the averages of φ over these blocks. We looked at[8]

$$A_{1,2} = \frac{1}{8} \sum_{<x',y'>} \left\langle (\phi_{x'} - \phi_{y'})^2 \right\rangle \ , \tag{2.110}$$

and

$$A_{3,2} = \frac{1}{4} \sum_{x'} \langle \cos(2\pi\phi_{x'}) \rangle \ . \tag{2.111}$$

It was demonstrated in ref. [BB7], that the matching with the BCSOS model can be performed by using just two block observables, e.g., $A_{1,2}$ and $A_{3,2}$. The matching conditions then fix β_c and the scale transformation. The matching of all the other block observables is then a consequence of universality and can be demonstrated.

[8]The notations are chosen to be consistent with the notations of ref. [BB7] and chapter 4.2

z	β	L	$W^2_{\rm MC}$	$W^2_{\rm PT}$
0.5	0.60	8	0.44624(69)	0.444773
0.5	0.60	16	0.57277(74)	0.572703
0.5	0.60	32	0.69975(84)	0.698515
0.5	0.60	64	0.82352(93)	0.822110
1.0	0.60	8	0.42250(83)	0.413632
1.0	0.60	16	0.53894(88)	0.527084
1.0	0.60	32	0.64558(98)	0.632884
1.0	0.60	64	0.7416(12)	0.730045
1.5	0.60	8	0.39822(90)	0.361730
1.5	0.60	16	0.50207(96)	0.451052
1.5	0.60	32	0.5862(12)	0.523500
1.5	0.60	64	0.6481(11)	0.576603
0.5	0.50	8	0.35450(67)	0.352331
0.5	0.50	16	0.44429(81)	0.438912
0.5	0.50	32	0.5167(10)	0.504380
0.5	0.50	64	0.5639(11)	0.531686
1.0	0.50	8	0.30370(83)	0.271438
1.0	0.50	16	0.35516(83)	0.285876
1.0	0.50	32	0.38203(71)	0.216543
1.0	0.50	64	0.38900(42)	-0.005254
1.5	0.50	8	0.25865(84)	0.136617
1.5	0.50	16	0.28566(66)	0.030816
1.5	0.50	32	0.29718(43)	-0.263186
1.5	0.50	64	0.29994(22)	-0.900152

Table 2.3: Monte Carlo estimates for the interface width in the smooth phase, and comparison with perturbation theory

z	$L=8$	$L=16$	$L=32$	$L=64$	$\beta_c(z)$
0.0					0.63662
0.5	0.6685(16)(12)	0.6709(13)(9)	0.6719(11)(8)	0.6683(18)(9)	0.670(2)
1.0	0.6989(13)(15)	0.6955(11)(13)	0.6984(9)(10)	0.6957(12)(8)	0.697(2)
1.5	0.7153(13)(16)	0.7137(10)(13)	0.7112(10)(10)	0.7105(12)(10)	0.711(2)
∞					0.7524(7)

Table 2.4: Estimates for the critical couplings $\beta_c(z)$ from matching of $A_{1,2}$ and $A_{3,2}$. β_c for $z=\infty$ is the roughening coupling for the DG model [BB7]

We tried to use the block BCSOS observables reported in [BB7] for a matching analysis of the SG model. We restricted ourselves to the quantities $A_{1,2}$ and $A_{3,2}$.

It turned out that the values of $A_{3,2}$ for the SG model close to the expected critical temperature are smaller than those of the BCSOS model on lattices of size up to $L=128$ [BB7]. Since $A_{3,2}$ vanishes like the inverse of the logarithm of the lattice size there is no hope to simulate the BCSOS model on lattices so large that the direct matching with the SG model at the z values under consideration can be performed.

From KT theory one expects that to leading order $A_{1,2}$ is a linear function of $A_{3,2}$. In figure 2.3 we plot for the BCSOS model the quantity $D_{1,2}$ as a function of $A_{3,2}$, where

$$D_{1,2}(L) = \frac{A_{1,2}(\infty)|_{z=0}}{A_{1,2}(L)|_{z=0}} A_{1,2}(L) \; . \tag{2.112}$$

In [BB7] we demonstrated that replacing $A_{1,2}$ by $D_{1,2}$ reduces finite lattice-spacing artefacts considerably. In addition to the BCSOS results the $z=0$ result is known. It is given by $A_{3,2}=0$ and $A_{1,2}=0.075425$. It seems that the linear interpolation between this $z=0$ point and the $L=128$ point of the BCSOS model is a reasonable approximation to the curve. On obtains $A_{1,2}=0.075425+0.034(2)A_{3,2}$. β_c is now computed from the condition that $A_{1,2}(\beta)$ and $A_{3,2}(\beta)$ are elements of the curve.

We simulated the SG model at β's close to the expected value for β_c on lattices up to $L=64$. We computed the values for the two observables in the neighborhood of this β using the reweighting technique [128]. Instead of $A_{1,2}$ itself we again considered $D_{1,2}$ in order to reduce finite lattice-spacing artefacts. The results for β_c stemming from different lattice sizes are summarized in table 2.4. We give two error bars. The first stems from the statistical error of the SG data itself, while the second is due to the error bar of the slope of the critical $A_{1,2}(A_{3,2})$ curve. Even the result from $L=8$ is consistent with the results from larger lattice sizes within the statistical errors.

From the exact result at $z=0$ and the estimate $\beta_c(0.5)=0.670(2)$ we derive a slope of the critical line of $S=14.98(0.9)$. This is obviously inconsistent with our estimate $S=17.945$ from the second order perturbation theory.

Beyond a three standard deviation statistical error there are two possible sources for a systematic error. First, the linear approximation of $A_{1,2}(A_{3,2})$ might be inadequate. Second, we

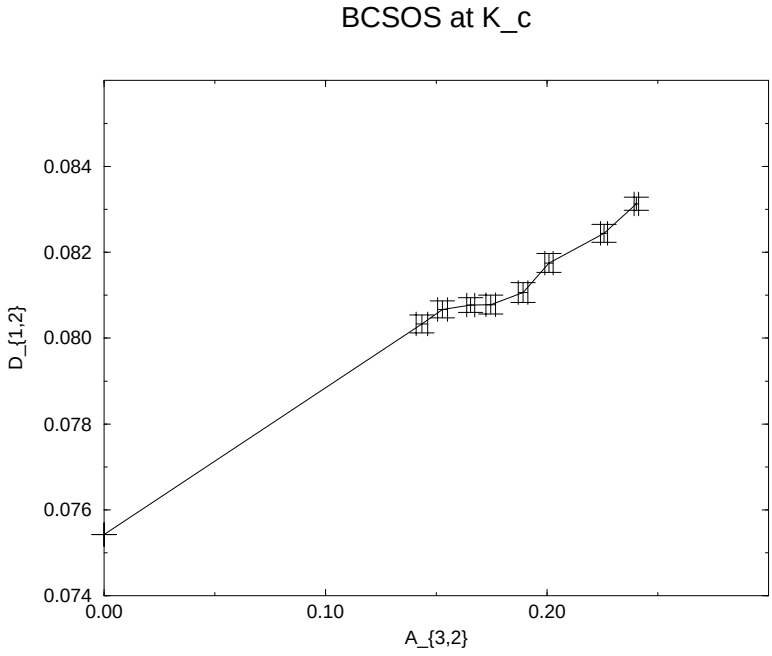

Figure 2.3: The quantity $D_{1,2}$ as a function of $A_{3,2}$ for the BCSOS model at criticality. The data are taken from ref. [BB7]

were not able to check whether higher orders in z of the interface width expansion can modify the slope of the critical curve. Such a modification would happen if the analogue of A_∞ at order z^n would diverge like $1/x^{n-1}$ for $x \to 0$.

Chapter 3

Monte Carlo Studies of the Solid-On-Solid Interfacial Width

3.1 The Solid-On-Solid Interface Width in the Rough Phase

A study is presented of the lattice size dependence of the Discrete Gaussian model interface width in the rough phase. This section is based on ref. [BB2].

We choose to work with the Discrete Gaussian model, cf. chapter 1. To each site x of a two-dimensional $L \times L$ square lattice with periodic boundary conditions we assign an integer valued spin h_x, which can be viewed as the height of a surface (interface) without overhangs. The partition function is

$$Z = \sum_{\{h\}} \exp\left\{ -\frac{1}{2T} \sum_{\langle x,y \rangle} (h_x - h_y)^2 \right\} . \tag{3.1}$$

T is the temperature (Boltzmann's constant is set to one). Note that we have defined

$$T = \frac{1}{2K_{DG}} , \tag{3.2}$$

where K_{DG} is the coupling constant of the Discrete Gaussian model introduced in chapter 1.

The square of the average interface width W on a finite lattice is defined by

$$W^2 = \frac{1}{L^2} \sum_x < (h_x - h_y)^2 >= 2 < (h_y - \overline{h})^2 > . \tag{3.3}$$

Here $\overline{h}$ is the average over the lattice of the h_x.

It follows from standard convergent expansion techniques that at low temperatures the SOS interface is smooth, i.e. the interface width W is finite. As the temperature T is increased, the interface fluctuates more and more. At high temperatures the discreteness of the spins is

L	8	16	32	64	128	256
W^2	0.75471(36)	0.97523(36)	1.19415(34)	1.41442(32)	1.63364(39)	1.85396(42)

Table 3.1: The squared interface width for the Discrete Gaussian model at $T = 1$

hardly felt. The interface width is infinite in the thermodynamic limit, i.e. the interface becomes rough. The large distance behavior is that of the massless free field theory (the model defined in eq. (3.1) with real instead of integer spins) [1, 2, 99]. In particular, we have the prediction

$$W^2 = \frac{T_{\rm eff}}{\pi} \left(\ln L + \text{const} \right) \ , \tag{3.4}$$

with the constant $T_{\rm eff}$ ("effective temperature") defined such that in the free field theory $T = T_{\rm eff}$.

Although for very high temperatures T the behavior of eq. (3.4) was proven in [99], doubts were repeatedly raised in the literature as to its validity for moderately high temperatures [35].

The phase transition, which is of the Kosterlitz-Thouless type, is located at $T_R = 0.7524(7)$ [BB7], see chapter 4. In [73], the value $T_R = 0.752(5)$ is estimated from a Monte Carlo simulation analysis of the XY model with Villain Hamiltonian (the dual of the Discrete Gaussian model).

We chose to perform our simulations at $T = 1$, which is not a very high temperature, but already far enough from T_R to expect only small deviations from eq. (3.4) (if the theoretical prediction is correct).

Let us give some technical details of these simulations. We considered lattice sizes $L =$ 8, 16, 32, 64, 128, and 256. For each lattice size we performed a total of between 3.5 and 4 million cluster updates. Each cluster was grown around a randomly chosen seed, according to the procedure which was found in [BB1] to have no critical slowing down at all. The average cluster size was between 0.3 and 0.4 of the lattice volume. We used a method for vectorizing the cluster update [133], which on a CRAY YMP resulted in a speed-up factor of around three. With vectorization, even a lattice of $L = 512$ is accessible, but the results up to $L = 256$ show that we do not really need it.

Table 3.1 presents our values for the interface thickness. Eq. (3.4) fits all data perfectly. Using only the values of W^2 for $L \geq 32$ we obtained $T_{\rm eff} = 0.9965(8)$. It is important to notice that the relation $T_{\rm eff} < T$ is true, as predicted by the flow diagram of the Kosterlitz-Thouless theory.

Eq. (3.4) is a finite volume continuum approximation for the r.h.s. of eq. (3.3). In order to minimize finite lattice spacing effects, we should compare the simulation results with the free field theory values of W^2 obtained on the same lattice as the Discrete Gaussian model, but at $T = T_{\rm eff}$. In this case the r.h.s. is a simple lattice sum that can be evaluated numerically with arbitrary precision. We checked however that for $L \geq 16$ the difference between these values and the continuum approximation eq. (3.4) is much smaller than the statistical errors of the Discrete Gaussian data. For $L = 8$ a difference can be seen; taking $L \geq 32$ for the result quoted in the last paragraph is thus very safe.

The data are very precise, so we hoped to exclude with a high degree of confidence certain types of behavior different from eq. (3.4). And indeed, the various least square fits we are going to discuss now all indicate that the data strongly favorize the linear dependence on $\ln L$.

We first tried a power fit, since quite often a logarithmic dependence looks very similar to a power law with a small exponent. The fits with

$$W^2 = c_1 L^a + c_2 \tag{3.5}$$

were not very stable, with the constants c_1 and c_2 having a tendency to grow very much. However, a reasonably small value for χ^2 per degree of freedom could only be obtained with very small values of a (≤ 0.001). Thus the power law eq. (3.5) is excluded.

An ansatz sometimes discussed in the literature [35] is the power-of-log form

$$W^2 = \frac{c_1}{\pi} (\ln L)^{1+b} + c_2 \ . \tag{3.6}$$

Fits with this form go rather well through all data. For $L \geq 32$ the fit results in $|b| < 0.009$, with $c_1 = 1.00(2)$ being consistent with the value we determined for $T_{\rm eff}$ using eq. (3.4). Thus a linear dependence on $\ln L$ is favored.

Next we tried to see if log-log corrections may play a role. We fitted the data with

$$W^2 = \frac{c_1}{\pi} \ln L + c_2 \ln \ln L + c_3 \ , \tag{3.7}$$

and the fits were good for all L-ranges. For $L \geq 32$ we got $c_2 = 0.01(5)$ and $c_1 = 0.994(11)$. Thus the absence of log-log corrections is favored.

Finally we fitted the data with

$$W^2 = \frac{T_{\rm eff}}{\pi} \ln L + \frac{1}{\pi^2} \ln(c_1 - L^{4-2\pi T_{\rm eff}}) + c_2 \ . \tag{3.8}$$

This is the renormalization group improvement of eq. (3.4) [BB5], see also section 3.2 below. For large enough L the difference between eqs. (3.8) and (3.4) is negligible. Close to but still above T_R we found this form to fit simulation results over a much wider L-range than eq. (3.4). Here, at $T = 1$, there was practically no difference between the fits with eq. (3.8) and with eq. (3.4). In particular, the fitted values for $T_{\rm eff}$ were almost identical in the two cases. Thus we have established that at $T = 1$ the asymptotic regime (large L) is reached very quickly. We conclude that we have confirmed the validity of eq. (3.4) with a high degree of accuracy.

3.2 The Interface Width Around the Roughening Transition

In this section, we investigate the interface width W of solid-on-solid interfaces in the vicinity of the roughening temperature T_R. Above T_R, W^2 diverges with the system size L like $\ln L$ [BB2], see section 3.1. However, close to T_R a clean $\ln L$ behavior can only be seen on extremely large lattices. Starting from the Kosterlitz-Thouless renormalization group, we derive an improved

formula that describes the small L behavior on both sides of T_R. For the Discrete Gaussian model, we used the valleys-to-mountains-reflections cluster algorithm in order to simulate the fluctuating solid-on-solid interface. In the simulation we took $8 \leq L \leq 256$. The improved formula fits the numerical results very well. From the analysis, we estimate the roughening temperature to be $T_R = 0.755(3)$. This section is based on ref. [BB5].

We stay with the Discrete Gaussian model. The model has two phases. At low temperatures the interface is smooth, and W stays finite as $L \to \infty$. When T is increased, we encounter the roughening transition at $T = T_R$. The KT theory predicts (see, e.g., [7]) that in the thermodynamic limit

$$W^2 \sim (T_R - T)^{-\frac{1}{2}} \sim \ln \xi \tag{3.9}$$

as T approaches T_R from below (ξ is the correlation length). For $T \geq T_R$, W diverges as $L \to \infty$. The prediction for asymptotically large L is the "free field" behavior (i.e. Continuous Gaussian – h_i is real instead of integer)

$$W^2 = \frac{T_{\text{eff}}}{\pi} \ln L + \text{const}\,. \tag{3.10}$$

T_{eff} is called the "effective temperature", and

$$T_{\text{eff}} = \frac{2}{\pi} \quad \text{for} \quad T = T_R\,. \tag{3.11}$$

Furthermore, as T approaches T_R from above,

$$T_{\text{eff}} - \frac{2}{\pi} \sim (T - T_R)^{\frac{1}{2}}\,. \tag{3.12}$$

In principle, these formulas could be used in a numerical study in order to verify or disprove the KT theory. In practice however this is problematic. In the smooth phase, we would need unrealistically large lattices in order to test the power law eq. (3.9). This problem is related to the difficulties encountered in the study of the dual (Villain, XY) spin models, where it is hard to cleanly distinguish an essential singularity in the correlation length ξ (as predicted by KT) from a power law singularity [73, 76]. In the rough phase, for large enough temperatures, the behavior eq. (3.10) could be unambiguously verified numerically [BB2], see also section 3.1 above.

However, it turns out that close to T_R a clean logarithm is only seen on very large lattices, and in order to extract the values of T_{eff} in practice we need to know the corrections to eq. (3.10). Otherwise we cannot determine T_R by checking eq. (3.11). Furthermore, for the largest lattice sizes accessible with present day computers and algorithms, it turns out that eq. (3.12) is not yet fulfilled for the region where eq. (3.10) holds. Actually, the status of eq. (3.12) is even worse, as will be argued later.

In order to overcome these problems, we developed a renormalization group (RG) improved formula for the dependence of W^2 on L. This is our main theoretical result. The numerical part of our work shows that the improved formula can be used for extracting T_{eff} as close as desired

to T_R, from numerical simulations on reasonably sized lattices. We mention that very high accuracy simulations were possible because we have a cluster algorithm that is free of critical slowing down (the valleys-to-mountains-reflections algorithm [BB1]). Vectorization [133] also helped. From our analysis, the best estimate for the roughening temperature is $T_R = 0.755(3)$.

In what follows, we first derive our improved formula, then present the analysis of the numerical results, and finally make some additional remarks and present our conclusions.

3.2.1 Renormalization Group Improved Finite L Formula

The RG flow of the SOS models can be described in an $x - y$ diagram, cf. chapter 2. The trajectories are parametrized by t, the logarithm of the changing length scale. $x(t)$ is related to the scale dependent ("running") temperature $T(t)$, $x(t) = \pi T(t) - 2$, while $y(t)$ is a constant times the fugacity. The KT flow equations are:

$$\begin{aligned} \dot{y}(t) &= -x(t)\, y(t) \\ \dot{x}(t) &= -y(t)^2 \,. \end{aligned} \tag{3.13}$$

The trajectories are hyperbolas, characterized by the constant E which depends on the temperature T of the model (not on the running $T(t)$!):

$$y(t)^2 - x(t)^2 = E \,. \tag{3.14}$$

Denoting $\epsilon = \mathrm{sign}(E)\sqrt{|E|}$, and $x_0 = x(0)$, the full solution of eq. (3.13) is:

$$\begin{aligned} E < 0: \quad & x(t) = \epsilon \left(1 + \frac{2\,(x_0 - \epsilon)}{(x_0 + \epsilon)\exp(2\epsilon\, t) - (x_0 - \epsilon)} \right) \\ E = 0: \quad & x(t) = \frac{x_0}{1 + x_0 t} \\ E > 0: \quad & x(t) = \epsilon\, \frac{x_0 - \epsilon \tan(\epsilon\, t)}{\epsilon + x_0 \tan(\epsilon\, t)} \,. \end{aligned} \tag{3.15}$$

The trajectories in the rough phase reach the free field theory, and have $\epsilon < 0$; in the smooth phase they have $\epsilon > 0$; at the KT transition the critical trajectory has $\epsilon = 0$, cf. chapter 2. Notice that in the rough phase $T_{\mathrm{eff}} = T(t = \infty) = (2 - \epsilon)/\pi$.

In order to use the RG for computing the interface width, we need to know the contributions corresponding to each length scale. Eq. (3.3) shows that W^2 is a sum of a two-point-function over all distances. When increasing the lattice size L, we get additional additive contributions from distances of order L. Let us choose

$$t = \ln \frac{L}{L_0} \,, \tag{3.16}$$

with L_0 some reference length scale, and let us approximate the sum in eq. (3.3) by an integral. For the free field theory, the additional contributions to W^2 coming from an infinitesimal change

in L are easily computed: since eq. (3.10) is always true, with $T_{\rm eff}$ replaced by the temperature T, we have $\mathrm{d}W^2/\mathrm{d}t = T/\pi$. In the case of the Discrete Gaussian model, the KT flow shows that for trajectories in the rough phase we are close to the free field theory if t is large enough. Moreover, we are also close to the free field theory for trajectories in the smooth phase, provided that L is much smaller than ξ but still large enough. Thus the main contribution to $\mathrm{d}W^2/\mathrm{d}t$ will be similar to the free field case, the only (important) difference being that we replace T by the running temperature $T(t)$:

$$\frac{\mathrm{d}W^2}{\mathrm{d}t} = \frac{T(t)}{\pi}\,. \tag{3.17}$$

Assuming that $T(t)$ behaves according to the KT flow for length scales larger than L_0, we can integrate eq. (3.17):

$$W^2 = \frac{1}{\pi^2}\int_0^t [x(t)+2]\,\mathrm{d}t \;+\; C\,. \tag{3.18}$$

The constant C contains the contributions of distances smaller than L_0. Using eq. (3.13) and eq. (3.14), we can express $\mathrm{d}t$ in terms of x and $\mathrm{d}x$, after which eq. (3.18) reduces to an elementary integral. We thus obtain our final formula for W^2:

$$W^2 = \frac{2}{\pi^2}t + \frac{1}{2\pi^2}\ln\left(\frac{x_0^2+E}{x^2+E}\right) + C\,, \tag{3.19}$$

which has to be used in conjunction with eqs. (3.15) and (3.16).

The crucial point in the derivation of our improved formula was the replacement, at the appropriate stage, of the temperature T with the running temperature $T(t)$. While this is a commonly used procedure in field theoretical RG arguments, it is not completely rigorous.

3.2.2 Simulation Results

We performed simulations of the Discrete Gaussian model for ten different values of the temperature T. At each T we considered lattice sizes of $L = 8$, 16, 32, 64, 128 and 256. Typically, we generated about 2 000 000 to 2 500 000 clusters for each temperature and lattice size. The expectation value of the cluster size varied in the range $0.3L^2$ to $0.35L^2$. The whole project required about 400 hours on one CRAY Y-MP processor. As will become clear from the analysis, we did not need more than half of our runs in order to obtain the best estimate for T_R. However, our aim was also to confirm our prediction for the L-dependence of W^2 and to determine the region in which the improved formula is really necessary. The simulation results for W^2 are given in table 3.2.

As a general rule, these data are extremely well fitted by eq. (3.19), with fit parameters ϵ, x_0 and C. Aside from the occasional statistical fluctuation, we did however notice that for $T \leq 0.755$ the quality of the fits deteriorated a little. The important results of such fits are the value of ϵ, which characterizes the trajectory, and the range of L for which the fits are good, which roughly tells us where the model enters the KT flow. Notice that we have to decide upon a value for L_0. The choice of L_0 only affects the values x_0 and C, as can be seen after a little

algebra. Table 3.3 contains the fit results for ϵ, for all our values of T and for various fit ranges. Clearly, for $T \geq 0.76$ the various fit ranges give compatible results. In fact the data for $L = 256$ hardly improve things here. For $T \leq 0.755$ however, the fit results for ϵ sometimes change by more than two standard deviations if we remove the data for $L = 8$. It may be that for these temperatures the KT flow is well reached only above $L = 8$.

From table 3.3 our first main numerical result strikes the eye: since $\epsilon > 0$ for $T \leq 0.75$ and $\epsilon < 0$ for $T \geq 0.76$, T_R is between 0.75 and 0.76. This result relies solely on the fact that eq. (3.19) fits the data well, and on eq. (3.11).

In order to give a more precise determination of T_R, we plotted for each fit range ϵ versus T, with error bars, and interpolated the two curves $\epsilon +$ error and $\epsilon -$ error. The intersection of the band thus obtained with the $\epsilon = 0$ line provides an estimate of T_R. In table 3.4 we collected these range-dependent estimates. They are quite consistent with one another. Thus, taking into account the above observations about the quality of the fits for $T \leq 0.755$, it would not be unreasonable to quote as our final result the value of T_R for the L-range $16 - 256$.

For a more conservative estimate of T_R we plotted the values of ϵ from the ranges $8 - 256$ and $16 - 256$, together with their error bars, on the same plot. We interpolated the upper and lower envelopes of the error bars. From the intersection of the band thus obtained with the $\epsilon = 0$ line we get the estimate $T_R = 0.755(3)$. Notice that the best estimate in the literature [BB7], $T_R = 0.7524(7)$, was obtained by a completely different method (matching with the critical block spin flow of the BCSOS model), that does not test directly any of the formulas derived from the KT theory. The best estimate by other authors [73], $T_R = 0.752(5)$ (from the analysis of the correlation length and susceptibility in the massive phase of the Villain model), is also consistent with the result presented here.

At the beginning of subsection 3.2.1 we explicitly wrote down the t dependence of the running temperature $T(t)$. With the numerically determined fit parameters ϵ and x_0, we can thus compute the flow of $T(t)$ numerically. If we use $x(t)$ instead of $T(t)$, we can neatly plot the points $(x(t), y(t))$ inside the standard KT flow diagram. We can now do the following consistency check. The differences $\pi \Delta W^2/\Delta t = (\pi/\ln 2)\,[W^2(2L) - W^2(L)]$, shown in table 3.5, should be discrete approximants of $T(t)$, by eqs. (3.16) and (3.17). Thus if we again plot the values of the points $(x(t), y(t))$, this time using the discrete approximation, we expect to obtain a similar diagram. We did this exercise, and indeed the two diagrams were almost identical.

In the last column of table 3.5 we show the values of $T_{\text{eff}} = (2 - \epsilon)/\pi$, obtained by again taking for each $T > T_R$ the envelope of the error bars from the fits with L-ranges $8 - 256$ and $16 - 256$. Above T_R, if L is large enough for eq. (3.10) to hold, the running temperature stabilizes to the value T_{eff}. By looking at how the the results in the rows of table 3.5 stabilize, we see that our data for W^2 enter the asymptotic regime of eq. (3.10) for $0.8 \leq T \leq 0.85$ clearly, and for $T = 0.78$ just barely. For $T_R \leq 0.77$ however, this is far from being true, even at $L = 256$. Notice that in order to understand the validity region of eq. (3.10) we did need the values of W^2 for $L = 256$. More importantly, notice that our results show that the use of eqs. (3.10) and (3.11) for determining T_R (like e.g. in [49, 52]) leads to a consistent underestimate.

In order to test eq. (3.12), we fitted the values for T_{eff} from table 3.5. The fit was not at all good. We then allowed for a free power instead of the power $\frac{1}{2}$. The fit was now good, but

T	$L=8$	$L=16$	$L=32$	$L=64$	$L=128$	$L=256$
0.740	0.51429(34)	0.66739(33)	0.81589(32)	0.96185(33)	1.10558(34)	1.24908(39)
0.745	0.51984(37)	0.67560(34)	0.82571(32)	0.97408(33)	1.12248(33)	1.26710(40)
0.750	0.52537(37)	0.68222(35)	0.83542(35)	0.98661(34)	1.13615(35)	1.28461(36)
0.755	0.53137(30)	0.69052(34)	0.84475(33)	0.99877(33)	1.15066(34)	1.30165(38)
0.760	0.53733(37)	0.69725(34)	0.85444(33)	1.00956(29)	1.16440(28)	1.31721(39)
0.770	0.54900(35)	0.71185(32)	0.87292(33)	1.03164(36)	1.18993(34)	1.34726(37)
0.780	0.55902(36)	0.72606(34)	0.88941(33)	1.05190(38)	1.21432(36)	1.37515(40)
0.800	0.58006(38)	0.75240(34)	0.92271(35)	1.09176(40)	1.26032(37)	1.42846(40)
0.820	0.59963(37)	0.77776(34)	0.95355(34)	1.12807(36)	1.30248(38)	1.47770(42)
0.850	0.62762(37)	0.81304(37)	0.99679(36)	1.18076(38)	1.36315(40)	1.54571(43)

Table 3.2: Simulation results for W^2

T	$8-256$	$16-256$	$32-256$	$8-128$	$16-128$
0.740	0.204(06)	0.178(10)	0.151(23)	0.226(08)	0.206(16)
0.745	0.171(07)	0.139(14)	0.165(21)	0.168(11)	0.060(57)
0.750	0.126(09)	0.109(17)	0.103(35)	0.137(14)	0.117(30)
0.755	0.030(38)	-0.078(25)	0.059(60)	0.054(33)	-0.102(33)
0.760	-0.124(10)	-0.130(14)	-0.128(27)	-0.131(13)	-0.151(21)
0.770	-0.211(06)	-0.210(09)	-0.221(17)	-0.211(09)	-0.205(17)
0.780	-0.277(05)	-0.287(07)	-0.278(14)	-0.278(07)	-0.300(12)
0.800	-0.387(04)	-0.387(06)	-0.388(11)	-0.386(06)	-0.387(10)
0.820	-0.478(03)	-0.484(05)	-0.494(09)	-0.471(05)	-0.474(09)
0.850	-0.601(03)	-0.599(04)	-0.590(08)	-0.603(04)	-0.601(07)

Table 3.3: Fit results for the parameter ϵ. The first row contains the L-range

fit range	$8-256$	$16-256$	$32-256$	$8-128$	$16-128$
estimated T_R	0.7555(25)	0.7535(15)	0.7550(30)	0.7555(25)	0.7515(55)

Table 3.4: T_R from the interpolated curves $\epsilon(T)$

T	$8-16$	$16-32$	$32-64$	$64-128$	$128-256$	T_{eff}
0.740	0.6939(21)	0.6731(21)	0.6615(21)	0.6514(22)	0.6504(24)	$T < T_R$
0.745	0.7059(23)	0.6804(21)	0.6724(21)	0.6726(21)	0.6555(23)	$T < T_R$
0.750	0.7109(23)	0.6944(22)	0.6852(22)	0.6778(22)	0.6729(23)	$T < T_R$
0.755	0.7213(21)	0.6990(22)	0.6981(21)	0.6884(21)	0.6843(23)	$T \approx T_R$
0.760	0.7248(23)	0.7124(21)	0.7031(20)	0.7018(18)	0.6926(22)	0.6777(48)
0.770	0.7381(21)	0.7300(21)	0.7194(22)	0.7174(22)	0.7131(23)	0.7035(29)
0.780	0.7571(22)	0.7404(22)	0.7365(23)	0.7361(24)	0.7290(24)	0.7267(35)
0.800	0.7811(23)	0.7719(22)	0.7662(24)	0.7640(25)	0.7620(25)	0.7598(19)
0.820	0.8074(23)	0.7967(22)	0.7910(22)	0.7905(24)	0.7942(26)	0.7900(22)
0.850	0.8404(24)	0.8328(23)	0.8338(24)	0.8267(25)	0.8274(27)	0.8273(16)

Table 3.5: The differences $\pi\,\Delta W^2/\Delta t$ compared to T_{eff}

the power was 0.60(4). Disregarding the point farthest away from T_R, $T = 0.85$, the situation did not improve: the power changed to 0.62(7). The fitted value for T_R was 0.753(2) with the point $T = 0.85$ included, and 0.752(4) without it. While these values for T_R are reasonable, the fact remains that the power $\frac{1}{2}$ is not yet seen even as close to T_R as our data in the rough phase are. Notice that this conclusion implies in particular that we cannot use eq. (3.12) in order to fit results in a region where the simple behavior eq. (3.10) applies on lattices of still manageable size.

As a last issue, let us remark that in the absence of a theory, one may be simply tempted to make some "reasonable" ansatz for the corrections to eq. (3.10). We tried to fit the data with a $\ln\ln L$ correction (the coefficient in front of $\ln\ln L$ is the third fit parameter besides T_{eff} and the constant). The fits were as good as those with eq. (3.19), if not better. However, the values of T_{eff} thus obtained were clearly wrong. It is not difficult to understand the numerics behind this phenomenon. The main point is, however, to view this as another example of the danger of analyzing simulation results without a solid theoretical basis.

Along the same lines, let us remark that we found a different modification of eq. (3.10) to also fit the data very well: instead of taking $\ln L$ we took a power of $\ln L$ (this power is the third fit parameter). The power that allowed for good fits very close to T_R never deviated from the value 1 by more than 10%. Nevertheless, the fitted values for T_{eff} were again clearly wrong with this procedure.

Let us summarize: We have derived a renormalization group improved formula for the finite size behavior of the SOS interface width in the vicinity of the roughening transition. The improved formula was tested in a high accuracy simulation of the Discrete Gaussian model, and found to describe the data excellently. As a result of our analysis, we verified an important aspect of the KT scenario; gave a precise determination of T_R; found the region in which eq. (3.10) cannot be used unless we consider much larger lattice sizes; found that the region of applicability of eq. (3.12) is much smaller than previously assumed.

Chapter 4

Renormalization Group Study of the SOS Roughening Transition

The KT scenario of the roughening transition is confirmed for the Discrete Gaussian (DG) model, the Absolute-Value-SOS (ASOS) model, and the dual transform of the XY model with standard (cosine) action.[1] *The method is based on a matching of the renormalization group flow of the candidate models with the flow of a bona fide Kosterlitz-Thouless model, the exactly solvable BCSOS model. The Monte Carlo simulations are performed using the VMR cluster algorithms described in [BB1, BB3]. Precise estimates for the critical couplings and other non-universal quantities are obtained. This chapter is based on ref. [BB7]. Part of that work is contained in [37].*

For nearly all of the SOS models there is no rigorous proof that their phase transition is really of the Kosterlitz-Thouless type. For rigorous work on the existence of a phase transition from a massive to a massless phase, see [99]. See also [149], where the KT nature of the transition is put into question, and [150].

In order to confirm or reject the KT nature of the roughening transition (or the corresponding transition in the dual spin models, e.g. the XY model), many Monte Carlo simulations were performed.

For Monte Carlo studies of SOS models, see, e.g., [47, 48, 49, 50, 51].

Many Monte Carlo simulations were done to investigate the phase transition for the XY model with cosine or Villain action, see [53]–[76].

Most of the Monte Carlo studies of KT candidate models are based on a direct computation of critical quantities such as the correlation length or the susceptibility.

By fitting the data with different ansätze one tries to rule out the power law singularities of conventional phase transitions. However, it turns out to be very demanding to get data for sufficiently large correlation lengths with good statistics. Only the results of the more recent simulations using cluster algorithms really favour a KT transition against a second-order phase

[1] These models were defined in chapter 1

transition, while the estimate for the transition temperature still has a relative error of order 1 per cent [71, 73].

There have also been attempts to study the KT scenario with the help of the Monte Carlo Renormalization Group (MCRG). See, e.g., [72].

In this chapter, a new method is presented to attack the problem. The method is based on the fact that one of the SOS models, the BCSOS model, can be solved exactly [100, 96, 97]. The BCSOS model has been *proved* to exhibit a KT transition. The critical coupling is exactly known. In addition, the correlation length and other quantities can be computed exactly [100], cf. chapter 1. For a detailed analysis of the BCSOS model with respect to roughening and surface structure, see [158, 16, 159].

It was proposed long ago to improve the numerical study of SOS models by a comparison with BCSOS results [49]. In this report we give this comparison a precise meaning in the framework of the renormalization group (RG). We verify the Kosterlitz Thouless scenario for several models - the ASOS model, the Discrete Gaussian (DG) model and the dual transform of the XY model with cosine action - by demonstrating that their long-distance RG flow at the critical point precisely matches with the flow of the critical BCSOS model. Stated differently, we demonstrate that the candidate models are in the same universality class (in the sense of Wilson's renormalization group [86]) as the BCSOS model.

The matching is demonstrated by comparing Monte Carlo data for expectation values of "blocked correlation functions". All data are generated using VMR cluster Monte Carlo algorithms that do not suffer from critical slowing down or have strongly reduced critical slowing down [BB1, BB3].

Our RG comparison is designed in such a way that finite-size effects are exactly cancelled. By simulations on reasonably small lattices we obtain results for the critical couplings, which are competitive in precision with estimates from much more expensive Monte Carlo studies. We also get estimates for the non-universal constants determining the asymptotic behavior of the correlation length.

The perhaps most important result of our study is, however, the demonstration that the models (with a high level of confidence) are in the same universality class as the BCSOS model. We consider this as an unambiguous confirmation that their phase transition is of the KT type.

4.1 Finite Lattice Renormalization Group

Universal properties of a statistical system do not depend on short distance details, but only on the nature of long wavelength fluctuations. This suggests to remove the irrelevant high frequency degrees of freedom by applying a coarse graining (block spin) procedure [86].

Universality, which was first introduced as the coincidence of the critical indices of various models, can be expressed as a convergence of the renormalization group flow to a universal flow as $T \to T_R$ and the number of block spin transformations goes to infinity. Here we use T as a representative for any coupling that is driven to a critical value in order to make the correlation length diverge and the system become critical.

Consider two models with different microscopic Hamiltonians that belong to the same universality class, i.e. that have the same critical indices. The above statement says that if the two models are both at criticality then their effective Hamiltonians will converge towards the same fixed point Hamiltonian. It might even happen that the two flows of Hamiltonians will come close to each other already a long time before they are really close to the fixed point. (We shall actually observe this phenomenon for the models studied in this chapter.) Note, however, that the two systems might need a different number of RG steps to reach a certain point on the universal trajectory.

It is suggestive to compare renormalization group flows in order to test for universality properties. To directly compare effective Hamiltonians, one would have to parametrize them in terms of coupling constants. However, there are infinitely many couplings already after a single renormalization group step. It turns out to be very difficult to determine the coupling constants of the blocked system by analytical calculations [88] or Monte Carlo simulations (MCRG) [89].

We shall deal with the problem in a similar fashion as Shenker and Tobochnik [90] did for the 2-dimensional O(3) model and Wilson [91] for the 4-dimensional SU(2) gauge model. As an example, let us assume that we deal with a model for real random variables (spins) φ_x, defined on a lattice Λ. Let the Hamiltonian be $\mathcal{H}(\varphi)$, and the partition function

$$Z = \int \prod_{x \in \Lambda} d\varphi_x \exp(-\mathcal{H}(\varphi)) \,. \tag{4.1}$$

We define effective Hamiltonians for *finite* lattices Λ that consist of $l \times l$ blocks, where each of the blocks contains $B \times B$ sites. The effective Hamiltonian $\mathcal{H}_{\text{eff}}^{(l,B)}$ defined through

$$\exp(-\mathcal{H}_{\text{eff}}^{(l,B)}(\phi)) = \int \prod_{x \in \Lambda} d\varphi_x \exp(-\mathcal{H}(\varphi)) \prod_{x' \in \Lambda'} \delta \left(\phi_{x'} - B^{-2} \sum_{x \in x'} \varphi_x \right) \tag{4.2}$$

is a function of l^2 block spin variables $\phi_{x'}$. A renormalization group flow is now defined as the sequence of effective Hamiltonians $\mathcal{H}_{\text{eff}}^{(l,B)}$, for fixed l and increasing B. Note that different l's lead to different flows.

In order to monitor the flow of the $\mathcal{H}_{\text{eff}}^{(l,B)}$, we do not necessarily have to compute the still infinitely many couplings in $\mathcal{H}_{\text{eff}}^{(l,B)}$. We can instead consider a set of suitably chosen observables,

$$E_i^{(l,B)} \equiv \langle A_i(\phi) \rangle_{l,B} = Z^{-1} \int D\phi \, \exp(-\mathcal{H}_{\text{eff}}^{(l,B)}) \, A_i(\phi) \,. \tag{4.3}$$

A convergence of the flow of effective Hamiltonians $\mathcal{H}_{\text{eff}}^{(l,B)}$ towards a fixed point will imply also the convergence of the flows of the $E_i^{(l,B)}$. The crucial point is that the $E_i^{(l,B)}$ can be expressed as expectation values in the original system with Hamiltonian $\mathcal{H}$ on a lattice with size $L = lB$. One just has to measure correlation functions of block averages of the original system, that can be simulated, e.g. with efficient Monte Carlo algorithms.

It is worth noting that the couplings $E_i^{(l,B)}$ introduced above can be interpreted as *phenomenological couplings* as introduced by Nightingale and by Binder [92, 93].

B	a	b	c	d	e	f
4	−8.99182	2.98941	−0.12121	−1.10822	−0.08032	0.05674
8	−9.83928	3.41193	−0.22512	−1.38204	−0.05261	0.06654
16	−10.0911	3.54303	−0.26380	−1.46882	−0.03870	0.06655
32	−10.1573	3.57796	−0.27464	−1.49208	−0.03453	0.06626
64	−10.1740	3.58685	−0.27744	−1.49801	−0.03343	0.06616
128	−10.1783	3.58908	−0.27815	−1.49950	−0.03315	0.06613
256	−10.1793	3.58964	−0.27833	−1.49988	−0.03308	0.06612
512	−10.1796	3.58978	−0.27837	−1.49997	−0.03307	0.06612
1024	−10.1796	3.58982	−0.27838	−1.49999	−0.03306	0.06612
2048	−10.1797	3.58983	−0.27838	−1.50000	−0.03306	0.06612

Table 4.1: Flow of the effective Laplacian for $l = 4$. The components are arranged as indicated in table (4.6)

We conclude this section by presenting results for the flow of the $\mathcal{H}_{\rm eff}^{(l,B)}$ for the free massless field theory (Gaussian model) in two dimensions. This may serve as an illustration for the convergence of the flow towards a fixed point. The Hamiltonian is

$$\mathcal{H}(\varphi) = \tfrac{1}{2}(\varphi, -\Delta\varphi) = \tfrac{1}{2}\sum_{<x,y>} (\varphi_x - \varphi_y)^2 \,. \tag{4.4}$$

For this theory the effective Hamiltonian can be computed exactly (see Appendix 2 in [BB7]),

$$\mathcal{H}_{\rm eff}^{(l,B)}(\phi) = \frac{1}{2}\left(\phi, -\Delta_{\rm eff}^{(l,B)}\phi\right) = \tfrac{1}{2}\sum_{x',y'} \phi_{x'}\left[-\Delta_{\rm eff}^{(l,B)}\right]_{x',y'}\phi_{y'} \,. \tag{4.5}$$

Table 4.1 shows the components of $\Delta_{\rm eff}^{(l,B)}$ on a 4×4 lattice, which are arranged according to the following scheme:

$$\begin{array}{cccc} a & b & d & b \\ b & c & e & c \\ d & e & f & e \\ b & c & e & c \end{array} \tag{4.6}$$

4.2 Renormalization Group Matching of SOS Models with the BCSOS Model

Using the cluster algorithm described in [BB3], we simulated the BCSOS model at the roughening coupling $K_R^{BCSOS} = \frac{1}{2}\ln 2$ on square lattices of size $L \times L$ with periodic boundary conditions. For a list of the used L's and the statistics, see table 4.2. There we give as an example the results for the squared interface width W^2, defined through

$$W^2 = \frac{1}{L^2}\sum_x < (h_x - h_y)^2 > \tag{4.7}$$

L	W^2	$stat$	L	W^2	$stat$
12	1.02860(32)	2.8	48	1.34674(34)	2.2
16	1.09624(42)	1.4	64	1.41080(26)	4.4
24	1.18996(40)	1.6	96	1.50038(30)	5.3
32	1.25464(38)	1.5	128	1.56362(32)	4.9

Table 4.2: Results for the squared interface width W^2 as function of the lattice size L for the critical BCSOS model. The statistics *stat* is given in units of 10^6 single cluster updates

Figure 4.1 shows $W^2 - (2/\pi^2)\ln L$ as a function of $\ln L$. KT theory predicts that this quantity should converge towards a constant for large L, see chapter 3.

The figure shows a significant deviation from this behavior. This means that for the lengths fitting on lattices with $L \leq 128$ the effective fugacity, which is a measure for the deviation from a massless Gaussian model, is not small. This is a consequence of the fact that along the critical line the flow towards the Gaussian fixed point is very slow (like $\sim 1/\ln L$, see chapter 2).

Our method to monitor the RG flow is to compute the flow of blocked observables (see section 4.1). The lattice is divided into $l \times l$ square blocks of size $B \times B$, with $l = 1, 2, 4$. [2] Linear block spins $\phi_{x'}$ are defined according to

$$\phi_{x'} = B^{-2} \sum_{x \in x'} h_x \,, \tag{4.8}$$

where the h_x are the height variables of the SOS model under consideration.

Motivated by KT theory we measured two types of block observables: those that are sensitive to the flow of the kinetic term (flow of K), and those that are sensitive to the fugacity. For the first type of observables we chose

$$A_{1,l} = \left\langle \frac{1}{2l^2} \sum_{<x',y'>} (\phi_{x'} - \phi_{y'})^2 \right\rangle \,, \tag{4.9}$$

where $< x', y' >$ are nearest-neighbor pairs on the block lattice, and

$$A_{2,l} = \left\langle \frac{1}{2l^2} \sum_{[x',y']} (\phi_{x'} - \phi_{y'})^2 \right\rangle \,, \tag{4.10}$$

where $[x', y']$ are next-to-nearest-neighbor pairs. These quantities are defined for $l > 1$. For the actual matching procedure to be described below, we also employed the quantities

$$D_{i,l} = \frac{A^{(0)}_{i,l}|_{B=\infty}}{A^{(0)}_{i,l}} A_{i,l} \quad \text{for } l = 1, 2 \,. \tag{4.11}$$

[2] A posteriori we found that measuring also $l > 4$ data would have been useful. However, the small l-values enabled us to save all block spin configurations on disk. This gave us flexibility in the data analysis.

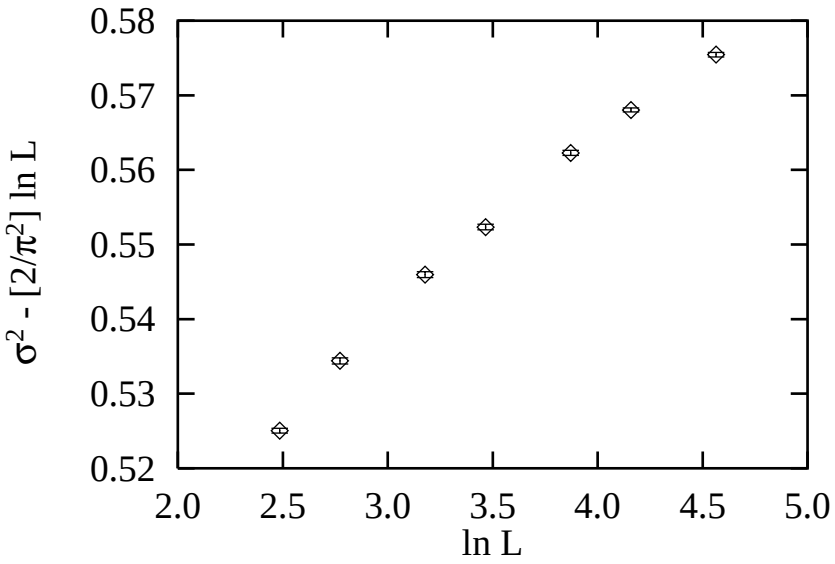

Figure 4.1: The squared interface width W^2 of the BCSOS model minus its large L behavior as anticipated from KT theory

Here, the $A_{i,l}^{(0)}$ denote the same quantities as defined in eqs. (4.9) and (4.10), taken, however, in the continuous Gaussian model with the Hamiltonian defined in eq. (4.4). The $A_{i,l}^{(0)}$ can be computed exactly, see Appendix 2 in [BB7]. In table 4.3 we give the values of $A_{1,l}^{(0)}$ and $A_{2,l}^{(0)}$ for $L \leq 8192$. Within the accuracy obtained (6 digits), the infinite B limit is reached for $L = 4096$.

As a monitor for the fugacity we chose the following set of quantities (defined for $l = 1, 2, 4$):

$$\begin{aligned} A_{3,l} &= \left\langle \frac{1}{l^2} \sum_{x'} \cos(1 \cdot 2\pi\phi_{x'}) \right\rangle , \\ A_{4,l} &= \left\langle \frac{1}{l^2} \sum_{x'} \cos(2 \cdot 2\pi\phi_{x'}) \right\rangle , \\ A_{5,l} &= \left\langle \frac{1}{l^2} \sum_{x'} \cos(3 \cdot 2\pi\phi_{x'}) \right\rangle . \end{aligned} \tag{4.12}$$

We believe that all important information about the large-distance RG flow of an SOS model close to or at criticality can be monitored by these observables or by a subset of them. The result for the flow of the $A's$ for the critical BCSOS model is summarized in table 4.4. We also give the exact limits that these quantities should approach when the block size B is scaled to ∞. KT theory predicts that $A_{3,l}$, $A_{4,l}$ and $A_{5,l}$ have to converge to zero. The quantities $A_{1,l}$ and $A_{2,l}$ are predicted to converge to $2/\pi$ times the $B \to \infty$ limit of the same observables in the free field

L	$A^{(0)}_{1,2}$	$A^{(0)}_{2,2}$	$A^{(0)}_{1,4}$	$A^{(0)}_{2,4}$
8	0.136719	0.187500	0.293527	0.380581
12	0.126721	0.175926	0.257225	0.340481
16	0.123147	0.171875	0.243918	0.326090
24	0.120565	0.168981	0.234147	0.315663
32	0.119655	0.167969	0.230662	0.311978
48	0.119002	0.167245	0.228148	0.309333
64	0.118773	0.166992	0.227263	0.308404
96	0.118609	0.166811	0.226628	0.307739
128	0.118551	0.166748	0.226406	0.307507
256	0.118496	0.166687	0.226191	0.307282
512	0.118482	0.166672	0.226137	0.307226
1024	0.118479	0.166668	0.226124	0.307212
2048	0.118478	0.166667	0.226120	0.307208
4096	0.118478	0.166667	0.226119	0.307207
8192	0.118478	0.166667	0.226119	0.307207

Table 4.3: Exact results for $A^{(0)}_{1,l}$ and $A^{(0)}_{2,l}$

theory. These limits can be read off from table 4.3. A close look at the data reveals that even for large B the $A's$ are still off their fixed points values. However, we shall see in the following that it does not matter that in the flow of the BCSOS data the fixed point is still somewhat away: The RG matching will take place a long time before the fixed point is close. Irrelevant couplings die out with a power of the length scale. The flow of the couplings is rapidly reduced to a 1-dimensional manifold. Along this remaining line, the fugacity dies out logarithmically with the length scale. Eventually the Gaussian fixed point with zero fugacity is reached. Since we know the 1-dimensional manifold from the BCSOS model, we just have to recover it in the other models. This can be done even far away from the fixed point.

The simulations of the DG model, the ASOS model and the dual of the XY model were also performed on quadratic lattices with periodic boundary conditions. We used the very efficient VMR cluster algorithms. The same blocking prescription as for the BCSOS model was employed. The lattice sizes and couplings involved will be specified below.

4.2.1 Determination of the Roughening Couplings

There are two parameters that have to be tuned in order to match the RG flow of one of the SOS models with that of the critical BCSOS model. One can vary the coupling K^{SOS} of the SOS model. This allows one to walk on the approximate starting line in figure 2. The flow of the SOS model can only match that of the critical BCSOS model if $K^{SOS} = K^{SOS}_R$. On the other hand, one can vary the ratio of the lattice sizes of the SOS model and the BCSOS model and, as a consequence, the ratio of the block sizes $b^{SOS}_m = B^{SOS}/B^{BCSOS}$. A ratio $b^{SOS}_m \neq 1$ turns out to be necessary to compensate for the different positions of the approximate starting lines in figure 4.2.

L	l	B	$A_{1,l}$	$A_{2,l}$	$A_{3,l}$	$A_{4,l}$	$A_{5,l}$
12	1	12			0.2842(17)	0.0777(14)	0.0229(13)
16	1	16			0.2655(27)	0.0669(20)	0.0212(18)
24	1	24			0.2383(31)	0.0551(22)	0.0149(19)
32	1	32			0.2261(36)	0.0511(24)	0.0105(20)
48	1	48			0.2056(36)	0.0394(23)	0.0077(18)
64	1	64			0.1969(30)	0.0372(18)	0.0051(13)
96	1	96			0.1821(37)	0.0296(20)	0.0052(14)
128	1	128			0.1719(43)	0.0283(21)	0.0058(15)
∞	1	∞			0.0	0.0	0.0
12	2	6	0.08891(16)	0.11983(26)	0.2403(10)	0.0668(7)	0.0227(6)
16	2	8	0.08569(22)	0.11745(36)	0.2258(16)	0.0582(10)	0.0157(9)
24	2	12	0.08319(22)	0.11505(37)	0.2009(19)	0.0445(11)	0.0101(9)
32	2	16	0.08187(23)	0.11395(39)	0.1892(22)	0.0390(11)	0.0084(10)
48	2	24	0.08114(22)	0.11343(37)	0.1746(22)	0.0328(11)	0.0058(9)
64	2	64	0.08097(17)	0.11339(29)	0.1655(18)	0.0263(8)	0.0042(7)
96	2	48	0.08076(20)	0.11326(33)	0.1528(22)	0.0239(9)	0.0046(7)
128	2	64	0.08038(21)	0.11268(35)	0.1435(26)	0.0208(10)	0.0033(7)
∞	2	∞	0.075425	0.106104	0.0	0.0	0.0
12	4	3	0.19524(17)	0.24472(24)	0.2438(5)	0.1121(4)	0.0586(4)
16	4	4	0.17686(21)	0.23046(31)	0.2226(7)	0.0781(5)	0.0407(5)
24	4	6	0.16521(20)	0.21978(30)	0.1933(8)	0.0535(6)	0.0177(5)
32	4	8	0.16087(21)	0.21539(31)	0.1793(9)	0.0438(6)	0.0122(5)
48	4	12	0.15798(18)	0.21278(28)	0.1632(9)	0.0349(5)	0.0087(4)
64	4	16	0.15646(14)	0.21136(21)	0.1522(8)	0.0296(4)	0.0064(3)
96	4	24	0.15522(16)	0.20995(25)	0.1395(9)	0.0248(5)	0.0049(4)
128	4	32	0.15471(17)	0.20928(27)	0.1322(11)	0.0219(5)	0.0045(4)
∞	4	∞	0.143952	0.195574	0.0	0.0	0.0

Table 4.4: Finite lattice renormalization group flow of the $A_{i,l}$ for the critical BCSOS model

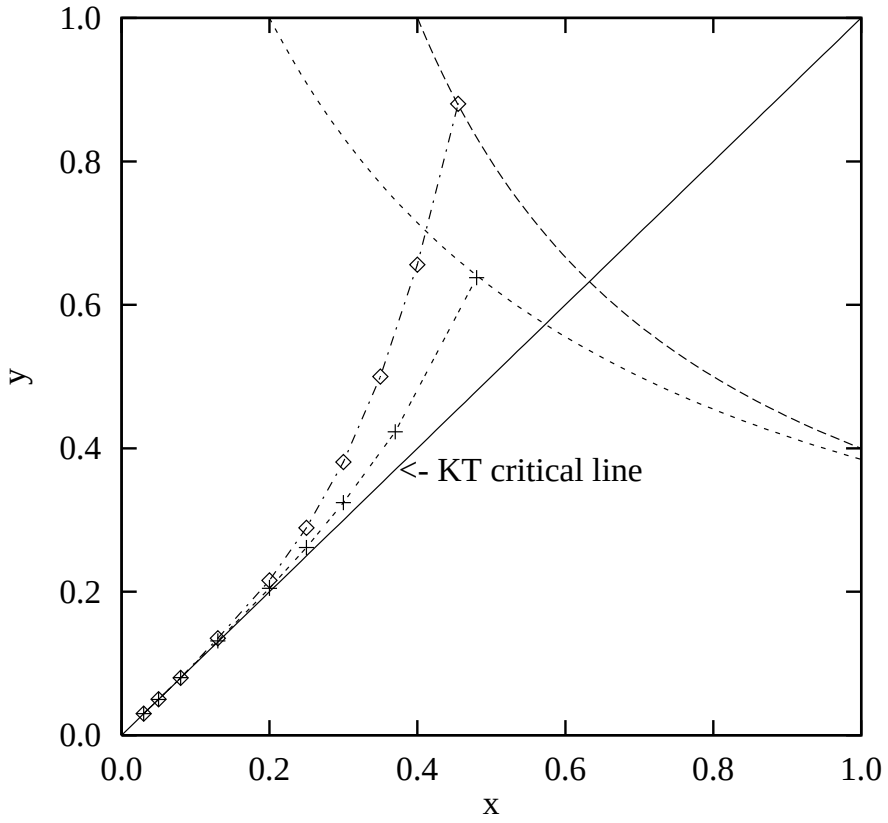

Figure 4.2: Matching of the finite size RG flow of two different SOS models in the KT flow diagram. Two successive points along the discrete trajectories are separated by a fixed scale factor. (In reality the models do not 'start' in the KT diagram but rather in a higher dimensional space of coupling constants.) Note that one of the models is one step 'ahead' of the other one. This explains that one needs the offset factor b_m in order to match the flows

Before we turn to the question of how to determine K_R^{SOS} and b_m^{SOS} in practice, let us write down the general condition for one of the SOS models to be in the same universality class as the critical BCSOS model.

Matching condition: Universality holds if there exists a b_m and a K_R^{SOS} such that for all i, l,

$$A_{i,l}^{SOS}\left(b_m^{SOS}B^{BCSOS}, K_R^{SOS}\right) = A_{i,l}^{BCSOS}\left(B^{BCSOS}, K_R^{BCSOS}\right) \tag{4.13}$$

in the limit of large B^{BCSOS}, and the corrections are of order $(B^{BCSOS})^{-\omega}$, with $\omega > 0$ the leading correction to scaling exponent. As we shall see below, moderate B^{BCSOS} are sufficient in practice.

In order to determine the SOS roughening coupling K_R^{SOS} from the RG flow data we proceeded as follows: For fixed values of L^{SOS} and for fixed l, we considered the two equations:

$$\begin{aligned} A_{1,l}^{SOS}\left(B^{SOS}, K_1^{SOS}\right) &\equiv A_{1,l}^{BCSOS}\left(B^{BCSOS}, K_R^{BCSOS}\right), \\ A_{3,l}^{SOS}\left(B^{SOS}, K_3^{SOS}\right) &\equiv A_{3,l}^{BCSOS}\left(B^{BCSOS}, K_R^{BCSOS}\right). \end{aligned} \tag{4.14}$$

We chose A_1 and A_3 because we consider these to be the most important observables for the monitoring of the RG flow. For each of the available values of B^{BCSOS} listed in table 4.4 we solved these two equations for the couplings K_i^{SOS}. To be able to do this we needed the $A's$ for a range of couplings. We simulated the SOS models at the (to that time) best known estimate for their roughening coupling. The expectation values in a neighborhood of the simulation point could then be obtained by extrapolating using a reweighting method [128].

For the determination of K_1^{SOS}, we did not use $A_{1,l}$ directly, but the 'improved' quantity $D_{1,l}$: matching of the $A_{i,l}$-flows of two models happens if and only if also the $D_{i,l}$-flows match. This is so because for $B \to \infty$ the factors $A_{i,l}^{(0)}(B)$ converge to fixed points $A_i^{(0)}(B = \infty)$. This proves that we are allowed to use the $D_{i,l}$ instead of the $A_{i,l}$ without losing any control on the RG flow. Furthermore, the $D_{i,l}$ flows converge more rapidly than those of the $A_{i,l}$. This will be demonstrated below. Roughly speaking, the $A_{i,l}^{(0)}$ factors cancel irrelevant terms in the flow that anyway die out under successive RG steps. These terms are strong as long as B is small, and are partly due to discretization details, e.g. of the lattice Laplacian. We want to stress the point that the use of the D's instead of the $A's$ is by no means necessary: the changes on the larger lattices are negligible. However, using the $D's$ allows one to observe a collapse to a universal trajectory on much smaller lattices.

The solution of eq. (4.14) yields, for each (L, l) pair, two values: K_1^{SOS} and K_3^{SOS}. For an illustration of this first step, see figure 4.3. Note that K_1^{SOS} and K_3^{SOS} will in general not be identical: one can expect matching only for a specific ratio b_m^{SOS}.

In a second step we plotted the values of K_1^{SOS} and K_3^{SOS} as a function of B^{BCSOS}. The couplings were linearly interpolated in $\log B^{BCSOS}$. The intersection of the two curves $K_1^{SOS}(B^{BCSOS})$ and $K_3^{SOS}(B^{BCSOS})$ then uniquely determines an estimate for the roughening coupling K_R^{SOS} of the SOS model, see figure 4.4.

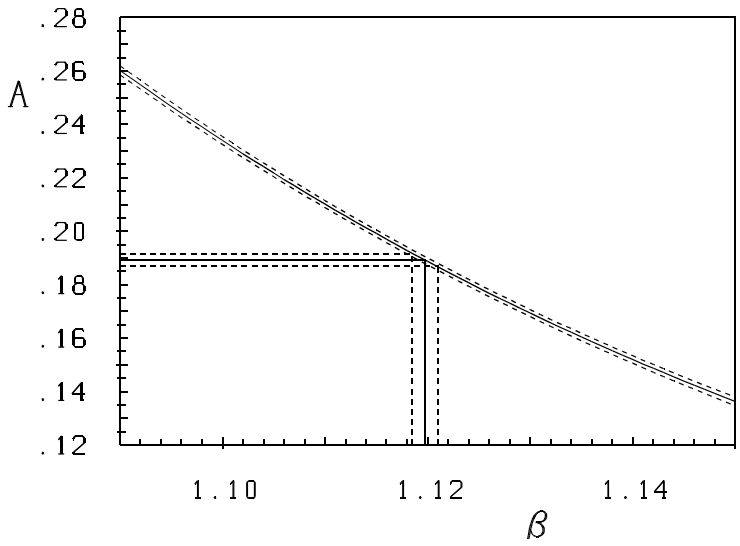

Figure 4.3: Determination of β_3^{XY} for $L^{XY} = 32$, $L^{BCSOS} = 32$ and $l = 2$. The solid curve gives $A_{3,2}^{XY}$ as a function of β^{XY}. The dashed curves indicate the statistical error. The solid straight horizontal line gives $A_{3,2}^{BCSOS}$ at K_R^{BCSOS}. The vertical lines give the result for $\beta_{3,2}^{XY}$ and its error

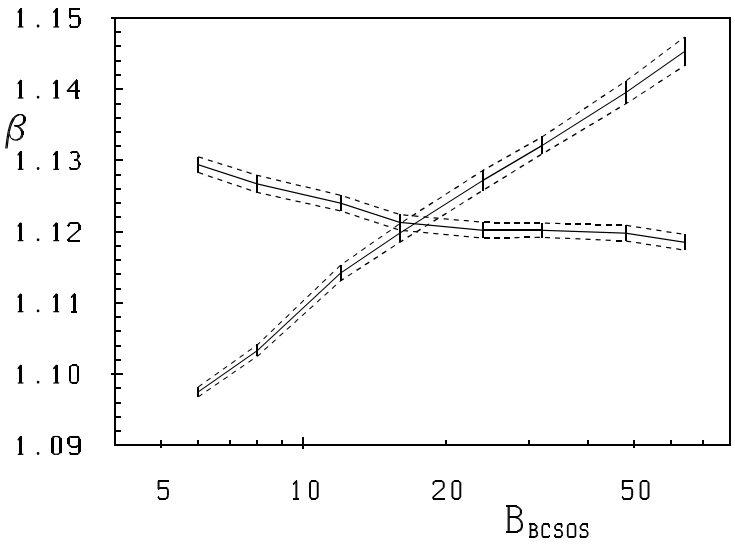

Figure 4.4: Determination of β_R^{XY} for $L^{XY} = 32$ and $l = 2$. The curves give β_1^{XY} and β_3^{XY} as functions of B_{BCSOS}. The intersection of the curves uniquely determines β_R^{XY} and the matching B_{BCSOS}

In addition we obtain for each B^{SOS} the BCSOS block size B^{BCSOS} that leads to a matching in the sense described above. The results for the matching for the three models are summarized in table 4.5.

For the three models, the results for the roughening coupling K_R obtained for the various lattice sizes L and sizes l of the blocked system are consistent with each other within statistical errors. Only the couplings for $l = 4$ on the smallest two lattice sizes and for $l = 2$ on the smallest lattice size deviate slightly from the rest. For the ratio of the matching block sizes $b_m = B^{SOS}/B^{BCSOS}$ the observation is the same. This indicates an extremely fast convergence to a universal RG flow of the models, since even for such small block sizes as $B^{BCSOS} = 16$ no deviation from the universal flow can be observed within our quite good statistics. To give estimates for the roughening coupling K_R for the three models we averaged the values obtained for the largest L with $l = 2$ and $l = 4$, and the second largest L only with $l = 2$. We arrive at the following results

$$\begin{aligned} \beta_R^{XY} &= 1.1197(5)\,, \\ K_R^{DG} &= 0.6645(6)\,, \\ K_R^{ASOS} &= 0.8061(3)\,. \end{aligned} \tag{4.15}$$

The quoted errors are statistical, but according to the discussion above, the systematic ones due to deviations from the universal parameter flow, should be much smaller. For the b_m we find in

Dual of XY model				
L	$\beta_R, l=2$	$\beta_R, l=4$	$b_m, l=2$	$b_m, l=4$
16	1.1220(12)	1.1257(8)	0.84(5)	0.75(1)
24	1.1214(13)	1.1225(8)	0.91(7)	0.84(2)
32	1.1211(12)	1.1214(8)	0.93(10)	0.85(3)
48	1.1199(11)	1.1205(7)	0.89(13)	0.89(3)
64	1.1212(11)	1.1201(7)	0.89(5)	0.82(12)
96	1.1189(11)	1.1194(7)	0.89(12)	0.95(7)
DG model				
L	$\beta_R, l=2$	$\beta_R, l=4$	$b_m, l=2$	$b_m, l=4$
12	0.6627(16)	0.6607(13)	0.31(4)	0.40(2)
16	0.6650(13)	0.6632(10)	0.32(5)	0.34(2)
24	0.6633(16)	0.6645(8)	0.30(6)	0.34(2)
32	0.6650(16)	0.6647(8)	0.28(5)	0.32(2)
ASOS model				
L	$\beta_R, l=2$	$\beta_R, l=4$	$b_m, l=2$	$b_m, l=4$
32	0.8052(4)		2.3(2)	
64	0.8061(6)	0.8058(3)	2.8(3)	2.4(1)
128	0.8061(6)	0.8060(3)	2.7(6)	2.6(2)
256	0.8060(5)	0.8062(3)	2.8(6)	2.9(4)

Table 4.5: K_R and $b_m = B^{SOS}/B^{BCSOS}$ for the three SOS models as obtained from the matching of $A_{1,l}$ and $A_{3,l}$

a similar way

$$\begin{aligned} b_m^{XY} &= 0.89(5)\,, \\ b_m^{DG} &= 0.31(2)\,, \\ b_m^{ASOS} &= 2.8(3)\,. \end{aligned} \tag{4.16}$$

4.2.2 Demonstration that the Matching is Universal

We want to demonstrate that all quantities $A_{i,l}$ ($D_{i,l}$) converge towards a universal flow with increasing B^{SOS}, provided that the couplings K^{SOS} are tuned to their critical values quoted in eq. (4.15), and that the block size ratios $b_m^{SOS} = B^{SOS}/B^{BCSOS}$ are taken to be the matching values quoted in eq. (4.16). Recall that the critical couplings and b_m's were determined by imposing the matching condition for $D_{1,l}$ and $A_{3,l}$ alone.

The first task was to evaluate the observables $A_{2,l}$, $A_{4,l}$ and $A_{5,l}$ at the critical couplings K_R determined above using $D_{1,l}$ and $A_{3,l}$ only. The results are summarized in tables 4.6 to 4.8. For the sake of completeness we also give the values of the $D_{i,l}$, in table 4.9. We furthermore demonstrated the universal matching by plotting all measured block observables at criticality as functions of the matching block size $B^{BCSOS} = B^{SOS}/b_m^{SOS}$. As an example we here show two representative plots for the quantities $D_{1,4}$ and $A_{1,4}$.[3] The reader is invited to look carefully at figs. 4.5 and 4.6. To correctly interpret the plots, it is necessary to realize that the scale of the y-axis might differ from plot to plot. The collapse of $D_{1,4}$ onto a universal curve is much faster than for the corresponding quantity $A_{1,4}$.

[3] A larger sample of plots can be found in ref. [BB7]

L	l	$A_{1,l}$	$A_{2,l}$	$A_{3,l}$	$A_{4,l}$	$A_{5,l}$
16	1			0.2601(19)	0.0669(17)	0.0175(13)
24	1			0.2381(28)	0.0497(20)	0.0110(17)
32	1			0.2260(22)	0.0493(18)	0.0113(16)
48	1			0.2029(24)	0.0391(21)	0.0084(18)
64	1			0.1946(31)	0.0354(19)	0.0072(19)
96	1			0.1748(31)	0.0256(26)	0.0032(18)
16	2	0.08486(17)	0.11735(30)	0.2187(13)	0.0531(8)	0.0140(7)
24	2	0.08255(20)	0.11505(32)	0.2000(16)	0.0436(10)	0.0101(7)
32	2	0.08146(20)	0.11373(32)	0.1893(13)	0.0377(10)	0.0088(8)
48	2	0.08109(23)	0.11337(37)	0.1712(14)	0.0306(10)	0.0071(9)
64	2	0.08051(23)	0.11234(35)	0.1629(18)	0.0266(8)	0.0026(9)
96	2	0.08087(26)	0.11337(44)	0.1470(20)	0.0207(11)	0.0038(10)
16	4	0.17102(20)	0.22671(30)	0.2088(6)	0.0624(5)	0.0240(4)
24	4	0.16283(18)	0.21812(28)	0.1883(6)	0.0479(5)	0.0144(3)
32	4	0.15965(18)	0.21477(26)	0.1755(7)	0.0414(5)	0.0107(4)
48	4	0.15721(16)	0.21206(23)	0.1602(7)	0.0338(5)	0.0076(5)
64	4	0.15602(20)	0.21065(29)	0.1489(8)	0.0283(6)	0.0071(5)
96	4	0.15531(20)	0.21012(30)	0.1377(9)	0.0234(6)	0.0050(6)

Table 4.6: Finite lattice renormalization group flow of the $A_{i,l}$ for the dual of the XY model at $\beta = 1.1197$

L	l	$A_{1,l}$	$A_{2,l}$	$A_{3,l}$	$A_{4,l}$	$A_{5,l}$
12	1			0.2170(31)	0.0474(22)	0.0125(17)
16	1			0.2061(23)	0.0403(27)	0.0068(15)
24	1			0.1944(45)	0.0407(32)	0.0057(25)
32	1			0.1729(41)	0.0312(29)	0.0058(27)
12	2	0.08611(30)	0.11901(45)	0.1850(18)	0.0409(12)	0.0090(10)
16	2	0.08408(27)	0.11711(40)	0.1725(16)	0.0314(11)	0.0062(12)
24	2	0.08185(38)	0.11418(58)	0.1603(27)	0.0275(14)	0.0064(11)
32	2	0.08140(34)	0.11431(59)	0.1458(27)	0.0246(15)	0.0051(13)
12	4	0.17782(32)	0.23433(45)	0.1875(8)	0.0588(6)	0.0327(6)
16	4	0.16839(24)	0.22388(35)	0.1663(8)	0.0413(6)	0.0143(6)
24	4	0.16100(26)	0.21601(40)	0.1488(10)	0.0305(8)	0.0068(6)
32	4	0.15800(25)	0.21312(37)	0.1380(10)	0.0254(7)	0.0050(5)

Table 4.7: Finite lattice renormalization group flow of the $A_{i,l}$ for the DG model at $K^{DG} = 0.6645$

L	l	$A_{1,l}$	$A_{2,l}$	$A_{3,l}$	$A_{4,l}$	$A_{5,l}$
32	1			0.2800(31)	0.0766(27)	0.0232(19)
64	1			0.2404(35)	0.0525(27)	0.0132(25)
128	1			0.2103(41)	0.0425(28)	0.0084(24)
256	1			0.1866(45)	0.0312(28)	0.0028(24)
32	2	0.08291(30)	0.11513(52)	0.2368(18)	0.0609(12)	0.0191(11)
64	2	0.08202(33)	0.11504(46)	0.2023(25)	0.0424(13)	0.0088(12)
128	2	0.08083(34)	0.11337(52)	0.1756(25)	0.0334(14)	0.0067(11)
256	2	0.08069(33)	0.11313(57)	0.1553(26)	0.0251(15)	0.0035(13)
32	4	0.16406(29)	0.21936(45)	0.2230(9)	0.0656(7)	0.0222(7)
64	4	0.15914(27)	0.21457(37)	0.1891(9)	0.0471(7)	0.0136(7)
128	4	0.15651(28)	0.21137(43)	0.1635(13)	0.0320(7)	0.0072(6)
256	4	0.15513(28)	0.21010(42)	0.1412(11)	0.0255(9)	0.0057(7)

Table 4.8: Finite lattice renormalization group flow of the $A_{i,l}$ for the ASOS model at $K^{ASOS} = 0.8061$

4.2.3 Determination of Non-Universal Constants

The matching also allows us to determine the non-universal constants appearing in the formulae for the divergence of observables near the roughening transition. Let us discuss this over the example of the correlation length ξ. Its critical behavior is

$$\xi \simeq A \, \exp\left(C\kappa^{-1/2}\right) , \quad \kappa = \tfrac{K-K_R}{K_R} . \tag{4.17}$$

Let us consider matching on an RG trajectory in the phase with finite correlation length (smooth phase), close to the critical trajectory. Let us assume that the BCSOS block observables match the SOS block observables for sufficiently large B^{BCSOS}, B^{SOS}, with $B^{SOS} = b_m^{SOS} B^{BCSOS}$. Then

$$\xi^{SOS} = b_m^{SOS} \xi^{BCSOS} . \tag{4.18}$$

Inserting eq. (4.17) in eq. (4.18) we get

$$\xi^{SOS} \simeq b_m^{SOS} A^{BCSOS} \exp\left(C^{BCSOS} \left(\kappa^{BCSOS}\right)^{-1/2}\right) . \tag{4.19}$$

It is a general assumption of the renormalization group that couplings on the blocked system are smooth functions of the block size and the coupling on the fine lattice. We thus assume that b_m^{SOS} is a smooth function of κ^{SOS}, even at the roughening transition,

$$b_m^{SOS}(K) = b_m^{SOS}(K_R) + O\left(\kappa^{SOS}\right) . \tag{4.20}$$

Furthermore, also κ^{BCSOS} is a smooth function of κ^{SOS},

$$\kappa^{BCSOS} = q\,\kappa^{SOS} + O\left(\left(\kappa^{SOS}\right)^2\right) . \tag{4.21}$$

BCSOS model					
B	$D_{1,2}$	$D_{2,2}$	B	$D_{1,4}$	$D_{2,4}$
6	0.08313(15)	0.11352(25)	3	0.17163(15)	0.22080(22)
8	0.08244(21)	0.11389(35)	4	0.16395(19)	0.21711(29)
12	0.08175(22)	0.11347(36)	6	0.15955(19)	0.21389(29)
16	0.08106(23)	0.11307(39)	8	0.15770(21)	0.21210(31)
24	0.08078(22)	0.11304(37)	12	0.15658(18)	0.21132(28)
32	0.08077(17)	0.11317(29)	16	0.15567(14)	0.21054(21)
48	0.08067(20)	0.11316(33)	24	0.15487(16)	0.20959(25)
64	0.08033(21)	0.11263(35)	32	0.15451(17)	0.20908(27)
Dual of XY model					
B	$D_{1,2}$	$D_{2,2}$	B	$D_{1,4}$	$D_{2,4}$
8	0.08164(16)	0.11379(29)	4	0.15854(19)	0.21358(28)
12	0.08112(20)	0.11347(32)	6	0.15725(17)	0.21228(27)
16	0.08066(20)	0.11285(32)	8	0.15651(18)	0.21149(26)
24	0.08073(23)	0.11298(37)	12	0.15581(16)	0.21060(23)
32	0.08031(23)	0.11212(35)	16	0.15523(20)	0.20983(29)
48	0.08078(26)	0.11327(44)	24	0.15496(20)	0.20976(30)
DG model					
B	$D_{1,2}$	$D_{2,2}$	B	$D_{1,4}$	$D_{2,4}$
6	0.08051(28)	0.11275(43)	3	0.15632(28)	0.21143(41)
8	0.08089(26)	0.11356(39)	4	0.15610(22)	0.21092(33)
12	0.08043(37)	0.11262(57)	6	0.15548(25)	0.21022(39)
16	0.08060(34)	0.11342(59)	8	0.15489(25)	0.20986(36)
ASOS model					
B	$D_{1,2}$	$D_{2,2}$	B	$D_{1,4}$	$D_{2,4}$
16	0.08209(30)	0.11424(52)	8	0.16083(28)	0.21601(44)
32	0.08182(33)	0.11482(46)	16	0.15834(27)	0.21374(37)
64	0.08078(34)	0.11331(52)	32	0.15631(28)	0.21116(43)
128	0.08068(33)	0.11312(57)	64	0.15508(28)	0.21005(42)

Table 4.9: Results for the flow of the $D_{i,l}$ at criticality

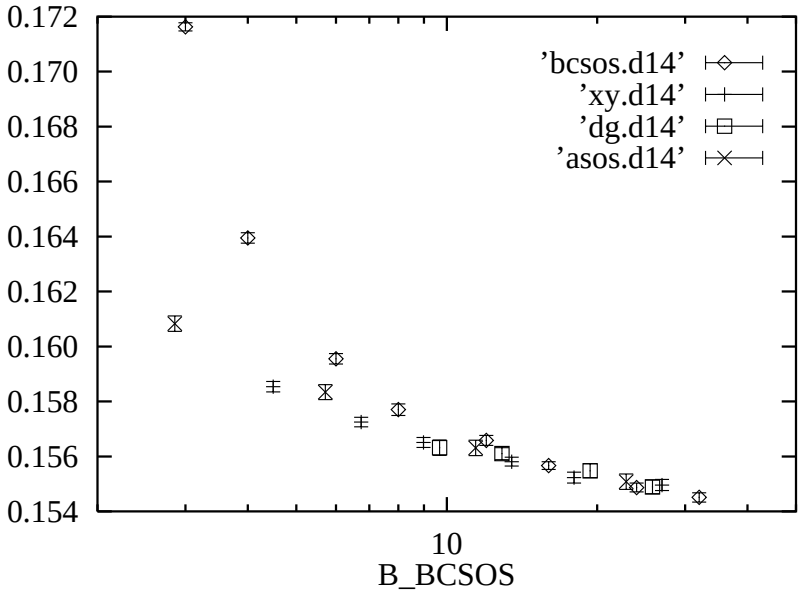

Figure 4.5: $D_{1,4}$ at criticality, plotted as a function of $B^{BCSOS} = B^{SOS}/b_m^{SOS}$

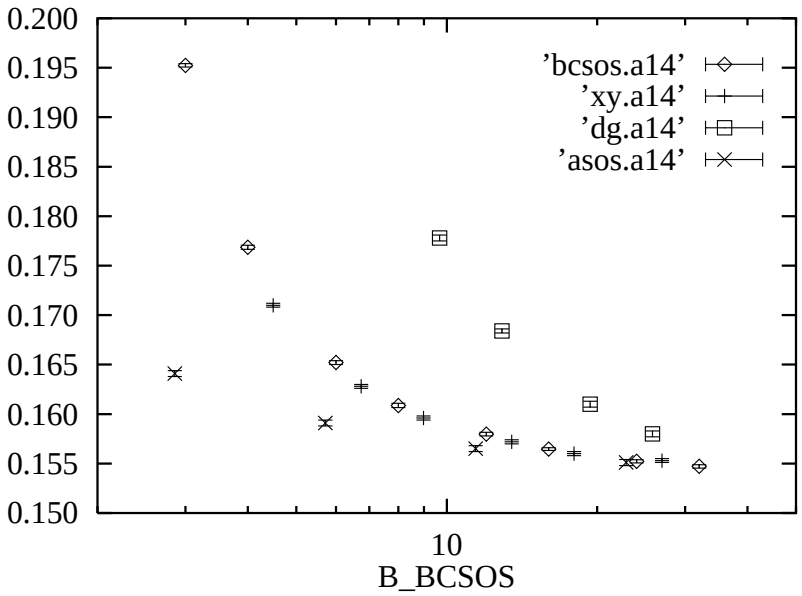

Figure 4.6: $A_{1,4}$ at criticality, plotted as a function of $B^{BCSOS} = B^{SOS}/b_m^{SOS}$

In the limit $\kappa^{SOS} \to 0$ we get

$$\xi^{SOS} \simeq A^{SOS} \exp\left(C^{SOS}(\kappa^{SOS})^{-1/2}\right) , \tag{4.22}$$

with

$$\begin{aligned} A^{SOS} &= b_m^{SOS} A^{BCSOS} , \\ C^{SOS} &= q^{-1/2}\, C^{BCSOS} . \end{aligned} \tag{4.23}$$

With the results obtained above for b_m and with $A^{BCSOS} = \frac{1}{4}$ we find

$$\begin{aligned} A^{XY} &= 0.223(13) , \\ A^{DG} &= 0.078(5) , \\ A^{ASOS} &= 0.70(8) . \end{aligned} \tag{4.24}$$

There remains to determine the constant q connecting κ^{SOS} and κ^{BCSOS}. For this purpose let us rewrite the matching condition for coupling constants in the neighborhood of the critical point. In order to keep the formulae compact, we shall write an 'S' for 'SOS' and a 'B' for 'BCSOS'. The matching condition reads

$$A_{i,l}^S\left(B^S, K_R^S + k^S\right) = A_{i,l}^B\left(B^B, K_R^B + k^B\right) . \tag{4.25}$$

A Taylor expansion around K_R^S and K_R^B, respectively, yields

$$\begin{aligned} A_{i,l}^S\left(B^S, K_R^S\right) &+ k^S \left(\frac{\partial A_{i,l}^S}{\partial K^S}\left(B^S, K_R^S\right) + \frac{\partial A_{i,l}^S}{\partial B^S}\left(B^S, K_R^S\right)\frac{\partial B^S}{\partial K^S}\left(K_R^S\right)\right) \\ &= \text{(same for BCSOS)} . \end{aligned} \tag{4.26}$$

These equations simplify since the observables match at criticality. As a consequence of the matching condition,

$$\begin{aligned} A_{i,l}^S\left(B^S, K_R^S\right) &\equiv A_{i,l}^B\left(B^B, K_R^B\right) , \\ \frac{\partial B^S}{\partial K^S}\left(K_R^S\right) &\equiv 0 . \end{aligned} \tag{4.27}$$

The second of these equations expresses the fact that we keep B^S fixed when tuning the other parameters in order to fulfil the matching condition. We are left with

$$k^S\left(\frac{\partial A_{i,l}^S}{\partial K^S}\left(B^S, K_R^S\right)\right) = k^B\left(\frac{\partial A_{i,l}^B}{\partial K^B}\left(B^B, K_R^B\right) + \underbrace{\frac{\partial A_{i,l}^B}{\partial B^B}\left(B^B, K_R^B\right)\frac{\partial B^B}{\partial K^B}(K_R^B)}_{d_{i,l}}\right) . \tag{4.28}$$

Let us now again restrict our attention to $i = 1, 3$. We can then solve eqs. (4.28) with respect to k^S/k^B:

$$\frac{k^S}{k^B} = \frac{\frac{\partial A^B_{1,l}}{\partial K^B} \Big/ \frac{\partial A^B_{1,l}}{\partial B^B} - \frac{\partial A^B_{3,l}}{\partial K^B} \Big/ \frac{\partial A^B_{3,l}}{\partial B^B}}{\frac{\partial A^S_{1,l}}{\partial K^S} \Big/ \frac{\partial A^B_{1,l}}{\partial B^B} - \frac{\partial A^S_{3,l}}{\partial K^S} \Big/ \frac{\partial A^B_{3,l}}{\partial B^B}} \,. \tag{4.29}$$

The partial derivatives $\partial A/\partial K$ can be determined with reweighting methods or with the help of the formula

$$\frac{\partial A}{\partial K} = -\langle AH \rangle + \langle A \rangle \langle H \rangle \,. \tag{4.30}$$

H is the Hamiltonian, and the expectation values are taken in the system with partition function $Z = \sum_{\rm conf} \exp(-KH)$. The partial derivatives $\partial A^B_{i,l}/\partial B^B$ can be extracted from table 4.4.

However, eq. (4.29) simplifies very much if the term $d_{i,l}$ in eq. (4.28) can be neglected. This is the case when

$$\frac{\partial B^B}{\partial K^B}(K^B_R) \approx 0 \,. \tag{4.31}$$

Equivalently, the simplification relies on the assumption that the expansion of the matching B^B around the roughening coupling K^B_R is of second order in k^B. Then we get

$$\left(\frac{k^S}{k^B}\right)^{\rm naive}_{i,l} = \frac{\partial A^B_{i,l}}{\partial K^B} \Big/ \frac{\partial A^S_{i,l}}{\partial K^S} \quad , \quad i = 1, 3 \,. \tag{4.32}$$

If the approximation is a good one, the $(k^S/k^B)^{\rm naive}_{i,l}$ should be independent of i, l. Our results for these quantities are summarized in table 4.10.

For all three models the numbers for $(k^S/k^B)^{\rm naive}_{i,l}$ for different (i, l) are consistent within the error bars. We arrive at the following estimates:

$$\begin{aligned} k^{BCSOS}/k^{XY} &= 0.43(1) \,, \\ k^{BCSOS}/k^{DG} &= 0.39(1) \,, \\ k^{BCSOS}/k^{ASOS} &= 1.46(6) \,. \end{aligned} \tag{4.33}$$

Dual of XY model					
L	$i=3, l=1$	$i=1, l=2$	$i=3, l=2$	$i=1, l=4$	$i=3, l=4$
16	0.413(8)	0.430(11)	0.406(8)	0.424(10)	0.400(7)
24	0.413(9)	0.436(14)	0.419(8)	0.431(14)	0.418(8)
32	0.427(12)	0.461(19)	0.429(10)	0.437(19)	0.421(9)
48	0.434(15)	0.441(21)	0.423(12)	0.445(22)	0.445(9)
64	0.449(17)	0.420(28)	0.445(13)	0.447(29)	0.434(11)
96	0.449(27)	0.447(46)	0.440(21)	0.437(45)	0.424(15)
Discrete Gaussian model					
L	$i=3, l=1$	$i=1, l=2$	$i=3, l=2$	$i=1, l=4$	$i=3, l=4$
12	0.381(12)	0.394(17)	0.375(10)	0.394(18)	0.369(9)
16	0.381(13)	0.384(18)	0.379(11)	0.385(19)	0.374(8)
24	0.388(17)	0.384(30)	0.381(13)	0.388(29)	0.374(11)
32	0.397(24)	0.364(38)	0.394(19)	0.372(39)	0.387(13)
ASOS model					
L	$i=3, l=1$	$i=1, l=2$	$i=3, l=2$	$i=1, l=4$	$i=3, l=4$
32	1.482(32)	1.504(35)	1.451(25)	1.426(40)	1.345(21)
64	1.385(42)	1.474(46)	1.345(40)	1.457(44)	1.447(42)
128	1.383(50)	1.416(66)	1.373(43)	1.510(72)	1.421(41)
256	1.909(106)	1.625(157)	1.712(75)	1.608(151)	1.586(57)

Table 4.10: $(k^S/k^B)^{\rm naive}_{i,l}$ for the three SOS models

Now we use that

$$C^{SOS} = \left(\frac{\kappa^{SOS}}{\kappa^{BCSOS}}\right)^{1/2} C^{BCSOS} \tag{4.34}$$

and $\kappa^{SOS} = k^{SOS}/K_R^{SOS}$. We get

$$\begin{aligned} C^{XY} &= 1.78(2)\,, \\ C^{DG} &= 2.44(3)\,, \\ C^{ASOS} &= 1.14(2)\,. \end{aligned} \tag{4.35}$$

4.2.4 Comparison With Other Monte Carlo Studies

We compared our results with those obtained in other Monte Carlo studies.

Janke and Nather [73] simulated the XY model with the Villain action in the vortex phase using Wolff's single cluster algorithm [129]. They measured correlation lengths up to $\xi = 140$ on lattices up to $L = 1200$, at β ranging from $\beta^V = 0.590$ up to $\beta^V = 0.675$, where $\beta^V = 0.5/K^{DG}$. They fitted their results for ξ to eq. (4.17). To check for systematical errors due to a too large distance to the critical point, they used two different definitions of κ:

$$\begin{aligned} \kappa_T &= |T - T_c|/T_c\,, \\ \kappa_\beta &= |\beta - \beta_c|/\beta_c\,. \end{aligned} \tag{4.36}$$

Definition of κ	β_c^V	A	C
κ_T	0.75106(36)	0.1204(18)	2.370(11)
κ_β	0.75814(40)	0.0287(7)	2.812(14)
This work	0.7524(7)	0.078(5)	2.44(3)

Table 4.11: Comparison of our results for the DG model with those of ref. [73]. The relation between β^V and K^{DG} is $\beta^V = 0.5/K^{DG}$

Authors	β_c	A	C
Gupta et al.	1.1218	0.2129	1.7258
Biferale	1.112(2)		1.74(20)
This work	1.1197(5)	0.223(13)	1.78(2)

Table 4.12: Comparison of our results for the XY model with those of refs. [74] and [72]

The two definitions agree to the first-order Taylor expansion around the critical point. Hence both fits should give consistent results when the data included are obtained in a sufficiently small neighborhood of the critical point. The comparison of the results of Janke and Nather with our results is given in table 4.11. The results of the two fits are not consistent within the error bars. One is therefore led to the conclusion that the systematic error due to a too large distance of the simulation points from criticality is much larger than the quoted statistical errors.

The authors give $\beta_c = 0.752(5)$ as an overall estimate for the critical coupling. Taking into account the systematic errors of the fits, the results of their simulation are well consistent with our results.

In [BB5], the roughening coupling of the DG model was estimated from fits of the finite size behavior of the interface width. The fits were done with a renormalization group improved formula. The best estimate was $\beta_c = 0.5/K_R = 0.755(3)$, which is nicely consistent with the estimate arrived at in the present paper, namely $\beta_c = 0.7524(7)$.

In the case of the XY model with cosine action we can compare our results with a fit given in [74], which includes data of [71] and data of the authors, see table 4.12. As in the case of the DG model one can say that the results compare well with ours taking the systematic errors of the fits into account. We also include the results of the MCRG study [72] in this comparison.

Chapter 5

Monte Carlo Studies of the Ising Model Interface

5.1 Ising Model Interface Properties for T from 0 to T_c

We compute properties of the interface of the 3-dimensional Ising model for a wide range of temperatures, covering the region from the low temperature domain through the roughening transition to the bulk critical point. The interface tension σ is obtained by integrating the interface energy density over the inverse temperature β. We use lattices of size $L \times L \times t$, with L up to 64, and t up to 27. The simulations with antiperiodic boundary conditions in t-direction are done with the Hasenbusch-Meyer interface cluster algorithm that turns out to be very efficient. We demonstrate that in the rough phase the large distance behavior of the interface is well described by a massless Gaussian dynamics. The interface stiffness coefficient κ is determined. We also attempt to determine the correlation length ξ and study universal quantities like $\xi^2\sigma$ and $\xi^2\kappa$. Results for the interfacial width on lattices up to $512 \times 512 \times 27$ are also presented. This section is based on ref. [BB4].

There has been continuous interest in the properties of interfaces separating coexisting phases. A prominent role is played by the 3-dimensional Ising model that is believed to share a universality class with binary systems in nature. The dominating method for quantitative studies of the interface of the 3-dimensional Ising model is the Monte Carlo (MC) method.[1]

A pioneering Monte Carlo study on the Ising interface is [29]. For more recent numerical work on the 3-dimensional Ising interface see, e.g., [30, 31, 32, 35, 33, 34, 30, 36, 38, 39, 40, 41, 42]. For related work in the 4-dimensional model, see [43, 44]. A numerical study based on on the transfer matrix formalism is ref. [46].

The Ising interface undergoes a roughening transition at an inverse temperature $\beta_R = 1/(k_B T_R)$ that is nearly twice as large as the bulk transition coupling β_c ($= 0.221652(3)$ [94]).

[1] For introductions to the Monte Carlo method, see refs. [120]–[123]. Important references for cluster algorithms are, e.g., [127, 129, 130, 131, 132, 134, 135]

The most precise estimate for the roughening coupling is $\beta_R = 0.4074(3)$ [37]. This value is consistent with a previous estimate $T_R/T_c = 0.542(5)$ in [35] and also with earlier results cited in [35].

For $\beta_c < \beta < \beta_R$ the interface is rough. It is believed that its infrared properties can be described by a massless Gaussian dynamics. This is the basic assumption of the theory of capillary waves that is widely used to describe long distance properties of rough interfaces, compare section 5.3. A Gaussian behavior in the infrared is also what is expected from a Kosterlitz-Thouless (KT) model in the massless phase [1, 2]. Indeed, it is believed that the roughening transition of the 3-dimensional Ising model is of the Kosterlitz-Thouless type. This belief is strongly substantiated by the renormalization group analysis in [37].

At and above the bulk transition temperature the system properties become independent of the boundary conditions in the infinite volume limit. The interface tension (free energy per unit area of the interface) vanishes like $\sigma \sim \sigma_0 \tau^\mu$, with $\tau = (\beta - \beta_c)/\beta_c$. If Widom scaling holds, the exponent μ should be twice the exponent ν that determines the critical behavior of the correlation length. The most precise estimates for ν are in the range to 0.624...0.630 (for an overview over the results obtained with different methods, see [94] and references cited therein. The amplitude σ_0 is of particular interest because it enters certain universal amplitudes that can also be measured in real life systems.

In this section, we report on a numerical study of properties of the Ising interface over a wide range of temperatures: from the low temperature regime through the rough domain up to the bulk transition region. The focus is mainly on the interface free energy, the interface tension, and on the long distance properties in the rough phase.

The interface free energy is determined by integrating the interface energy over β.[2] We start the integration both at high and at low temperatures and compare the results.

The integration method allows us to include interfaces with extension up to 64×64 in the analysis. Close to criticality we also use a finite step method that allows to directly obtain the change of the interface free energy over a small interval $\Delta\beta$.

From the interface free energies we get estimates for the interface tension σ and make fits with the critical law cited above. We also determine the correlation length ξ in order to study the quantity $\xi^2\sigma$ where the factors $\tau^{-2\nu}$ and τ^μ cancel each other.

In the rough phase, we study the long distance behavior of the interface by measuring block spin correlation functions of suitably defined interface "height variables". An effective coupling β_{eff} (well known in KT theory) is obtained that parameterizes the asymptotic Gaussian dynamics. β_{eff} is related to the interface stiffness coefficient κ that enters the interface Hamiltonian of the capillary wave model.

We also study the interface width. In the rough phase, the squared width is expected to grow logarithmically with the interface extension, with a coefficient that is proportional to β_{eff}. For a simulation at $\beta = \beta_c/0.8$ we verify this behavior with good accuracy.

[2] To the best of our knowledge, this method to obtain interface free energies was first used by Bürkner and Stauffer [31]

5.1.1 Interfacial Properties

We shall give a short account of important interfacial properties: interface width, interface tension and interface stiffness. For the definition of our model, see the first section of chapter 1. Some (but not all) of the definitions given there will be repeated here.

Interface Width

For sufficiently large β and large enough L, the imposure of antiperiodic boundary conditions forces the system to develop exactly one interface, a region where the magnetization rapidly changes from a large negative value to a large positive value. (Situations where more than one interface can occur are discussed below.) An important property of an interface is its width. The definition of the interfacial width is not unique. We adopt the following definition:

A magnetization profile for lattice planes perpendicular to the x_3-direction is defined by

$$M(x_3) = L^{-2} \sum_{x_1,x_2} \sigma_x \,. \tag{5.1}$$

The antiperiodic boundary condition allows us to shift the configuration in x_3-direction such that the interface comes close to $x_3 = 0$. To this end we first roughly locate the interface by looking for the lattice plane where the magnetization profile takes its minimum. Then we shift the configuration such that this position comes close to $x_3 = 0$. Of course, spins have to flipped when passing the antiperiodic boundary at $x_3 = \pm D$ during the shift process.

We introduce an auxiliary coordinate z that assumes half-integer values (labeling positions between adjacent lattice layers perpendicular to the x_3-direction). z takes values $-D+1/2, -D+3/2, \ldots, D-3/2, D-1/2$. Following [35], a normalized magnetization gradient is defined as

$$\rho(z) = \frac{1}{M(D) - M(-D)} \left[M(z+\tfrac{1}{2}) - M(z-\tfrac{1}{2}) \right] \,. \tag{5.2}$$

For a given configuration of the spin field, the position of the interface is defined as the sum over $z\rho(z)$. The square of the interface width is then defined [47, 35] as the expectation value

$$W^2 = \left\langle \sum_z \rho(z)\, z^2 - \left(\sum_z \rho(z)\, z \right)^2 \right\rangle \,. \tag{5.3}$$

Especially on small lattices, fluctuations in the two bulk phases can deteriorate the results. Due to bubbles, $\rho(z)$ can be accidentially large even far away from the interface position. Since such fluctuations contribute to the interface width with a weight proportional to the distance from the interface position, the true signal can disappear in the noise. One possibility to reduce noise that stems from fluctuations of bubbles in the bulk is to take the lattice extension t as small as possible. In the framework of a study based on a Metropolis algorithm, this approach is proposed in [31, 35]. However, one has to be careful not to disturb the free fluctuation of the interface (the properties of which we are interested in). We therefore follow the method proposed

in refs. [37, 132].[3] There it is proposed to implement a procedure to remove the bubbles before measurement of the actual magnetization profile. Note that when the bulk correlation length is small, then also the bubbles are small. One then can assume that the interface width changes little when one removes all bubbles. The procedure is as follows: All nearest neighbor pairs with a saturated bond are frozen together. (A bond with $k_{xy} = +1$ is saturated when the two spins connected by this bond are parallel. A bond connecting top and bottom layer of the lattice, i.e. a bond with $k_{xy} = -1$, is saturated when the spins have different signs.) The freezing procedure defines a configuration of clusters. By flipping all spins sitting in the largest cluster, all first order bubbles (bubbles which do not contain smaller bubbles) are completely removed. Iterating the procedure, one can quickly get rid of all bubbles in the configuration. We denote the interface width (measured as described above) on the bubble free configuration by W_0.

Interface Tension

The interface tension σ of a d-dimensional Ising model is defined by

$$\sigma = \lim_{t\to\infty} \lim_{L\to\infty} \frac{1}{L^{d-1}} (F_I - F_0)\,. \tag{5.4}$$

Here, $F_I = -\ln Z_I$ is the *reduced* free energy of the system (no factor β included) with boundary conditions such that an interface perpendicular to the x_3-direction is introduced at a fixed position. The boundary conditions of the system labeled by the subscript "0" are such that no interface is forced into the system.

There are many possibilities to obtain estimates for the interface tension from Monte Carlo simulations on finite lattices, see the references given at the beginning of this section.

One has to do essentially with two sources of systematic errors that are distinct in nature but intimately related. Effects from too small L and effects from too small t.

To minimize the finite size effects in x_3-direction we choose antiperiodic boundary conditions as described above. These boundary conditions do not fix the position of the interface: it can wander freely in x_3-direction and is less affected by the presence of a boundary compared to a system with fixed "$+-$" boundary conditions. However, it is still important that t is large compared to the width of the interface.

The finite L-effect is as follows: For $\beta_c < \beta < \beta_R$, the interface is rough, which means that its thickness grows like the square root of $\ln L$. This means, that if we go to large interface areas we simultaneously have to increase t in order to avoid strong effects from confining a wildly fluctuating interface to a flat box. On the other hand, if we choose L too small, the formation of more than one interface becomes more likely.

The finite size effects become the stronger the closer one approaches the bulk critical point where no interface survives the thermodynamic limit. This means that close to the bulk critical point one needs large and thick lattices to keep systematic errors under control.

Let us assume that there is only one interface in the system with antiperiodic boundary conditions (referred to by an index a), and that there are no interfaces in the corresponding

[3] Compare also the procedure described in [45]

periodic system (which is referred to by an index p. Then the effect of the free motion of the interface in x_3-direction on the interfacial free energy amounts to adding $\ln t$:

$$F_s = F_a - F_p + \ln t \,. \tag{5.5}$$

What happens to the interface free energy if there are several interfaces in the system? If one assumes that the interfaces do not interact which each other, one finds

$$\tanh\left(\exp(-F_s + \ln t)\right) = \frac{Z_a}{Z_p} \,. \tag{5.6}$$

If we resolve this equation with respect to F_s we get

$$F_s = \ln t - \ln\left(\frac{1}{2}\ln(\frac{1+Z_a/Z_p}{1-Z_a/Z_p})\right) \,. \tag{5.7}$$

In general one has no direct access to the partition function in Monte Carlo simulations. (For not too large systems, the interface free energy can be obtained directly from a Monte Carlo simulation of a statistical ensemble that includes the boundary conditions as dynamical variables. These variables are updated using a modified cluster algorithm [42].) We shall employ two methods to get estimates for the interface free energy.

Note that the derivative of the free energy with respect to the coupling β is a well defined observable,

$$\frac{\partial F}{\partial \beta} = \langle H \rangle \,. \tag{5.8}$$

In the case of a single interface one therefore gets

$$\frac{\partial F_s}{\partial \beta} = \langle H \rangle_a - \langle H \rangle_p \,. \tag{5.9}$$

Here, the expectation values are defined in the systems with periodic or antiperiodic boundary conditions, respectively. Let us introduce the abbreviation

$$E_s = \langle H \rangle_a - \langle H \rangle_p \,. \tag{5.10}$$

The interface free energy can then be obtained by integration over β:

$$F_s(\beta) = F_s(\beta_0) + \int_{\beta_0}^{\beta} d\beta' \, E_s(\beta') \,, \tag{5.11}$$

where β_0 is arbitrary. Our approach is to compute by Monte Carlo simulation the interface energy for β-values ranging from low temperatures around $\beta = 0.6$ up to the bulk critical region around β_c. Note that we can integrate our data starting both from the hot and the cold side since the initial conditions for the integration are known in both cases: For large β we can employ a low temperature expansion for the interface tension by Weeks et al. (published in an

article by Shaw and Fisher [82]) to obtain the interface free energy of an interface *at a fixed position.*[4]

In the thermodynamic limit the interface tension vanishes in the high temperature phase, while it is finite in the low temperature phase. For finite systems the difference $F_a - F_p$ strictly vanishes only at $\beta = 0$ where only the entropy and not the energy enters the free energy. But $F_a - F_p$ will remain negligibly small until β comes close to β_c. For our numerical purpose we set this point where the difference of the energies with periodic and antiperiodic boundary conditions exceeds a certain amount (which we define as the statistical error we can achieve in our simulations). Let us call this coupling β_1.

Starting from β_1 where the difference $F_a - F_p$ is negligible within the obtainable accuracy, we can integrate the energy differences to obtain the free energy for any β. In this case we have $\ln t$ as the integration constant: $F_s(\beta_1) = \ln t$.

An alternative way to determine free energies is to add finite differences in the free energy from small intervals $\Delta\beta$. For sufficiently small $\Delta\beta$ and for not too large transverse lattice extension L we can get the change of the free energy directly from a single Monte Carlo simulation. It is easy to show that

$$F(\beta + \Delta\beta) = F(\beta) - \ln\langle \exp(-\Delta\beta H)\rangle_\beta \,. \tag{5.12}$$

We put an extra subscript β here to make explicit that the expectation value is in the system simulated at inverse temperature β. Results based on the use of eq. (5.12) can be easily checked for accuracy and consistency: by simulating at a certain point β one gets estimates for the free energies in a whole neighborhood of β. Note that one can use negative $\Delta\beta$'s as well. Now assume that we do another simulation at $\beta' > \beta$ not too far away from β. Then we have two sets of estimates for the points between β and β', namely the ones from the simulation at β with positive $\Delta\beta$'s and the ones from the simulation at β' with negative $\Delta\beta$'s. If all the results are consistent (within the statistical accuracy), we assume that the step from β to β' was safe, and we proceed to the next larger β-value.

We shall now describe how we extract estimates for the interface tension σ from the finite L data for the interface free energy F_s. The fundamental definition of σ as given in eq. (5.4) requires to actually perform the limit $L \to \infty$. However, we observed that with very good precision the interface free energy behaves like

$$F_s = C_s + \sigma' L^2 \,. \tag{5.13}$$

This behavior is anticipated on the basis of a description of a rough interface by a massless Gaussian dynamics. We found that eq. (5.13) is obeyed with very good precision already for moderate interface extension L. It is therefore natural to identify the coefficient σ' in eq. (5.13) with the interface tension σ.

Let us discuss how this definition of an interface tension on finite lattices relates to another one used in the literature. In [38], the interface tension is computed via the finite L behavior of

[4] After completion of the present study, the series was extended to 17^{th} order by Arisue [77], cf. section 5.2, eq. (5.45) and table 5.20

the energy splitting in finite volumes E_{0a},

$$E_{0a} = C \exp(-\sigma L^2) \,. \tag{5.14}$$

Note that the constant C is not identical with the constant C_s introduced in eq. (5.13). However, there is an approximate relation between the two constants that can be derived by approximating the Ising system in a long cylinder by a 1-dimensional Ising model with a β-value chosen according to $2\beta = F_s$. (This approximation assumes that the interfaces are sharply defined and do not interact with each other. Both conditions are fulfilled if β and L are large enough.) With the abbreviation $v = \exp(-2\beta)$ one finds

$$E_{0a} = \ln((1+v)/(1-v)) \,. \tag{5.15}$$

For large β one has approximately $E_{0a} \approx 2v$, and thus

$$2v = 2\exp(-C_s - \sigma L^2) \approx C \exp(-\sigma L^2) \,. \tag{5.16}$$

So we finally obtain the relation

$$\ln 2 - C_s \approx \ln C \,. \tag{5.17}$$

Interface Stiffness

In the theory of interfaces the interface stiffness coefficient κ plays an important role. It is defined as follows. In generalization of the interface tension definition given in eq. (5.4) one defines

$$\sigma(\theta) = \lim_{t\to\infty} \lim_{L\to\infty} \frac{1}{L^{d-1}/\cos(\theta)} (F_I - F_0) \,, \tag{5.18}$$

where by suitable boundary conditions in the system "I" a single interface is enforced that makes an angle θ e.g. with the x-axis. Expanding for small inclination angle θ,

$$\sigma(\theta)/\cos(\theta) = \sigma(0) + \sigma'(\theta)\,\theta + \frac{1}{2}\,\kappa\,\theta^2 + \dots \,, \tag{5.19}$$

one defines the stiffness coefficient κ,

$$\kappa = \sigma(0) + \left.\frac{d^2\sigma}{d\theta^2}\right|_{\theta=0} \,. \tag{5.20}$$

(This definition of the interface stiffness is the one used e.g. in [14, 113].)

The coefficient κ plays an important role in the capillary wave model of rough interfaces, see e.g. [113]. Roughly speaking, this model assumes that the interface dynamics of a rough interface is well described by a Gaussian model for interface "height" variables $h(X_1, X_2, ..., X_{d-1})$. The model Hamiltonian is

$$H_{cw} = \frac{1}{2} \int dX_1 dX_2 \dots dX_{d-1} \sum_{i=1}^{d-1} \kappa_i \left(\frac{dh}{dX_i}\right)^2 \,, \tag{5.21}$$

where the κ_i are the stiffness coefficients corresponding to inclinations of the interface with respect to the i'th lattice plane perpendicular to the d'th direction. In our case of a 3-dimensional Ising model on a simple cubic lattice, $\kappa_1 = \kappa_2 \equiv \kappa$, and we define

$$\beta_{\text{eff}} = \frac{1}{\kappa} \,. \tag{5.22}$$

Capillary wave theory then says that the long distance properties should be encoded in a $(d-1)$-dimensional Gaussian model (massless free field theory) with partition function

$$Z_0 = \int \prod_x dh_x \exp\left(-\frac{1}{2\beta_{\text{eff}}} \sum_{<x,y>} (h_x - h_y)^2 \right) \,. \tag{5.23}$$

Long distance properties are most systematically studied via the block spin renormalization group [86]. For the Gaussian model defined through eq. (5.23) one defines block spins $\Phi_{x'}$ as averages over cubic blocks x' of size L_B^{d-1}:

$$\Phi_{x'} = L_B^{-(d-1)} \sum_{x \in x'} h_x \,. \tag{5.24}$$

Usually the renormalization group flow is described in terms of effective Hamiltonians parameterized by effective coupling constants. For our purpose it is sufficient to consider expectation values of block spin observables which can be directly measured with the Monte Carlo method. We define the two quantities

$$A_{1,l}^{(0)} = \left\langle \frac{1}{l^2} \sum_{<x',y'>} (\phi_{x'} - \phi_{y'})^2 \right\rangle \,, \tag{5.25}$$

where x' and y' are nearest neighbors in the block lattice, and

$$A_{2,l}^{(0)} = \left\langle \frac{1}{l^2} \sum_{[x',y']} (\phi_{x'} - \phi_{y'})^2 \right\rangle \,, \tag{5.26}$$

where x' and y' are next to nearest neighbors. l is the extension of the block lattice, i.e. $l = L/L_B$. For the Gaussian model, the A's can be computed exactly with the help of Fourier transformation. The results for a variety of lattice sizes are quoted in table 4.3 of chapter 4. These values are computed for $\beta = 1$. The results for arbitrary β' can be obtained by just multiplying with β'/β.

How do we now do the blocking for the Ising interface? Block spin "height variables" $\bar{h}_{x'}$ are defined as follows: Blocks x' are defined as sets that are quadratic in $x_1 - x_2$ direction with extension $L_B \times L_B$ and that extend through the *whole* lattice in x_3-direction. One block thus contains $L_B^2 t$ lattice points. A magnetization profile and an interface position in a block can be determined exactly as in the case of the full lattice. We define

$$\bar{h}_{x'} = \text{ interface position in block } x' \,. \tag{5.27}$$

Note that the blocked height variables can also be defined "with and without bubbles". Blocked observables for the Ising interface are introduced analogously to eqs. (5.25) and (5.26):

$$A_{1,l}^{(\mathrm{Ising})} = \left\langle \frac{1}{l^2} \sum_{<x',y'>} (\bar{h}_{x'} - \bar{h}_{y'})^2 \right\rangle , \tag{5.28}$$

where x' and y' are nearest neighbors in the block lattice, and

$$A_{2,l}^{(\mathrm{Ising})} = \left\langle \frac{1}{l^2} \sum_{[x',y']} (\bar{h}_{x'} - \bar{h}_{y'})^2 \right\rangle , \tag{5.29}$$

where x' and y' are next to nearest neighbor blocks. For a rough Ising interface, we define an effective coupling β_{eff} as follows:

$$\beta_{\mathrm{eff}} = \lim_{L_B \to \infty} \frac{A_{i,l}^{(\mathrm{Ising})}}{A_{i,l}^{(0)}} , \tag{5.30}$$

We expect that the so defined β_{eff} does not depend on i or l. In Monte Carlo studies we can not really do the infinite L_B-limit. Instead, one has to convince oneself that the results have negligible finite size effects. This can, of course, only be checked within the given statistical accuracy.

5.1.2 Data Analysis and Monte Carlo Results

Interface Free Energies and Interface Tension

As described above, one of our methods to access the interface free energy is to integrate the interface energy over β. Here we now describe how we did this in practice.

We did simulations with antiperiodic boundary conditions in x_3-direction on lattices with $L = 8, 16, 32, 64$ for β-values ranging from the bulk critical region up to $\beta = 0.6$ which is deep in the low temperature domain. For many β-values we made runs with different D to control the effects of a finite thickness of the lattice in x_3-direction. In total, we made more than 250 different simulations with antiperiodic boundary conditions. Typically, we made 10000 measurements of several quantities, separated always by 8 cluster updates and a single Metropolis sweep. A major part of the simulations was done on RISC workstations (≈ 1000 hours).[5]

The simulations supplied us with a sufficiently dense grid of β-values for the energies E_a. For most of the β-values, we fortunately did not have to do extra simulations to access the energies with periodic boundary E_p. Instead we used the diagonal Padé approximation (order of numerator = order of denominator = 12) of the low temperature series by Bhanot et al. [85].[6] By comparing with Monte Carlo simulations we found that this approximation is safe for a sizeable range of β-values, cf. table 5.1. In the table we quote the β-values above which we used the Padé approximant throughout. For smaller β values we used the cluster Monte

[5] For more details on the algorithm and computer performance, see [BB4]

[6] After completion of this study, the series was extended to order 34 by Vohwinkel [84]

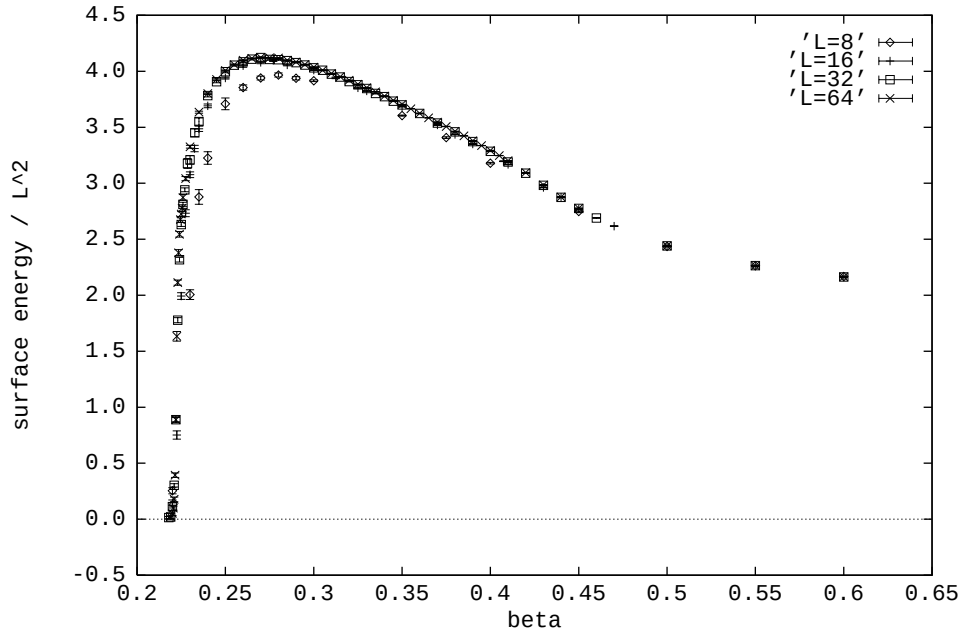

Figure 5.1: The results for the interface energy per area as function of β for spatial lattice extensions $L = 8, 16, 32, 64$. These are the data to be interpolated by splines and integrated over in order to determine the interface free energies

Carlo method to determine E_p. To give an impression of the data we display our results for the interface energies (divided by L^2) in figure 5.1.

In order to do the integration over β we interpolated the data with the help of cubic splines which can easily be integrated over arbitrary intervals numerically. Estimates for the statistical error of the interface free energy were obtained as follows. For each of the β-values, we have an energy value and an error bar. Note that the data for different β are statistically independent. We simulated a whole sequence of outcomes "energy as function of β" by generating independent Gaussian random numbers centered around the Monte Carlo averages and with variances determined by the error bars, respectively. For each of these outcomes, a spline was generated and integrated. The error of the result of the integration (the free energy) was then obtained as the mean square deviation over this "data Monte Carlo".

We employed this method to do the integration over β starting from large β as well as from small β. The integration from large β was always started at $\beta = 0.6$, where the integration constant can be safely taken from the low temperature series for the interface tension. The "initial conditions" for the integration starting at small β were already described in section 5.1.1.

The results for the free energies for $L = 8$, 16, 32 and 64 were then used to make fits with the

L	D	β	MC	Padé	Padé used for ...
8	9	0.2350	1.5381(8)	1.5472	
8	9	0.2400	1.6826(7)	1.6844	
8	8	0.2500	1.9082(20)	1.9083	$\beta \geq 0.26$
16	16	0.2300	1.3849(6)	1.3860	
16	16	0.2325	1.4702(7)	1.4701	
16	16	0.2350	1.5469(6)	1.5472	$\beta \geq 0.24$
32	16	0.2300	1.3839(9)	1.3860	
32	16	0.2327	1.4764(8)	1.4765	
32	16	0.2350	1.5466(8)	1.5472	$\beta \geq 0.24$
64	16	0.2265	1.2498(6)	1.2537	
64	16	0.2275	1.2901(6)	1.2935	
64	16	0.2300	1.3852(5)	1.3860	$\beta \geq 0.235$

Table 5.1: Comparison of Monte Carlo results for energy per site ($= 3\langle s_x s_y \rangle$, with x and y nearest neighbors, periodic boundary conditions) with results from the Padé approximation of the low temperature series. In the last column we quote the β value above which we consider the use of the Padé approximation as safe

ansatz eq. (5.13) to obtain estimates for the interface tension σ. Two typical fits are displayed in figure 5.2. We determined σ's both from the two different integration directions. A subset of our results is displayed in table 5.2. The χ^2's quoted in the last column show that the fits for the data from the integration started at small β have a significantly higher χ^2. We also made fits with the $L = 8$ data excluded, and they had a better χ^2 per degree of freedom (d.o.f.). We conclude that close to the critical point the inclusion of larger lattices might be necessary to give reliable estimates for σ. Our method would allow us to do this.

With figure 5.3, we demonstrate how nicely the results from the two integration directions match within the error bars. The constants C_s, however, show deviations indicating systematic effects which we do not have under control. This, of course, carries over to the approximate determination of the constant C defined in equation (5.17).

In figure 5.4 we display our results for the interface tension σ (the plot shows the quantity σ/β) and the constant C_s as obtained from the integration started at large β.

We also tried to estimate the critical exponent μ that governs the critical behavior of the interface tension. To this end we fitted our results for σ according to the critical law $\sigma = \sigma_0 \tau^\mu$. Since our estimates for the σ's at different β-values are strongly correlated we took the covariance matrix into account when doing the "data Monte Carlo" for the error estimates. We made two sorts of fits: Fits with the definition $\tau = 1 - \beta_c/\beta$ and fits with the definition $\tau = \beta/\beta_c - 1$. We also varied the interval, over which the β dependence of σ was fitted. Our results are shown in tabs. 5.3, 5.4, and 5.5.

The fits were always done using four different β-values. Using more data points would not make very much sense since the data are correlated anyhow. Note however, that our statistical

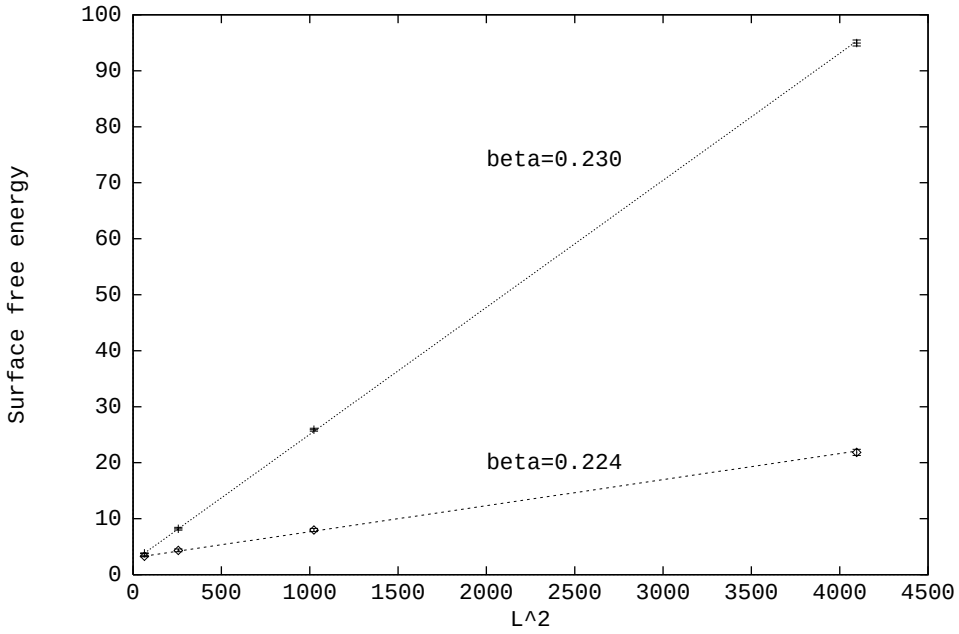

Figure 5.2: Two examples for our results for the interface free energy as function of L. These data are fitted with the law $F_s = C_s + \sigma L^2$ to determine the interface tension

β	type	C_s	σ	$-\ln C$	χ^2/d.o.f
0.225	l	2.885(81)	0.00733(12)	2.192(81)	1.09
	s	2.663(20)	0.007489(38)	1.970(20)	7.45
0.226	l	2.770(83)	0.01014(13)	2.077(83)	1.33
	s	2.539(22)	0.010318(44)	1.846(22)	5.35
0.227	l	2.651(77)	0.01310(12)	1.958(77)	1.27
	s	2.425(21)	0.013303(52)	1.732(21)	4.65
0.228	l	2.554(76)	0.01620(12)	1.861(76)	1.39
	s	2.324(21)	0.016406(55)	1.631(21)	6.16
0.229	l	2.477(81)	0.01938(11)	1.784(81)	1.62
	s	2.235(22)	0.019589(56)	1.542(22)	7.43
0.230	l	2.388(73)	0.02268(11)	1.695(73)	1.84
	s	2.151(21)	0.022863(68)	1.458(21)	6.46
0.231	l	2.298(80)	0.02606(11)	1.605(80)	1.72
	s	2.073(24)	0.026226(63)	1.380(24)	5.82
0.232	l	2.232(76)	0.02952(11)	1.539(76)	1.27
	s	1.999(26)	0.029684(82)	1.306(26)	5.03
0.233	l	2.165(77)	0.03305(11)	1.472(77)	1.25
	s	1.934(25)	0.033221(82)	1.241(25)	5.27
0.234	l	2.097(73)	0.03665(11)	1.404(73)	1.20
	s	1.877(26)	0.036808(89)	1.184(26)	5.24
0.235	l	2.048(69)	0.04025(10)	1.355(69)	1.14
	s	1.831(24)	0.040429(84)	1.138(24)	5.25
0.236	l	1.999(72)	0.04392(11)	1.306(72)	1.13
	s	1.785(31)	0.044077(95)	1.092(31)	5.31
0.237	l	1.947(71)	0.04760(10)	1.281(71)	1.01
	s	1.747(32)	0.047758(85)	1.054(32)	5.68
0.238	l	1.909(75)	0.05133(10)	1.216(75)	1.15
	s	1.707(35)	0.05149(10)	1.014(35)	5.69
0.239	l	1.869(70)	0.05509(10)	1.176(70)	1.08
	s	1.671(30)	0.05524(10)	0.978(30)	5.35
0.240	l	1.840(66)	0.05889(10)	1.147(66)	1.11
	s	1.636(33)	0.05905(11)	0.943(33)	5.68

Table 5.2: Results for the constant C_s and for the interface tension σ. Type l means: obtained by integration starting at large β, type s means: obtained by integration starting at small β. We also quote the logarithm of the constant C defined in section 3.2.3. The last column gives χ^2 per degree of freedom, averaged over the "data Monte Carlo"

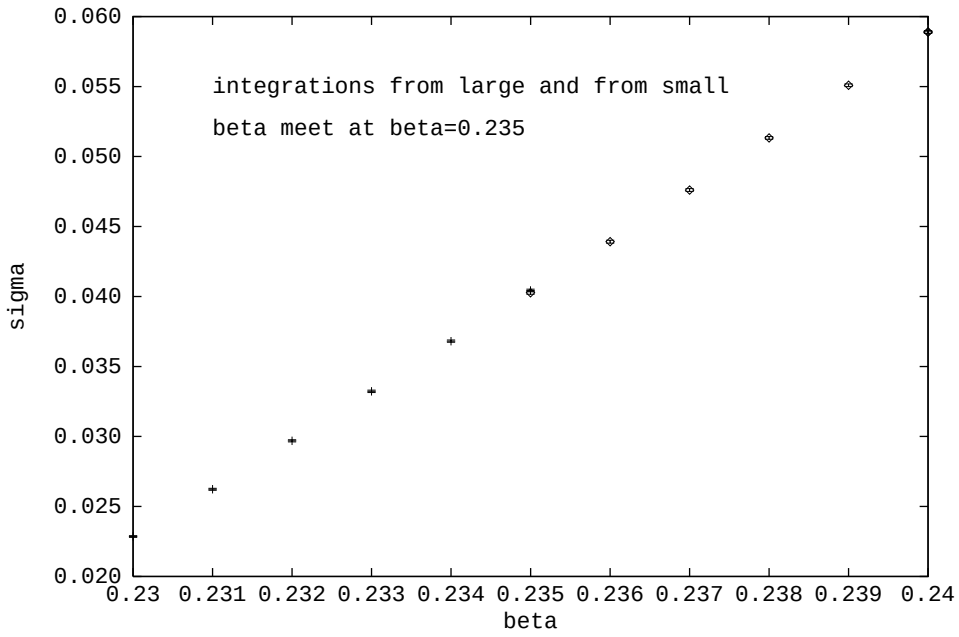

Figure 5.3: With this figure, we demonstrate the consistency of the results for σ obtained from the integration started at large β with that obtained from the integration started at small β. The left half of the figure contains only the "small β" data, whereas the right part contains only the "large β" data. Here they meet at $\beta = 0.235$. (The data from both methods cover the whole β range. We chose this specific presentation only to demonstrate the consistency.) For small β, the $\sigma's$ obtained by integrating from below have smaller error bars

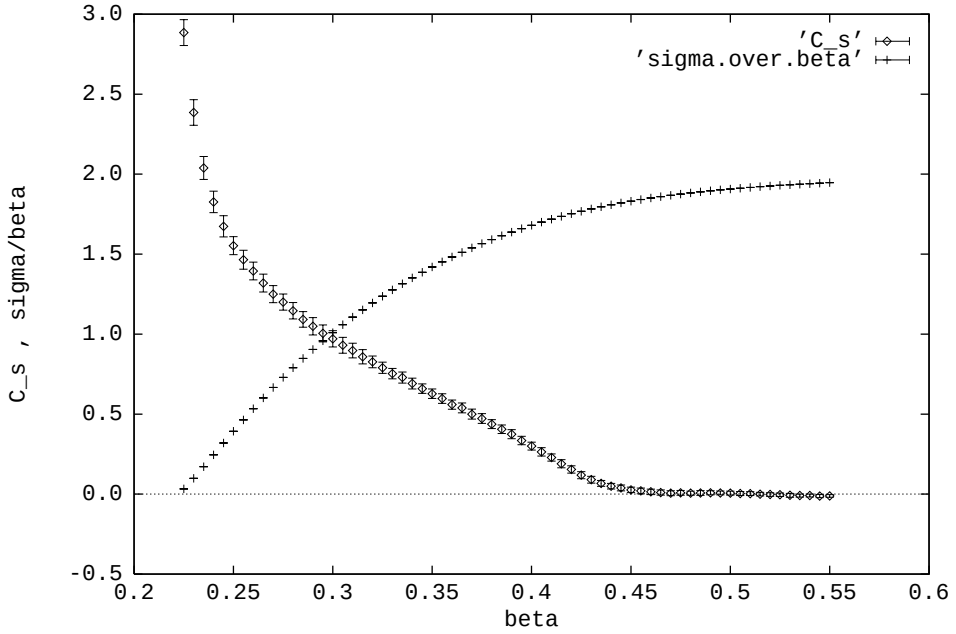

Figure 5.4: Our results for the interface tension σ and the constant C_s. Instead of σ we here plot the ratio σ/β

type of fit	fit interval	all lattice sizes	$-(L=8)$	$-(L=64)$
1	0.224 - 0.2300	1.274(16) [0.27]	1.276(19) [0.52]	1.266(31) [0.13]
2		1.243(15) [0.57]	1.244(18) [0.90]	1.234(30) [0.08]
1	0.224 - 0.2313	1.270(12) [0.21]	1.275(17) [0.35]	1.257(28) [0.19]
2		1.234(11) [0.48]	1.239(17) [0.72]	1.222(27) [0.20]
1	0.224 - 0.2325	1.278(9) [0.38]	1.282(12) [0.67]	1.252(22) [0.25]
2		1.238(9) [1.18]	1.241(11) [1.38]	1.213(21) [0.33]
1	0.224 - 0.2338	1.277(8) [0.25]	1.281(11) [0.52]	1.259(21) [0.28]
2		1.232(7) [1.02]	1.236(19) [1.33]	1.216(20) [0.34]
1	0.224 - 0.2350	1.276(8) [0.57]	1.281(11) [0.59]	1.248(18) [0.43]
2		1.226(8) [0.96]	1.232(19) [1.24]	1.200(17) [0.25]

Table 5.3: Results for the critical exponent μ as obtained from fitting the logarithm of the interface tension with the critical law $\ln\sigma = \ln\sigma_0 + \mu\ln\tau$. For this table we used the σ's from the integration starting at *large* β. Type 1 is a fit with $\tau = 1 - \beta_c/\beta$, and type 2 is a fit with $\tau = \beta/\beta_c - 1$. The fourth and fifth columns give the results using σ's obtained only from subsets of the data ($L = 8$ data excluded or $L = 64$ data excluded, respectively). The fits were done using four equidistant β-values. The numbers in square brackets give the average χ^2 in the "data Monte Carlo", not divided by d.o.f.

type of fit	fit interval	all lattice sizes	$-(L=8)$	$-(L=64)$
1	0.224 - 0.2300	1.252(5) [0.24]	1.268(7) [3.63]	1.240(7) [3.27]
2		1.223(5) [1.07]	1.238(7) [7.41]	1.212(7) [1.21]
1	0.224 - 0.2313	1.253(4) [0.56]	1.266(5) [3.3]	1.242(7) [3.40]
2		1.221(4) [1.30]	1.233(5) [8.5]	1.211(7) [1.31]
1	0.224 - 0.2325	1.254(4) [2.18]	1.268(5) [2.79]	1.244(7) [4.57]
2		1.219(4) [0.87]	1.231(4) [8.58]	1.210(6) [1.72]
1	0.224 - 0.2338	1.257(4) [5.01]	1.270(5) [2.96]	1.246(6) [5.87]
2		1.218(4) [0.86]	1.230(5) [9.34]	1.208(5) [1.40]
1	0.224 - 0.2350	1.261(3) [3.90]	1.269(3) [2.48]	1.249(5) [4.56]
2		1.218(3) [1.83]	1.226(3) [11.11]	1.208(5) [0.70]

Table 5.4: Same as table 5.3, however based on results for σ obtained from the integration starting at *small* β

type of fit	fit interval	all lattice sizes	$-(L=8)$	$-(L=64)$
1	0.224 - 0.2300	0.372(18) [0.24]	0.423(22) [3.63]	0.341(23) [3.27]
2		0.232(17) [1.07]	0.281(22) [7.41]	0.206(22) [1.21]
1	0.224 - 0.2313	0.376(15) [0.56]	0.416(17) [3.30]	0.349(25) [3.39]
2		0.223(15) [1.30]	0.261(17) [8.52]	0.239(24) [1.31]
1	0.224 - 0.2325	0.383(12) [2.17]	0.422(14) [2.79]	0.357(23) [4.57]
2		0.216(11) [0.87]	0.253(13) [8.58]	0.198(21) [1.72]
1	0.224 - 0.2338	0.392(11) [5.01]	0.429(15) [2.96]	0.364(18) [5.87]
2		0.214(11) [0.85]	0.248(14) [9.34]	0.192(16) [1.39]
1	0.224 - 0.2350	0.404(10) [3.90]	0.427(9) [2.48]	0.374(17) [4.56]
2		0.213(10) [1.83]	0.234(9) [11.11]	0.189(16) [0.70]

Table 5.5: Results for $\ln \sigma_0$ as obtained from fitting the logarithm of the interface tension $\ln \sigma$ with the critical law $\ln \sigma = \ln \sigma_0 + \mu \ln \tau$. For this table we used the σ's from the integration starting at *small* β. Type 1 is a fit with $\tau = 1 - \beta_c/\beta$, and type 2 is a fit with $\tau = \beta/\beta_c - 1$. The fourth and fifth columns give the results using σ's obtained only from subsets of the data ($L = 8$ data excluded or $L = 64$ data excluded, respectively). The fits were done using four equidistant β-values. The numbers in square brackets give the average χ^2 in the "data Monte Carlo", not divided by d.o.f

errors are nevertheless correct since our "data Monte Carlo" takes the covariances correctly into account. The comparison of the two different fits (using the two different definitions of τ) clearly shows that there are systematic effects larger than the error bars: one still is not close enough to criticality. However we think that it is fair to say that our results are consistent with the value of $\mu \approx 1.26$ expected from Widom scaling. The results for the critical amplitude σ_0 show even stronger dependency on the type of the fit, and we can not say very much more than that $\ln \sigma_0$ is probably something between 0.2 and 0.4.

The method to compute interface free energies by finite $\Delta\beta$-steps worked quite well. In tabs. 5.6 and 5.7 we present some of our results for the interface free energy on lattices with $L = 8, 16, 32$ and 64. We there display the naive free energy $F_{s,\mathrm{n}}(L)$ obtained by assuming only a single interface, and the "improved" free energy $F_{s,\mathrm{i}}(L)$ that is computed taking into account the presence of several interfaces. For small interface area and for β close to the critical point the difference between the two definitions becomes significant. We also determined estimates for the interface tension σ from the interface free energies. The results are quoted in table 5.8. Again the fits have relatively large χ^2, and in some cases discarding the $L = 8$ data changes the results beyond the statistical error. We again consider this as a warning that too small L's might lead to systematic errors in σ.

In order to study the behavior of the products $\xi^2\sigma$ we tried also to extract the correlation length from the simulations of the systems with periodic boundary conditions. We also tried to compute the correlation length from low temperature series [79, 143]. For details see reference

β	$F_{s,\mathrm{n}}(8)$	$F_{s,\mathrm{i}}(8)$	$F_{s,\mathrm{n}}(16)$	$F_{s,\mathrm{i}}(16)$
0.222	3.026(12)	2.475(43)	3.688(19)	3.337(40)
0.223	3.060(14)	2.589(41)	3.882(24)	3.684(36)
0.224	3.103(16)	2.706(39)	4.200(30)	4.108(36)
0.225	3.156(19)	2.827(39)	4.649(32)	4.614(40)
0.226	3.228(19)	2.964(33)	5.208(35)	5.197(36)
0.227	3.311(20)	3.103(30)	5.849(37)	5.846(37)

Table 5.6: Interface free energies obtained by the step-by-step method, for $L = 8$ and $L = 16$. We here display the naive free energy (subscript n) obtained by assuming only a single interface, and the "improved" free energy (subscript i) that is computed taking into account the presence of several interfaces

β	$F_{s,\mathrm{n}}(32)$	$F_{s,\mathrm{i}}(32)$	$F_{s,\mathrm{n}}(64)$	$F_{s,\mathrm{i}}(64)$
0.222	4.340(28)	4.272(32)	5.82(11)	5.82(11)
0.223	5.706(36)	5.702(37)	12.19(15)	12.19(15)
0.224	7.841(43)	7.841(43)	21.90(17)	21.90(17)
0.225	10.386(48)	10.386(48)	32.78(19)	32.78(19)
0.226	13.179(52)	13.179(52)	44.21(20)	44.21(20)
0.227	16.123(56)	16.123(56)		

Table 5.7: Same as table 5.6, however for $L = 32$ and $L = 64$

β	L's used	C_s	σ	χ^2/d.o.f.
0.227	8,16,32	2.28(3)	0.01356(7)	10.7
0.227	16,32	2.42(5)	0.01338(9)	
0.226	16,32,64	2.61(4)	0.01023(5)	6.2
0.225	16,32,64	2.76(4)	0.00738(4)	4.0
0.224	16,32,64	2.96(4)	0.00469(4)	8.
0.224	32,64	3.16(8)	0.00457(6)	
0.223	16,32,64	3.20(4)	0.00231(4)	34.
0.223	32,64	3.54(7)	0.00211(5)	

Table 5.8: Results of the fit of the form $F_{im} = C_s + \sigma L^2$ for the data obtained by the step-by-step method. The last column gives χ^2 per degrees of freedom

[BB4]. Our estimates are summarized in table 5.9. In figure 5.5 we show our results for the quantity $\xi\tau^\nu$, with $\nu = 0.625$.

Interface Stiffness

In all simulations we measured the block spin correlation functions $A_{i,l}^{(\mathrm{Ising})}$ as defined in section 5.1.1 for $i = 1, 2$ and $l = 2, 4$. We define auxiliary quantities

$$\beta_{\mathrm{eff}}^{i,l} = \frac{A_{i,l}^{(\mathrm{Ising})}}{A_{i,l}^{(0)}}, \tag{5.31}$$

where the $A^{(0)}$'s are taken for $L = 256$ (cf. table 4.3 in chapter 4), which is essentially the infinite block size limit. We thus get eight values that all (in the large L limit) should converge towards the same β_{eff}. In table 5.10 we show two examples for these eight values (for two different values of the lattice thickness t) at $\beta = 0.24$. The values for the different i, l are fairly consistent within the statistical accuracy. Closer to the critical point the estimates from the bubble free configurations are more stable. We therefore decided to use only the bubble free data for the determination of the β-dependence of β_{eff}. In tabs. 5.11 and 5.12 we present our estimates for β_{eff}. The values were determined by averaging over the two quantities $\beta_{\mathrm{eff}}^{i,l}$ with $i = 1$ and $i = 2$. The first two lines of table 5.11 shows that our results become unstable close to the critical point where β_{eff} diverges. For $\beta = 0.43$ and $\beta = 0.45$, both points are in the smooth phase, β_{eff} decreases with increasing block size, in agreement with the Kosterlitz-Thouless picture of the roughening transition. This behavior is consistent with an infinite macroscopic stiffness for $\beta > \beta_R$.

In figure 5.6, we show our results for two combined quantities, namely $\xi^2\sigma$ and $\xi^2\kappa$. In the product $\xi^2\sigma$, the exponents μ and -2ν of the reduced temperature τ should cancel, and we expect that this product should be fairly constant in a neighborhood of the critical point. The full line in figure 5.6 was obtained by combining our $\sigma's$ from the integration method with the

β	L	t	ξ
0.2250	64	65	3.57(10)
0.2275	64	33	2.45(7)
0.2285	32	33	2.16(6)
0.2300	64	33	2.04(6)
0.2327	32	33	1.66(3)
0.2350	32	33	1.48(3)
0.2391	16	23	1.28(3)
0.2400	16	23	1.22(3)
0.2500	16	23	0.92(1)
0.2600	16	11	0.76(1)
0.2700	16	11	0.68(1)
0.2800	16	11	0.61(1)
0.2900	16	11	0.55(1)
0.3000	16	11	0.52(1)
0.3200	8	11	0.46(1)
0.3400	8	11	0.40(1)
0.3600	8	11	0.36(1)

Table 5.9: Results for the correlation length ξ. L and t specify the extensions of the lattices used in the Monte Carlo calculation

i	l	(b) $t = 19$	(nb) $t = 19$	(b) $t = 27$	(nb) $t = 27$
1	2	16.88(44)	16.98(47)	16.94(47)	16.59(46)
2	2	16.82(52)	16.85(52)	16.27(56)	16.06(55)
1	4	16.82(20)	17.18(20)	17.64(22)	16.86(21)
2	4	16.79(23)	17.04(23)	17.35(25)	16.79(24)

Table 5.10: The auxiliary quantities $\beta_{\text{eff}}^{i,l}$ for $\beta = 0.24$ on a $64 \times 64 \times t$ lattice, with (b) and without (nb) bubbles

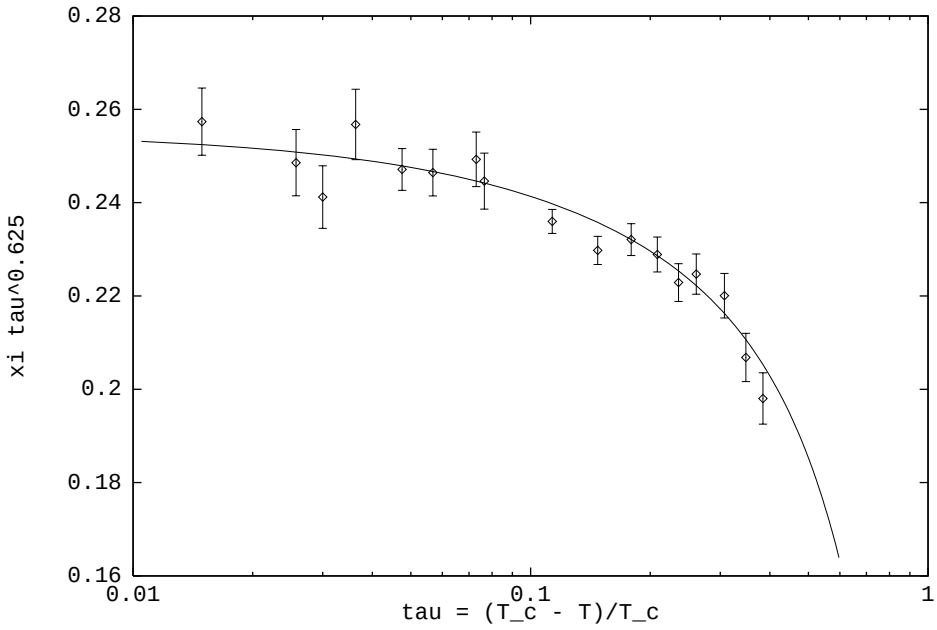

Figure 5.5: Comparison of our Monte Carlo results (points with error bars) for the correlation length in the broken phase with the Padé approximation of the low temperature series of ref. [79] (full line). The figure shows the result for the quantity $\xi\tau^{\nu}$, with $\nu = 0.625$

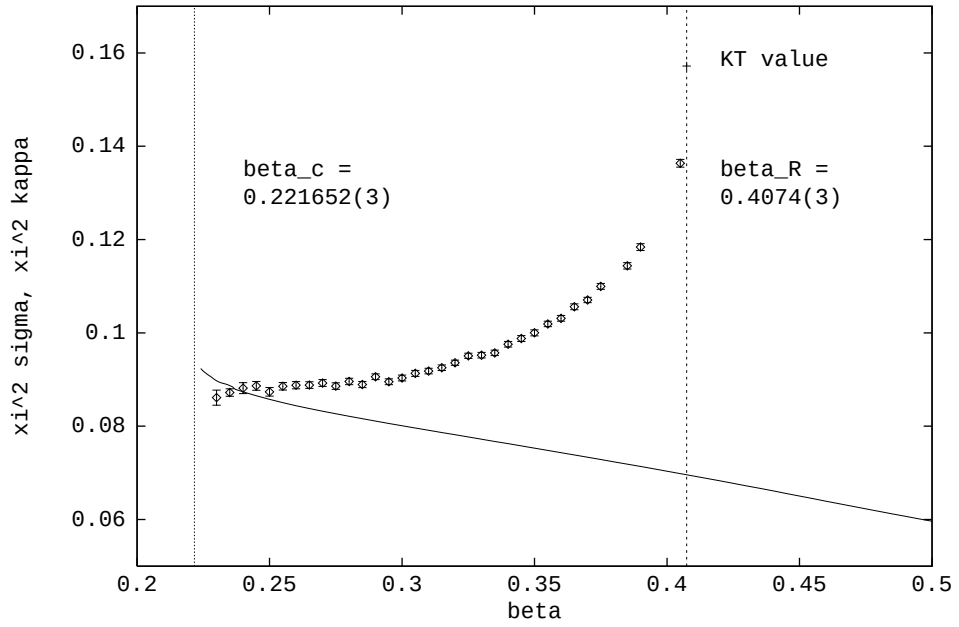

Figure 5.6: Plot of our results for the combined quantities $\xi^2\sigma$ (full line) and $\xi^2\kappa$ (points with error bars). Details are explained in the text

correlation lengths as obtained from the Padé. Since we do not know the error of the Padé approximation of the low temperature series we base our error estimate for this quantity on our error bars for the measured correlation length as reported in table 5.9 and on the statistical errors on the interface tension σ. We estimate the relative precision of our results for $\xi^2\sigma$ to be around 5 per cent for the smaller β's, certainly better in the large β region. This takes into account statistical errors only. There might also be systematic errors (due to too small L's) in the interface tension close to the critical point. They might be responsible for another 5 percent relative uncertainty. The points with error bars in figure 5.6 show the product $\xi^2\kappa$. The plot shows that in the critical limit the interface stiffness becomes the same as the interface tension. This is a consequence of the restoration of rotational symmetry at the bulk critical point.

Using our results for both $\xi^2\sigma$ and $\xi^2\kappa$, we estimate that in the limit $\beta \to \beta_c$ both quantities have the limiting value $R_- = 0.090(5)$. This is in nice agreement with the result obtained in [38], namely $R_- = 0.090(3)$.

In the theory of critical wetting, the following quantity plays an important role [17]:

$$\omega(\beta) = 1/(4\pi\kappa\xi^2)\,. \tag{5.32}$$

In [17] we find an estimate $\omega(T/T_c = 0.8) = 0.88$. Our result $\omega(T/T_c = 0.8) = 0.882(5)$ is in

	$L=16$		$L=32$		$L=64$	
β	$l=2$	$l=4$	$l=2$	$l=4$	$l=2$	$l=4$
0.230			62.3(36)	73.6(89)	45.5 (20)	45.59(86)
0.235	28.84(61)	28.30(43)	28.67(42)	28.65(20)	24.50(72)	25.16(23)
0.240	16.54(22)	16.02(11)	16.99(27)	17.01(12)	16.32(50)	16.83(22)
0.245			12.24(19)	12.42(8)	12.46(32)	12.47(13)
0.250	9.80(13)	9.69(7)	9.68(17)	9.74(7)	9.91(23)	10.00(10)
0.255			8.26(14)	8.12(5)	8.02(17)	8.11(7)
0.260	6.75(9)	6.90(5)	6.89(12)	6.87(5)	6.83(14)	6.85(6)
0.265			5.78(10)	5.95(5)	5.88(11)	5.92(5)
0.270	5.25(7)	5.31(3)	5.19(10)	5.23(4)	5.26(10)	5.18(4)
0.275			4.57(8)	4.63(3)	4.65(8)	4.65(4)
0.280			4.05(8)	4.16(3)	4.13(7)	4.14(3)
0.285	3.81(6)	3.89(2)	3.83(7)	3.81(3)	3.79(7)	3.80(3)
0.290			3.57(7)	3.52(3)	3.43(6)	3.41(2)
0.295			3.21(5)	3.19(2)	3.17(5)	3.19(2)
0.300	2.97(5)	3.01(2)	2.87(5)	2.93(2)	2.96(5)	2.93(2)
0.305			2.71(4)	2.73(2)	2.72(4)	2.70(2)
0.310			2.55(4)	2.53(2)	2.55(4)	2.51(2)
0.315			2.37(3)	2.36(1)	2.33(4)	2.34(2)
0.320			2.15(3)	2.18(1)	2.15(4)	2.18(2)

Table 5.11: β_{eff} for $\beta = 0.24 \ldots 0.32$ as obtained from 2×2 and 4×4 blocking on lattices with $L = 16, 32, 64$. Only bubble free configuration were used. For each value of l, the estimate for β_{eff} was obtained by taking the average of $\beta_{\text{eff}}^{1,l}$ and $\beta_{\text{eff}}^{2,l}$. The data for $\beta = 0.230$ and $\beta = 0.235$ are shown to demonstrate that the results are not yet stable there

	$L=16$		$L=32$		$L=64$	
β	$l=2$	$l=4$	$l=2$	$l=4$	$l=2$	$l=4$
0.325	2.04(3)	2.11(1)	2.03(3)	2.07(1)	2.05(3)	2.03(1)
0.330			1.93(3)	1.95(1)	1.94(3)	1.92(1)
0.335			1.80(3)	1.81(1)	1.79(3)	1.82(1)
0.340			1.71(2)	1.73(1)	1.72(3)	1.70(1)
0.345			1.58(2)	1.62(1)	1.58(2)	1.60(1)
0.350	1.57(3)	1.60(1)	1.53(2)	1.53(1)	1.51(2)	1.52(1)
0.355					1.40(2)	1.42(1)
0.360					1.32(2)	1.35(1)
0.365					1.23(2)	1.27(1)
0.370	1.20(1)	1.28(1)	1.19(1)	1.22(1)	1.19(2)	1.20(1)
0.375					1.13(2)	1.13(1)
0.385					1.00(1)	1.01(1)
0.390	0.94(1)	1.00(1)	0.93(1)	0.96(1)	0.94(1)	0.94(1)
0.405					0.74(1)	0.74(0)
0.410	0.70(1)	0.76(1)	0.66(1)	0.69(1)		
0.430	0.44(1)	0.50(0)	0.35(1)	0.39(0)	0.22(0)	0.27(0)
0.450	0.24(0)	0.31(0)	0.13(0)	0.17(0)	0.05(0)	0.08(0)

Table 5.12: β_{eff} for $\beta = 0.325 \ldots 0.45$ as obtained from 2×2 and 4×4 blocking on lattices with $L = 16, 32, 64$

	$L=32$	$L=64$	$L=128$	$L=256$	$L=512$
W^2	2.341(42)	2.889(42)	3.365(29)	3.855(35)	4.313(60)
				3.811(33)	4.335(64)
W_0^2	3.094(9)	3.619(16)	4.098(20)	4.573(35)	5.059(66)
				4.542(30)	5.069(58)
stat	10000	3000	2430	550 / 820	187/260

Table 5.13: Squared interface width W^2 (measured on configurations with bubbles) and W_0^2 (measured after removal of the bubbles) at $\beta = \beta_c/0.8$ on lattices $L \times L \times 27$. *stat* denotes the number of measurements. Between two subsequent measurements we always performed eight single cluster updates (alternating type O and B) and a single Metropolis sweep. For $L = 256$ and $L = 512$ we show results of two independent runs

nice agreement with this prediction. In the limit $\beta \to \beta_R$, Kosterlitz-Thouless theory states that $\beta_{\text{eff}} \to 2/\pi$. We use the estimate for β_R cited in the introduction, and find $\xi(\beta_{\text{eff}}) = 0.3163$ (from the Padé that here certainly is reliable). We then find a "KT-value" of $\xi^2\kappa$ which is 0.1572.

Interface Width

To check the prediction of the finite size behavior of the interface width (cf. eq. (5.33) below). We redid the interface width computation of Mon et al. [35] at $\beta = \beta_c/0.8 = 0.2771$ on lattices of size $L \times L \times 27$, with $L = 32, 64, \ldots, 512$. Our results for W^2 and W_0^2 are summarized in table 5.13.

We performed fits of the data using the ansatz

$$W^2 = \text{const} + \frac{\beta_{\text{eff}}}{2\pi} \ln L \tag{5.33}$$

that is motivated by Kosterlitz-Thouless theory of a rough interface and that should become precise for large enough L (depending, of course, on β). At the roughening transition at β_R, the amplitude β_{eff} is believed to jump from $2/\pi$ to zero. We performed several fits on subsets of the data. Our results for β_{eff} are summarized in table 5.14. The errors were determined by a "data Monte Carlo" as described in section 5.1.2. We conclude that the $L = 32$ data should not be included in the fit and estimate that $\beta_{\text{eff}} = 4.3(2)$. The corresponding data and the fit are displayed in figure 5.7.

The result has to be compared with the β_{eff} as obtained from the renormalization group quantities A introduced in section 5.1.1. Because of the moderate statistics we used only quantities measured on the bubble free configurations. We computed the auxiliary quantities $\beta_{\text{eff}}^{i,l}$, as defined in eq. (5.31), measured on bubble free configurations only. The quantities $\beta_{\text{eff}}^{i,l}$ should converge to β_{eff} for large L. Our findings are summarized in table 5.15. One should not overemphasize the $L = 512$-results, which suffer a bit from poor statistics. Instead we focus on the

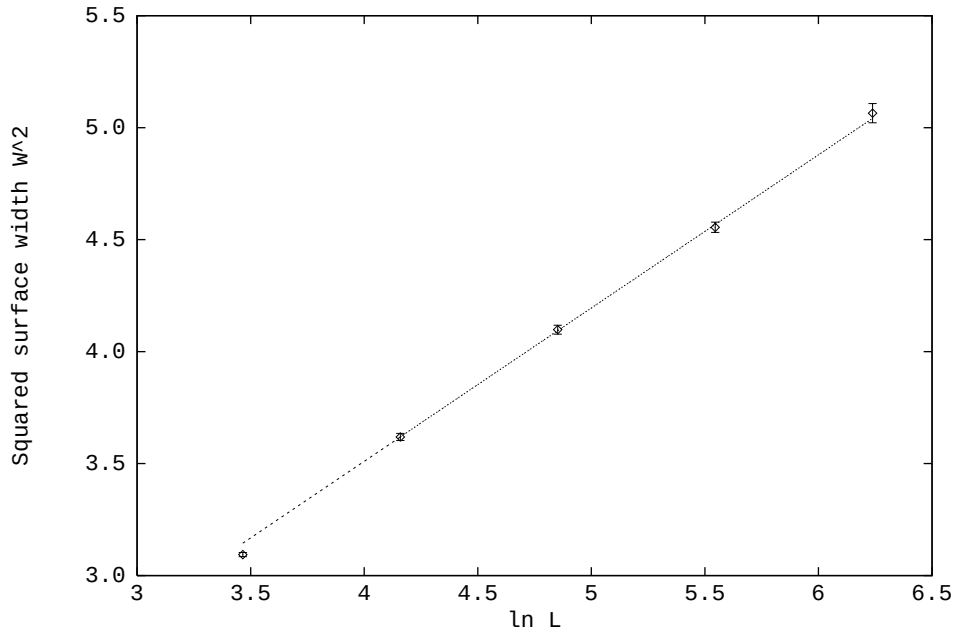

Figure 5.7: Plot of the squared interface width W_0^2 (measured from the configurations without bubbles) versus $\ln L$. The full line shows the fit with $\beta_{\text{eff}} = 4.3$. This fit does not include the $L = 32$ data

data used	all	all – $(L = 32)$	all – $(L = 32, 64)$	all – $(L = 512)$
from W^2	4.45(12) [1.33]	4.30(16) [1.05]	4.30(23) [1.22]	4.44(14) [1.87]
from W_0^2	4.48(6) [2.29]	4.3(1) [1.31]	4.3(2) [1.70]	4.48(6) [3.62]

Table 5.14: Fit results for β_{eff}. The numbers in square brackets give the average χ^2 per degree of freedom in the "data Monte Carlo"

L	$\beta_{\rm eff}^{1,2}$	$\beta_{\rm eff}^{1,4}$	$\beta_{\rm eff}^{2,2}$	$\beta_{\rm eff}^{2,4}$
32	4.50(8)	4.41(9)	4.46(3)	4.45(4)
64	4.7(2)	4.74(20)	4.50(6)	4.48(7)
128	4.04(18)	4.03(21)	4.433(82)	4.434(95)
256	4.26(37)	4.07(39)	4.37(17)	4.35(17)
	3.9(3)	3.8(3)	4.30(15)	4.29(16)
512	4.65(62)	3.16(64)	5.02(35)	4.62(31)
	5.1(6)	5.9(8)	4.25(21)	4.6(3)

Table 5.15: $\beta_{\rm eff}^{i,l}$ for $\beta = \beta_c/0.8$ as obtained from 2×2 and 4×4 blocking on lattices with $L = 32, \ldots, 512$. The quantity $\beta_{\rm eff}^{i,l}$ is defined in the text. For $L = 256$ and $L = 512$ we show results of two independent runs

$L = 128$ and on the $L = 256$ results. Within the statistical accuracy these data are fairly compatible with the value for $\beta_{\rm eff}$ obtained from the interface thickness fits. We interpret our results as a further confirmation that the long distance properties of the Ising interface are correctly described by a massless Gaussian dynamics, that means by uncoupled capillary waves with an energy proportional to the squared wave vector.

To summarize this section: We have presented a numerical study of the Ising interface in three dimensions over a wide range of temperatures. The method to obtain the interface free energies by integration over β requires many separate simulations but turns out to be practicable and useful. Inclusion of large interfaces is possible because of the use of a cluster algorithm also for the simulations with antiperiodic boundary conditions.

Our analysis of the interface tension showed that closer to the critical point large interface extensions L are necessary to get reliable values (σ has a tendency to come out too large when the lattices are too small). A high precision computation of σ_0 and μ seems difficult, the systematic effects from a too large reduced temperature τ are strong.

The large interfaces allowed us to study the infrared interface properties. We could confirm the massless Gaussian behavior in the rough phase and also extract the stiffness coefficient from the renormalization group behavior.

5.2 Monte Carlo Results Versus Extrapolated Low Temperature Expansions

We compare Monte Carlo results for the interface tension and for the interface energy of the 3-dimensional Ising model with Padé and inhomogeneous differential approximants of the low temperature series that was recently extended by Arisue to 17^{th} order in $u = \exp(-4\beta)$. The series is expected to suffer from the roughening singularity at $u \approx 0.196$. The comparison with the Monte Carlo data shows that the Padé and inhomogeneous differential approximants fail to improve the truncated series result of the interface tension and the interface energy in the region around the roughening transition. The Monte Carlo data show that the specific heat displays a peak in the smooth phase. Neither the truncated series nor the Padé approximants find this peak. This section is based on ref. [BB6].

The Ising interface undergoes a roughening transition at an inverse temperature $\beta_R = 0.4074(3)$ [37]. The roughening transition is believed to be of the Kosterlitz-Thouless (KT) nature [1, 2], with the interface free energy having an essential singularity at β_R of the type

$$f_{\text{sing}} \sim \exp[-A(\beta - \beta_R)^{-1/2}]\,. \tag{5.34}$$

Though the free energy and all its derivatives with respect to β stay finite at the roughening point, one has to expect that low temperature series for interface properties suffer from the transition.

The first low temperature expansion of the 3D Ising interface tension σ was given by Weeks et al. to 9^{th} order in the variable $u = \exp(-4\beta)$. Shaw and Fisher [82] analyzed the series with the help of Padé and inhomogeneous differential approximants. They claimed that the Padé and differential approximants allow to compute the interface tension accurately for temperatures below the roughening point.

Recently, Arisue put forward the series to 17^{th} order in u [77]. It is interesting to note that the coefficients of the series change their sign at order 13. This behavior does not come unexpected and confirms that the roughening transition of the Ising interface is of Kosterlitz-Thouless type: Expanding eq. (5.34) in the variable u, one also obtains a series with coefficients that change their sign at a certain order. The order where the change of sign happens depends on the non-universal parameters A and β_R.

In [BB4] (see section 5.1 of this chapter), we reported on a numerical study of properties of the Ising interface over the whole range from low temperatures up to the bulk critical point. In particular we determined the interface energy and, by integration over β, also the interface free energy and interface tension.

In this section, we give a more detailed account of the numerical results and compare them with Padé and inhomogeneous differential approximants for the extended low temperature series. In order to demonstrate that the disagreement of series and numerical data is not due to finite size effects, we provide data for various lattice extensions and demonstrate that the systematic errors in the determination of interface energy and interface tension are under control.

5.2.1 The Model and Quantities Studied

We consider the Ising model on a simple cubic lattice, with the same notation as in the previous section. Let us define

$$G = -\left(\ln Z_a - \ln Z_p\right) , \tag{5.35}$$

where the subscript a (p) means antiperiodic (periodic) boundary conditions. The *interface tension* can be defined as the limit

$$\sigma = \lim_{t\to\infty} \lim_{L\to\infty} \frac{G}{L^2} . \tag{5.36}$$

With numerical simulations only a rather limited range of L and t values is accessible. Hence a careful discussion of finite size effects is needed. Let us express the partition functions of the periodic and antiperiodic Ising system in terms of the transfer matrix $\mathbf{T}$. The antiperiodic boundary conditions are represented by a spin-flip operator $\mathbf{P}$ that flips the sign of all spins in a given x_3-slice.

The partition function of the periodic system is given by $Z_p = \mathrm{Tr}\mathbf{T}^t$, while the partition function of the antiperiodic system is given by $Z_a = \mathrm{Tr}\mathbf{T}^t\mathbf{P}$. The operators $\mathbf{T}$ and $\mathbf{P}$ commute and thus have a common set of eigenfunctions. Say the eigenvalues of $\mathbf{T}$ are λ_i and those of $\mathbf{P}$ are p_i. The possible values of p_i are 1 and -1. The partition functions take the form $Z_p = \sum_i \lambda_i^t$ and $Z_a = \sum_i \lambda_i^t p_i$.

Let us consider the ratio of the partition functions in the broken phase of the model. Here the two largest eigenvalues λ_{0s} and λ_{0a} are much larger than the other eigenvalues [144]. (The subscripts s and a label eigenfunctions with $p = 1$ and $p = -1$, respectively.) Hence the ratio of the two partition functions can be well approximated by

$$\frac{Z_a}{Z_p} \simeq \frac{\lambda_{0s}^t - \lambda_{0a}^t}{\lambda_{0s}^t + \lambda_{0a}^t} . \tag{5.37}$$

The corrections are of order $(\lambda_{1s}/\lambda_{0s})^t$. This means that the extension t of the lattice in x_3-direction has to be much larger than the bulk correlation length ξ. For $\xi_{0a} >> t$ ($\xi_{0a} = -1/\ln(\lambda_{0a}/\lambda_{0s})$ is the tunneling correlation length) we can write

$$\frac{Z_a}{Z_p} \simeq \frac{t}{2}\left(1 - \frac{\lambda_{0a}}{\lambda_{0s}}\right) . \tag{5.38}$$

Note that within this approximation the derivative of G with respect to β does not depend on t.

According to this discussion, if $\xi << t << \xi_{0a}$ then already for finite L an interface free energy is rather well defined by

$$F_s \simeq G + \ln t . \tag{5.39}$$

Phenomenologically one can interpret this situation as follows: The lattice is short enough that the creation of interfaces in the system with periodic boundary conditions is sufficiently suppressed while for the system with antiperiodic boundaries only the interface induced by the

boundary conditions is present. On the other hand the extension of the lattice is large enough not to restrict the fluctuations of the interface.

In order to discuss the L dependence of the interface free energy a model for the interface is needed.

Theoretical studies of the interface are based on the SOS (solid-on-solid) approximation which essentially neglects overhangs and bulk fluctuations. SOS models predict that the roughening transition is of the Kosterlitz-Thouless type (cf. chapters 1 and 2).

That the Ising interface at the roughening point is indeed in the same universality class as various SOS models was demonstrated by Hasenbusch using a renormalization group matching procedure [37]. For large β there are also rigorous results from linked cluster expansions. Borgs and Imbrie have shown [106] for sufficiently large β, i.e., when the interface is smooth, that

$$F_s \simeq \sigma L^2 . \tag{5.40}$$

It is believed that this result holds for all $\beta > \beta_R$.

A model for the interface in the rough phase is the capillary wave model [113]. In its quadratic approximation it essentially states that the infrared fluctuations of the interface are massless Gaussian. This assumption has been verified numerically in a number of cases, see e.g. [BB4] and also section 5.3 of this chapter. The massless Gaussian dynamics leads to the following finite L behavior of the interface free energy in the rough phase [145, 15, 112, 114]:

$$F_s \simeq C_s + \sigma L^2 . \tag{5.41}$$

Gelfand and Fisher [111] predicted in addition a logarithmic dependence of the interface free energy on the lattice size. They did not take into account a prefactor L in the partition function that arises when the average position of the interface is fixed via a δ-function.

At the roughening transition one has still a Gaussian fixed point, however, with logarithmic corrections. Hence eq. (5.41) should be still valid for sufficiently large L.

It is difficult to compute free energies directly by Monte Carlo (however, cf. [42]). But the derivative of G with respect to β is a quantity that can be computed by Monte Carlo:

$$\frac{\partial G}{\partial \beta} = \langle H \rangle_a - \langle H \rangle_p \equiv E_s . \tag{5.42}$$

G can then be obtained by integration over β:

$$G(\beta) = G(\beta_0) + \int_{\beta_0}^{\beta} d\beta' \, E_s(\beta') , \tag{5.43}$$

where β_0 is arbitrary. In the case that there is only one interface in the system, E_s is the *interface energy*. The interface energy per area is defined as

$$\epsilon_s = E_s / L^2 . \tag{5.44}$$

In [BB4] (see section 5.1) we used the method of 'integration over β' to determine the interface free energies for a wide range of temperatures, for $L = 8, 16, 32, 64$. We found that the interface free energy can be fitted accurately with eq. (5.41). We thus identify the coefficient σ in front of the factor L^2 with the *interface tension*.

5.2.2 Monte Carlo Algorithms

For the production of the Monte Carlo results of ref. [BB4] and for part of the new results to be presented below we employed the cluster algorithm of Hasenbusch and Meyer [132]. A detailed description of this algorithm can be found in [BB4].

When the focus is on the determination of the energy with antiperiodic boundary conditions, it is helpful to use a local algorithm instead of the cluster algorithm. It is much easier to adapt a local Monte Carlo algorithm for vectorization, parallelization or multi-spin coding.

It turns out that the energy of the system with antiperiodic boundary conditions does almost not couple to the slow modes of the local algorithm.

For the update of the 3-dimensional Ising model we therefore also used a micro-canonical demon algorithm [124, 125, 126] in combination with a particularly efficient canonical update [136] of the demons. The algorithm was implemented using the multi-spin coding technique [125, 126]. Every bit of a computer word carries one Ising spin. In order to avoid restrictions of the geometry of the systems 32 independent systems are run in parallel. For more details see [BB5].

5.2.3 Discussion of Results

The Interface Energy. We first explain how we obtained estimates for the interface energy defined in eq. (5.42). The quantity $\langle H \rangle_a$ was always computed using either the interface cluster algorithm or the local demon algorithm. For the determination of the energy with periodic boundary conditions we used a Padé approximant of the low temperature series for the energy (for details cf. [BB4]). The series was extended to order 24 in $u = \exp(-4\beta)$ by Bhanot et al. [85] and a little later to order 32 by Vohwinkel [84]. In [BB4], we found by comparing with Monte Carlo results, that the use of the Padé approximation was safe for $\beta \geq 0.26$ for $L = 8$, $\beta \geq 0.24$ for $L = 16$ and $L = 32$, and for $\beta \geq 0.235$ for $L = 64$. For the range of couplings that we want to focus on in this paper ($\beta \geq 0.35$), the use of the Padé approximant is safe (for the accuracy required).

When computing the interface energy per area ϵ_s one has to deal with systematic effects from the finite extension of the lattice in t- and in L-direction.[7].

First we carefully studied the t-dependence of the interface energy for three different β-values, namely $\beta = 0.45$ (which is in the smooth phase of the interface), $\beta = 0.4074$ (the roughening point) and $\beta = 0.3500$ (which is in the rough phase of the interface, but still far away from the bulk critical point). The results for ϵ_s for interfaces with extension $L = 4, 8, 16, 32, 64$ and for lattices with various values of t are quoted in the tables 5.16, 5.17 and 5.18. The statistics is as follows: For the runs with the cluster algorithm we performed 400 000 measurements, separated by an update step made up from generating and flipping 8 clusters of two different types, cf. [BB4], and a subsequent Metropolis sweep. For the runs with the demon algorithm we made 100 000 measurements on each of the 32 independent copies, separated by always 5 cycles as described in section 5.2.2. For some sets of parameters we made runs with two different random

[7] For a study of finite size effects in a previous high precision simulation performed by Ito see [41]

number generators and found perfect consistency. As a further check we compared Monte Carlo results for $L = t = 4$ with the *exact* result for the energy.

t	$L = 4$	$L = 8$	$L = 16$	$L = 32$	$L = 64$
2	2.67433(63)	2.78942(42)	2.83759(30)	2.85006(21)	2.85225(12)
3	2.66940(57)	2.75544(34)	2.77860(21)	2.78114(11)	2.781092(56)
4	2.66799(63)	2.75238(38)	2.77445(23)	2.77717(13)	2.776936(68)
5	2.66775(57)	2.75246(35)	2.77440(20)	2.77677(11)	2.776790(64)
9	2.6700(16)	2.7517(9)	2.7746(5)		
10	2.66645(75)	2.75223(42)	2.77442(25)	2.77683(15)	2.776835(83)
17	2.6688(19)	2.7541(11)	2.774(1)		

Table 5.16: Ising interface energy at $\beta = 0.4500$

An inspection of the tables reveals that (for fixed L) the estimates for ϵ_s are consistent within error bars for $t \geq 4$ and $\beta = 0.45$. For $\beta = 0.4074$ we find consistency for $t \geq 5$ if $L \leq 32$ and for $t \geq 6$ if $L = 64$, cf. the discussion of finite t effects in section 5.2.1. In this context it might be interesting to note that the bulk correlation length ξ which governs the exponential decay of the connected correlation function is 0.2809 for $\beta = 0.45$. For $\beta = 0.4074$, one has $\xi = 0.3162$, and for $\beta = 0.35$ the correlation length is $\xi = 0.3897$. These estimates are based on a Padé evaluation of a low temperature series by Arisue and Fujiwara [79]. Correlation length estimates from the series truncated at 13^{th} order for $\beta = 0.35$ differ from the Padé approximants in the third digit.

Using the safe values of t found for the smaller β-values we computed the interface energies presented in table 5.19 for the range from $\beta = 0.35$ to $\beta = 0.6$ in steps of 0.01 or 0.005. The table also contains estimates for the $L = \infty$ interface energy from the low temperature series, truncated at 17^{th} and at 12^{th} order, cf. the discussion below.

Concerning the convergence of the interface energies to the infinite L limits we make the following observations: For $\beta \geq 0.45$ we find that (within the statistical accuracy obtained) the estimates converged well, consistent with exponentially small L-corrections. Of course, the convergence becomes better for larger β.

In the rough phase the interface energy is expected to behave like $A + B\,L^2$. We fitted the $\beta = 0.35$ data for $L \geq 8$ and $t = 13$ with this ansatz and found $A = -5.96(47)$ and $B = 3.70428(9)$ with $\chi^2/\mathrm{dof} = 1.135$.[8]

At the roughening transition the situation is more difficult. We studied the differences $E_s(2L) - E_s(L)$ for $L \leq 64$ and found that this quantity scales down with a factor of at least 3 always when L is doubled. This gives us confidence that $E_s(\infty) - E_s(128)$ is not bigger than $E_s(128) - E_s(64) = 0.0022(1)$.

Comparison with Extrapolated Series. The estimates for the interface energies can be compared with results from the low temperature expansion of the same quantity. The series for

[8] Infinite L-extrapolations according to the law $A + B\,L^2$ for data in the rough phase were also done by Ito [41]

t	$L=4$	$L=8$	$L=16$	$L=32$	$L=64$
2	2.9542(7)	3.2408(5)	3.42063(27)	3.48668(12)	3.492507(59)
3	2.9479(7)	3.14030(37)	3.21718(22)	3.24322(12)	3.25120(7)
4	2.9419(8)	3.1244(4)	3.19578(24)	3.21901(14)	3.226227(83)
5	2.9414(7)	3.12342(37)	3.19428(22)	3.21745(12)	3.224334(62)
6	2.9427(8)	3.1230(5)	3.19410(24)	3.21735(14)	3.224389(83)
9	2.9384(20)	3.1235(11)	3.1936(6)	3.21723(30)	
10					3.224219(88)
11	2.9520(10)	3.1237(5)	3.19443(28)	3.21756(16)	
17	2.9431(25)	3.1247(14)	3.1941(7)		
33			3.1946(9)		

Table 5.17: Ising interface energy at $\beta = 0.4074$. We made an additional run with $L = 128$ and $t = 11$. The result for the interface energy is 3.226375(45)

t	$L=4$	$L=8$	$L=16$	$L=32$	$L=64$
2	3.3173(7)	3.69719(30)	3.77344(14)	3.77574(7)	3.775673(34)
3	3.3684(8)	3.70942(48)	3.85405(31)	3.92648(21)	3.95577(11)
4	3.3479(9)	3.62530(50)	3.70230(29)	3.72218(16)	3.726973(76)
5	3.3432(9)	3.61092(48)	3.68357(28)	3.70146(14)	3.705558(61)
6	3.3437(11)	3.60982(55)	3.68145(28)	3.69886(16)	3.703239(76)
7	3.3446(13)	3.61025(63)	3.68106(32)	3.69870(17)	3.702884(85)
9	3.3431(28)	3.6094(15)	3.6816(8)	3.69854(39)	
13	3.3440(16)	3.61122(78)	3.68080(39)	3.69851(20)	3.70282(10)
17	3.3411(38)	3.6102(19)	3.6836(10)		

Table 5.18: Ising interface energy at $\beta = 0.3500$

β	$L=8$	$L=16$	$L=32$	$L=64$	S_{17}	S_{12}
0.350	3.61122(78)	3.68080(39)	3.69851(20)	3.70282(11)	4.59933	5.77307
0.360	3.53379(70)	3.60450(36)	3.62157(19)	3.62574(9)	4.47093	5.09037
0.370	3.45279(67)	3.52385(35)	3.54189(18)	3.54621(9)	4.23424	4.56179
0.380	3.36878(64)	3.44095(33)	3.46002(16)	3.46462(8)	3.97351	4.14707
0.390	3.28038(59)	3.35522(34)	3.37550(16)	3.38049(7)	3.72531	3.81746
0.395			3.33163(16)		3.61065	3.67785
0.400	3.19154(55)	3.26458(30)	3.28669(16)	3.29260(8)	3.50320	3.55224
0.405			3.24002(15)		3.40309	3.43889
0.410	3.09971(53)	3.16889(29)	3.19217(16)	3.19938(9)	3.31017	3.33632
0.415		3.11972(29)	3.14166(16)		3.22415	3.24326
0.420	3.00972(50)	3.06903(29)	3.09000(17)	3.09669(11)	3.14463	3.15860
0.425		3.01806(28)	3.03614(18)		3.07117	3.08140
0.430	2.91929(48)	2.96759(27)	2.98205(18)	2.98512(11)	3.00334	3.01083
0.435		2.91664(28)	2.92813(18)		2.94069	2.94618
0.440	2.83342(47)	2.86806(27)	2.87502(16)	2.87575(9)	2.88278	2.88681
0.445		2.82025(26)	2.82450(16)		2.82923	2.83218
0.450	2.75223(42)	2.77442(25)	2.77682(15)	2.77683(8)	2.77965	2.78182
0.455		2.73093(23)	2.73180(14)		2.73370	2.73529
0.460	2.67688(41)	2.68951(23)	2.68978(14)	2.68991(7)	2.69107	2.69224
0.465		2.65063(21)	2.65065(13)		2.65148	2.65234
0.470	2.60753(38)	2.61440(20)	2.61426(13)	2.61408(6)	2.61465	2.61528
0.475			2.57979(12)		2.58036	2.58083
0.480	2.54599(36)	2.54823(19)	2.54813(12)	2.54813(6)	2.54840	2.54874
0.485			2.51866(11)		2.51856	2.51882
0.490	2.48992(32)	2.49041(18)	2.49060(10)	2.49054(5)	2.49068	2.49087
0.500	2.44055(30)	2.44052(18)	2.44014(10)	2.44014(5)	2.44018	2.44028
0.510	2.39611(28)	2.39613(18)	2.39578(9)		2.39580	2.39586
0.520	2.35725(25)	2.35658(17)	2.35657(8)		2.35665	2.35668
0.530	2.32212(23)	2.32219(16)	2.32208(8)		2.32198	2.32200
0.540	2.29135(23)	2.29123(14)	2.29129(7)		2.29118	2.29119
0.550	2.26399(20)	2.26403(14)	2.26363(7)		2.26374	2.26375
0.560	2.23930(20)	2.23943(13)	2.23904(7)		2.23922	2.23923
0.570	2.21751(19)	2.21728(12)	2.21724(6)		2.21726	2.21726
0.580	2.19748(19)	2.19757(11)			2.19755	2.19755
0.590	2.17986(17)	2.17989(11)			2.17981	2.17981
0.600	2.16378(17)	2.16387(10)			2.16383	2.16383

Table 5.19: Ising interface energy, Monte Carlo and truncated low temperature series results (S_i corresponds to truncation at i^{th} order)

the interface tension is

$$\sigma = 2\beta + \sum_{n=2}^{17} a_n \, u^n + \mathcal{O}(u^{18}) \, . \tag{5.45}$$

The coefficients up to order u^9 in the low temperature variable $u = \exp(-4\beta_{\rm Ising})$ were first determined by Weeks et al. They can be found in a paper by Shaw and Fisher [82]. The higher coefficients (order u^{10} through u^{17}) were computed recently by Arisue [77]. The coefficients a_n are quoted in table 5.20. In order to get ϵ_s from σ, one has to differentiate eq. (5.45) with respect to β. The result is a power series in u (there is no longer a term $\ln(u)$ present). We compared the truncated series and its Padé approximants with the Monte Carlo results as follows: For order k, with $7 \le k \le 17$, we plotted the result of the truncated series (truncated at order k) together with the results of 4 or 5 close-to-diagonal Padé approximants $[m/n]$, with $m+n=k$. For even k we took the five Padeś with $m = k/2-2, \ldots, k/2+2$, for odd k we took the four Padés with $m = (k-1)/2-1, \ldots, (k-1)/2+2$. In all figures the truncated series estimates are plotted with a '+' and connected with a broken line. For the Padé estimates we use diamonds. On the right hand side of the plots we present our Monte Carlo estimates of the interface energy for different lattice sizes. The $L = 64$ result is also plotted with two horizontal lines for easier comparison with the series results.

n	$a_n^{\rm Ising}$
2	– 2
3	– 2
4	– 10
5	– 16
6	– 242/3
7	– 150
8	– 734
9	– 4334/3
10	– 32122/5
11	– 10224
12	– 106348/3
13	+ 53076
14	+ 3491304/7
15	+ 74013814/15
16	+ 27330236
17	+ 160071418

Table 5.20: Coefficients of the low temperature series for the 3D Ising interface tension as computed by Arisue [77]

Figure 5.8 shows this comparison for $\beta = 0.50$ which is in the smooth phase of the interface

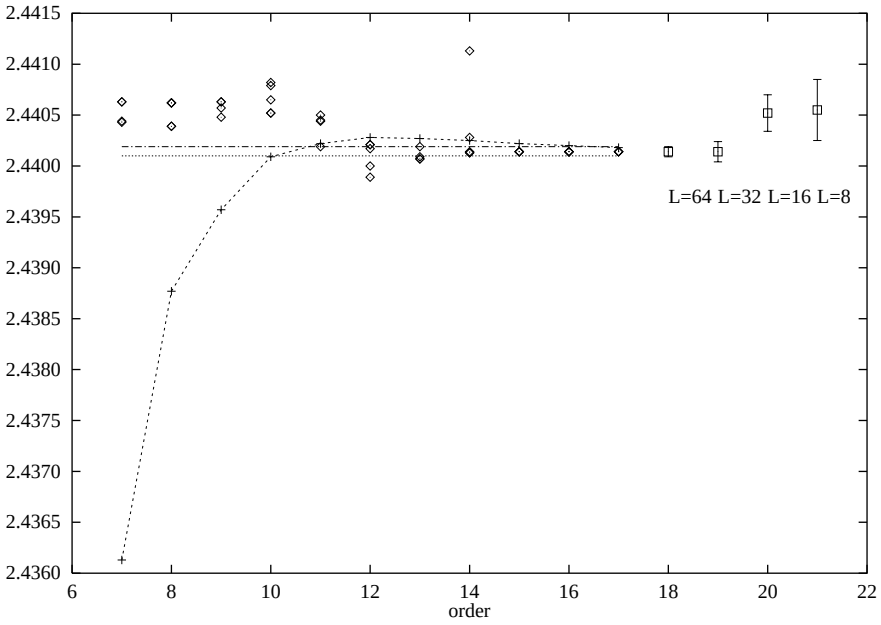

Figure 5.8: Ising interface energy at $\beta = 0.5000$ from Padé, truncated series and Monte Carlo. Truncated series estimates are plotted with a '+' and connected with a broken line. The close to diagonal Padé estimates are given with diamonds. The data with error bars present our Monte Carlo results for the different lattice sizes. The $L = 64$ estimate is also given by two horizontal lines.

and far away from the roughening transition. For order ≥ 16 the truncated series and the Padé approximants have become consistent with the Monte Carlo estimate. Note however, that there is no apparent advantage in using the Padé approximants instead of the truncated series.

$\beta = 0.45$ is still in the smooth phase. The comparison is summarized in figure 5.9. Notice the much larger scale of the y-axis in this plot compared to figure 5.8. The Padé approximants scatter a lot, especially around order 13 where the series changes its sign. If one looks only at order ≤ 12, the truncated series seems to be even superior to the Padé approximations.

The scenario becomes even more drastic if one proceeds to the roughening region. In figure 5.10 we show the comparison of the different approximations at the roughening point $\beta = 0.4074$. Here obviously neither the truncated series nor the Padé approximants lead to a reasonable approximation.

The Interface Tension. The estimates for the interface tension quoted in this paper were obtained with the method described in [BB4].

However, for the β-range above 0.35 we used the new and much more precise estimates for the

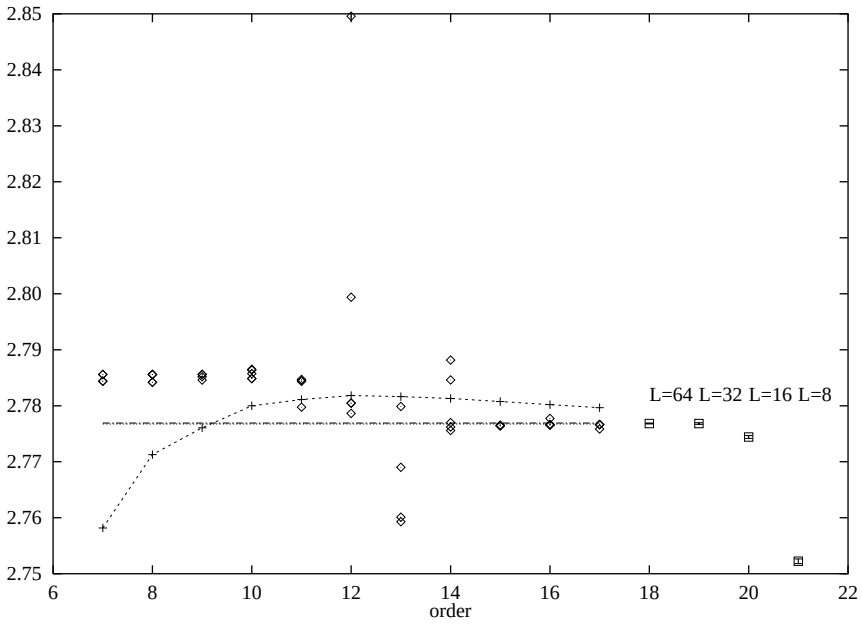

Figure 5.9: Ising interface energy at $\beta = 0.4500$ from Padé, truncated series and Monte Carlo. The symbols are the same as in figure 5.8

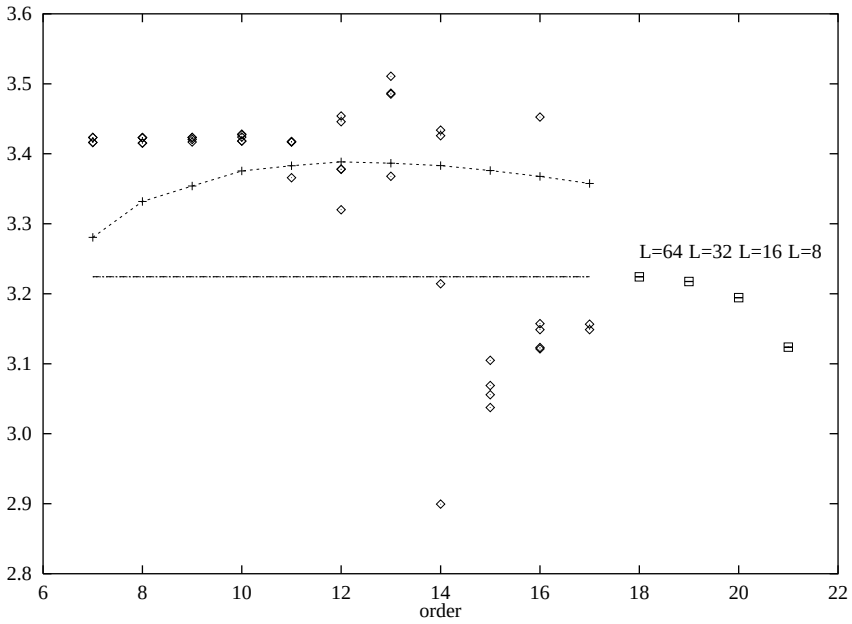

Figure 5.10: Ising interface energy at $\beta = 0.4074$ from Padé, truncated series and Monte Carlo. The symbols are the same as in figure 5.8

interface energy as quoted in table 5.19. From the results for the interface energy we determined the interface tension using the method of 'integration over β' as outlined in section 5.2.1. In [BB4] we used two different starting points β_0 for the integration, namely $\beta_0 \approx \beta_c$ and $\beta_0 = 0.6$. Both methods yielded compatible results. In table 5.21 we quote our new results obtained by starting the integration at the following β values: For $L = 8$ and $L = 16$ we took $\beta_0 = 0.545$, for $L = 32$ we used $\beta_0 = 0.515$, and for $L = 64$ we started the integration at $\beta_0 = 0.495$. The starting point was determined such that the Monte Carlo interface energy estimate and the 17^{th} order low temperature series for the same quantity are consistent within the present error bars. Note that the errors quoted in table 5.21 are statistical errors (1σ error bars) that do not include systematic effects. The estimates rely on fits of the finite L behavior of the free energy with the law $C_s + \sigma L^2$.

For the estimation of systematical errors we used the following procedure: One defines

$$\sigma(L) = F_s(L)/L^2 \,. \tag{5.46}$$

By the very definition this quantity converges to the interface tension in the infinite L limit, however, with stronger finite size effects than definition eq. (5.41). So looking at the variation of $\sigma(L)$ gives one a feeling of the maximal systematic error possible.

It is also instructive to obtain estimates for σ based on the law eq. (5.41), however, using just pairs of adjacent L-values. Then no fit is needed. In table 5.22 we quote these quantities for $\beta = 0.402359$ (which corresponds to $u = 0.2$) and for $\beta = 0.45$. We adopt the following rule for the estimation of a systematical error: Take the estimates for σ from the pair $L = 16, 32$ and from the pair $L = 32, 64$ and compute the difference. Take this as the systematic error of the interface tension determined with the fit method. For the two examples studied in table 5.22 we conclude that for $\beta = 0.45$ the systematic error is smaller than the statistical error. For $\beta = 0.402359$ we arrive at $\sigma/(2\beta) = 0.84487(3)$.

In figs. 5.11 and 5.12 we show the comparison of the Monte Carlo results for the two β values quoted above[9] with the truncated series and the Padé approximations. The Padés were not performed directly for the series for σ but (as in [82]) for the quantity $Q(u) = u \exp(2\sigma)$.

The conclusions are similar to the ones for the interface energy. Figure 5.12 demonstrates the trap one can get into when the series is too short. Shaw and Fisher might have been misled by the convergence and consistency of the Padé and differential approximants at order 9 and concluded that the interface tension could well be approximated by Padés of ninth order for temperatures below the roughening temperature. The now longer series shows that this is a wrong conclusion. Note that the Padés seem to converge again at the by now highest available order. But still, the value is definitely off from our Monte Carlo estimate.[10]

Shaw and Fisher pointed out that the use of inhomogeneous differential approximants [83] might be superior to using Padés. In fact, these approximants generalize Padés and are suitable

[9] We chose $u = 0.2$ ($\beta = 0.402359$) for easier comparison with the work of Shaw and Fisher. We compared our Monte Carlo results with the series extrapolations also at the more recent estimate $\beta_R = 0.4074$, with the same conclusions

[10] A preliminary Padé analysis for the interface tension was already performed by Arisue in [77]. His results are perfectly consistent with ours. However, he could not compare with an independent Monte Carlo result

β	$\sigma/(2\beta)$	X	β	$\sigma/(2\beta)$	X	β	$\sigma/(2\beta)$	X
.225	.01629(30)	2.3	.315	.575804(38)	7.0	.405	.8499891(27)	6.2
	.01622(25)	2.0		.575824(38)	5.8		.8499979(26)	21.5
.230	.04929(25)	4.8	.320	.597570(31)	6.9	.410	.8592883(27)	2.1
	.04921(20)	3.0		.597585(35)	6.5		.8592906(22)	3.2
.235	.08565(18)	1.9	.325	.618399(28)	5.6	.415	.8680694(26)	2.0
	.08562(20)	1.5		.618420(25)	8.1		.8680646(22)	7.8
.240	.12262(18)	1.1	.330	.638353(26)	7.4	.420	.8763354(26)	10.0
	.12263(16)	1.1		.638390(25)	11.3		.8763233(21)	49.7
.245	.15971(15)	1.4	.335	.657448(21)	4.9	.425	.8840889(24)	19.2
	.15972(14)	1.2		.657500(16)	15.1		.8840714(19)	117.0
.250	.19623(14)	1.2	.340	.675699(13)	2.8	.430	.8913357(25)	24.3
	.19627(12)	1.2		.675751(12)	23.6		.8913154(18)	178.7
.255	.23200(12)	1.4	.345	.6931576(53)	3.7	.435	.8980930(21)	13.9
	.23202(12)	1.5		.6931802(49)	39.6		.8980731(16)	195.0
.260	.266799(93)	1.7	.350	.7098453(66)	1.0	.440	.9043836(18)	5.2
	.266831(94)	1.8		.7098713(62)	34.5		.9043665(16)	175.3
.265	.300562(97)	1.5	.355	.7258015(44)	2.5	.445	.9102364(18)	2.0
	.300592(92)	2.2		.7258219(36)	43.5		.9102225(14)	137.8
.270	.333177(90)	2.4	.360	.7410463(39)	5.6	.450	.9156833(14)	.9
	.333196(80)	2.6		.7410681(34)	51.9		.9156726(12)	97.3
.275	.364607(73)	2.9	.365	.7556038(42)	5.1	.455	.9207540(12)	1.6
	.364639(82)	2.7		.7556250(33)	59.9		.9207468(12)	61.3
.280	.394894(71)	1.7	.370	.7694993(37)	4.7	.460	.9254779(11)	1.6
	.394923(66)	2.3		.7695206(34)	64.3		.9254730(10)	36.2
.285	.424033(66)	1.8	.375	.7827565(36)	6.7	.465	.9298820(12)	1.3
	.424051(60)	2.3		.7827780(30)	68.5		.9298786(10)	20.3
.290	.451998(61)	1.8	.380	.7953967(37)	8.4	.470	.9339903(10)	2.1
	.452023(60)	2.6		.7954174(32)	70.4		.9339883(09)	9.2
.295	.478878(63)	2.2	.385	.8074397(33)	9.2	.475	.9378262(08)	1.3
	.478887(55)	2.6		.8074602(31)	69.4		.9378251(07)	3.9
.300	.504651(53)	2.8	.390	.8189052(34)	10.6	.480	.9414105(06)	1.0
	.504664(52)	2.9		.8189246(26)	66.9		.9414100(06)	2.5
.305	.529376(47)	3.8	.395	.8298090(32)	10.5	.485	.9447624(04)	1.6
	.529393(46)	3.5		.8298263(28)	59.4		.9447621(03)	1.8
.310	.553076(44)	5.2	.400	.8401660(29)	10.1	.490	.9478999(04)	1.8
	.553089(42)	4.3		.8401801(25)	43.6		.9478997(03)	1.1

Table 5.21: Monte Carlo results for the interface tension. We always quote two numbers. For the upper number the $L = 16, 32, 64$ data were included. For lower number also the $L = 8$ data were included. X denotes χ^2 per degree of freedom for the fit of the free energies with $C_s + \sigma L^2$

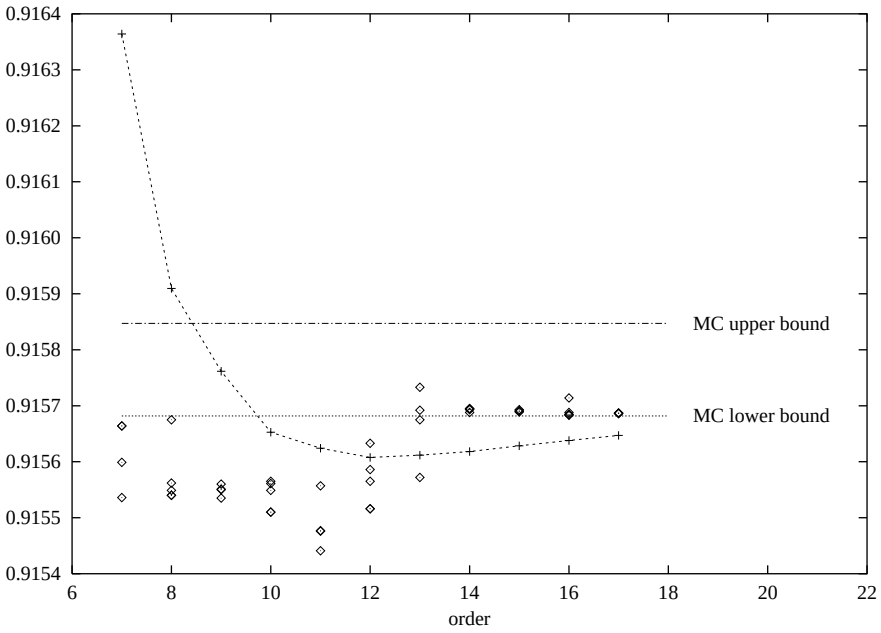

Figure 5.11: Ising interface tension at $\beta = 0.4500$ from Padé, truncated series and Monte Carlo. The symbols are the same as in figure 5.8

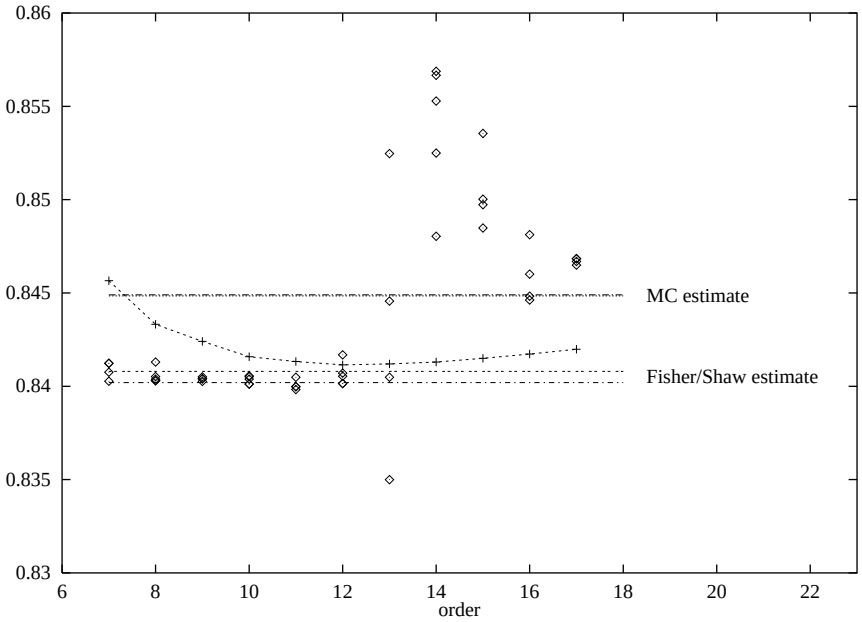

Figure 5.12: Ising interface tension at $u = 0.2$ ($\beta = 0.4204$) from Padé, truncated series and Monte Carlo. For comparison we also quote here the Shaw and Fisher estimate (based on the ninth order series evaluation). The symbols are the same as in figure 5.8

to deal with functions that have a critical behavior like $\sim A(x)(x-x_c)^{-\gamma}+B(x)$. Note, however, that the singularity of the free energy of the Ising interface is not of this type.

Table 5.23 shows the results obtained by evaluating inhomogeneous differential approximants for $\sigma/(2\beta)$ at $\beta = 0.402359$ which corresponds to $u = 0.2$. Like Shaw and Fisher, we computed the approximant for the quantity $Q(u)$ defined above and then took the logarithm. We here only discuss the order 9 and order 17 approximants. The order 9 approximants are fairly stable, however yield too small results (as the Padé approximants of this order do). Recall that the Monte Carlo estimate for this β-value is $\sigma/(2\beta) = 0.84487(3)$. The order 17 approximants are also fairly stable, however, they now overshoot the Monte Carlo estimate definitely. We conclude that using inhomogeneous differential approximants does not cure the problem (as was to be expected). The analysis of the interface tension at $\beta = 0.4074$ leads to a similar result.

In figure 5.13 we compare our results for the interface tension with the whole range approximant of Fisher et al. [81, 82, 17] in the β-range $0.35 - 0.50$. The approximant provided by Fisher and Wen [81] is obtained as discussed in ref. [82]. In addition the critical amplitude of the interface tension is fixed to the value given by Mon [34]. The mismatch of the two curves can be explained by the failure of the approximants to the low temperature series of order 9 at $u = 0.20$. The interface tension at $u = 0.20$ is underestimated and since the interface energy is overestimated the gap between the two curves increases with decreasing β.

For β-values close to the bulk critical temperature the Monte Carlo result and the interpolation are consistent again. This fact confirms the validity of the result for the interface tension amplitude obtained by Mon [34].

The Specific Heat. The specific heat of models undergoing a KT phase transition was investigated in a number of Monte Carlo studies. For the XY model a peak of the specific heat is found, which is located in the massive phase of the model at about $0.9\beta_c$, see e.g. refs. [54, 70, 71]. Swendsen [47] also found a peak of the specific heat for the DGSOS and ASOS models in the massive (smooth) phase of the models. For the BCSOS model (or F-model) that is an SOS model with the constraint that two neighboring height variables must differ by +1 or –1, the specific heat can be computed exactly (chapter 8 in the book of Baxter [100]). The peak of the specific heat lies clearly in the massive phase.

In contrast to these findings, Shaw and Fisher [82] arrive at the conclusion (based on their series analysis) that the peak of the specific heat of the 3D Ising interface is located in the massless (rough) phase.

The position of the specific heat peak is, of course, not a universal feature of the KT transition since the specific heat stays finite for all temperatures. However, the ASOS model is supposed to approximate the Ising interface at the roughening transition even quantitatively quite well. Hence it would be quite surprising if the specific heat peak of the Ising interface should be in the massless phase while that of the ASOS model is located in the massive phase.

We computed the derivative of the interface energy with respect to the inverse temperature β from finite differences of the energy. The results for $L = 8, 16, 32$ and 64 are given in figure 5.14. For comparison we give the truncated series result for order 12 and 17. For the lattices of size $L = 16, 32$ and 64 the derivative of the energy clearly exhibits a peak for $\beta \sim 0.43 > \beta_R$. The

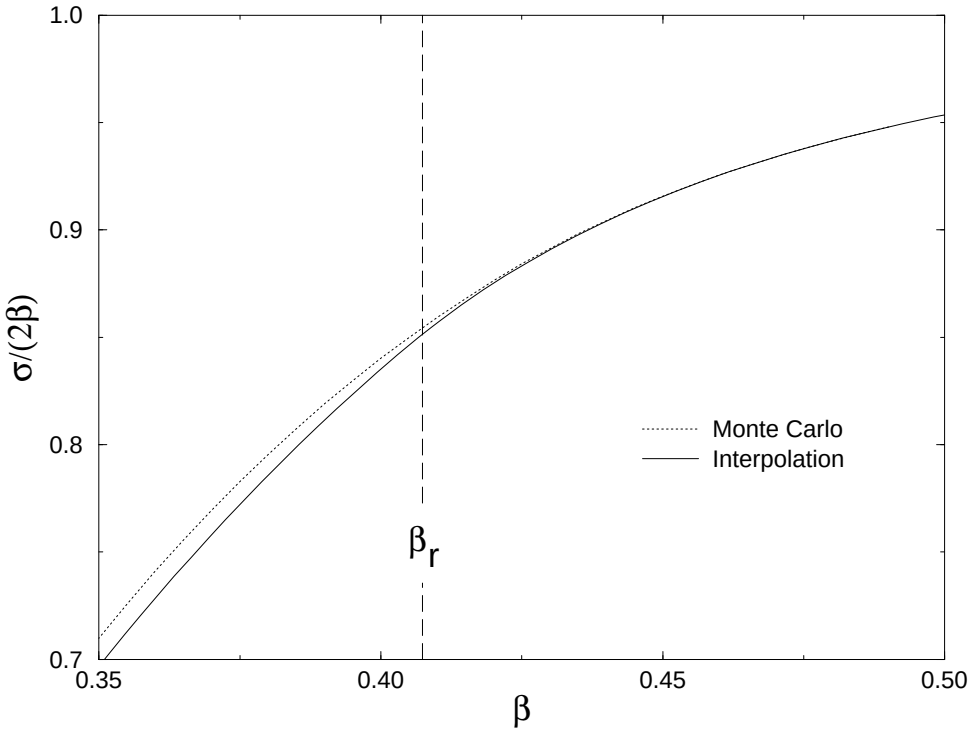

Figure 5.13: The surface tension obtained by Monte Carlo simulation (dotted line) is plotted as a function of the inverse temperature β. The error bars are smaller than the line width. For comparison we give the interpolation result of Fisher et al. [81, 82, 17] (solid line). The roughening transition at $\beta_R = 0.4074(3)$ is indicated by a vertical dashed line

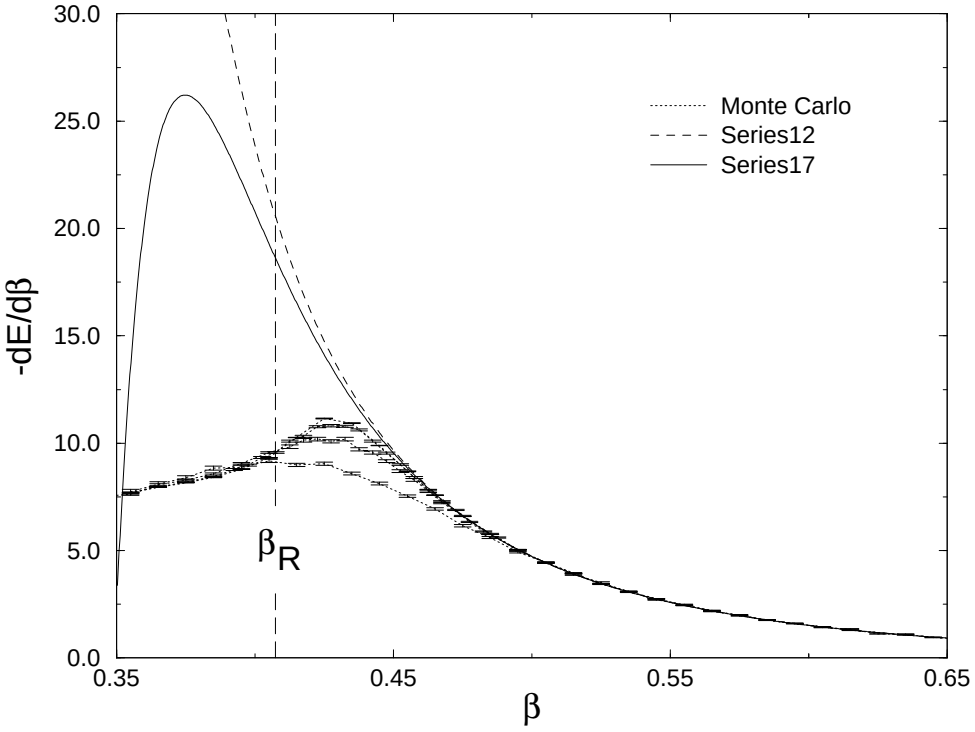

Figure 5.14: The derivative of the surface energy with respect to β is plotted as a function of the inverse temperature β. The dotted lines gives the derivative obtained from finite differences of the surface energy for L = 8,16,32, and 64, computed by Monte Carlo. The height of the peak grows with increasing L. For comparison we give the result from the series truncated at order 12 (Series12) and truncated at order 17 (Series17). The roughening transition at β_R is indicated by a vertical dashed line

peak of the specific heat $C = -\frac{1}{T^2}\frac{dE}{d\beta}$ itself is even slightly deeper in the massless phase. This is in contradiction to the Shaw and Fisher result. The peak height still increases considerably for $L = 64$ compared to $L = 32$. This fact indicates that length scales of order 10 lattice spacings are largely involved in the generation of the specific heat peak. On the other hand the correlation length at $\beta = 0.43$ is finite. It should be of order 100.

For $\beta > 0.46$ the derivative of the energy obtained from the 12^{th} and 17^{th} order truncated series are close together and reproduce the Monte Carlo result within error bars. The 12^{th} order truncated series contains only coefficients with positive sign and is hence increasing monotonically with increasing u. Obviously it cannot predict the peak of the specific heat. The situation is slightly different for the 17^{th} order truncated series. The curve displays a peak at $\beta = 0.3747...$ deep in the massless phase, but obviously wrong.

One expects the low temperature series of the free energy to converge for $\beta > \beta_R$. Hence in principle one should be able to obtain the specific heat peak accurately from the truncated series of sufficiently high order. However, since length scales of more than ten are involved one would have to compute diagrams of this extension.

We presented a comparison of Monte Carlo results for interface properties with low temperature series. We took the obvious discrepancy between the methods as a motivation to improve confidence in the Monte Carlo estimates by providing a detailed study of possible systematic errors.

The failure of the series approximations to improve the series result compared with the truncated series as discussed in this article is not completely unexpected. However, our detailed study reveals the seriousness of the problem and calls for new approaches to deal with essential singularities in series expansions.

In ref. [BB6], we performed a similar analysis for the ASOS model (based on the low temperature series by Weeks et al. extended by us to order 12). Recently, the series was further extended to order 23 and analyzed by Arisue [80].

$\beta = 0.402359$ ($u = 0.2$)			
L	$\sigma(L)/(2\beta)$	pair	$\sigma/(2\beta)$
8	0.849503(17)	8-16	0.844959
16	0.8460946(87)	16-32	0.844882
32	0.8451848(42)	32-64	0.844858
64	0.8449398(30)		
$\beta = 0.45$			
L	$\sigma(L)/(2\beta)$	pair	$\sigma/(2\beta)$
8	0.916039(10)	8-16	0.915567
16	0.9156853(56)	16-32	0.915683
32	0.9156838(24)	32-64	0.915683
64	0.9156833(14)		

Table 5.22: Interface tension $\sigma(L)/(2\beta)$ together with estimates for the same quantity obtained from interface free energies for pairs of L-values

order 17		order 15		order 12		order 9	
$[9/5,1]$	–	$[7/5,1]$	0.849 19	$[6/3,1]$	0.841 35	$[4/2,1]$	0.840 73
$[8/6,1]$	0.845 08	$[6/6,1]$	0.846 21	$[5/4,1]$	0.843 64	$[3/3,1]$	0.840 69
$[7/7,1]$	–	$[5/7,1]$	0.846 18	$[4/5,1]$	0.841 26	$[2/4,1]$	–
$[6/8,1]$	–			$[3/6,1]$	0.841 25		
$[9/4,2]$	0.846 06	$[7/4,2]$	–	$[5/3,2]$	0.841 45	$[3/2,2]$	0.840 41
$[8/5,2]$	0.845 66	$[6/5,2]$	0.844 80	$[4/4,2]$	0.841 43	$[2/3,2]$	0.840 29
$[7/6,2]$	0.845 75	$[5/6,2]$	0.846 82	$[3/5,2]$	0.841 15		
$[6/7,2]$	0.845 45	$[4/7,2]$	0.844 75				
$[5/8,2]$	0.845 92						
$[4/9,2]$	0.845 90						
$[7/5,3]$	–	$[6/4,3]$	–	$[5/2,3]$	0.841 67	$[3/1,3]$	0.840 70
$[6/6,3]$	–	$[5/5,3]$	0.845 79	$[4/3,3]$	–	$[2/2,3]$	0.840 25
$[5/7,3]$	0.845 49	$[4/6,3]$	0.845 52	$[3/4,3]$	0.841 74	$[1/3,3]$	0.840 32
$[4/8,3]$	–			$[2/5,3]$	0.842 06		
$[7/4,4]$	–	$[6/3,4]$	–	$[4/2,4]$	–		
$[6/5,4]$	0.845 55	$[5/4,4]$	–	$[3/3,4]$	0.842 96		
$[5/6,4]$	0.845 49	$[4/5,4]$	–	$[2/4,4]$	0.842 08		
$[4/7,4]$	–	$[3/6,4]$	0.844 90				
$[7/3,5]$	0.845 63	$[5/3,5]$	–				
$[6/4,5]$	0.845 68	$[4/4,5]$	–				
$[5/5,5]$	0.845 63	$[3/5,5]$	0.845 54				
$[4/6,5]$	–						
$[3/7,5]$	0.845 66						

Table 5.23: Interface tension $\sigma/(2\beta)$ at $u = 0.2$ ($\beta = 0.4024$) estimated from inhomogeneous differential approximants $[N/M, L]$ for $Q(u)$. The symbol '–' means that the corresponding approximant could not be computed because it did not exist or the numerics was unstable

5.3 Comparison with the Capillary Wave Model

We compare predictions of the Capillary Wave Model beyond its Gaussian approximation with Monte Carlo results for the energy gap and the interface energy of the 3-dimensional Ising model in the scaling region. Our study reveals that the finite size effects of these quantities are well described by the Capillary Wave Model, expanded to two–loop order (one order beyond the Gaussian approximation). This section is based on ref. [BB8].

Soft modes play an essential role in the description of *finite size effects* (FSEs) in the fluid interface's free energy (see for instance [111, 113] and references therein). 3-dimensional spin systems offer a simple context where these effects appear and can be studied, e.g. by using numerical simulations to check theoretical predictions. It is well known that, between the roughening and the critical temperature of the 3-dimensional Ising model, interfaces are dominated by long wavelength fluctuations (i.e. they behave as *fluid* interfaces). Because of these fluctuations, a complete control on the description of interfaces, starting from the microscopic Hamiltonian, has not yet been reached in the rough phase. The usual approach consists in assuming an effective Hamiltonian describing the collective degrees of freedom.

An effective model widely used to describe a rough interface is the *capillary wave model* (CWM) [107]. In its simplest formulation one assumes an effective Hamiltonian proportional to the variation of the surface's area with respect to the classical solution. Because of its non–polynomial nature, until recently the CWM has been studied only in its quadratic approximation, the Hamiltonian being equivalent to a (massless) 2-dimensional Gaussian model. The CWM has been often identified with the Gaussian model. This model was shown to give a good description of several features of the interfaces of the 3-dimensional Ising model, like the logarithmic growth (as a function of the lattice size) of the interfacial width in the whole rough phase [BB4] (see also section 5.1), and the FSEs (as a function of the shape of the lattice) of the free interface energy in the scaling region of the model [114].

The corrections that arise when passing from the classical approximation to the Gaussian one [148, 112, 114], (which we shall term from now on *one–loop* contributions), only depend on one dimensionless parameter (namely on the asymmetry $u = L_2/L_1$ of the transverse sizes of the lattice) and on the boundary conditions. They reduce on symmetric lattices ($u = 1$) to the well known finite–size behavior of the free energy [142, 145, 144, 15] in the large L limit

$$\frac{F}{k_B T} \propto \sigma L^2 \ , \tag{5.47}$$

σ being the reduced interface tension.

As mentioned above, the CWM has been often identified with its Gaussian approximation. However, the full CWM is interesting in itself because of its simple geometrical meaning (see for instance ref. [110] and references therein). Also, it coincides with the Nambu–Goto string action in a particular gauge. The improvement of Monte Carlo simulations reached in the last years allows now to test the CWM beyond the Gaussian approximation. This is the aim of this

study, in which we investigate the presence of corrections to the pure Gaussian description of the free energy of a rough interface in the scaling region of the 3-dimensional Ising model.

A similar analysis was recently made in the context of the 3-dimensional three–state Potts model [116]. It was shown that higher order corrections to the Gaussian approximation of the CWM (from now on called *two–loop* contributions) give contributions to the functional form of the interface's free energy which can be exactly estimated.

The contributions to the interface free energy (i.e. vacuum diagrams on finite volumes) due to higher order expansion of the CWM Hamiltonian are finite and can be evaluated in a simple way [108]. In this study we present evidence that the results are independent of the regularization used.

It turns out that the two–loop contributions do not depend only on the asymmetry parameter u but also on the dimensionless expansion parameter proportional to the minimal area of the surface, namely $\sigma A \equiv \sigma L_1 L_2$. As a consequence and in contrast to what happens for the Gaussian model, even for symmetric ($L_1 = L_2 \equiv L$) lattices the finite–size behavior of the free energy defined in eq. (5.47) gets corrections proportional to $(\sigma L^2)^{-1}$ which are important in extracting the interface tension value using a fitting procedure. In this study we discuss this picture for the Ising model, checking the theoretical prediction by means of Monte Carlo simulations and using very different techniques and algorithms.

Note that the 3-dimensional Ising model is related through duality to 3-dimensional Z_2 gauge theory. In particular, the physics of interfaces is directly linked to the physics of their dual gauge observables, i.e. the Wilson loops, and, as a consequence, to the properties of the chromo–electric flux tube in the confining phase [117]. This means that all the results that we describe in this study have a direct counterpart in the context of lattice gauge theories, and could help to better understand the possible string–like descriptions of their infrared behavior.

5.3.1 The Models

The Ising Model

We consider the 3-dimensional Ising model on a regular cubic lattice of size L_1, L_2 in the x_1–, x_2–directions, where $L_2 \geq L_1$, and size t in the x_3–direction. In the x_1– and the x_2–direction periodic boundary conditions are imposed, while in the x_3–direction either periodic or anti-periodic boundary conditions are used, depending on the Monte Carlo method that is applied. The Hamiltonian is defined by

$$H = -\sum_{<xy>} s_x s_y \quad , \tag{5.48}$$

where the sum is over all nearest–neighbor pairs $< xy >$, and $s_x = \pm 1$. The corresponding partition function is

$$Z_I = \sum_{\{s\}} e^{-\beta H} \quad , \tag{5.49}$$

where $\beta = 1/(k_B T)$.

We study the model between the critical and the roughening temperature, namely in the region $\beta_R > \beta > \beta_c$.

While in infinite volume, for $\beta > \beta_c$, the system shows a spontaneous symmetry breaking, in finite volume this cannot occur, and interfaces appear, separating extended domains of different magnetization.

In particular, we will consider interfaces that are parallel to the $x_1 - x_2$ plane and fluctuate freely in the third, orthogonal, x_3–direction. We shall discuss below how such interfaces can be generated in a Monte Carlo simulation.

Above the roughening temperature ($\beta_R > \beta > \beta_c$) the step free energy of the interface goes to zero. As a consequence the interface behaves essentially as a 2-dimensional critical system: it may be freely translated through the medium and the long-wavelength, transverse fluctuations in the interface position, i.e. capillary waves, have a small cost in energy (hence cannot be neglected in calculations). They can be viewed as the Goldstone modes associated with the spontaneous breaking of the transverse translational invariance [26]. To describe the interface free energy one is therefore forced to assume an effective model. On the other side, one has the advantage of choosing a Hamiltonian defined directly on the continuum to make analytical computations.

The Effective Model

We assume the effective Hamiltonian of the interface to be proportional to its area. Denoting by $x_i(\xi_1, \xi_2)$, $i = 1, 2, 3$, the coordinates of a point of the interface as functions of the parameters ξ_α, $\alpha = 1, 2$, with $0 \leq \xi_\alpha \leq 1$, we can write the area in the standard reparametrization invariant form,

$$\mathcal{A} = \int_0^1 d\xi_1 \int_0^1 d\xi_2 \ \sqrt{g} \quad , \tag{5.50}$$

where $g = \det(g_{\alpha\beta})$, with

$$g_{\alpha\beta} = \frac{\partial x_i}{\partial \xi_\alpha} \frac{\partial x^i}{\partial \xi_\beta} \quad . \tag{5.51}$$

A system with a Hamiltonian proportional to $\mathcal{A}$ coincides with the Nambu–Goto model for the bosonic string. The corresponding quantum theory is anomalous: depending on the quantization method one finds either the breaking of rotational invariance or the appearance of interacting longitudinal modes (Liouville field). We are, however, interested in interfaces of very large size where these difficulties disappear and the rotational invariance is restored [109]; in the infrared limit the theory flows to the massless Gaussian model. In order to study the first perturbative correction to this limit it is convenient to assume that the main contribution to the interface free energy is given in this region by small and smooth deformations of the minimal surface (which is a flat torus of area $L_1 L_2$). More precisely, we assume that there are no foldings nor self-intersections nor overhangs.[11] Under these conditions we can choose as parameters the two

[11] From the microscopic point of view this is not obvious *a priori*: in fact it has been observed that the interface at small scales is much more similar to a sponge than to a smooth surface [115, 118]. The strong linear correlation

longitudinal coordinates $x = x_1$ and $y = x_2$, by putting $\xi_1 = x_1/L_1$ and $\xi_2 = x_2/L_2$; as a consequence, the transverse displacement x_3 of the surface becomes a single–valued function of them: $x_3 = \phi(x, y)$. In such a frame eq. (5.50) can be written as

$$A[\phi] = \int_0^{L_1} dx \int_0^{L_2} dy \sqrt{1 + \left(\frac{\partial \phi}{\partial x}\right)^2 + \left(\frac{\partial \phi}{\partial y}\right)^2} \quad . \tag{5.52}$$

Using these notations, the free energy of a fluid interface can be described by

$$F = -k_B T \ln Z \tag{5.53}$$

$$Z = \lambda \, e^{-\sigma L_1 L_2} Z_q(\sigma, L_1, L_2) \tag{5.54}$$

$$Z_q = \int [D\phi] \exp\{-\mathcal{H}[\phi]\} \quad , \tag{5.55}$$

where λ is an undetermined constant within this approach. The reduced Hamiltonian $\mathcal{H}$ is given by

$$\mathcal{H}[\phi] = \sigma (A[\phi] - L_1 L_2) \quad . \tag{5.56}$$

In words, $\mathcal{H}[\phi]$ is given by the change produced by the deformation ϕ in the interface's area, measured in units of the interface tension σ. [12]

One can then take into account the quantum contributions by expanding eq. (5.56) in the natural dimensionless parameter $(\sigma A)^{-1}$, $A = L_1 L_2$. The interface tension is the only dimensionful parameter of this theory.

Coming back to the dimensionless parameters $\xi_\alpha = x_\alpha / L_\alpha$, and putting $\phi' = \sqrt{\sigma}\phi$, the Hamiltonian can be written as

$$\mathcal{H}[\phi] = \sigma A \int_0^1 d\xi_1 \int_0^1 d\xi_2 \left[\sqrt{1 + \frac{1}{\sigma A}(\nabla\phi)^2} - 1\right] \tag{5.57}$$

$$(\nabla\phi)^2 = u \left(\frac{\partial \phi}{\partial \xi_1}\right)^2 + \frac{1}{u}\left(\frac{\partial \phi}{\partial \xi_2}\right)^2 \quad , \tag{5.58}$$

where $u = L_2/L_1$, and the primes have been omitted. For $(\sigma A)^{-1} \to 0$, expanding up to the second order, one obtains

$$\mathcal{H}[\phi] = \mathcal{H}_g[\phi] - \frac{1}{8\sigma A}\mathcal{H}_p[\phi] + O\left((\sigma A)^{-2}\right) \tag{5.59}$$

$$\mathcal{H}_g[\phi] = \frac{1}{2}\int_0^1 d\xi_1 \int_0^1 d\xi_2 \, (\nabla\phi)^2 \tag{5.60}$$

$$\mathcal{H}_p[\phi] = \int_0^1 d\xi_1 \int_0^1 d\xi_2 \left((\nabla\phi)^2\right)^2 \quad . \tag{5.61}$$

between the area and the genus of the surface (number of microscopic handles), together with the evidence that the partition function summed over all genera behaves like a smooth surface, has led to conjecture that a simple non–perturbative renormalization of the physical quantities associated to the surface occurs [118]

[12] Far from the scaling region, the interface tension σ in eq. (5.56) should be replaced by the stiffness κ. However, in the scaling region, as the bulk correlation length increases and the rotational invariance is restored, κ approaches σ and for all the values of β that we studied the difference between them can be safely neglected [BB4]

Retaining only the quadratic term of eq. (5.60) in the Hamiltonian (5.59), one obtains from eq. (5.55) the one–loop contribution which constitutes the Gaussian approximation

$$Z_q^{(g)}(u) = \frac{1}{\sqrt{u}} \left| \eta(iu)/\eta(i) \right|^{-2} \quad , \tag{5.62}$$

where η is the Dedekind eta function

$$\eta(\tau) = q^{1/24} \prod_{n=1}^{\infty} (1-q^n) \quad , \qquad q \equiv \exp(2\pi i \tau) \quad . \tag{5.63}$$

This is a well known result in string theory and conformal field theory, and coincides[13] with the partition function of a 2-dimensional conformal invariant free boson on a torus of modular parameter $\tau = iu$ [148, 112, 114].

Within this approximation, the interface partition function takes the form

$$Z \;=\; \lambda \, e^{-\sigma L_1 L_2} Z_q^{(g)}(u) \quad . \tag{5.64}$$

For $u = 1$, i.e. $L_1 = L_2 \equiv L$, one recovers the well known finite size behavior of the interface partition function given in eq. (5.47),

$$Z \;=\; \lambda \, e^{-\sigma L^2} \quad . \tag{5.65}$$

It has been already verified [114] that the inclusion of the one–loop contribution (5.64) allows to describe accurately finite size effects on asymmetric lattices ($u > 1$): these turn out to be strong enough to make the classical approximation (5.65) completely inadequate. However, this result does not give a definitive answer about the reliability of the CWM hypothesis expressed by eq. (5.56): it is in fact well known that the Gaussian model is the fixed point of a wide class of possible effective descriptions [26]. To identify the particular effective Hamiltonian which describes the free fluid interface it is then crucial to test higher–order contributions.

Let us also stress that, among various possibilities, eq. (5.56) is the simplest and most intuitive from a geometrical point of view. Moreover, it does not add any new free parameter and, even if this hypothesis is rather old [107], it has never been tested beyond the Gaussian approximation until recently [116].

5.3.2 Two-Loop Calculation

We shall now calculate the contribution to the partition function Z from the term given in the eq. (5.61) which is the first correction to the Gaussian Hamiltonian. We write Z in the form

$$Z \;=\; \lambda_o \, \mathrm{e}^{-\sigma_o A} Z_q^{(g)}(u) \, Z_q^{(2l)}(u, \sigma_o A, \varrho_o) \tag{5.66}$$

$$\begin{aligned} Z_q^{(2l)} &= 1 + \frac{\varrho_o}{8\sigma_o A \, Z_q^{(g)}} \int [D\phi] \, \mathcal{H}_p[\phi] \, e^{-\mathcal{H}_g[\phi]} + O\left((\sigma A)^{-2}\right) \\ &= 1 + \frac{\varrho_o}{8\sigma_o A} \langle \int_0^1 d\xi_1 \int_0^1 d\xi_2 \, \left((\nabla\phi)^2 \right)^2 \rangle \quad , \end{aligned} \tag{5.67}$$

[13] The constant $\eta(i)$ has been introduced just to normalize $Z_q^{(g)}(1) = 1$

where the expectation value is taken in the free theory. A subscript $_o$ is added to the bare quantities in order to distinguish them from the corresponding renormalized ones. In the Nambu-Goto model $\varrho_o = 1$.

Eq. (5.67) shows that the two–loop contribution can be expressed in terms of products of double derivatives of the free Green function. Wick's theorem gives

$$\begin{aligned} \langle \int_0^1 d\xi_1 \int_0^1 d\xi_2 \left((\nabla\phi)^2 \right)^2 \rangle &= \Big[3u^2 (\partial^2_{\xi_1} G)^2 + 3u^{-2} (\partial^2_{\xi_2} G)^2 + \\ 2\partial^2_{\xi_1} G \partial^2_{\xi_2} G &+ 4(\partial_{\xi_1}\partial_{\xi_2} G)^2 \Big]_{\xi \to \xi'} \end{aligned} \tag{5.68}$$

with

$$G(z - z') = \langle \phi(\xi)\phi(\xi') \rangle \quad , \tag{5.69}$$

where we have introduced the complex variable $z = \xi_1 + iu\xi_2$.

Let us denote by $\{\omega\}$ the period lattice, namely the set of points of the complex plane of the form $\{\omega = \mathrm{m} + in u,\ \mathrm{m}, \mathrm{n} \in Z\}$. Then the periodic boundary conditions can be written simply as

$$G(z + \omega) = G(z) \quad . \tag{5.70}$$

The Green function should also satisfy

$$-\Delta \, \langle \phi(\xi)\phi(0) \rangle = \delta^{(2)}(\xi) - 1 \tag{5.71}$$

where

$$\Delta = u \frac{\partial^2}{\partial \xi_1^2} + \frac{1}{u} \frac{\partial^2}{\partial \xi_2^2} \quad . \tag{5.72}$$

The -1 term on the right-hand side of eq. (5.71) represents the subtraction of the zero mode due to the translational invariance of the interface in the x_3–direction: this is the standard procedure making Δ invertible in the subspace orthogonal to the zero mode (see for instance ref. [146]).

The solution of the above equation can be expressed in terms of the Weierstrass σ function, defined through the infinite product

$$\sigma(z) = z \prod_{\omega \neq 0} \left(1 - \frac{z}{\omega} \right) \mathrm{e}^{z/\omega + \frac{1}{2}(z/\omega)^2} \quad . \tag{5.73}$$

We can write the solution as a sum of three terms,

$$G(z) = -\frac{1}{2\pi} \ln \Big| \sigma(z) \Big| + \frac{\pi E_2(iu)}{12} \, \Re e(z^2) + \frac{1}{2u} \Big(\Im m(z) \Big)^2 \quad , \tag{5.74}$$

where $E_2(\tau)$ is the first Eisenstein series

$$E_2(\tau) = 1 - 24 \sum_{n=1}^{\infty} \frac{n \, q^n}{1 - q^n} \quad , \qquad q \equiv \exp(2\pi i \tau) \quad . \tag{5.75}$$

The last term in eq. (5.74) accounts for the zero mode subtraction, while the first two may be thought of as the real part of an analytic function $f(z)$, hence they satisfy $\Delta \Re e f(z) = 0$ outside the singularities at $z \in \{\omega\}$. For z near a node of the period lattice the second term is regular while the first one behaves like $-\frac{1}{2\pi}\ln|z-\omega|$ as it should in order to yield the correct normalization of the delta function. The coefficient of the second term is uniquely fixed by imposing the periodic boundary conditions of eq. (5.70) (for a different, but equivalent form of the solution see for instance ref. [146] p. 571).

The double derivative of the Green function can be easily calculated using the the formula

$$\wp(z) = -\frac{\mathrm{d}^2}{\mathrm{d}z^2}\ln\Big(\sigma(z)\Big) \quad , \tag{5.76}$$

where $\wp(z)$ is the Weierstrass $\wp$–function. We need only the first few terms of its Laurent expansion about the origin

$$\wp(z) = \frac{1}{z^2} + \frac{\pi^4}{15}E_4(iu)z^2 + \dots \quad , \tag{5.77}$$

where $E_4(\tau)$ is the second Eisenstein series. The double pole at the origin implies that the limit for $\xi \to \xi'$ in eq. (5.68) is singular. In order to regularize this theory we keep $\xi - \xi'$ different from zero by putting $z = \mathrm{e}^{i\alpha}|z| = \mathrm{e}^{i\alpha}\varepsilon/L_1$ where ε is used as an ultraviolet spatial cut-off. We get

$$Z_q^{(2l)} = 1 + \frac{\varrho_o}{\sigma_o}\left[\frac{A}{8\pi^2\varepsilon^4} + \frac{\cos(2\alpha)c(u)}{4\pi\varepsilon^2} + \frac{\cos(4\alpha)d(u)}{A}\right] + \frac{\varrho_o f(u)}{\sigma_o A} + O(\varepsilon) \quad , \tag{5.78}$$

with $c(u) = (\pi u E_2(iu)/3 - 1)$, $d(u) = \pi^2 u^2 E_4(iu)/60$ and

$$f(u) = \frac{1}{2}\left\{\left[\frac{\pi}{6}uE_2(iu)\right]^2 - \frac{\pi}{6}uE_2(iu) + \frac{3}{4}\right\} \quad . \tag{5.79}$$

The three terms in the square brackets of eq. (5.78) are cut-off dependent quantities. They can be reabsorbed in the renormalization of the couplings σ, λ and ϱ, respectively. In fact, putting $\sigma = \sigma_o + \delta\sigma_o$, $\lambda = \lambda_o + \delta\lambda_o$ and $\varrho = \varrho_o + \delta\varrho_o$ in eq. (5.66), comparison with eq. (5.78) yields

$$\delta\sigma_o = -\frac{\varrho_o}{8\pi^2\varepsilon^4\sigma_o} \tag{5.80}$$

$$\delta\lambda_o = \frac{\lambda_o\varrho_o\cos(2\alpha)c(u)}{4\pi\varepsilon^2\sigma_o} \tag{5.81}$$

$$\delta\varrho_o = \varrho_o\cos(4\alpha)\frac{d(u)}{f(u)} \quad . \tag{5.82}$$

Of course the renormalized quantities σ, λ and ϱ should not depend on the regularization scheme and in particular on the choice of the parameter α. On the other hand, choosing $\alpha = \frac{\pi}{8}$, we get $\delta\varrho_o = 0$, which shows that ϱ is not renormalized, at least at the first perturbative order. Thus we can safely put the Nambu-Goto value $\varrho = 1$ in the final formula

$$Z = \frac{\lambda}{\sqrt{u}}\mathrm{e}^{-\sigma L_1 L_2}\Big|\eta(iu)/\eta(i)\Big|^{-2}\left[1 + \frac{f(u)}{\sigma L_1 L_2} + O\left(\frac{1}{(\sigma L_1 L_2)^2}\right)\right] \quad , \tag{5.83}$$

where $f(u)$ is defined in eq. (5.79). Note that eq. (5.83) is symmetric under the exchange $L_1 \leftrightarrow L_2$ as a consequence of the functional relation

$$E_2\left(-\frac{1}{\tau}\right) = \tau^2 E_2(\tau) - i\frac{6\tau}{\pi}\,. \tag{5.84}$$

Similarly, it can be shown that also eqs. (5.80-5.82) are symmetric under such exchange. Our two–loop result coincides with the one obtained some years ago in the context of string theory [108], using the ζ–function regularization.

The fact that two completely independent regularization schemes tell us that the coupling ϱ is not renormalized suggests that this a general property, even if we have not yet found a rigorous argument to support it. Note that in our derivation the splitting between the cut-off dependent part and the remainder in eq. (5.78) is a crucial point. Such a separation arises in a natural way in our regularization, but it is conceivable that different cut-off schemes might generate a different splitting. We notice, however, that the functional form of the two-loop contribution is preserved by the modular invariance. This is not obvious in our derivation because, for sake of simplicity, we dealt with a rectangular torus with a purely imaginary modulus $\tau = iu$. It is possible to develop the theory on a generic torus associated to an arbitrary complex modulus τ. Any physical quantity must be invariant under the two generators of modular group:

$$S \;:\; \tau \;\to -1/\tau \tag{5.85}$$

$$T \;:\; \tau \;\to \tau + 1\,. \tag{5.86}$$

The terms in the square brackets of eq. (5.78) are not modular invariant because the angle α has not an intrinsic geometric meaning. On the contrary, the function $F(iu) = f(u)$ which yields the functional form of the two-loop contribution (5.83) is modular invariant. Its form in a general frame (i.e. τ arbitrary complex number) is given by

$$F\left(\tau\right) = \frac{1}{2}\left\{\left|\frac{\pi}{6}\Im m(\tau) E_2\left(\tau\right) - \tfrac{1}{2}\right|^2 + \tfrac{1}{2}\right\} \quad . \tag{5.87}$$

Notice that eq. (5.83) has no longer the functional form of the classical approximation (5.65) even on symmetric lattices: for $u = 1$ it can be easily seen that eq. (5.83) gives

$$Z \;=\; \lambda\, e^{-\sigma L^2}\left(1 + \frac{1}{4\sigma L^2}\right) \quad , \tag{5.88}$$

where the identity $E_2(i) = \frac{3}{\pi}$ has been used, which follows directly from eq. (5.84).

Let us stress finally that no new free parameter is introduced within this approach.

5.3.3 Observables and Monte Carlo Simulations

Let us discuss the observables of the Ising model that we can use to test the functional form of the interface free energy.

In the finite geometry the degeneracy of the ground state is removed: the energy of the symmetric, Z_2 invariant, ground state is separated by a small energy gap ΔE (or inverse tunneling correlation length) from the antisymmetric ground state energy.

This energy splitting is due to tunneling between the two vacua and is directly linked to the free energy of the interface. In the dilute gas approximation, in which multi–interface configurations are summed over, but interactions between interfaces are neglected, the energy splitting is directly proportional to the interface partition function Z, where Z is given by eqs. (5.64,5.65,5.83). It is then easy to show (see e.g. [147]) that

$$\Delta E \;=\; Z(\sigma, L_1, L_2) \quad , \tag{5.89}$$

where the usual factor 2 has been reabsorbed into the parameter λ appearing in the definitions of Z. Let us notice that λ has the physical dimensions of an energy. In the scaling region of the Ising model all dimensionful quantities should depend on β according to the scaling law

$$\xi\,(\beta) \;\simeq\; \xi_\infty \left(1 - \frac{\beta_c}{\beta}\right)^{-\nu} \quad , \tag{5.90}$$

where ξ_∞ is the bulk correlation length in the continuum limit. The most precise estimates for ν are in the range from 0.624 to 0.630 [94]. Since the interface tension is the only dimensionful physical quantity appearing in the interface free energy, in the following we express all physical observables in units of the square root of the interface tension $\sqrt{\sigma_\infty}$ according to the scaling law

$$\sqrt{\sigma\,(\beta)} \;=\; \sqrt{\sigma_\infty} \left(1 - \frac{\beta_c}{\beta}\right)^{\nu} \quad . \tag{5.91}$$

The measurements of the energy gap ΔE, for different choices of the lattice sizes, provides then a first direct check on the functional form of the interface free energy and allows one to estimate the interface tension σ. To this end, we have used two different methods, as explained in the following.

A second observable we have used to check our theoretical prediction is the surface energy E_S defined by

$$E_S(\sigma, L_1, L_2) = -\frac{1}{Z}\frac{\partial Z}{\partial \beta} \quad . \tag{5.92}$$

This observable is particularly useful because it enables us to isolate explicitly quantum contributions beyond the Gaussian one, as it will be discussed below.

Before describing the method we used to estimate these quantities, let us make some general remarks, independent from the observable and MC method used, on the range of values of β and on the lattice sizes where our formulae can be used.

Applying eq. (5.83), one should pay attention to avoiding spurious effects like the incomplete restoration of rotational invariance and the residual presence of lattice artifacts, as already discussed. To this end we made our simulation in the scaling region of the Ising model: the lowest temperature used corresponds to $\beta = 0.240$. In table 5.24 we present besides other quantities to be introduced below estimates for the bulk correlation length of the Ising model

β	L_c	$L_1^{(min)}$	$\xi_{\rm bulk}^{\rm MC}$	$\xi_{\rm bulk}^{\rm IDA}$
0.2240	12.1	18		4.527
0.2246	10.5	13		3.926
0.2258	8.5	12		3.170
0.2275	6.8	10	2.62(2)	2.556
0.2400	3.4	8		1.251

Table 5.24: The first column shows the β–values used in the present study. The corresponding inverse critical temperature L_c (in units of the lattice spacing) is given in second column. In the third column appear the corresponding minimal sizes used in Monte Carlo simulations. In the last two columns we present estimates for the bulk correlation length from a Monte Carlo simulation and from an analysis of the low temperature series with inhomogeneous differential approximants [83]

at the β–values used in the present study. The MC estimate is taken from ref. [152]. The other estimates are based on the low temperature series that was extended to 15th order by Arisue [78]. We analysed the series with the help of inhomogeneous differential approximants [83]. The numbers in the table are the results from the $[1;7,7]$ approximation.

The expansion parameter σA should be small enough to justify the perturbative calculation.

Interactions between interfaces should be negligible, which means that the dilute gas approximation must be satisfied: the dominant contribution in the probability of creating an interface is proportional to $e^{-\sigma A}$. Too small lattice size can give rise to a high density of interfaces and to non–negligible interactions.

Finally, the smallest size of the lattice (L_1 in our conventions) should not only be greater than the bulk correlation length but also greater than the (inverse) deconfinement temperature of the dual gauge model. In fact, by duality (see for instance [154], see also [114]), the broken phase of the Ising model on an asymmetric 3-dimensional lattice corresponds to the confined phase of the 3-dimensional Z_2 gauge model at a finite temperature $T^{(g)} = 1/L_1$.

Precise information on the finite temperature deconfinement transition can be found, for instance, in [95]. β is mapped to the gauge coupling constant $\tilde{\beta} = -\frac{1}{2}\ln\tanh\beta$. For each β there exists a value $L_c(\beta)$ such that for $L_1 \leq L_c$ the gauge system is in the deconfined phase, and eq. (5.83) cannot be applied.

The values of L_c for the β's used are given in table 5.24. These have been obtained using data taken from ref. [95] and the scaling law

$$\frac{1}{L_c(\beta)} \;=\; T_c^{(g)}\;(\tilde{\beta}_c - \tilde{\beta}(L_c))^{\nu} \quad , \tag{5.93}$$

where $T_{(g)}^c = 2.3(1)$, $\tilde{\beta}_c \simeq 0.7614$ and $\nu \simeq 0.630$ (see [117]).

Energy Gap: the Time–Slice Correlations Method

The first method we have used to extract the energy splitting ΔE follows the procedure explained in ref. [38] (see also refs. [43, 114]); we refer to it as the *time–slice correlations* method (TSC).

Consider a cylindrical geometry, with $t \gg L_1, L_2$ and periodic boundary conditions in all directions, and define the time–slice magnetization S_k, where $k = 0, 1, \ldots, t/2$, as

$$S_k \equiv \frac{1}{L_1 L_2} \sum_{n_1=1}^{L_1} \sum_{n_2=1}^{L_2} s_{\vec{n}} \,, \tag{5.94}$$

with $\vec{n} \equiv (n_1, n_2, k)$. If one computes the two–point correlation function

$$G(k) \equiv \langle S_0 S_k \rangle \quad , \tag{5.95}$$

the low energy levels of the transfer matrix spectrum can be obtained from the asymptotic k–dependence of $G(k)$

$$\begin{aligned} G(k) \cdot Z_I &= c_0^2 \left(e^{-k\Delta E} + e^{-(t-k)\Delta E} \right) + \\ &\quad c_1^2 \left(e^{-k\Delta E'} + e^{-(t-k)\Delta E'} \right) + \ldots \qquad (5.96) \\ Z_I &= 1 + e^{-t\Delta E} + \ldots \qquad (5.97) \end{aligned}$$

where $Z_I \equiv \mathrm{tr}\ e^{-tH}$ is the partition function of the Ising model in the transfer matrix formalism.

$\Delta E'$ is the energy of the first (antisymmetric) excited state and turns out to be (at least) one order of magnitude greater than ΔE in the range of parameters we have used. The coefficient c_0 corresponds to the magnetization expectation value and can be used to check the consistency of the MC results.

To perform our MC simulations we used a Swendsen–Wang cluster algorithm [127]. For each value of β considered, i.e. $\beta = 0.2246, 0.2258$ and 0.2275, L_1 and L_2 ranged from 10 to 35. We usually fixed $t = 120$, using, for simulations with particularly large L_1 and L_2, bigger sizes $t = 240 - 360$. The values of the energy gap ΔE, extracted using eq. (5.96), are reported in tabs. 5.25, 5.26 and 5.27 (for table 5.27 see also the table caption) [14]; the confidence levels of these fits are always above 70%.

Using this approach one should pay attention to correlations in MC time. In particular it turns out that the two–point correlation functions $G(k)$ are affected by very strong cross–correlations in MC time. To take under control this problem, we followed the procedure used in ref. [114], scattering the evaluation of time–slice correlations in Monte Carlo time. This has the advantage of reducing the cross–correlation matrix to an almost–diagonal form and simplify the non–linear fitting procedure. For each β and each lattice we made about $0.6 - 1.2 \cdot 10^6$ sweeps (after thermalization) with $1 - 2 \cdot 10^3$ measurements/observable. A standard jackknife procedure was used to evaluate errors.

[14] Some of these data have appeared preliminarily in ref. [119]

L_1	L_2	ΔE	$\Delta E^{(CWM)}$	x
13	13	0.04437(28)	0.04441	0.226
13	26	0.01657(28)	0.01682	0.181
13	30	0.01321(57)	0.01326	0.196
13	34	0.01069(40)	0.01059	0.217
14	14	0.03617(32)	0.03627	0.267
14	28	0.01157(62)	0.01156	0.156
14	32	0.00916(51)	0.00880	0.168
14	34	0.00723(65)	0.00771	0.176
16	16	0.02398(29)	0.02355	0.149
18	18	0.01451(46)	0.01468	0.118

Table 5.25: The energy gaps ΔE obtained at $\beta = 0.2246$ from MC simulations with the TSC method are reported together with the best fit values to the CWM at 2–loop approximation given by eq. (5.83). In the last column the values of the two–loop parameter x defined in eq. (5.112) are given

L_1	L_2	ΔE	$\Delta E^{(CWM)}$	x
12	12	0.03750(23)	0.03765	0.184
12	24	0.01126(13)	0.01117	0.212
12	26	0.00939(13)	0.00940	0.154
12	28	0.00769(29)	0.00793	0.161
12	30	0.00665(21)	0.00672	0.170
13	26	0.00662(23)	0.00684	0.126
13	28	0.00554(32)	0.00562	0.130
14	14	0.02225(16)	0.02212	0.135
16	16	0.01236(45)	0.01222	0.104
18	18	0.00617(48)	0.00631	0.082

Table 5.26: The same as table 5.25, but for $\beta = 0.2258$

L_1	L_2	ΔE	$\Delta E^{(CWM)}$	x
10	10	$0.04334(8)^a$	0.04335	0.265
10	18	$0.01439(26)^b$	0.01457	0.131
10	20	$0.01099(23)^b$	0.01148	0.136
10	23	$0.00797(23)^b$	0.00813	0.147
10	26	$0.00584(23)^b$	0.00583	0.162
10	28	$0.00396(44)^b$	0.00469	0.174
10	32	$0.00289(32)^b$	0.00307	0.200
11	30	0.00169(35)	0.00213	0.140
11	35	0.00114(38)	0.00113	0.164
12	12	$0.0217(1)^a$	0.0217	0.118
12	15	$0.01296(21)^c$	0.01274	0.099
14	14	$0.00989(7)^a$	0.00979	0.087
14	18	$0.00431(7)^c$	0.00432	0.071
16	16	$0.00400(7)^a$	0.00397	0.066
18	18	$0.00151(8)^a$	0.00144	0.052
20	20	$0.000454(11)^c$	0.000466	0.042
24	24	$0.000035(2)^c$	0.000034	0.029
26	26	$0.000009(1)^c$	0.000008	0.025

Table 5.27: The same as table 5.25, but for $\beta = 0.2275$. The (a) and (b) are data taken from ref. [38] and [114], respectively; the (c) data have been obtained with the BF method

Figure 5.15 shows a histogram of the magnetization for a typical lattice size. Almost all configurations contain zero or two interfaces, which indicates that the dilute gas approximation is respected. The plateau corresponds to configurations of the system with two interfaces (because of the periodic boundary conditions in the x_3-direction). It is easy to see that the presence of more interfaces would have the effect of strongly modify it. The two peaks correspond to configurations without interfaces.

Energy Gap: the Boundary Flip Method

Another method (which we refer to as the *boundary flip* (BF) method) to evaluate the energy gap ΔE was introduced by M. Hasenbusch in refs. [42, 137].

We consider a system which allows both periodic (p) and antiperiodic (a) boundary conditions (bc). The partition function of this system is given by

$$Z = Z_a + Z_p = \sum_{bc} \sum_{\{s\}} e^{-\beta H(s,bc)} \tag{5.98}$$

and the fraction of configurations with antiperiodic boundary conditions is given by

$$\frac{Z_a}{Z} = \frac{1}{Z} \sum_{\{s\}} e^{-\beta H(s,a)} = \frac{1}{Z} \sum_{bc} \sum_{\{s\}} \delta_{bc,a}\, e^{-\beta H(s,bc)} = < \delta_{bc,a} > \ . \tag{5.99}$$

An analogous result can be found for periodic boundary conditions.

We can express the ratio Z_a/Z_p as a ratio of observables in this system,

$$\frac{Z_a}{Z_p} = \frac{< \delta_{bc,a} >}{< \delta_{bc,p} >} , \tag{5.100}$$

which turns out to be directly connected to the energy gap ΔE.

To see this, let us express the partition functions of the periodic and antiperiodic Ising system in terms of the transfer matrix $\mathbf{T}$. The antiperiodic boundary conditions are represented by a spin–flip operator $\mathbf{P}$, which flips the sign of all spins in a given x_3–slice.

The partition function of the periodic system is given by

$$Z_p = Tr \mathbf{T}^t \ , \tag{5.101}$$

while the partition function of the antiperiodic system is given by

$$Z_a = Tr \mathbf{T}^t \mathbf{P} \ . \tag{5.102}$$

Since the operators $\mathbf{T}$ and $\mathbf{P}$ commute, they have a common set of eigenfunctions. Say the eigenvalues of $\mathbf{T}$ are λ_i and those of $\mathbf{P}$ are p_i. The possible values of p_i are 1 and -1. States that are symmetric in the magnetization have $p_i = 1$ and those that are antisymmetric have $p_i = -1$. The partition functions take the form

$$Z_p = \sum_i \lambda_i^t \tag{5.103}$$

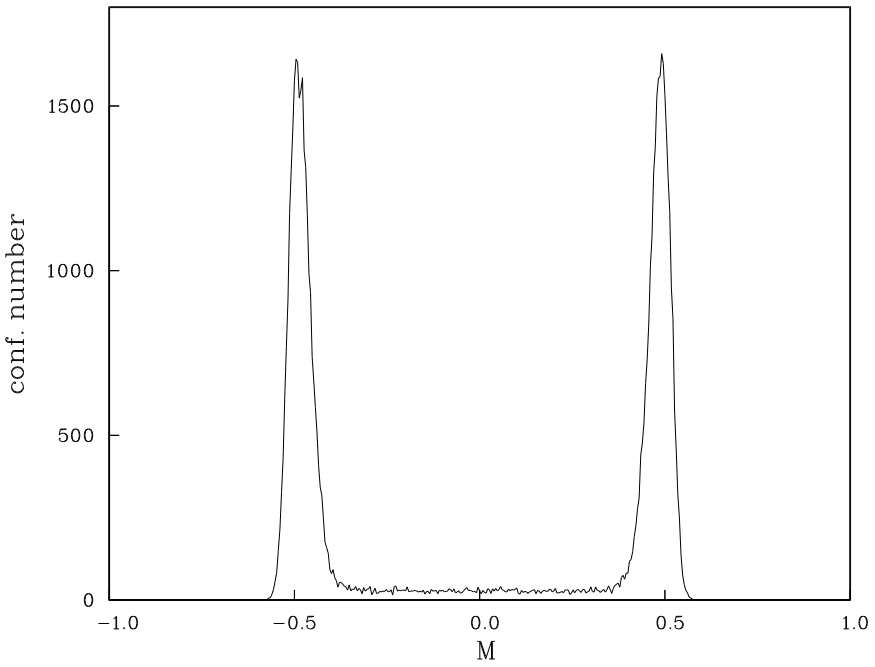

Figure 5.15: Histogram of the magnetization for a typical Monte Carlo ensemble at $\beta = 0.2275$, with lattice sizes $L_1 = 20$, $L_2 = 23$ and $t = 120$

and

$$Z_a = \sum_i \lambda_i^t p_i \quad . \tag{5.104}$$

Let us consider the ratio of the partition functions in the low temperature phase. If we assume that

$$\lambda_{0s}, \lambda_{0a} >> \lambda_{1s} \ , \lambda_{1a} \ , ... \tag{5.105}$$

then, ignoring terms of order $O\left[(\lambda_{1s}/\lambda_{0s})^t\right]$, it is easy to show that

$$\left(\frac{\lambda_{0a}}{\lambda_{0s}}\right)^t \ = \ \frac{Z_p - Z_a}{Z_p + Z_a} \ = \ 1 - 2 < \delta_{bc,a} > \quad . \tag{5.106}$$

The interface free energy (inverse of the tunneling mass) is then given by

$$\Delta E \ = \ -\ln(\lambda_{0a}/\lambda_{0s}) \ = \ -\frac{1}{t}\ln\left(1 - 2 < \delta_{bc,a} >\right) \quad . \tag{5.107}$$

Assuming that the number of interfaces is even for periodic boundary conditions and odd for anti-periodic boundary conditions, the dilute gas approximation leads to exactly the same relation between the interface free energy and the boundary statistics [42].

We have used the BF method at $\beta = 0.2240$ for a large number of lattices, as reported in table 5.28. In a few cases we studied two or three values of t, in order to check the stability of the results. In general, however, the t value needed is smaller than the one we would have needed when using the TSC method. For this reason, the BF method is particularly useful near the critical point where large L_1 and L_2 must be used.

For the determination of the ratio of partition functions Z_a/Z_p we employed the boundary cluster algorithm of M. Hasenbusch [42, 137].

For each simulation given in table 5.27 (case c) and in table 5.28 we have made, after thermalization, $0.7 - 1.4 \cdot 10^5$ sweeps, depending on the lattice size.

Moreover, the BF method bypasses the fitting procedure of eq. (5.96) required by the TSC method, reducing from $t/2$ to one ($< \delta_{bc,a} >$) the observables needed to evaluate E. This allows to save MC time as well as drastically reduces the problems connected to correlations in MC time.

Surface Energy

As stated above, one can also measure the surface energy and compare the MC results with the CWM predictions.

If one assumes eq. (5.83), it follows from eq. (5.92) ($\sigma' \equiv \partial_\beta \sigma$ and $\lambda' \equiv \partial_\beta \lambda$) that

$$E_S^{(CWM)}(\sigma, L_1, L_2) = \sigma' L_1 L_2 - \frac{\lambda'}{\lambda} - \frac{1}{Z_q^{(2l)}} \partial_\beta Z_q^{(2l)} \quad . \tag{5.108}$$

L_1	L_2	t	ΔE	$\Delta E^{(CWM)}$	x
18	18	54	0.0230(2)[a]	0.0229	0.161
18	30	60	0.008628(95)	0.008650	0.124
18	35	70	0.005993(74)	0.006046	0.128
18	40	120	0.004242(42)	0.004289	0.137
18	45	90	0.003034(41)	0.003076	0.149
18	50	100	0.002214(35)	0.002224	0.164
20	30	80	0.006156(90)	0.006149	0.101
20	35	70	0.004010(72)	0.004021	0.101
20	40	80	0.002681(53)	0.002669	0.105
20	45	90	0.001810(39)	0.001790	0.112
20	50	150	0.001205(14)	0.001210	0.121
24	24	72	0.00657(8)[a]	0.00646	0.091
24	35	70	0.001925(32)	0.001885	0.071
24	40	80	0.001102(22)	0.001107	0.070
24	45	180	0.000652(11)	0.000657	0.071
24	50	100	0.000407(10)	0.000393	0.074
24	60	120	0.000145(5)	0.000143	0.084
30	30	90	0.00136(3)[a]	0.00133	0.058

Table 5.28: Data at $\beta = 0.2240$ obtained with the BF method, where the data with index (a) have been taken from ref. [42]. The best fit values to eq. (5.83) are given in the fourth column. The t–extensions of the lattices in the x_3–direction are also reported

On the other hand, if one uses eq. (5.65) or eq. (5.64) one gets

$$E_S^{(1l)}(\sigma, L_1, L_2) = \sigma' L_1 L_2 - \frac{\lambda'}{\lambda} \quad , \tag{5.109}$$

because one–loop quantum contributions do not depend on β. In particular, from eq. (5.83) one expects corrections proportional to $(Area)^{-1}$ due to the two–loop corrections to the CWM which would be absent for a pure Gaussian model.

To measure the surface energy we follow the MC procedure which was already used in ref. [BB6]. Consider again the ratio Z_a/Z_p. From eq. (5.106) one can express the ratio Z_a/Z_p in terms of the two largest transfer matrix eigenvalues

$$\frac{Z_a}{Z_p} \simeq \frac{t}{2}\left(1 - \frac{\lambda_{0a}}{\lambda_{0s}}\right) , \tag{5.110}$$

where we again ignore terms of order $O\left[(\lambda_{1s}/\lambda_{0s})^t\right]$. In addition we assume that $t << 1/\Delta E$. This means that for periodic boundary conditions the configurations without an interface dominate while for anti-periodic boundary conditions there is only one interface present in almost all configurations. Then, within this approximation, one obtains from eq. (5.110) a definition of surface energy which does not depend on the extension t, and

$$E_S \equiv E_p - E_a \quad , \tag{5.111}$$

with $E_p =< H >_p$ and $E_a =< H >_a$.

We have applied this method at $\beta = 0.240$ for many lattice sizes with t ranging from 10 to 40. The surface energies E_S for each lattice are given in table 5.29.

Local Demon Algorithm

The variance of the energy stems to a major part from fluctuations on small scales. Hence an optimally implemented local algorithm is superior to a cluster algorithm in solving this particular problem. We used a micro-canonical demon algorithm [124, 125, 126] in combination with a particularly efficient canonical update [136] of the demons. This type of algorithm circumvents the frequent use of random numbers. The algorithm is implemented using the multi-spin coding technique [125, 126]. Every bit of a computer word carries one Ising spin. In order to avoid restrictions of the geometry we simulate 32 (the number of bits in a word) independent systems.

We have chosen demons that carry the energies 4, 8, and 16. We take one demon for each lattice site.

First we used the cycle described in [BB6] to simulate the systems with periodic and anti-periodic boundary conditions independently. However, it turned out that in contrast to the situation close to the roughening transition, near the bulk critical point also frequent updates of the demons carrying the energies 8 and 16 are needed to obtain autocorrelation times close to that of the Metropolis algorithm. As one can see from the CPU times summarized in table 1 of ref. [BB6], this would mean a considerable increase of the CPU time needed.

L_1	L_2	t	E_S	$E_S^{(CWM)}$	x
4	16	20	188.57(22)		0.40
5	20	30	348.49(22)		0.26
6	24	30,40	521.73(16)		0.18
7	28	40	720.90(28)		0.13
8	8	30	214.19(8)		0.07
8	32	30,40	949.58(18)		0.08
9	9	30	278.85(7)		0.05
9	16	20	518.58(17)		0.04
9	36	30,40	1207.47(17)		0.08
9	64	30	2173.99(53)		0.16
10	10	30	350.96(7)	351.06	0.04
10	40	30,40	1496.65(19)	1496.47	0.06
11	11	30	430.66(8)	430.62	0.03
11	44	30,40	1816.17(25)	1815.98	0.05
12	12	30,40	517.94(9)	517.93	0.03
12	48	40	2165.83(35)	2166.18	0.05
13	13	30	613.07(9)	612.95	0.02
14	14	30,40	715.73(17)	715.66	0.02
15	15	30	825.83(19)	826.04	0.02
16	16	30,40	944.16(18)	944.08	0.02
18	18	30,40	1203.11(15)	1203.12	0.01
20	20	30,40	1492.86(20)	1492.73	0.01
22	22	30,40	1812.86(21)	1812.89	0.009
24	24	30,40	2163.25(23)	2163.58	0.007

Table 5.29: Data for the surface energy at $\beta = 0.240$ obtained by MC simulations with the local demon algorithm. The CWM best fit values of eq. (5.83) to these data are given in the case $L_1 \geq 10$. In the last column the values of the two–loop parameter x defined in eq. (5.112) are given

We could, however, overcome this problem by simulating systems with periodic and anti-periodic boundary conditions in a single simulation and coupling them to the same demon system. It turned out that for our particular choice of the update cycle, the integrated autocorrelation time of $E_p - E_a$ was almost one order of magnitude smaller than the integrated autocorrelation time of E_p and E_a as separate quantities.

The cycle that we used mostly can be explained as follows. The simulation was done by performing a cycle of 6 groups, where each group consisted of a *micro-canonical* update of the 32 periodic systems and the demon, the 32 anti-periodic systems plus the demon and a *translation* or a shift with respect to the 32 copies of the spin system of the demon layer with energy 4, 8, or 16 (alternating). Each group was finished by updating the demons with energy 4. The whole cycle was completed by updating the demons with energy 8. We performed a measurement twice in this cycle.

For the $24 \times 24 \times 40$ lattice at $\beta = 0.24$ we observed the integrated autocorrelation times $\tau_p = 5.3$ and $\tau_a = 5.1$ of the energy with periodic and anti-periodic boundary conditions, while the integrated autocorrelation time of the surface energy $\tau_s = 0.6$ was about one order of magnitude smaller. As unit of the autocorrelation time we took one cycle. The simulation with 200000 cycles took about 104 h on a SPARC 10 workstation.

We used the drand48 random number generator from the C-library and the G05CAF from the NAGLIB. For some choices of the parameters we simulated with both random number generators. The results are consistent within the error bars.

5.3.4 Monte Carlo Data Analysis

We shall now compare the CWM predictions with data extracted from MC simulations for the two observables defined in eqs. (5.89,5.92).

FSEs of the Interface Free Energy

Let us first discuss the fits of the energy gap formula eq. (5.89) to the data given in tabs. 5.25–5.28, using different functional forms for the interface partition function Z, in analogy with refs. [116, 119].

We call *classical*, *one–loop* and *two–loop* fits those made with Z given by eq. (5.65), eq. (5.64) and eq. (5.83), respectively.

The values of the energy gaps we used range over nearly four orders of magnitude, the biggest value being $\Delta E = 0.0444$ at $\beta = 0.2246$, for a $L_1 = L_2 = 13$ lattice size, and the smallest $\Delta E = 0.09 \cdot 10^{-4}$ at $\beta = 0.2275$, with $L_1 = L_2 = 26$ (see tabs. 5.25 and 5.27).

To obtain estimates of ΔE for large lattice sizes the BF method is more efficient than the TSC method. For this reason we have principally used it at $\beta = 0.2240$ (table 5.28), which (from our set of values) is the closest to to the critical point. Rather large lattices are needed here (see also table 5.24). The BF algorithm has been also used to take some measurements at $\beta = 0.2275$, to obtain energy gaps for particularly small value of the two–loop contribution

β	approx.	χ^2/dof	C.L.	dof	σ	$\lambda/\sqrt{\sigma}$
0.2240	2l	0.63	86%	16	0.004778(14)	1.343(13)
	1l	2.02	1 %	16	0.004839(14)	1.561(15)
	cl	66.0	0 %	16	0.004534(14)	1.480(13)
0.2246	2l	0.54	82%	8	0.006547(69)	1.354(16)
	1l	1.89	6 %	8	0.006792(69)	1.681(18)
	cl	17.5	0 %	8	0.005987(73)	1.539(16)
0.2258	2l	0.45	89%	8	0.009418(61)	1.271(14)
	1l	1.50	15%	8	0.009587(61)	1.511(15)
	cl	20.2	0 %	8	0.008363(63)	1.324(13)
0.2275	2l	1.05	40%	16	0.014728(40)	1.332(5)
	1l	2.36	0 %	16	0.015283(40)	1.612(6)
	cl	18.3	0 %	16	0.015114(39)	1.594(6)

Table 5.30: For each β, we report the best fit results obtained using eq. (5.83), eq. (5.64) and eq. (5.65), which correspond to 2–loop, 1–loop and classical approximation, respectively

parameter

$$x \equiv f(u)/(\sigma A) \quad , \tag{5.112}$$

where $f(u)$ is defined by eq. (5.79), with $u = L_2/L_1$ and $A = L_1 L_2$.

In table 5.30 we report the fits we made for each β: the reduced χ^2 of the classical fits turns out to be always more than one order of magnitude greater than those of one and two–loop fits, in agreement with what was already shown in [114, 116]. Moreover, two–loop fits show a level of confidence which is higher than the one–loop fits for all β's: this is the first evidence that the two–loop corrections discussed above correctly describe the data.

For $\beta = 0.2246$, 0.2258 and 0.2275 the MC data[15] are given in figure 5.16, while those referring to $\beta = 0.2240$, which range over a rather different scale both in ΔE and in A, are plotted in figure 5.17. The lines represent the best two–loop fits; their values in correspondence of the MC data are also given in tabs. 5.25–5.28 ($\Delta E^{(CWM)}$).

Both the high χ^2 values of the fits and the clear u–dependence of the MC data in figure 5.16 and figure 5.17 show that the classical contribution, eq. (5.65), being only function of A and not of u is completely ruled out.

Therefore, from now on, we concentrate on the one and two–loop functional forms.

Let us now make some further considerations on the different results one obtains with the one–loop and the two–loop approximations to the CWM. The parameter x, at fixed β and for any given lattice, gives the relative weight of the two–loop correction with respect to the classical and one-loop contributions (see eq. (5.83)). One expects that a fit on a sample of data for which $x \ll 1$ should give consistent results both at one and two–loop and that, as one increases the

[15]Some data at $\beta = 0.2275$ and $\beta = 0.2240$ do not appear in the figures: their behavior is analogous to that of the other data. They have been omitted only in order to have a better resolution in the figures

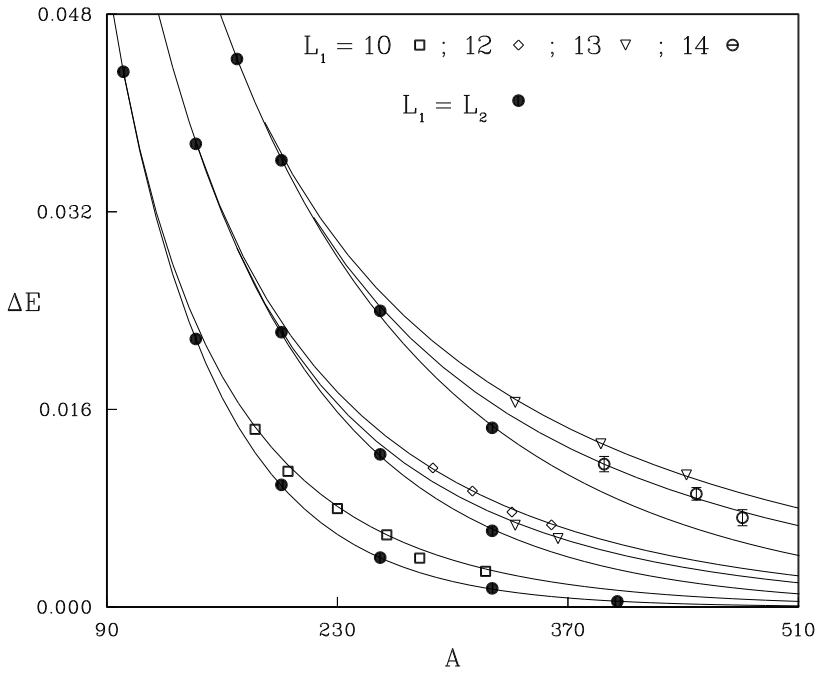

Figure 5.16: MC data and best fit curves obtained with the two–loop formula (5.83) plotted for different values of β versus the classical interface area $A = L_1 L_2$. From top to bottom, the first three lines correspond to $\beta = 0.2246$, the next three to $\beta = 0.2258$ and the last two to $\beta = 0.2275$. The values are also given in tables 5.25, 5.26 and 5.27, respectively

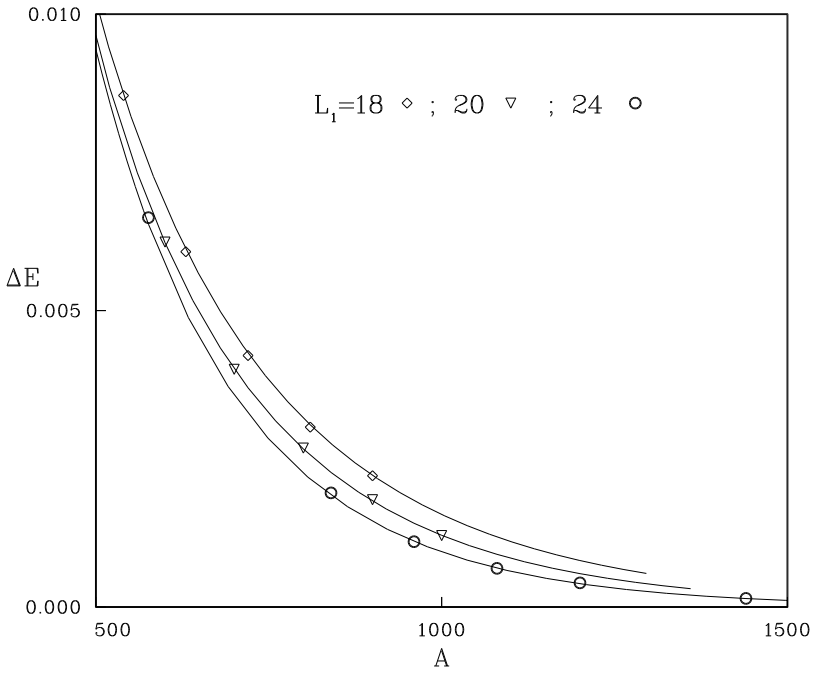

Figure 5.17: The same as figure 5.16 but for $\beta = 0.2240$

value of x, the fits made with the two–loop contributions should have better confidence levels than those made with the one–loop only. Finally, if the CWM is the correct picture, an upper value of x should exists at which higher order corrections should become important and fits with the two–loop contribution should start to show higher χ^2's.

The values of x for all samples of data are given, in tables 5.25–5.28 in the last columns, while the values of σ which have been used to evaluate it (see eq. (5.112)) are given in table 5.30 (the differences between the one and two–loop values are not appreciable in this case). One can see that x ranges from 0.03 up to the rather large value of 0.27.

In order to make more stringent fits, we can use all the data we have by expressing σ through the scaling law (5.91): the free parameters then become $\lambda/\sqrt{\sigma}$, σ_∞ and ν. With this assumption eqs. (5.64,5.83) take the form

$$Z_{1l} = \frac{\lambda}{\sqrt{\sigma}} \sqrt{\sigma_\infty} \left(1 - \beta_c/\beta\right)^\nu e^{-\sigma_\infty A (1-\beta_c/\beta)^{2\nu}} Z_q^{(g)}(u) \tag{5.113}$$

$$Z_{2l} = Z_{1l} \cdot \left[1 + \frac{f(u)\left(1-\beta_c/\beta\right)^{-2\nu}}{\sigma_\infty A} + O\left(\frac{\left(1-\beta_c/\beta\right)^{-4\nu}}{(\sigma_\infty A)^2}\right)\right] \quad . \tag{5.114}$$

According to the usual attitude, we make the fits also using the other scaling law

$$\sqrt{\sigma(\beta)} = \sqrt{\sigma_\infty}\left(\frac{\beta}{\beta_c} - 1\right)^\nu \tag{5.115}$$

with the obvious modifications of eqs. (5.113,5.114).

We performed the fits on the samples of energy gaps

$$\left\{ \Delta E(x) \mid x \le x_{cut} \right\} \quad , \tag{5.116}$$

starting from the first six data ($x_{cut} = 0.058$) and adding two data each time, so that the last fits contain all the 56 data. The corresponding χ^2/dof obtained with the one–loop (empty circles) and two–loop (full circles) formulae written above, as functions of x_{cut}, are reported in figure 5.18.

From the figure one can see that the one–loop formula (5.113) has a 50% confidence level (or more) for $x_{cut} \sim 0.15$, which corresponds to 36 data over 56 of our sample, while the two–loop formula (5.114) reaches, with the same confidence level, $x_{cut} \sim 0.20$, which corresponds to 47 data. The fact that both fits on the first sample have a reduced χ^2 greater than one is instead due to the lack of statistics (only 6 data points). For $x_{cut} > 0.2$, the reduced χ^2 of the fits made with the two–loop correction indicates that higher order corrections could be important. Notice, however, that the confidence levels for the two–loop fits are better than those for the one–loop fits. The parameter of the fits turns out be very stable, for both types of fits, until the $\chi^2/dof \approx 1$: these are given in table 5.31 for the two limiting samples discussed above. The results obtained for σ_∞ and ν are consistent with the values reported in the literature and, almost, with each other, the only difference being in the constant $\lambda/\sqrt{\sigma}$. Let us point out that, if the two–loop contributions obtained from the CWM Hamiltonian (5.57) are physical,

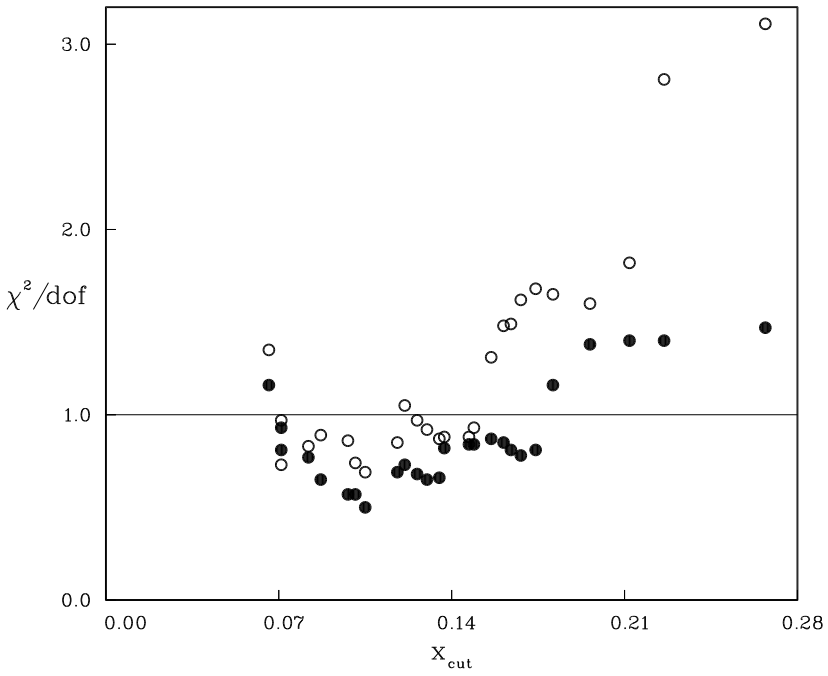

Figure 5.18: χ^2/dof of the fits made with the one–loop eq. (5.113) (empty circles) and two–loop eq. (5.114) (full circles) on the samples defined by eq. (5.116)

scaling law	approx.	χ^2/dof	C.L.	dof	σ_∞	ν	$\lambda/\sqrt{\sigma}$
Eq. (5.91)	2l	0.86	74%	44	1.47(1)	0.629(1)	1.333(8)
	1l	0.94	56%	33	1.55(2)	0.633(1)	1.535(10)
Eq. (5.115)	2l	0.88	70%	44	1.32(1)	0.618(1)	1.331(8)
	1l	0.94	56%	33	1.38(1)	0.622(1)	1.533(10)

Table 5.31: Fits on the samples defined by eq. (5.116), with $x_{cut} \approx 0.2$ and $x_{cut} \approx 0.15$ for the two–loop eq. (5.114) and the one–loop eq. (5.113), respectively

one expects the two formulae (5.113,5.114) to give the same constant when the above fitting procedure is applied to a sample with $x_{cut} \approx 0$. As we can observe looking at our sample of data, it is rather difficult to reduce x_{cut} below 0.05 without spoiling the reliability of the statistics of our analysis, but we can significantly check the constance of $\lambda/\sqrt{\sigma}$ making fits on (independent) samples in which the x values included are approximately constant. That is, we define the sample

$$\{ \quad \Delta E\,(x) \quad | \quad x_i \leq x \leq x_{i+\epsilon} \quad \} \tag{5.117}$$

and we denote with x_{av} the average value of x within each sample.

The results are given in table 5.32 and in figure 5.19. It turns out that both the ν and σ_∞ values are very stable on the whole sample, discarding the last one where x_{av} is too big. However, while the one–loop and two–loop constants are compatible for $x_{av} = 0.04 - 0.07$, moving toward greater x_{av} values $\lambda/\sqrt{\sigma}$ increases systematically in the one–loop case but remains stable when the two–loop formula is used. This indicates that the absence of the $1/(\sigma A)$ corrections in the Gaussian formula is artificially compensated by the enhancements of its constant, already for $x_{av} \sim 0.1$. As a final comment, let us note that a comparison with a semiclassical ϕ^4 approach [15] suggests to fix $\lambda/\sqrt{\sigma}$ to $[4\ \Gamma(3/4)/\Gamma(1/4)] \simeq 1.352$, in good agreement with the two–loop value $\simeq 1.33(1)$ of table 5.31 and table 5.32.

FSEs of the Surface Energy

In this section we discuss the finite size behavior of the interface partition function from MC measurements of the surface energy defined by eq. (5.92).

As already before, this approach has the advantage that the two–loop contribution appears as an additive correction to the surface free energy calculated at the Gaussian (and classical) level, as given by eq. (5.108) and eq. (5.109), respectively. We decided to make our simulations at $\beta = 0.240$ also because very precise estimates of σ and σ' (two of the three parameters on which eqs. (5.108,5.109) depend) are known,

$$\sigma = 0.0590(2) \quad , \text{ from } [\text{BB4}] \tag{5.118}$$

$$\sigma' = 3.813(2) \quad , \text{ from } [41] \ . \tag{5.119}$$

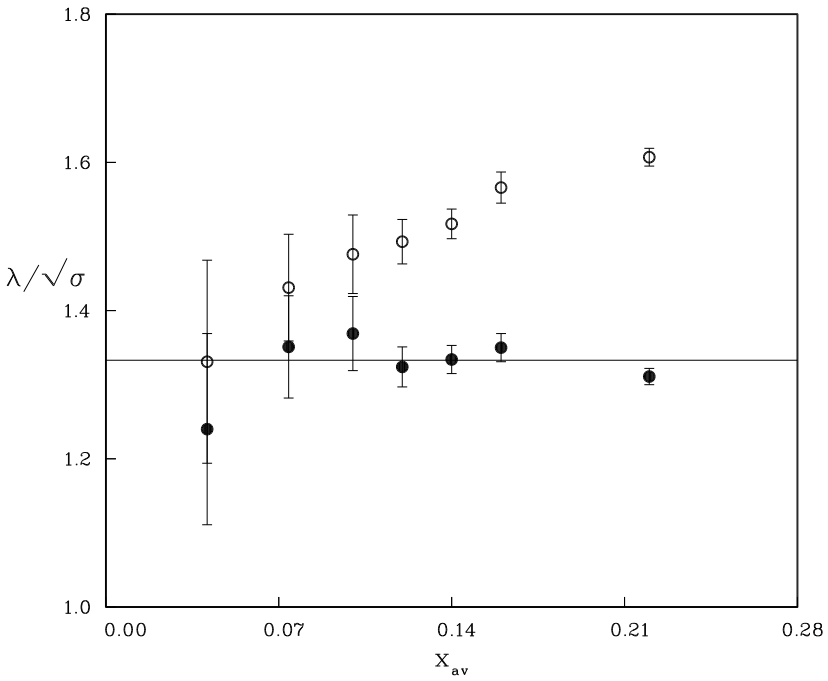

Figure 5.19: Values of the constant $\lambda/\sqrt{\sigma}$ obtained fitting on the samples defined by eq. (5.117) with the one–loop eq. (5.113) (empty circles) and two–loop eq. (5.114) (full circles)

scaling law	x_{av}	approx.	χ^2/dof	C.L.	dof	σ_∞	ν	$\lambda/\sqrt{\sigma}$
Eq. (5.91)	0.04	2l	1.39	25%	2	1.53(6)	0.636(7)	1.24(13)
		1l	1.50	22%	2	1.55(6)	0.637(7)	1.33(14)
	0.07	2l	0.65	66%	5	1.49(6)	0.630(3)	1.35(7)
		1l	0.72	61%	5	1.48(6)	0.630(3)	1.43(7)
	0.10	2l	0.24	95%	5	1.48(4)	0.629(2)	1.37(5)
		1l	0.35	88%	5	1.50(5)	0.631(2)	1.48(5)
	0.12	2l	0.78	54%	4	1.44(6)	0.627(4)	1.32(3)
		1l	0.82	51%	4	1.47(6)	0.629(4)	1.49(3)
	0.14	2l	1.31	25%	6	1.49(4)	0.630(3)	1.33(2)
		1l	1.96	7%	6	1.51(4)	0.631(3)	1.52(2)
	0.16	2l	0.78	59%	6	1.50(7)	0.630(5)	1.35(2)
		1l	0.74	62%	6	1.50(7)	0.630(5)	1.57(2)
	0.21	2l	2.87	1%	7	1.28(4)	0.612(3)	1.31(1)
		1l	6.16	0%	7	1.58(5)	0.634(4)	1.61(1)
Eq. (5.115)	0.04	2l	1.39	25%	2	1.37(5)	0.625(7)	1.24(13)
		1l	1.50	22%	2	1.39(5)	0.626(7)	1.33(14)
	0.07	2l	0.66	65%	5	1.33(5)	0.619(3)	1.35(7)
		1l	0.72	61%	5	1.33(5)	0.619(3)	1.43(7)
	0.10	2l	0.24	95%	5	1.33(4)	0.618(2)	1.37(5)
		1l	0.34	89%	5	1.34(5)	0.620(2)	1.48(5)
	0.12	2l	0.87	48%	4	1.29(5)	0.616(4)	1.32(3)
		1l	0.88	47%	4	1.32(5)	0.618(4)	1.49(3)
	0.14	2l	1.07	38%	6	1.34(4)	0.620(3)	1.33(2)
		1l	1.70	12%	6	1.35(4)	0.621(3)	1.51(2)
	0.16	2l	0.77	59%	6	1.35(6)	0.620(5)	1.35(2)
		1l	0.73	62%	6	1.35(6)	0.620(5)	1.57(2)
	0.21	2l	2.83	1%	7	1.14(3)	0.600(3)	1.31(1)
		1l	6.19	0%	7	1.40(4)	0.622(4)	1.61(1)

Table 5.32: Fits on the samples defined by eq. (5.117)

Our preliminary step is to assume as external inputs these values and, assuming they are not biased, to use them to test the reliability of the functional form of the second order quantum contribution to the interface free energy.

Let us define the following surface energy differences (at fixed β)

$$\Delta E_S\left(L\right) = E_S\left(2L, L/2\right) - E_S\left(L, L\right) \tag{5.120}$$

considering two different lattices, one with $u = L_2/L_1 = 4$ and the other with $u = 1$, but with the same area $A = L_1 L_2 = L^2$. Then, from eqs. (5.109,5.108) one obtains

$$\Delta E_S^{(1l)}\left(L\right) = 0 \tag{5.121}$$

$$\Delta E_S^{(CWM)}\left(L\right) = \left.\frac{\partial_\beta Z_q^{(2l)}}{Z_q^{(2l)}}\right|_{u=4} - \left.\frac{\partial_\beta Z_q^{(2l)}}{Z_q^{(2l)}}\right|_{u=1} . \tag{5.122}$$

The theoretical prediction of the Gaussian model requires these differences to be zero, while that of the CWM at two–loop does not depend any more on the third parameter, λ'/λ. Eq. (5.122) can be written explicitly as

$$\Delta E_S^{(CWM)} = \frac{\sigma'}{\sigma^2 L^2}\ \left[f\left(4\right) - f\left(1\right)\right] \tag{5.123}$$

where $f(u)$ is given by eq. (5.79) and in the two points we are considering takes the values $f(1) = 0.25$ and $f(4) \simeq 1.52$.

Using the MC data given in table 5.29 (taken at $\beta = 0.240$) one can easily construct these differences. They are given in the first column of table 5.33, where we have assumed $L \equiv 2L_1 = L_2/2$. It is clear that all these data are not compatible with zero. Assuming the validity of eqs. (5.118,5.119) and plugging the values into eq. (5.123) we obtain the theoretical predictions reported in the second column of table 5.33. Monte Carlo data and theoretical predictions are plotted in figure 5.20.

A nice $Area^{-1}$ behavior is clearly seen in the MC data for $L \geq 16$, in good agreement with eq. (5.123). Comparing the last column of table 5.29 with table 5.33 one sees that this corresponds to $x \sim 0.1$, while for $x \geq 0.13$ higher order corrections would be needed and for $x \geq 0.20$ the two–loop contributions are definitively too small.

Then we follow the same approach of the preceding discussion, that is we assume different forms of the free energy and choose among them using the reduced χ^2s of the fits with equal number of parameters. In this case, our main parameters are fixed from the fits.

We fit eq. (5.108), which can be written explicitly as

$$E_S^{(CWM)}\left(L_1, L_2\right) = \sigma' L_1 L_2 + \frac{\sigma'}{\sigma^2 L_1 L_2} f(u) - \frac{\lambda'}{\lambda} \tag{5.124}$$

and eq. (5.109). The results are given in table 5.34, where the parameters refer to the two–loop fits while, for the Gaussian fits, only the reduced χ^2's are given in the second column.

L	ΔE_S	ΔE_S^{CWM}
8	-25.62(30)	21.754(159)
10	-2.47(29)	13.923(102)
12	3.79(25)	9.669(71)
14	5.17(45)	7.103(52)
16	5.42(36)	5.439(40)
18	4.36(32)	4.297(31)
20	3.79(39)	3.481(25)
22	3.31(46)	2.877(21)
24	2.58(58)	2.417(18)

Table 5.33: Differences of surface energies at $\beta = 0.240$, obtained from eq. (5.120) with the data of table 5.29 and the notation $L = 2L_1 = L_2/2$. The theoretical predictions $\Delta E_S^{(CWM)}$ are given by eqs. (5.123,5.118,5.119)

$L_1 \geq$	χ^2_{1l}/dof	χ^2/dof	C.L.	dof	σ	σ'	λ'/λ
8	107.2	8.02	0.00	17	0.0620(7)	3.81383(24)	33.10(8)
9	83.3	2.25	0.00	15	0.0593(8)	3.81321(25)	33.12(9)
10	48.5	0.96	0.48	11	0.0569(12)	3.81292(29)	33.17(13)
11	24.1	0.66	0.74	9	0.0565(18)	3.81261(36)	33.10(17)
12	8.4	0.57	0.78	7	0.0596(37)	3.81213(50)	32.83(27)
13	1.7	0.72	0.60	5	0.057(11)	3.8123(14)	32.95(87)

Table 5.34: Data of table 5.29 are fitted using eq. (5.124). For comparison, the reduced χ^2's are reported of the fits on the same sample of data using eq. (5.109)

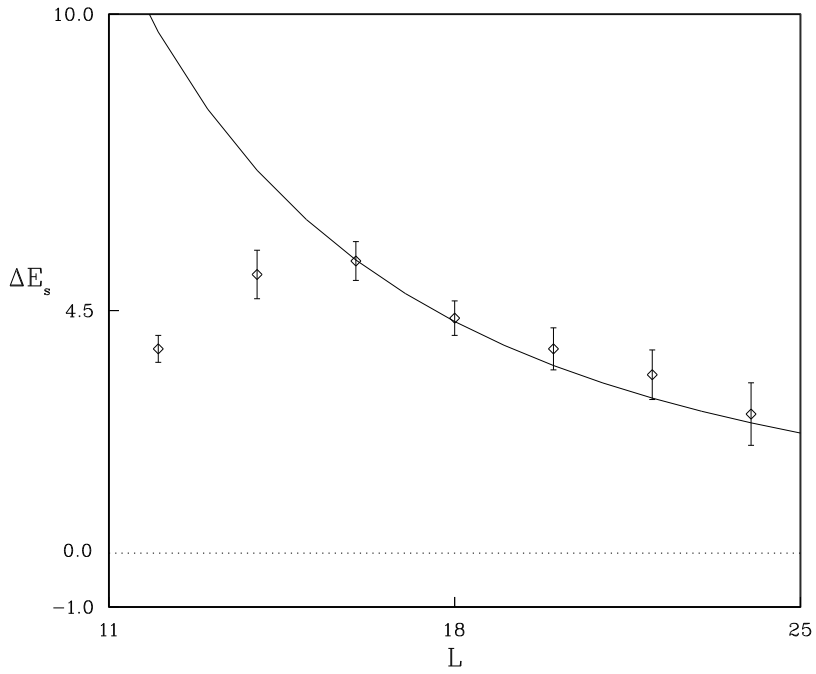

Figure 5.20: Comparison between Monte Carlo data and theoretical predictions (see eq. (5.123) in the text) for the surface energy differences defined in eq. (5.120). The corresponding values are also given in table 5.33. The dotted line is the theoretical expectation if two–loop corrections are neglected

$L_1 \geq$	σ	σ'	$\sigma'/(2\sigma)$	ν
Eq. (5.118,5.119)	0.0590(2)	3.813(2)	32.31(13)	0.593(2)
10	0.0569(12)	3.81292(29)	33.5(7)	0.615(13)
11	0.0565(18)	3.81261(36)	33.7(1.1)	0.619(20)

Table 5.35: The scaling ratio $\sigma'/(2\sigma)$ is evaluated according to eq. (5.125), with $\nu \simeq 0.63$ for three estimates of σ and σ'. In the last column the corresponding estimates of ν, using eq. (5.126), are given

Finally, we can make an interesting check comparing the ratio of σ' and σ with the equation one obtains from the asymptotic scaling laws. Taking the derivative with respect to β in eq. (5.115), one gets

$$\frac{\sigma'}{2\sigma} = \frac{\nu}{(\beta - \beta_c)} \quad . \tag{5.125}$$

To compute this ratio we take the last two results of table 5.34, the values of eqs. (5.118,5.119) and assume $\nu \simeq 0.63$. The results are given in the fourth column of table 5.35. Notice that the RHS of eq. (5.125) should also be obtained from λ'/λ: from table 5.34 one sees that the two estimates agree within errors.

On the other side, one can also assume this ratio as an input to evaluate the critical index ν, inverting eq. (5.125); one gets

$$\nu = \frac{\sigma' \, (\beta - \beta_c)}{2\sigma} \quad . \tag{5.126}$$

The corresponding values are given in the last column of table 5.35. The agreement with the expected values is good, though the errors are still large.

In this study we have demonstrated that the finite size effects of interface properties in the 3-dimensional Ising model are rather well described by the two–loop expansion of the CWM. Our MC data for the energy gap and the surface energy prove that there are corrections to the Gaussian approximation, and the various fits indicate that these corrections are indeed given (up to even higher corrections) by the two–loop result, with no extra coefficients introduced into the game. Since there is (yet) no rigorous proof that the two-loop corrections are universal (i.e., independent from the regularization scheme) we have to consider the predictive power of the two–loop CWM model a little bit as a miracle. We consider the present contribution as a first step towards a deeper understanding of the physics of rough interfaces in terms of effective models.

Acknowledgments

This work was supported in part by the German-Israeli Foundation for Research and Development (GIF).

I would like to thank all my collaborators, especially Martin Hasenbusch, who was involved in all the projects.

It is a pleasure to thank my friends in Israel and Italy for their kind hospitality.

A very interesting and stimulating correspondence with M.E. Fisher on the issues of chapter 5.2 is gratefully acknowledged.

Finally I would like to appreciate stimulating discussions with H. Arisue, G. Münster, and C. Wieczerkowski.

Bibliography

In this bibliography, I quote in addition to the journal references in most cases the title of the article, and, in many cases, the abstract or a short version thereof. Note that my way of shortening the abstract might be different from what the authors themselves would consider the right way to summarize.

Articles by the Author and Collaborators that form the Backbone of this Work

[BB1] H.G. Evertz, M. Hasenbusch, M. Marcu, K. Pinn, and S. Solomon,
Phys. Lett. B 254, 185 (1991).
'Stochastic Cluster Algorithms for Discrete Gaussian (SOS) Models.' We present new Monte Carlo cluster algorithms which eliminate critical slowing down in the simulation of 2-dimensional SOS models. The algorithms are based on reflecting the integer valued spin variables with respect to appropriately chosen reflection planes. The algorithm is applied and studied in simulations of the 2-dimensional discrete Gaussian model.
Conference contributions by the same authors: 'Surface Simulations without Critical Slowing Down', Nucl. Phys. B (Proc. Suppl.) 20 (1991) 80, and 'Cluster Algorithms for Surfaces', in: Proceedings of the Workshop on Fermion Algorithms, Jülich 1991, eds. H.J. Herrmann and F. Karsch, World Scientific, Singapore 1991.

[BB2] H.G. Evertz, M. Hasenbusch, M. Marcu, K. Pinn, and S. Solomon,
J. Phys. I France, 1669 (1991).
'High Precision Measurement of the SOS Surface Thickness in the Rough Phase.' Using a cluster algorithm without critical slowing down for the discrete Gaussian SOS model, we verify to high precision the linear dependence of the surface thickness on the logarithm of the lattice size.

[BB3] M. Hasenbusch, G. Lana, M. Marcu, and K. Pinn,
Phys. Rev. B 46, 10472 (1992).
'Cluster Algorithm for a Solid-On-Solid Model with Constraints.' We adapt the cluster algorithm described in ref. [BB1] to the simulation of the BCSOS model, which is an SOS model with constraints. A significant reduction of critical slowing down is observed.

[BB4] M. Hasenbusch and K. Pinn,
Physica A 192, 342 (1993).
'Surface Tension, Surface Stiffness, and Surface Width of the 3-dimensional Ising Model on a Cubic Lattice.' We compute properties of the interface of the 3-dimensional Ising model in the whole region from the low-temperature domain through the roughening transition to the bulk critical point. The interface tension is obtained by integrating the surface energy over the inverse temperature β. It is demonstrated that in the rough phase the large distance behavior of the interface is well described by a massless Gaussian dynamics. Results for the interfacial width on lattices up to $512 \times 512 \times 27$ are also presented.
Conference contribution by the same authors: 'Surface Tension, Surface Stiffness, and Surface Width of the 3-dimensional Ising Model on a Cubic Lattice', Nucl. Phys. B (Proc. Suppl.) 30, 857 (1993).

[BB5] H.G. Evertz, M. Hasenbusch, M. Marcu, and K. Pinn,
Physica A 199, 31 (1993).
'The Solid-on-Solid Surface Width Around the Roughening Transition.' We investigate the surface width W of solid-on-solid surfaces in the vicinity of the roughening temperature T_r. For temperatures above T_r, W^2 is expected to diverge with the system size L like $\ln L$. However, close to T_r, a clean $\ln L$ behavior can be seen only on extremely large lattices. Starting from the Kosterlitz-Thouless renormalization group, we derive an improved formula that describes the small L behavior of W on both sides of T_r. The formula is applied in the evaluation of data for the Discrete Gaussian model that we obtained with the cluster algorithms of ref. [BB1].

[BB6] M. Hasenbusch and K. Pinn,
Physica A 203, 189 (1994).
'Comparison of Monte Carlo Results for the 3D Ising Interface Tension and Interface Energy with (Extrapolated) Series Expansions.' We compare Monte Carlo results for the interface tension and interface energy of the 3-dimensional Ising model with Padé and inhomogeneous differential approximants of the low temperature series in $u = \exp(-4\beta)$. The series is expected to suffer from the roughening singularity at $u \approx 0.196$. The comparison with the Monte Carlo data shows that the series extrapolations fail to improve on the naive truncated series results in the region around the roughening transition.

[BB7] M. Hasenbusch, M. Marcu, and K. Pinn,
Physica A 208, 124 (1994).
'High Precision Renormalization Group Study of the Roughening Transition.' We confirm the Kosterlitz-Thouless scenario of the roughening transition for three different SOS models: the Discrete Gaussian model, the Absolute-Value-Solid-On-Solid model and the dual transform of the XY-model. The method is based on a matching of the renormalization group flow of the candidate models with the flow of a bona fide KT model, the exactly solvable BCSOS model. We obtain high precision estimates for the critical couplings and other non-universal quantities.
Conference contribution by the same authors: 'High Precision Verification of the Kosterlitz-Thouless Scenario', Nucl. Phys. B (Proc. Suppl.) 26, 598 (1992).

[BB8] M. Caselle, R. Fiore, F. Gliozzi, M. Hasenbusch, K. Pinn, and S. Vinti, Nucl. Phys. B 432, 590 (1994).
'Rough Interfaces Beyond the Gaussian Approximation.' We compare predictions of the Capillary Wave Model beyond its Gaussian approximation with Monte Carlo results for the energy gap and the surface energy of the 3D Ising model in the scaling region. Our study reveals that the finite size effects of these quantities are well described by the Capillary Wave Model, expanded to two-loop order (one order beyond the Gaussian approximation).

[BB9] M. Hasenbusch, M. Marcu, and K. Pinn, Physica A 211, 255 (1994).
'The Sine Gordon Model: Perturbation Theory and Cluster Monte Carlo.' We study the expansion of the surface thickness in the 2-dimensional lattice Sine Gordon model in powers of the fugacity z. Using the expansion to order z^2, we derive lines of constant physics in the rough phase. We describe and test a VMR cluster algorithm for the Monte Carlo simulation of the model. The algorithm shows nearly no critical slowing down. We apply the algorithm in a comparison of our perturbative results with Monte Carlo data.

KT Transition, Interfaces, SOS Models, and Roughening

[1] J.M. Kosterlitz and D.J. Thouless, J. Phys. C 6, 1181 (1973).
'Ordering, metastability and phase transitions in two-dimensional systems.' A new definition of order called topological order is proposed for two-dimensional systems in which no long-range order of the conventional type exists. The possibility of a phase transition characterized by a change in the response of the system to an external perturbation is discussed in the context of a mean field type of approximation. The critical behaviour found in this model displays very weak singularities. The application of these ideas to the XY model of magnetism, the solid-liquid-transition, and the neutral superfluid are discussed. This type of phase transition cannot occur in a superconductor nor in a Heisenberg ferromagnet, for reasons that are given.

[2] J.M. Kosterlitz, J. Phys. C 7, 1046 (1974).
'The critical properties of the two-dimensional XY model.' The critical properties of the XY model with nearest-neighbour interactions on a two-dimensional square lattice are studied by a renormalization group technique. The mean magnetization is zero for all temperatures, and the transition is from a state of finite to one of infinite susceptibility. The correlation length is found to diverge faster than any power of the deviation from the critical temperature. Analogues of the strong scaling laws are derived and the critical exponents, η and δ, are the same as for the two-dimensional Ising model.

[3] J.D. Weeks, G.H. Gilmer, and H.J. Leamy, Phys. Rev. Lett. 31, 549 (1973).
'Structural Transition in the Ising-Model Interface.' Low temperature expansions of moments of the gradient of the density profile and of the slope at its midpoint suggest that the interface width diverges at a temperature T_R about half of the critical temperature.

[4] S. Coleman, Phys. Rev. D 11, 2088 (1975).
'Quantum sine-Gordon equation as the massive Thirring model.' It is shown that the Sine Gordon

model with interaction term $\cos(\beta\varphi)$ has unbounded energy density for $\beta^2 > 8\pi$. The theory is equivalent to the zero-charge sector of the theory of a free massive Fermi field for $\beta^2 = 4\pi$. For other values of β the theory is equivalent to the zero-charge sector of the massive Thirring model. The Sine Gordon soliton is identified with the fundamental fermion of the Thirring model.

[5] S.T. Chui and J.D. Weeks, Phys. Rev. B 14, 4978 (1976).
'Phase transition in the two-dimensional Coulomb gas, and the interfacial roughening transition.' The behavior of the interface in the 3-D Ising system is modeled using a 2-D array of columns of varying height. It is shown that the roughening transition is directly related to the metal-insulator transition in a 2-D coulomb gas.

[6] J.V. José, L.P. Kadanoff, S. Kirkpatrick, and D.R. Nelson,
Phys. Rev. B 16, 1217 (1977).
'Renormalization, vortices, and symmetry-breaking perturbations in the two-dimensional planar model.' The XY model is studied at low temperatures by means of renormalization theory and a series of exact transformations.

[7] T. Ohta and K. Kawasaki, Prog. Theor. Phys. 60, 365 (1978).
'Renormalization Group Theory of the Interfacial Roughening Transition.' Interfacial properties near the roughening transition of a modified discrete Gaussian model in two dimensions are discussed.

[8] T. Ohta, Prog. Theor. Phys. 60, 968 (1978).
'Phase Transition in 2-D Sine-Gordon System.' The RG equations for the sine-Gordon system with a short wave-length cutoff in two dimensions are derived by means of a momentum-shell recursion method. The analysis gives rise to a possibility that certain classes of phase transitions can be described in a unified way with the Sine Gordon Hamiltonian.

[9] H. Yamamoto, Prog. Theor. Phys. 61, 363 (1979).
'Exact relation between the Sine-Gordon system and the Coulomb Gas system.'

[10] S. Samuel, Phys. Rev. D 18, 1916 (1978).
'Grand partition function in field theory with applications to sine-Gordon field theory.' Certain relativistic field theories are shown to be equivalent to the grand partition function of an interacting gas.

[11] D.J. Amit, Y.Y. Goldschmidt, and G. Grinstein, J. Phys. A13, 585 (1980).
'Renormalization group analysis of the phase transition in the 2D Coulomb gas, Sine-Gordon theory and XY-model.' A systematic renormalization group technique for studying the 2D Sine Gordon theory (Coulomb gas, XY model) is presented.

[12] R.H. Swendsen, Phys. Rev. B 17, 3710 (1978).
'Correlation functions in XY models and step free energies in roughening models.' A duality relation derived by José et al. is exploited to calculate properties of XY and roughening models from known properties of the dual models.

[13] B. Nienhuis, J. Stat. Phys. 34, 731 (1984).
'Critical Behavior of Two-Dimensional Spin Models and Charge Asymmetry in the Coulomb Gas.' If possible, a transformation of a two-dimensional spin model into a Coulomb gas system can lead to a much better understanding of the phase transition.

[14] V. Privman, Phys. Rev. Lett. 61, 183 (1988).
'Finite Size Properties of the Angle-Dependent Surface Tension of Rough Interfaces.'

[15] G. Münster, Nucl. Phys. B 340, 559 (1990).
'Interface Tension in Three-Dimensional Systems From Field Theory.'

[16] I. Nolden, 'Equilibrium Crystal Shapes', PhD thesis, Utrecht 1990. Detailed analysis of the BCSOS model with respect to roughening and surface structure.

[17] M.E. Fisher and H. Wen, Phys. Rev. Lett. 68, 3564 (1992).
'Interfacial Stiffness and the Wetting Parameter: The Simple Cubic Ising Model.'

Roughening Experiments and Comparison with Theory

[18] F. Gallet, S. Balibar, and E. Rolley, J. Physique 48, 353 (1987).
'The roughening transition of crystal surfaces. I. Static and dynamic renormalization theory, crystal shape and facet growth.'

[19] F. Gallet, S. Balibar, and E. Rolley, J. Physique 48, 369 (1987).
'The roughening transition of crystal surfaces. II. Experiments on static and dynamic properties near the first roughening transition of hcp ^{4}He.'

[20] I.K. Robinson, E. Vlieg, H. Hornis, and E.H. Conrad,
Phys. Rev. Lett. 67, 1890 (1991).
'Surface Morphology of Ag(110) Close to Its Roughening Transition.' Report on an experimental investigation of the Ag(110) surface using synchrotron x-ray diffraction.

[21] H. Häkkinen, J. Merikoski, M. Manninen, J. Timonen, and K. Kaski,
Phys. Rev. Lett. 70, 2451 (1993).
'Roughening of the CU(110) Surface.' The structure of the Cu(110) surface is studied at high temperatures using a combination of lattice-gas Monte Carlo and molecular dynamics methods with many-atom interactions. A roughening transition is found around 1000 K.

Roughening in Lattice Gauge Theories

[22] C. Itzykson, M.E. Peskin, and J.B. Zuber, Phys. Lett. B 95, 259 (1980).
'Roughening of Wilson's Surface.'

[23] A. Hasenfratz, E. Hasenfratz, and P. Hasenfratz, Nucl. Phys. B 180, 353 (1981).
'Generalized Roughening Transition and Its Effect on the String Tension.'

[24] G. Münster and P. Weisz, Nucl. Phys. B 180, 13 (1981).
'On the Roughening Transition in Abelian Lattice Gauge Theories.'

[25] G. Münster and P. Weisz, Nucl. Phys. B 180, 330 (1981).
'On the Roughening Transition in Non-Abelian Lattice Gauge Theories.'

[26] M. Lüscher, Nucl. Phys. B 180, 317 (1981).
'Symmetry Breaking Aspects of the Roughening Transition in Gauge Theories.'

[27] J.M. Drouffe and J.B. Zuber, Nucl. Phys. B 180, 253 (1981).
'Roughening Transition in Lattice Gauge Theories in Arbitrary Dimension. (I) The Z_2 case.'

[28] J.M. Drouffe and J.B. Zuber, Nucl. Phys. B 180, 264 (1981).
'Roughening Transition in Lattice Gauge Theories in Arbitrary Dimension. (II) The groups Z_3, $U(1)$, $SU(2)$, $SU(3)$.'

Monte Carlo Studies of Ising Interfaces and Similar

[29] H.J. Leamy, G.H. Gilmer, K.A. Jackson, and P. Bennema,
Phys. Rev. Lett. 30, 601 (1973).
'Lattice-Gas Interface Structure: A Monte Carlo Simulation.' The (100), simple-cubic, lattice-gas interface structure has been simulated by Monte Carlo methods. For the interface width L we find $L = (1.05 \pm 0.04)(1 - T/T_c)^{-0.69}$, in the range $T \geq 0.5T_c$. This is larger than the bulk correlation length ξ by a factor of ~ 3.

[30] K. Binder, Phys. Rev. A 25, 1699 (1982).
'Monte Carlo calculation of the surface tension for two- and three-dimensional lattice-gas models.' It is suggested that the interface free energy between bulk phases with a macroscopically flat interface can be estimated from the variation of certain probability distribution functions of finite blocks with block size.

[31] E. Bürkner and D. Stauffer, Z. Phys. B 53, 241 (1983).
'Monte Carlo Study of Surface Roughening in the Three-Dimensional Ising Model.' Above a roughening temperature of about 0.56 T_c the thickness of the two-dimensional interface separating domain on a simple cubic lattice is found to increase roughly logarithmically with system size. Also, the interface tension is determined for temperatures below T_c.

[32] K.K. Mon, S. Wansleben, D.P. Landau, and K. Binder,
Phys. Rev. Lett. 60, 708 (1988).
'Anisotropic Surface Tension, Step Free Energy, and Interfacial Roughening in the Three-Dimensional Ising Model.' The anisotropic interfacial tension is calculated by Monte Carlo. The size dependence of the step free energy is used to probe the correlation length near the roughening transition.

[33] K.K. Mon and D. Jasnow, Phys. Rev. A 31, 4008 (1985).
'Monte Carlo evaluations of interfacial tension and universal amplitude ratios of the three-dimensional Ising model.' The interfacial tension of the simple-cubic Ising model near the transition temperature has been calculated with use of an extension of a recently proposed novel Monte Carlo method. Finite-size scaling theory was used to analyze the results and to obtain the surface tension amplitude. Universal ratios involving the surface tension amplitude are evaluated. Previous ambiguities in the theoretical value of the ratio involving the surface tension and specific-heat amplitudes have been clarified.

[34] K.K. Mon, Phys. Rev. Lett. 60, 2749 (1988).
'New Monte Carlo Estimates of Critical Interfacial Amplitudes and the Universality of Amplitude Ratios.' Critical interfacial tension amplitudes are obtained without calculating the related excess free energy.

[35] K.K. Mon, D.P. Landau, and D. Stauffer, Phys. Rev. B 42, 545 (1990).
'Interface roughening in the three-dimensional Ising model.' Based on a Monte Carlo determination of the interface thickness, the roughening temperature of a (100) interface in the three-dimensional Ising model is determined to be about 0.542 ± 0.005 in units of the critical temperature. The squared interface width in the rough phase is found to diverge logarithmically with the system size.

[36] H. Meyer-Ortmanns and T. Trappenberg, J. Stat. Phys. 58, 185 (1990).
'Surface Tension from Finite-Volume Vacuum Tunneling in the 3D Ising Model.' We measure the surface tension σ in the broken phase of the 3D Ising model at a temperature $T = 0.955\,T_c$ with two different methods which are taken from quantum field theory in finite volumes. Both methods rely on finite-size effects close to the phase transition.

[37] M. Hasenbusch, PhD thesis, Universität Kaiserslautern, 1992.

[38] S. Klessinger and G. Münster, Nucl. Phys. B 386, 701 (1992).
'Numerical Investigation of the interface tension in the three-dimensional Ising model.' The interface tension together with other physically relevant quantities is obtained from a calculation of time-slice correlation functions in a cylindrical geometry. The results are in good agreement with predictions from a semiclassical approximation in the framework of ϕ^4 theory.

[39] B.A. Berg, U. Hansmann, and T. Neuhaus, Z. Phys. B 90, 229 (1993).
'Properties of Interfaces in the two and three dimensional Ising model.' Interfacial properties of the 2D and 3D Ising model are calculated with the help of multimagnetical simulations. Following Binder, the interfacial free energy is extracted from the infinite volume limit of the magnetic probability density.

[40] H. Gausterer, J. Potvin, C. Rebbi, and S. Sanielevici, Physica A 192, 525 (1993).
'Surface Tension and Universality in the Ising Model.' Presentation of a numerical computation of the surface tension in the Ising model in two and three dimensions. The method is based on

a partition of the lattice into two halves, which are slowly driven from one magnetization state to the other.

[41] N. Ito, Physica A 196, 591 (1993).
'Non-equilibrium relaxation and interface energy of the Ising model.' Besides other quantities, the critical exponent ν and the critical amplitude of the surface tension σ_o of the three-dimensional Ising model are determined from a non-equilibrium critical relaxation study.

[42] M. Hasenbusch, J. Phys. I France 3, 753 (1993).
'Direct Monte Carlo measurement of the surface tension in Ising models.' A cluster algorithm is presented that gives direct access to the interface free energy of the Ising models. One simulates an ensemble that contains configurations with both periodic and with antiperiodic boundary conditions.

[43] K. Jansen, J. Jersák, I. Montvay, G. Münster, T. Trappenberg, and U. Wolff,
Phys. Lett. B 213, 203 (1988).
'Vacuum Tunneling in the Four-Dimensional Ising Model.' In the broken phase of the four-dimensional Ising model tunneling between the two degenerate minima of the effective potential takes place in a finite volume. We study this phenomenon numerically.

[44] K. Jansen and Y. Shen, Nucl. Phys. B 393, 658 (1993).
'Tunneling and Energy Splitting in Ising Models.' The energy splitting E_{0a} in two and four dimensional Ising models is measured in a cylindrical geometry on finite lattices. The results are compared with two different theoretical predictions.

[45] S. Kremer and D.E. Wolf, Physica A 182, 543 (1992).
'Numerical method for analyzing surface fluctuations.' A method for measuring the width of an interface in the presence of overhangs and holes is presented.

[46] H.L. Richards, M.A. Novotny, and P.A. Rikvold, Phys. Rev. B 48, 14584 (1993).
'A numerical transfer-matrix study of surface-tension anisotropy in Ising models on square and cubic lattices.' Computation of surface free energy, surface stiffness and single-step free energy by numerical transfer matrix methods.

Monte Carlo Studies of SOS Models

[47] R.H. Swendsen, Phys. Rev. B 15, 5421 (1977).
'Monte Carlo studies of the interface roughening transition.' Monte Carlo study of the roughening transition in the Discrete Gaussian and ASOS models.

[48] R.H. Swendsen, Phys. Rev. B 18, 492 (1978).
'Monte Carlo study of the Coulomb gas and the Villain XY model in the discrete Gaussian roughening representation.'

[49] W.J. Shugard, J.D. Weeks, and G.H. Gilmer, Phys. Rev. Lett. 41, 1399 (1978).
'Monte Carlo test of theories for the planar model, the F model, and related systems.' Monte Carlo results are compared to predictions of KT theory.

[50] R.H. Swendsen, Phys. Rev. B 25, 2019 (1982).
'Comment on a Monte Carlo test of theories for the planar model, the F model and related systems.'

[51] W.J. Shugard, J.D. Weeks, and G.H. Gilmer, Phys. Rev. B 25, 2022 (1982).
'Reply to Comment on a Monte Carlo test of theories for the planar model, the F model and related systems.'

[52] W. Janke and H. Kleinert, Phys. Rev. B 41, 6848 (1990).
'Monte Carlo study of two-step defect melting.'

Monte Carlo Studies of the XY Model

[53] S. Miyashita, H. Nishimori, A. Kuroda, and M. Suzuki,
Prog. Theor. Phys. 60, 1669 (1978).
'Monte Carlo Simulation and Static and Dynamic Critical Behavior of the Plane Rotator Model.' The properties of phase transition and the low temperature phase of the plane rotator model are studied with the Monte Carlo method.

[54] J. Tobochnik and G.V. Chester, Phys. Rev. B 20, 3761 (1979).
'Monte Carlo study of the planar spin model.'

[55] S. Miyashita, Prog. Theor. Phys. 63, 797 (1980).
'Monte Carlo Simulation of the Plane Rotator Model. II.' Results of ref. [53] are confirmed, and response to an external field is newly studied.

[56] S. Miyashita, Prog. Theor. Phys. 65, 1595 (1981).
'Monte Carlo Simulation of the Plane Rotator Model. III.' Features of the phase transition of the plane rotator model are investigated by the renormalization group method on energy, spin configuration and local order parameter density.

[57] H. Betsuyaku, Physica A 106, 311 (1981).
'Monte Carlo realization of Kadanoff block transformation in the 2d plane-rotator model.'

[58] J.E. Van Himbergen and S. Chakravarty, Phys. Rev. B 23, 359 (1981).
Helicity Modulus and Specific Heat of Classical XY Model in Two Dimensions.'

[59] J.E. Van Himbergen, Phys. Rev. B 25, 5977 (1982).
Helicity modulus and specific heat of the periodic Gaussian model in two dimensions.'

[60] F. Fucito and S. Solomon, Phys. Lett. B 134, 235 (1984).
'Does Monte Carlo Support the Kosterlitz-Thouless Scenario?' A modified Monte Carlo procedure is employed that permits tunneling between configurations with different numbers of free vortices. The data do not match the predictions of the vortex liberation scenario for the topological susceptibility. The results are interpreted as lack of support for the KT picture.

[61] J.E. Van Himbergen, J. Phys. C 17, 5039 (1984).

[62] G.G. Batrouni, G.R. Katz, A.S. Kronfeld, G.P. Lepage, B. Svetitsky,
and K.G. Wilson, Phys. Rev. D 32, 2736 (1985).
'Langevin simulations of lattice field theories.' An analysis of Langevin simulation techniques is presented, including a general discussion of errors and algorithm speed. Fourier techniques accelerate simulations on large lattices. As one of the many numerical examples the XY model is considered.

[63] J. Kogut and J. Polonyi, Nucl. Phys. B 265, 313 (1986).
'Microcanonical Study of the Planar Spin Model.' Average action, topological charge density and spin-spin correlation function of the XY model around criticality is studied by microcanonical and canonical Monte Carlo algorithms. Lattices are up to 30×30. A small shift (of order 1/volume) of the temperature brings the two ensembles into excellent agreement.

[64] P. Harten and P. Suranyi, Nucl. Phys. B 265, 615 (1986).
'Monte Carlo Renormalization Group Study of the XY Model.' The $\Delta\beta$ method is applied to investigate the phase structure of the XY model. The results support the KT scenario.

[65] M.S.S. Challa and D.P. Landau, Phys. Rev. B 33, 437 (1986).
'Critical behaviour of the six-state clock model in two dimensions.'

[66] J.F. Fernández, M.F. Ferreira, and J. Stankiewicz, Phys. Rev. B 34, 292 (1986).
'Critical behaviour of the two-dimensional XY-model: A Monte Carlo simulation.'

[67] H. Weber and P. Minnhagen, Phys. Rev. B 37, 5986 (1988).
'Monte Carlo determination of the critical temperature for the two-dimensional XY model.'

[68] W. Bernreuther and M. Göckeler, Phys. Lett. B 214, 109 (1988).
'An Investigation of the Phase Structure of the Two-Dimensional O(2) and O(4) Symmetric Nonlinear Sigma-Models.' Monte Carlo investigation of the phase structure using Binder's phenomenological renormalization group. Confirmation of KT scenario for O(2). No critical point is found for the O(4) case.

[69] R.G. Edwards and A.D. Sokal, Phys. Rev. D 38, 2009 (1988).
'Generalization of the Fortuin-Kasteleyn-Swendsen-Wang Representation and Monte Carlo Algorithm.'

[70] R. Gupta, J. DeLapp, G.G. Batrouni, G.C. Fox, C.F. Baillie, and J. Apostolakis, Phys. Rev. Lett. 61, 1996 (1988).
'Phase Transition in the 2D XY Model.' Detailed Monte Carlo results are presented for the critical quantities of the 2D XY model. The best fits are obtained with the KT scaling form with $\nu = 0.500(1)$, but η shows a considerable deviation from 1/4 down to $T = 1.03$. The critical temperature is estimated to be $T_c = 0.898(2)$.

[71] U. Wolff, Nucl. Phys. B 322, 759 (1989).
'Collective Monte Carlo Updating in a High Precision Study of the XY Model.'

[72] L. Biferale and R. Petronzio, Nucl. Phys. B 328, 677 (1989).
'Renormalization Group Study of XY and Heisenberg Models in Two Dimensions.' Numerical study based on the finite size RG. Confirmation of the KT picture and strong evidence against a standard algebraic divergence of the correlation length.

[73] W. Janke and K. Nather, Phys. Lett. A 157, 11 (1991).
'Numerical Evidence for Kosterlitz-Thouless Transition in the 2-D XY Villain Model.'

[74] C.F. Baillie and R. Gupta, Nucl. Phys. B (Proc. Suppl.) 20, 669 (1991).
'Critical Behavior of 3D Ising and 2D XY Spin Models.' Large-scale computer simulations of the 3D Ising and the 2D XY models using the Monte Carlo Renormalization Group (MCRG) method.

[75] R.G. Edwards, J. Goodman, and A.D. Sokal, Nucl. Phys. B 354, 289 (1991).
'Multigrid Monte Carlo. 2. Two-Dimensional XY Model.

[76] C.F. Baillie and R. Gupta, Phys. Rev. B 45, 2883 (1992).
'Critical Behavior of the 2D XY Model.' Detailed Monte Carlo results for the XY model are presented. The data favor a KT singularity over a second order transition, however, do not confirm the predicted values $\nu = 0.5$ and $\eta = 0.25$.

Series Expansions

[77] H. Arisue, Phys. Lett. B 313 (1993) 187.
'Strong coupling expansion of string tension for Z_2 lattice gauge theory in three dimensions.' We calculate the strong coupling expansion of string tension to order β^{34} in $D = 3$ Z_2 lattice gauge theory, which is equivalent to the low temperature expansion of the surface tension in the $D = 3$ Ising model. We obtain the expansion series by a linear combination of the string tension on finite size lattices, whose coefficients are determined recursively. A preliminary Padé analysis of the string tension at the roughening transition is also given.

[78] H. Arisue, Phys. Lett. B 322 (1994) 224.
'Strong coupling expansion of the mass gap for Z_2 lattice gauge theory in three dimensions.' We calculate the strong coupling expansion of the mass gap in three-dimensional Z_2 lattice gauge

theory, which is equivalent to the low temperature expansion of the inverse correlation length for the Ising model on a three-dimensional simple cubic lattice. The finite lattice method is used and the expansion series are obtained to order β^{30}.

[79] H. Arisue and T. Fujiwara, Nucl. Phys. B 285 [FS 19], 253 (1987).
'High Order Calculation of the strong coupling expansion for the mass gap in lattice gauge theory.'

[80] H. Arisue, preprint OPCT-94-3, hep-lat/9412109.
'Low-Temperature Expansion of the Free Energy in ASOS Model.' The low-temperature series of the free energy in the ASOS model is calculated to order u^{23} using the finite-lattice-method.

[81] M.E. Fisher, private communication.

[82] L.J. Shaw and M.E. Fisher, Phys. Rev. A 39, 2189 (1989).
Surface tension of the three-dimensional Ising model: A low-temperature analysis.'

[83] M.E. Fisher and H. Au-Yang, J. Phys. A 12 (1979) 1677.
'Inhomogeneous differential approximants for power series.'

[84] C. Vohwinkel, Phys. Lett. B 301, 208 (1993), and private communication.
'Yet another way to obtain low temperature expansions for discrete spin systems.' I present a modification of the shadow-technique, which allows one to derive low temperature series for discrete spin models to high orders. Results are given for the 3D Ising model up to 64 excited bonds, for the 4D Ising model up to 96 excited bond and the 3D Potts model up to 56 excited bonds.

[85] G. Bhanot, M. Creutz, and J. Lacki, Phys. Rev. Lett. 69, 1841 (1992).
'Low temperature expansion for the 3-d Ising Model.' Weak coupling expansion for the energy and magnetization of the 3-dimensional simple cubic Ising model using a finite lattice method. Order u^{25} for energy, u^{21} for magnetization, where $u = \exp(-4\beta)$.

Renormalization Group and Related

[86] K.G. Wilson and J. Kogut, Phys. Rep. C12, 75 (1974).
'The Renormalization group and the ϵ-Expansion.'

[87] J. Polchinski, Nucl. Phys. B 231, 269 (1984).
'Renormalization and Effective Lagrangians.'

[88] T. Niemeijer and J.M.J. Van Leeuwen, in: 'Phase transitions and Critical Phenomena', Vol. 6, C. Domb and M.S. Green, eds., Academic London 1976.

[89] S.K. Ma, Phys. Rev. Lett. 37, 461 (1976).
'Renormalization Group by Monte Carlo Methods.'

[90] S.H. Shenker and J. Tobochnik, Phys. Rev. B 22, 4462 (1980).
'Monte Carlo renormalization-group analysis of the classical Heisenberg model in two dimensions.'

[91] K.G. Wilson, in: 'Recent developments of gauge theories', G. 't Hooft et al., eds., Plenum, New York, 1980.

[92] M.P. Nightingale, Physica A 83, 561 (1976).
'Scaling Theory and Finite Systems.' A RG theory is introduced with the help of which the critical properties of infinite systems can be related to finite systems. As a numerical example the method is applied to the two-dimensional Ising model.

[93] K. Binder, Z. Phys. B 43, 119 (1981).
'Finite Size Scaling Analysis of Ising Model Block Distribution Functions.' The distribution function of the local order parameters in finite blocks of linear dimension L is studied for Ising lattices. A Monte Carlo RG similar to Nightingale's phenomenological RG is proposed.

[94] C.F. Baillie, R. Gupta, K.A. Hawick, and G.S. Pawley,
Phys. Rev. B 45, 10438 (1992).
'Monte Carlo renormalization-group study of the three-dimensional Ising model.' Results are presented of a MCRG study of the 3-dimensional Ising model on simple cubic 64^3 and 128^3 lattices. The estimate for the critical coupling is $0.221652 \pm 0.000003 \pm 0.000001$ where the first error is statistical and the second due to the finite number of blocking steps. The results for the relevant exponents are $\nu = 0.624(2)$ and $\eta = 0.026(3)$. The correction to scaling exponent is found to lie in the range $\omega = 0.8 - 0.85$.

[95] S. Wansleben and J. Zittarz, Nucl. Phys. B 280, 108 (1987).
'Monte Carlo Renormalization Group Calculations For Critical Exponents of the Finite Temperature Deconfinement Transition.' By using the Monte Carlo Renormalization group method we have calculated the critical exponents β/ν and ν for the $(2+1)$-dimensional Z(2) lattice gauge model at finite temperatures.

Rigorous Work on Kosterlitz-Thouless Theory and Related

[96] E.H. Lieb, Phys. Rev. 162, 162 (1967).
'Residual Entropy of Square Ice.'

[97] E.H. Lieb and F.Y. Wu, in: 'Phase Transitions and Critical Phenomena', C. Domb and M.S. Green, eds., Vol. 1, Academic London 1972.

[98] H. van Beijeren, Phys. Rev. Lett. 38, 993 (1977).
'Exactly Solvable Model for the Roughening Transition of a Crystal Surface.' An exactly solvable model (the BCSOS model) of the crystal-vacuum interface is constructed which exhibits a roughening transition. The model is isomorphic to the symmetric six-vertex model. Some of the thermodynamic properties are discussed.

[99] J.M. Fröhlich and T. Spencer, Phys. Rev. Lett. 46, 1006 (1981).
'Kosterlitz-Thouless Transition in the Two-Dimensional Plane Rotator and Coulomb Gas.' A rigorous argument is described establishing the KT transition in a class of two-dimensional models including the plane rotator and the Coulomb gas.
J.M. Fröhlich and T. Spencer, Commun. Math. Phys. 81, 527 (1981).
'The Kosterlitz-Thouless Transition in Two-Dimensional Abelian Spin Systems and the Coulomb Gas.'
J.M. Fröhlich and T. Spencer,
'The Berezinskii-Kosterlitz-Thouless Transition. Energy-Entropy Arguments and Renormalization in Defect Gases', in: 'Scaling and Selfsimilarity in Physics', J. Fröhlich, ed., Birkhäuser 1984.

[100] R.J. Baxter, 'Exactly Solved Models in Statistical Mechanics', Academic 1982.

[101] M. Göpfert and G. Mack, Commun. Math. Phys. 82, 545 (1982).
'Proof of Confinement of Static Quarks in 3-Dimensional Lattice Gauge Theory for all Values of the Coupling Constant.'

[102] K.R. Ito, Nucl. Phys. B 205 [FS5], 440 (1982).
'Upper and Lower Bound for the String Tension in the Three-Dimensional Lattice Quantum Electrodynamics.'

[103] J. Glimm and A. Jaffe, 'Quantum Physics - A Functional Integral Point of View', Springer, New York, 1987.

[104] J. Dimock, T.R. Hurd, Commun. Math. Phys. 137, 263 (1991).
'A Renormalization Group Analysis of the Kosterlitz-Thouless Phase.' For a 2D Sine Gordon theory with short distance cutoff, a complete RG analysis is given for $\beta > 8\pi$ and fugacity z sufficiently small. It is shown that the flow of the effective measures is toward a free field (infrared asymptotic freedom).

[105] J. Dimock, T.R. Hurd, Commun. Math. Phys. 156, 547 (1993).
'Construction of the Two-Dimensional sine-Gordon Model for $\beta < 8\pi$.' A rigorous construction of the two-dimensional massless and massive Sine Gordon models in finite volume is given for $\beta < 8\pi$. Analyticity in the coupling constant is proven and thus convergence of perturbation theory. The short distance behavior of the theory is that of the free field theory.

[106] C. Borgs and J.Z. Imbrie, Comm. Math. Phys. 145, 235 (1992).
'Finite Size Scaling and Surface Tension From Effective One-Dimensional Systems.'

Capillary Wave Model and Related

[107] F.P. Buff, R.A. Lovett, and F.H. Stillinger, Phys. Rev. Lett. 15, 621 (1965).
'Interfacial Density Profile for Fluids in the Critical Region.' The capillary wave model is proposed for the description of fluid interfaces.

[108] K. Dietz and T. Filk, Phys. Rev. D 27, 2944 (1983).
'Renormalization of string functionals.'

[109] P. Olesen, Phys. Lett. B 160, 144 (1985).
'Strings and QCD.' It is pointed out that the occurence of a large-distance "Coulomb" term in the static quark-antiquark potential is related to tachyons in the underlying string model.

[110] R.K.P. Zia, Nucl. Phys. B 251 [FS13], 676 (1985).
'Normal Coordinates and Curvature Terms in an Interface Hamiltonian.' For a system displaying two-phase coexisting at low temperature, the dominant modes are those associated with fluctuations of an interface between the phases. The lowest-order terms in the effective hamiltonian are proportional to the area and curvatures of the interface. A geometrically transparent approach to these terms is shown.

[111] M.P. Gelfand and M.E. Fisher, Physica A 166, 1 (1990).
'Finite-Size Effects in Fluid Interfaces.' Finite size effects are studied at the level of the Gaussian model of capillary waves.

[112] B. Bunk, Int. J. Mod. Phys. C 3, 889 (1992).
('Proceedings of the Workshop on Fermion Algorithms', Jülich 1991, ed. H.J. Herrmann and F. Karsch, World Scientific, Singapore 1991.)
'A Note on Interfaces with Periodic Boundaries.'

[113] V. Privman, Int. J. Mod. Phys. C 3, 857 (1992).
('Proceedings of the Workshop on Fermion Algorithms', Jülich 1991, ed. H.J. Herrmann and F. Karsch, World Scientific, Singapore 1991.)
'Fluctuating Interfaces, Surface Tension, and Capillary Waves: An Introduction.' Introduction to theories of interfacial fluctuations and the associated interfacial parameters: surface tension and surface stiffness, as well as their interpretation within the capillary wave model.

[114] M. Caselle, F. Gliozzi, and S. Vinti, Phys. Lett. B 302, 74 (1993).
'Finite-size effects in the interface of the 3D Ising model.' The 3D Ising model interface displays universal finite size effects which can be described in terms of a gaussian model of capillary waves. The finite-size effects depend strongly on the shape of the lattice.

[115] V. S. Dotsenko, G. Harris, E. Marinari, E. Martinec, M. Picco, and P. Windey,
Phys. Rev. Lett. 71, 811 (1993).
'Critical and Topological Properties of Cluster Boundaries in the 3D Ising Model.'

[116] P. Provero and S. Vinti, Physica A 211, 436 (1994).
'Capillary wave approach to order-order fluid interfaces in the 3D three-state Potts model.'

[117] M. Caselle, R. Fiore, F. Gliozzi, P. Guaita, and S. Vinti,
Nucl. Phys. B 422, 397 (1994). 'On the behaviour of spatial Wilson loops in the high-temperature phase of LGT.'

M. Caselle, F. Gliozzi, and S. Vinti, Nucl. Phys. B (Proc. Suppl.) 34, 263 (1994).
'On the relation between the width of the flux tube and T_c^{-1} in lattice gauge theories.
For a review on the subject see F. Gliozzi, Acta Phys. Pol. 23 B, 971 (1992).

[118] M. Caselle, F. Gliozzi, and S. Vinti, Nucl. Phys. B (Proc. Suppl.) 34, 726 (1994).
'Self-avoiding random surfaces with fluctuating topology.'

[119] M. Caselle, F. Gliozzi, P. Provero, and S. Vinti,
Nucl. Phys. B (Proc. Suppl.) 34, 720 (1994).
'Finite size effects in fluid interfaces.'

Monte Carlo Methods

[120] K. Binder, 'Monte Carlo Investigations', in: 'Phase Transitions and Critical Phenomena', Vol. 5b, C. Domb and M.S. Green, eds., Academic Press, New York 1976.

[121] K. Binder (ed.), 'Applications of the Monte Carlo Methods in Statistical Physics', Springer, 1984.

[122] K. Binder and D.W. Heermann, 'Monte Carlo Simulation in Statistical Physics', Springer, 1984.

[123] A.D. Sokal, 'Monte Carlo Methods in Statistical Mechanics: Foundations and New Algorithms', Lecture Notes "Cours de Troisième Cycle de la Physique en Suisse Romande, Lausanne 1989."

[124] M. Creutz, Phys. Rev. Lett. 50, 1411 (1983).
'Microcanonical Monte Carlo Simulation.' A new algorithm for the simulation of statistical systems is presented. The procedure produces a random walk through configurations of a constant total energy. It is computationally simple and applicable to systems of both discrete and continuous variables.

[125] G. Bhanot, M. Creutz, and H. Neuberger, Nucl. Phys. B 235 [FS11], 417 (1984).
'Microcanonical Simulation of Ising Systems.' Numerical simulations of the microcanonical ensemble for Ising systems are described. We explain how to write very fast algorithms for such simulations, relate correlations measured in the microcanonical ensemble to those in the canonical ensemble and discuss criteria for convergence and ergodicity.

[126] M. Creutz, K.J.M. Moriarty, and M. O'Brien,
Comput. Phys. Comm. 42 (1986) 191.
'Vectorization of the Three-Dimensional Ising Model Program on the CDC Cyber-205.'

[127] R.H. Swendsen and J.S. Wang, Phys. Rev. Lett. 58, 86 (1987).
'Nonuniversal Critical Dynamics in Monte Carlo Simulations.' A new approach to Monte Carlo simulations is presented, giving a highly efficient method of simulation for large systems near

criticality. The algorithm violates dynamic universality at second-order phase transitions, producing unusually small values of the dynamical critical exponent.

[128] A.M. Ferrenberg and R.H. Swendsen, Phys. Rev. Lett. 61, 2635 (1988).
'New Monte Carlo Technique for Studying Phase Transitions.' A method is presented for using the data from Monte Carlo simulations. A single MC simulation is sufficient to obtain complete information over the entire scaling region near a phase transition. The method is generally applicable to statistical models.

[129] U. Wolff, Phys. Rev. Lett. 62, 361 (1989).
'Collective Monte Carlo Updating for Spin Systems.' Description and investigation of the single cluster algorithm for $O(N)$ spin models.

[130] R.C. Brower and P. Tamayo, Phys. Rev. Lett. 62, 1087 (1989).
'Embedded Dynamics for ϕ^4 Theory.' Discrete Ising variables are embedded into the ϕ^4 theory, so that large-scale tunneling events can be induced via a modified Swendsen-Wang algorithm with fluctuating site-bond percolation probabilities. The results are consistent with the conjecture that this embedded dynamics lies in the same universality class as the Swendsen-Wang dynamics.

[131] D. Kandel and E. Domany, Phys. Rev. B 43, 8539 (1991).
'General Cluster Monte Carlo Dynamics.' A general cluster method for Monte Carlo simulations is presented that unifies many of previously developed algorithms.

[132] M. Hasenbusch and S. Meyer, Phys. Rev. Lett. 66, 530 (1991).
'Cluster-Update Acceleration of Interface Roughening in the 3D Ising Model.' A cluster update Monte Carlo algorithm for a fluctuating interface in the 3D Ising model is presented that drastically reduces critical slowing down. At the roughening point, the dynamical critical exponent is found to be $z = 0.44 \pm 0.03$.

[133] H.G. Evertz, J. Stat. Phys. 70 (1993) 1075.
'Vectorized Search for Single Clusters.' Breadth-first search for a single cluster on a regular lattice is shown to be vectorizable. It is applied to construct clusters in the single-cluster variant of the Swendsen-Wang algorithm. On a Cray-YMP, total CPU time has been reduced by factors of $3.5 - 7$ in large-scale applications. A multiple-cluster version is also described.

[134] H.G. Evertz, G. Lana, and M. Marcu, Phys. Rev. Lett. 70, 875 (1993).
'Cluster Algorithm for Vertex Models.' A cluster algorithm is presented that strongly reduces Critical Slowing Down in the simulations of vertex models. The clusters are closed paths of bonds. The algorithm is tested for the case of the F model. It is applicable also to other vertex models and to two-dimensional quantum spin systems.

[135] M. Marcu and E. Naftali, in preparation.

[136] K. Rummukainen, Nucl. Phys. B 390, 621 (1993).
'Multicanonical cluster algorithm and the two-dimensional 7-state Potts model.' I present a

hybrid-like two-step algorithm, which combines a microcanoincal update of a spin system using demons, with a multicanoincal demon refresh. The algorithm is free from supercritical slowing down. It is demonstrated with the 7-state Potts model.

[137] M. Hasenbusch, Physica A 197, 423 (1993).
'Monte Carlo simulation with fluctuating boundary conditions.' Study of the finite size behavior of the ratio of partion functions with periodic and antiperiodic boundary conditions in the vicinity of the critical coupling of the 3D Ising model. This ratio is obtained as a simple expectation value in an ensemble where the average is over both kinds of boundary conditions. Results for β_c and ν obtained from such simulations are compared with those from fourth order cumulant results obtained in the same Monte Carlo simulations.

Miscellaneous

[138] G.H. Hardy, Mess. Math. 49, 85 (1919).

[139] L. Onsager, Phys. Rev. 65, 117 (1944). 'Crystal Statistics. I. A Two-Dimensional Model with an Order-Disorder-Transition.'

[140] B. Kaufman, Phys. Rev. 76, 1232 (1949).
'Crystal Statistics. II. Partition Function Evaluated by Spinor Analysis.'

[141] W. Magnus, F. Oberhettinger, F.G. Tricomi, 'Higher Transcendental Functions', Vol. 1, A. Erdélyi, ed., McGraw-Hill, New York, 1953.

[142] M.E. Fisher, J. Phys. Soc. Jap. Suppl. 26, 87 (1969).

[143] M.E. Fisher and H.B. Tarko, Phys. Rev. B 11, 1217 (1975).
'Tests of strong scaling in the three-dimensional Ising model.'

[144] V. Privman and M.E. Fisher, J. Stat. Phys. 33, 385 (1983).
'Finite-Size Effects at First-Order Transitions.'

[145] E. Brézin and J. Zinn-Justin, Nucl. Phys. B 257, 867 (1985).
'Finite Size Effects in Phase Transitions.'

[146] C. Itzykson, J.M. Drouffe, 'Statistical Field Theory', Cambridge University Press 1989.

[147] S. Coleman, 'Aspects of Symmetry', Cambridge (1985).

[148] C. Itzykson and J.B. Zuber, Nucl. Phys. B 275 [FS17], 580 (1986).
'Two-dimensional Conformal Invariant Theories on a Torus.'

[149] A. Patrascioiu and E. Seiler, Phys. Rev. Lett. 60, 875 (1988).
'Different Perspective of the Kosterlitz-Thouless Phase Transition.' An interpretation of the KT transition is given that is different from the standard one.

[150] E. Seiler, I.O. Stamatescu, A. Patrascioiu, and V. Linke,
Nucl. Phys. B 305, 623 (1988).
'Critical Behaviour, Scaling and Universality in some Two-Dimensional Spin Models.' Numerical studies are presented of certain two-dimensional spin models, in particular the Z(10) model that is a discrete version of the O(2) model. We find strong evidence that this model has two transitions: the well-known freezing transition at low temperatures, and a KT transition at higher temperatures. The latter transition is well described by a power law singularity.

[151] C.F. Baillie, W. Janke, and D.A. Johnston, Phys. Lett. B 318, 424 (1993).
'DGSOS on DRTS.' Simulations of a discrete gaussian solid on solid (DGSOS) model on dynamical ϕ^3 graphs, using the cluster algorithms recently developed by Evertz et. al for use on fixed lattices.

[152] M. Hasenbusch, K. Rummukainen, and K. Pinn, in preparation.

Reviews

[153] R. Savit, Rev. Mod. Phys. 52, 453 (1980).
'Duality in field theory and statistical systems.' Pedagogical review of duality (in the sense of Kramers and Wannier) and its application to a wide range of field theories and statistical systems.

[154] J.M. Drouffe and J.B. Zuber, Phys. Rep. C 102, 1 (1983).
'Strong Coupling and Mean Field Methods in Lattice Gauge Theories.'

[155] D.B. Abraham, 'Surface Structures and Phase Transitions – Exact Results', in: 'Phase Transitions and Critical Phenomena', Vol. 10, C. Domb and J.L. Lebowitz, eds., Academic 1986. Some rigorous and exact results are discussed which relate to structure and phase transitions in interfaces and boundaries.

[156] H.W. Diehl, 'Field-theoretic Approach to Critical Behaviour at Surfaces', in: 'Phase Transitions and Critical Phenomena', Vol. 10, C. Domb and J.L. Lebowitz, eds., Academic 1986.

[157] D. Jasnow, 'Renormalization Group Theory of Interfaces', in: 'Phase Transitions and Critical Phenomena', Vol. 10, C. Domb and J.L. Lebowitz, eds., Academic 1986.

[158] H. van Beijeren and I. Nolden, 'The Roughening Transition', in: 'Structure and Dynamics of Surfaces II', W. Schommers and P. van Blanckenhagen, eds., Topics in Current Physics Vol. 43, Springer 1987.

[159] G. Forgacs, R. Lipowsky, and Th. M. Nieuwenhuizen, 'The Behaviour of Interfaces in Ordered and Disordered Systems', in: 'Phase Transitions and Critical Phenomena', Vol. 14, C. Domb and J.L. Lebowitz, eds., Academic 1991.